

Evaluation of Infiltration Practices as a Means to Control Stormwater Runoff

A Thesis

Submitted to the Faculty

of

Villanova University

by

Clay Hunter Emerson

in partial fulfillment of the

requirements for the degree

of

Doctor of Philosophy

May 2008

**© Copyright 2008
Clay Hunter Emerson. All Rights Reserved**

Acknowledgements

I have been very fortunate to have had the opportunity to work in such an exciting and fascinating field. The program conceived and created by Dr. Robert Traver is without equal. Dr. Traver has been and will continue to be a great advisor, role model, and friend. I am especially grateful for the unique opportunity he has given me. The impression he has left on me reaches far beyond the scope of this dissertation and is more valuable than any degree.

I am also thankful to have been able to work with Dr. Andrea Welker. She has been an indispensable, and always available, resource for all things geotechnical or otherwise. I would also like to thank the other members of my committee who have graciously provided their time and expertise. I thank Dr. Chadderton for his help in the preparation of this document and for his logical and objective recommendations and guidance, Dr. Baehr for his insightful observations and recommendations regarding all things groundwater related, and Dr. Wieder for his unique perspective on the subject. I would also like to acknowledge the insight, experience, example, and camaraderie provided by Bill Heasom.

This work would not have been possible without the love and support of my family and friends. Taryn, thank you for your continued unbridled love and support through all my endeavors. I am also thankful to have been raised by some of the most supporting parents and family one could imagine; thank you Mom, Dad, Amy, and Wendy.

I have had the opportunity to come to know many wonderful people during my time at Villanova. Specifically I would like to thank George Pappas for his help and direction in designing and building anything I could ever imagine, and Linda DeAngelis for her help in all things administrative including countless seminars, symposiums, and workshops. I am also grateful for the advice provided by Dr. Duran and Dr. Wadzuk. In addition to the faculty and staff of the department, I have had the pleasure to get to know many graduate students while at Villanova. They have provided support and friendships that I will treasure for a lifetime.

Finally, I would like to express my gratitude for the various funding sources that have made my work at Villanova possible.

Table of Contents

| | |
|--|-----|
| Acknowledgements..... | ii |
| Table of Contents..... | iii |
| List of Tables..... | vi |
| List of Figures..... | vii |
| Abstract | xiv |
| Chapter 1. Introduction..... | 1 |
| 1.1 Background..... | 1 |
| 1.2 Statement of Objectives..... | 6 |
| 1.3 Villanova University BMP Site Descriptions..... | 7 |
| 1.3.1 Pervious Concrete Infiltration Basin (PCIB)..... | 8 |
| 1.3.2 BioInfiltration Traffic Island (BTI)..... | 10 |
| 1.3.3 Infiltration Trench (IT)..... | 15 |
| 1.3.4 Summary of Infiltration BMPs..... | 18 |
| Chapter 2. Long-term and Seasonal Performance of the Infiltration Process in Stormwater Management BMPs..... | 24 |
| 2.1 Introduction and Background..... | 24 |
| 2.2 Characterization of the Long-Term and Seasonal Performance of Infiltration BMPs..... | 27 |
| 2.2.1 Long-Term and Seasonal Performance of the PCIB..... | 36 |
| 2.2.2 Long-Term and Seasonal Performance of the BTI..... | 62 |
| 2.2.3 Long-Term and Seasonal Performance of the IT..... | 85 |
| 2.2.4 Summary of Long-Term and Seasonal Performance of BMPs..... | 112 |
| 2.2.4.1 Temperature Dependency..... | 112 |
| 2.2.4.2 Longevity..... | 120 |

| | |
|---|-----|
| 2.3 Discussion and Review of Processes that Influence Infiltration..... | 126 |
| 2.3.1 Temperature Dependency | 126 |
| 2.3.1.1 Examples from Literature | 128 |
| 2.3.1.2 Relation to Villanova Infiltration BMPs..... | 140 |
| 2.3.2 Soil Surface Evolution and BMP Longevity | 142 |
| 2.3.2.1 Examples from Literature | 145 |
| 2.3.2.2 Relation to Villanova Infiltration BMPs..... | 163 |
| Chapter 3. Soil Testing for Infiltration BMPs | 173 |
| 3.1 Introduction..... | 173 |
| 3.2 Particle-size distribution and Soil Classification | 173 |
| 3.3 Preconstruction Investigative Infiltration Testing | 178 |
| 3.3.1 Pervious Concrete Infiltration Basin..... | 178 |
| 3.3.2 BioInfiltration Traffic Island..... | 180 |
| 3.3.3 Infiltration Trench..... | 182 |
| 3.3.4 Summary | 187 |
| 3.4 In-situ Infiltration Testing at the BTI..... | 190 |
| 3.4.1 Introduction..... | 190 |
| 3.4.2 Results..... | 199 |
| 3.4.3 VS2D Simulations | 205 |
| 3.4.3.1 Introduction..... | 205 |
| 3.4.3.2 VS2D Background..... | 208 |
| 3.4.3.3 Model Development..... | 208 |
| 3.4.3.4 Sensitivity Analysis | 212 |
| 3.4.3.5 Energy Transport | 218 |

| | |
|--|-----|
| 3.4.3.6 Results..... | 219 |
| 3.4.3.7 Summary and Implications | 228 |
| 3.5 Conclusion | 229 |
| Chapter 4. Groundwater Modeling of Infiltration BMPs..... | 232 |
| 4.1 Introduction and Purpose | 232 |
| 4.2 Pervious Concrete Infiltration Basin..... | 233 |
| 4.3 BioInfiltration Traffic Island..... | 238 |
| 4.4 Conclusion | 243 |
| Chapter 5. Summary and Conclusions..... | 245 |
| Chapter 6. Design Recommendations for Infiltration BMPs..... | 253 |
| 6.1 Infiltration Testing | 254 |
| 6.2 BMP Design..... | 256 |
| 6.3 Infiltration BMP Assessment..... | 260 |
| Chapter 7. Future Work | 263 |
| List of References | 267 |
| Appendix A. SlopeFinder Program..... | 274 |
| Appendix B. Time Interval Conversion Program: Visual Basic Code | 280 |
| Appendix C. Monte Carlo Green and Ampt Sensitivity Analysis | 282 |
| Appendix D. Method to Correct for Oscillations in Level Data from the BTI..... | 288 |
| Appendix E. Infiltration Trench Model (McKsat)..... | 293 |
| Appendix F. Green and Ampt Model for Infiltration BMPs | 297 |

List of Tables

| | |
|---|-----|
| 1. Planting list for the BTI. | 12 |
| 2. Summary of the contributing areas to the three infiltration BMPs. | 23 |
| 3. Student’s T-test for incremental slopes from 2004 and 2005. | 42 |
| 4. Summary of the observed temperature dependency for all three BMPs (blue lines). | 114 |
| 5. Summary of the fluidity corrections for all three BMPs (green lines). | 115 |
| 6. Summary of multiple linear regressions. | 120 |
| 7. Relevant dates including the start and end of the data record used in this study along with equivalent age comparisons for the three infiltration BMPs. | 125 |
| 8. Summary of the observed and predicted temperature dependencies for the three BMPs. | 141 |
| 9. Summary of approximate textural breakdown and USDA soil classifications for the three infiltration BMPs. | 178 |
| 10. Summary of preconstruction infiltration test at the three infiltration BMPs. | 188 |
| 11. Summary of VS2D solver options for single-ring infiltrometer simulations. | 210 |
| 12. Summary of van Genuchten parameters for the three infiltration BMPs. | 212 |
| 13. Summary of energy transport parameters used in VS2DH simulations. | 219 |
| 14. Summary of single-ring infiltrometer data and VS2DH simulations for the east ring infiltrometer. | 224 |
| 15. Model soil profile properties for the PCIB. | 234 |
| 16. Model soil profile properties for the BTI. | 240 |
| 17. Example output from SlopeFinder program. | 275 |
| 18. Summary of the Monte Carlo Green and Ampt sensitivity analysis. | 283 |

List of Figures

| | |
|--|----|
| 1. Two detention basins located in Chester County, PA..... | 3 |
| 2. Excavation of the lower bed (left) and placement of the middle bed crushed stone (right)..... | 9 |
| 3. Fully excavated original soil (left) and composite soil placement process (right). | 11 |
| 4. Contour view of BTI (based on survey conducted by William Heasom in June of 2002)..... | 11 |
| 5. Cross section of outflow conditions via the modified 2×4 ft inlet box (image by William Heasom)..... | 13 |
| 6. Completed BTI (August 28 th 2007)..... | 15 |
| 7. Preconstruction view of BMP location (left) and BMP excavation with retaining wall in place..... | 16 |
| 8. IT prior to the installation of the Eco-Pavers (left) and the completed BMP (right)... | 18 |
| 9. Representative cross sections of all three infiltration BMPs with crushed stone and overflow depth shown..... | 20 |
| 10. Aerial view of contributing areas (outlined in blue) to three infiltration BMPs (outlined in green)..... | 22 |
| 11. Sedimentation occurring in two detention basins in Chester County, PA..... | 25 |
| 12. Depth records from all three infiltration BMPs for the April 1 st 2005 storm event... | 31 |
| 13. Incremental slope approximations for December 15 th 2005 storm event at the PCIB..... | 34 |
| 14. Comparison of recorded five-minute data to derived 15-minute data..... | 37 |
| 15. Calendar years 2004 and 2005 data for the PCIB..... | 39 |
| 16. Average recession rates and temperature for each of the seven incremental depth ranges for the PCIB data record (2004-2005)..... | 40 |
| 17. Comparison for averaged incremental slopes for data from calendar years 2004 and 2005..... | 41 |
| 18. Incremental slopes found for the PCIB..... | 43 |

| | |
|--|----|
| 19. Recession limb comparison for October 29 th 2003 and October 9 th 2005..... | 44 |
| 20. Temperature dependency linear regression for the PCIB..... | 46 |
| 21. Histogram of regression residuals for PCIB..... | 47 |
| 22. Check for homoscedasticity for PCIB regression..... | 48 |
| 23. Check for autocorrelation of residuals for PCIB..... | 49 |
| 24. Relative variation of density and viscosity of water with temperature..... | 51 |
| 25. Rainfall, depth, and soil moisture reading for the October 7 th , 2005 storm event at the PCIB..... | 53 |
| 26. Fluidity of water as a function of temperature..... | 55 |
| 27. Temperature dependency of the predicted and observed estimates of hydraulic conductivity for the PCIB..... | 58 |
| 28. Original data regression and predicted fluidity correction for hydraulic conductivity as a function of measured temperature over the two year data record for the PCIB.. | 60 |
| 29. Data set used for analysis of the BTI..... | 63 |
| 30. Comparison of three storm events at the BTI..... | 65 |
| 31. Full Range (1.4 to 0.4 ft) slopes for BTI..... | 67 |
| 32. Measured recession rates between water levels of 1.4 and 0.4 ft with a minimum recession time of 12 hours for the BTI without full-range constraint, displayed with one, two and four year linear regressions..... | 68 |
| 33. Recession rate data from the BTI fit with seven-point moving average and best-fit periodic function..... | 69 |
| 34. Two-year data record with measured temperature at the BTI..... | 70 |
| 35. Temperature dependency linear regression for the BTI..... | 72 |
| 36. Histogram of regression residuals for BTI..... | 73 |
| 37. Check for homoscedasticity for BTI regression..... | 74 |
| 38. Check for autocorrelation of residuals for BTI..... | 75 |

| | |
|--|-----|
| 39. Rainfall, level, and soil moisture reading for the July 12 th , 2004 storm event at the BTI. | 77 |
| 40. Temperature dependency of the predicted and observed estimates of hydraulic conductivity for the BTI..... | 80 |
| 41. Original data regression and predicted fluidity correction for hydraulic conductivity as a function of measured temperature over the two-year data record for the BTI. ... | 83 |
| 42. Depth data record for the IT..... | 87 |
| 43. Incremental slope method for IT for the November 29 th , 2005 storm. | 88 |
| 44. Incremental slopes between five and four feet for the IT before and after sorting.... | 90 |
| 45. Incremental slopes for the IT from July 2004 to March 2007. | 91 |
| 46. Depth duration curves for first two years of data at IT..... | 92 |
| 47. Scaled incremental slopes for the IT from July 2004 to March 2007..... | 94 |
| 48. Representative theoretical recession limbs for the IT..... | 96 |
| 49. Conceptual diagram of hydraulic conductivity for McKsat model of the IT. | 99 |
| 50. Geometric relationships for the IT BMP. | 100 |
| 51. Sensitivity of the McKsat model for the April 8 th , 2005 storm event..... | 103 |
| 52. Observed and simulated (McKsat) infiltration hydrographs for four selected storms at the IT..... | 104 |
| 53. Results for all 72 storms from McKsat for the IT..... | 105 |
| 54. Autocorrelation check for average hydraulic conductivity vs. temperature regression for the IT for two-year data record. | 106 |
| 55. Temperature dependency linear regression for the IT for the last full year of data. | 108 |
| 56. Check for autocorrelation of residuals for IT (last full year of data only)..... | 109 |
| 57. Temperature dependency of the predicted and observed average hydraulic conductivity for the IT (last full year of data record). | 110 |
| 58. Observed data (McKsat) regression and predicted fluidity correction for hydraulic conductivity as a function of measured temperature over a one year data record for the IT..... | 111 |

| | |
|---|-----|
| 59. Overlay of linear regressions for all three infiltration BMPs. | 114 |
| 60. Particle-size distributions for the three infiltration BMPs. | 118 |
| 61. Incremental slopes found for a hypothetically shortened data span for the IT. | 124 |
| 62. Seasonal changes in vegetation, April 2006 (left) and September 2006 (right). | 165 |
| 63. Approximately six years of sediment build-up in a riprap swale at the BTI (photo taken on May 16 th 2007). | 167 |
| 64. Desiccated surface crust with emerging vegetation at the BTI (photo taken on May 16 th 2007). | 168 |
| 65. Incremental slopes from initial six months of operation at the IT. | 169 |
| 66. Sieve analyses for three infiltration BMPs. | 174 |
| 67. Sieve and hydrometer data for the IT. | 176 |
| 68. Complete particle-size distributions for the BTI. | 177 |
| 69. Location of two test pits (left) and an ongoing infiltration test in one of the test pits (right). | 179 |
| 70. Ongoing flexible wall hydraulic conductivity test. | 180 |
| 71. Ongoing infiltration test at the BTI. | 181 |
| 72. Depth versus time for three trials at the BTI. | 182 |
| 73. Test pit location and fully excavated pit during constant head infiltrometer test. | 183 |
| 74. Simulated moisture content at one hour of the single-ring constant head infiltrometer test at the IT ($K = 2.8$ in/hr). | 184 |
| 75. Three inch PVC pipe installed for Maryland infiltration test. | 186 |
| 76. Results from the Maryland infiltration test using a three inch pipe at the IT. | 187 |
| 77. Photographs of the west ring (left) and east ring (right) taken on November 21, 2006. | 193 |
| 78. Approximate locations of single-ring infiltrometers in the BTI. | 193 |
| 79. Single-ring infiltrometer experimental setup for the west ring on August 3 rd , 2006. | 196 |

| | |
|--|-----|
| 80. Submerged soil surface within the east ring during an experimental run..... | 196 |
| 81. Excavations left by two soil cores taken from soil adjacent to the west ring..... | 198 |
| 82. Intake curve from eight separate infiltration tests on the east ring infiltrometer located in the BTI..... | 200 |
| 83. Six intake curves from the west ring infiltrometer in the BTI..... | 200 |
| 84. Steady-state intake rate and temperatures from single-ring infiltrometer runs at the BTI..... | 202 |
| 85. Steady-state intake rates vs. temperature for the east ring..... | 204 |
| 86. Green and Ampt approximation of August 23 rd , 2006 west ring infiltrometer data..... | 206 |
| 87. Full scale and ring close-up of axisymmetric VS2D single-ring infiltrometer simulation..... | 211 |
| 88. VS2D intake curves for the single-ring infiltrometer using the soil hydraulic parameters for three soil types at both a dry ($\theta = 0.10$) and wet ($\theta = 0.30$) initial condition. Intake rate at two hours labeled on plots [in/hr]..... | 213 |
| 89. VS2D intake curves using the soil hydraulic parameters for three soil types with a constant saturated hydraulic conductivity at both a dry ($\theta = 0.10$) and wet ($\theta = 0.30$) initial condition. Intake rate at two hours labeled on plots [in/hr]..... | 214 |
| 90. VS2D intake curves using the soil hydraulic parameters for sandy loam at three different initial moisture contents ($\theta = 0.10, 0.20,$ and 0.30). Intake rate at two hours labeled on plots [in/hr]..... | 215 |
| 91. VS2D intake curves using the soil hydraulic parameters for sandy loam at a constant moisture content ($\theta = 0.20$) and three saturated hydraulic conductivities ($K = 0.31, 0.63,$ and 1.3 in/hr). Intake rate at two hours labeled on plots [in/hr]..... | 216 |
| 92. Steady-state intake rate for sandy loam as a function of saturated hydraulic conductivity (left) and initial moisture content (right). | 217 |
| 93. Initial temperature profile for the west ring infiltrometer experiment conducted on August 23 rd , 2006..... | 221 |
| 94. Observed and VS2DH intake curves with various hydraulic conductivities for the west ring infiltrometer on the August 23 rd , 2007 run. Intake rate at two hours labeled on plots [in/hr]..... | 222 |
| 95. Observed and VS2DH intake curves for the six east ring infiltrometer runs. | 224 |
| 96. Observed and simulated intake rates for all six east ring runs..... | 225 |

| | |
|--|-----|
| 97. Axisymmetric view of volumetric moisture content from VS2D at 0.25 hr increments for the August 23 rd , 2006 east ring infiltrometer simulation. Black lines represent grid cell flow velocity vectors..... | 227 |
| 98. PCIB model profile diagram..... | 234 |
| 99. Total head condition (bed depth) and resulting soil profile intake curves for three VS2D simulations at the PCIB. | 236 |
| 100. Total head condition (bed depth) and resulting volumetric moisture content output for three depths in soil profile at the PCIB. | 237 |
| 101. BTI model profile diagram. | 239 |
| 102. Bed depth and resulting soil profile intake curves for three VS2D simulations at the BTI. | 241 |
| 103. Total head condition (average bed depth) and resulting volumetric moisture content output for three depths in soil profile at the BTI. | 242 |
| 104. Conceptual program flow chart for SlopeFinder. | 274 |
| 105. Recession rate vs. hydraulic conductivity for Green and Ampt sensitivity analysis for the BioInfiltration Traffic Island. | 284 |
| 106. Screenshot of the spreadsheet used to implement the Monte Carlo Green and Ampt sensitivity analysis, results for the BioInfiltration Traffic Island shown. | 285 |
| 107. Ultrasonic transducer oscillations and temperature at the BioInfiltration Traffic Island..... | 288 |
| 108. Running calculation of a three-hour slope of the ultrasonic transducer oscillation. | 289 |
| 109. Recession limb (from 1.4 to 0.4 ft) for the July 9 th 2005 storm, showing two calculated slopes as found with the SlopeFinder program..... | 290 |
| 110. Recession limb for July 9 th 2005 storm showing both 15-minute and two-hour data. | 291 |
| 111. Comparison of original two-point method and linear regression method for the BioInfiltration Traffic Island..... | 292 |
| 112. Program flow chart for the McKsat model of the IT. | 293 |
| 113. BioInfiltration Traffic Island readings for depth, rainfall and two foot depth moisture meter, July 2004..... | 298 |

| | |
|--|-----|
| 114. Bioinfiltration Traffic Island storage basin geometry..... | 299 |
| 115. Observed and simulated depth using Green and Ampt model with tabled geometric data..... | 301 |
| 116. Green and Ampt model used to simulate recession limb of BioInfiltration Traffic Island for same storm mentioned previously..... | 302 |
| 117. Green and Ampt model with flat bottom approximation of BioInfiltration Traffic Island..... | 304 |
| 118. Observed data and Green and Ampt continuous simulation data for July and August 2005..... | 306 |
| 119. Cumulative plot for two month simulation period..... | 307 |
| 120. Screenshot of spreadsheet used to implement Green and Ampt infiltration BMP model..... | 311 |

Abstract

Evaluation of Infiltration Practices as a Means to Control Stormwater Runoff

Clay Hunter Emerson

Robert G. Traver Ph.D. PE

The objective of this research is to provide a comprehensive explanation of the infiltration process as it relates to stormwater best management practices (BMPs), with the purpose of improving the current application of infiltration BMPs. Recent regulations have focused on, and in many cases required, the use of engineered infiltration practices to mitigate the excess volume of stormwater runoff created from developed areas. The widespread implementation of infiltration BMPs is a relatively new concept in the engineering community. Infiltration BMPs are currently designed and built without a full understanding of the physical process that dictates their operation. This investigation focuses on the analysis of data collected at three infiltration BMPs constructed on the campus of Villanova University. The three infiltration BMPs include a Pervious Concrete Infiltration Basin, a BioInfiltration Traffic Island, and an Infiltration Trench. The goal of this analysis is to resolve many of the remaining questions regarding stormwater infiltration BMPs. How does the infiltration process within a BMP change over time, and what design factors may influence its long-term performance? Other questions remain about potential seasonal variations in performance of infiltration BMPs. What is the magnitude and source of these variations and what type of design and BMP assessment implications might these variations suggest? Various performance normalization techniques and assessment protocols for infiltration BMPs are developed in an effort to determine the long-term and seasonal variations present at the three infiltration BMPs. Finally, this work examines and proposes infiltration testing techniques to be used to determine the adequacy of a site for infiltration. The results of

this study indicate that properly designed infiltration BMPs can provide a long-term solution to manage the increase in runoff volume from developed areas. Seasonal variations in performance are significant and primarily a result of temperature-induced viscosity effects of the ponded water. Generally, infiltration tests which focused on the determination of the hydraulic conductivity were shown to provide the best prediction of BMP performance. In summary, this work seeks to improve the current status of stormwater infiltration BMP design and implementation.

Chapter 1. Introduction

1.1 Background

The world's population is ever more reliant on already stressed water resources.

Consequently, a sustainable approach to water resource planning and management is crucial. Sustainability, with regard to water resources, has been defined as follows

(ASCE and UNESCO 1998):

Sustainable water resources systems are those designed and managed to fully contribute to the objectives of society, now and in the future, while maintaining their ecological, environmental, and hydrological integrity.

For society to meet the ideals of sustainability it must protect and preserve the hydrologic cycle through sound water resources planning and management.

One of the major ways our society impacts the hydrologic cycle is through land use modifications. The conversion of land from forested and agricultural areas to urban and suburban land uses has been the dominant succession in recent years, especially in regions surrounding existing urban areas. Common land development practices entail the removal of large amounts of vegetation, soil grading and compaction, and the construction of impervious surfaces. These alterations have drastic impacts on the hydrologic cycle including an increase in the volume, frequency, and peak rate of runoff along with an associated decrease in water quality and base flow. Prior to development, the hydrologic balance was dominated by evapotranspiration and groundwater recharge. However, in the post construction condition the hydrologic balance of the site shifts towards an increase in surface runoff.

These local hydrologic alterations act in a cumulative fashion over the landscape and have many adverse impacts including an increase in the magnitude and frequency of flooding and flood-related damage. Surface water supply is often compromised by decreased water quality, and groundwater supplies are stressed by a decrease in groundwater recharge. These changes also have a profound impact on the biological and ecological integrity of receiving water bodies. Streams and rivers experience a characteristic shift in their annual flow regime. This change results in excess channel erosion and sedimentation. This process further degrades aquatic habitat with associated decreases in invertebrate and fish species richness/diversity indices (Paul and Meyer 2001; Steffy and Kilham 2006). Additionally, diminished groundwater recharge can result in decreased baseflow and a decline in groundwater levels which can have a profound ecological impact on shallow wetlands (Simmons and Reynolds 1982; Gibbs 1993). The recreational, aesthetic, and economic values of waterways are compromised as a result of these alterations.

Stormwater runoff generated by the development process was viewed as a nuisance in the recent past. The strategy was to collect and convey the runoff away from the developed area towards the nearest watercourse as quickly as possible. Inlets and culverts created an efficient conveyance system which brought the runoff directly into streams and rivers. During the 1960's and 1970's communities began to notice the effects of excess uncontrolled runoff from development. Flooding resulted in property damage and, in some cases, loss of life. In response, regulations were passed in an effort to control the

runoff from developing areas. This was the dawn of modern stormwater management. Initially focus was placed specifically on peak flow rate. Typical regulations required that the engineer ensure that the post construction peak flow rate not exceed the preconstruction peak flow rate for large infrequent storm events (2 – 100 year return period). This was accomplished by constructing detention basins, which are designed to temporarily detain higher flows while releasing flow at a lower controlled rate. This requires a storage volume and outlet structure both sized to meet the peak flow requirement. Figure 1 shows two typical detention basins.



Figure 1. Two detention basins located in Chester County, PA.

This practice became commonplace and detention basins became the staple of stormwater management. Over the following decades, numerous detention basins were built to control the runoff from their individual drainage areas. Because each basin was typically designed on a site-by-site basis, the detention basins act in an uncoordinated fashion across a watershed. Natural spatial variability of precipitation also makes a truly coordinated system unrealistic. Nevertheless, the perception was that controlling peak flow rate on a site-by-site basis would result in watershed-wide peak flow control. The

watershed-wide effectiveness of a network of uncoordinated detention basins is at best questionable (McCuen 1979; Traver and Chadderton 1992). One evaluation of the watershed-wide effectiveness of peak flow control showed that detention basins have little impact on the watershed-wide storm flow regime. It also illustrated that while they may limit peak flow at their outlet, detention basins lose their effectiveness at the watershed scale and in fact have the potential to increase peak flow downstream (Emerson 2003; Emerson, Welty et al. 2005).

Detention basins and peak flow control, do not address the quantity of runoff. Under the post construction conditions, compacted soils and impervious surfaces generate runoff well in excess of the predevelopment conditions. These increases in the quantity or volume of runoff act in a cumulative fashion over a watershed. The individual peak-attenuated hydrographs from the detention basins accumulate and coincide with one another in an uncoordinated fashion resulting in higher peak flow rates compared to predevelopment conditions and even higher peak flow rates than there may be with uncontrolled development (no detention basins) (Emerson, Welty et al. 2005). Therefore, flooding, channel erosion, and aquatic habitat degradation will continue under a peak flow based system.

Controlling the peak flow rate from developed areas is only one piece of a complete solution to stormwater management. In hindsight, detention basins represent an “end of the pipe” solution to managing the increased runoff. The term stormwater management has often been used to describe the structural measures taken to counteract the negative

impacts of typical land development practices. A more comprehensive outlook on stormwater management is to develop land in a way that first minimizes the amount of structural measures required to offset the hydrologic impacts of the development process. These methods are often collectively referred to as Low Impact Development (LID). One of the main objectives is to limit the volume of runoff that leaves the site. This is first accomplished by limiting the amount of soil compaction and impervious surfaces. The next step is to reduce the runoff that is generated through capture and reuse, evapotranspiration and infiltration.

In addition to limiting the volume of runoff, infiltration BMPs provide groundwater recharge which helps maintain baseflow. This method of controlling the volume of runoff, unlike detention control, is cumulative when scaled up from the site to watershed level. Consequently, when a volume-based method is applied at a watershed scale, watershed-wide peak flow rates are attenuated (Emerson, Welty et al. 2005). Because of the continued degradation under detention control regulations, recent stormwater regulations and guidance are placing an increasingly larger focus on volume-based infiltration stormwater management practices (MDE 2000; NJDEP 2004; PADEP 2006). A volume-based approach is the first step towards a more sustainable land development process. By controlling the volume of runoff, the magnitude and frequency of flooding and flood related damage is minimized. Under a volume control system stream channel erosion and sedimentation approaches natural levels. This approach results in flow regimes that more closely mimic predevelopment levels. The improved flow regime and the resulting physical improvements to stream and river channels provide a basis for a

healthier aquatic ecosystem. All of these changes result in water resources that have enhanced water supply, recreational, and aesthetic value.

However, infiltration BMPs are still a relatively new stormwater management approach. There is a lack of long-term continuous hydrologic monitoring to support their design and implementation. Many questions remain regarding the proper design techniques, operation, maintenance, and performance assessment of infiltration BMPs. Most importantly, there are uncertainties regarding the long-term and seasonal infiltration performance for this class of stormwater BMPs. To insure that the benefits of a volume-based (specifically infiltration) system are attained, it is imperative to gain an understanding of the long-term operation of infiltration BMPs. A complete understanding of infiltration BMPs includes a solid understanding of how design and construction techniques impact the long-term effectiveness. Furthermore, sufficient attention needs to be given to the assessment methods used to gauge the performance of these BMPs.

1.2 Statement of Objectives

The objective of this research is to investigate all aspects of stormwater infiltration with the intention of improving the performance prediction, design, implementation, and assessment of stormwater infiltration practices. The goal is to provide the engineering community with conclusions and recommendations that support proper methods of design, construction, operation, and assessment of infiltration BMPs. The primary instrument used in this examination is the analysis of continuous monitoring data

collected at three infiltration BMPs on the campus of Villanova University. Infiltration BMP performance characteristics revealed from the continuous monitoring data are explained in the context of the relevant and dominant physical processes that dictate their performance. The infiltration BMPs central to this investigation include a Pervious Concrete Infiltration Basin (PCIB), a BioInfiltration Traffic Island (BTI), and an Infiltration Trench (IT). Each of the three BMPs is unique in terms of its specific design parameters. Together, they represent nearly the full spectrum of various applications of infiltration to manage stormwater runoff from developed areas. The focus of this examination is on the actual infiltration process itself and not on the capture efficiency of any individual BMP. Therefore, steps have been taken to normalize the performance of the BMPs so that their performance can be evaluated over time, relative to one another, and relative to other BMPs outside of this research. This research also compares findings to existing literature on topics relevant to stormwater infiltration. Preconstruction infiltration testing techniques are addressed as to how they relate to BMP design and performance. Unsaturated groundwater modeling is used to provide a conceptual explanation of the subsurface flow processes at the infiltration BMPs. An ancillary objective is to develop performance assessment methods and techniques that could be applied to other infiltration BMPs besides those at the focus of this study.

1.3 Villanova University BMP Site Descriptions

The Villanova Urban Stormwater Partnership (VUSP) was formed to provide research, demonstration and technical outreach for innovative stormwater practices. The VUSP has built and or retrofitted more than seven stormwater BMPs on campus. These BMPs

include among others a Stormwater Wetlands, BioInfiltration Traffic Island, Pervious Concrete Infiltration Basin, Infiltration Trench, and a Green Roof. As part of the mission of the VUSP many of these BMPs have been instrumented in an effort to provide valuable hydrologic and water quality monitoring data related to the operation of such innovative BMPs. The three infiltration BMPs central to this study are further detailed in the following sections. The overall site design and configuration of the infiltration BMPs, along with details regarding their construction and the relevant hydrologic monitoring instrumentation, are provided.

1.3.1 Pervious Concrete Infiltration Basin (PCIB)

The PCIB is a retrofit of an existing courtyard and walkway constructed in the summer of 2002. The courtyard was previously paved with standard asphalt and curbed. The purpose of the retrofit was to capture and infiltrate runoff from the courtyard and adjacent dormitory rooftops and also to improve the overall aesthetics of the courtyard. Because of the linear form and slope of the site, the design called for a tiered system. The BMP consists of three subsurface infiltration beds which are filled with crushed stone aggregate to create a storage basin with approximately 40% void space. The storage beds were constructed in such a manner as to avoid excess compaction of the subsoil. The beds were excavated in a sequential manner and filled with the crushed stone in the same sequential fashion. Therefore the soil in the storage beds was never directly driven on by any equipment. Once the beds were backfilled with crushed stone they could be driven over by various equipment without significantly compacting the soil surface. The construction sequencing of the storage beds is shown in Figure 2.



Figure 2. Excavation of the lower bed (left) and placement of the middle bed crushed stone (right).

The storage beds were also lined with a nonwoven geotextile to separate the natural sub soils from the stone bed as can be seen in Figure 2. The downspouts from the adjacent dormitories are directly connected to the storage bed via flexible plastic pipe. The rooftops are four-story slate roofs and therefore the runoff collected by the downspouts has characteristically low suspended solids concentrations. The courtyard area consists of standard concrete outlined with a strip of pervious concrete which is then outlined with standard decorative pavers. The standard concrete is crowned towards the pervious concrete. While the BMP gets its name from the pervious concrete it should be noted that the directly connected downspouts likely make up the majority of the inflow to the BMP. The contributing area to the PCIB is approximately 1.3 acres and is 62% impervious which results in a Directly Connected Impervious Area (DCIA) to BMP footprint of approximately 6:1. Further details on the design, construction and contributing area of this BMP are provided in Kwiatkowski (2004), Ladd (2004) and Kwiatkowski, Welker, et al. (2007).

Instrumentation at this BMP includes a pressure-temperature transducer in the lower bed to monitor the depth and temperature of the ponded water. The lower bed was also equipped with an array of Time Domain Reflectometer (TDR) soil moisture probes located one, two and four feet beneath the storage bed. This investigation only uses the data collected at the lower bed. The lower bed itself has a DCIA to BMP footprint ratio of only approximately 3:1. A rain gauge was also installed on the rooftop of one of the adjacent buildings.

1.3.2 BioInfiltration Traffic Island (BTI)

The BTI is a retrofit of an existing curbed traffic divider/island. The BMP is located on the University's west campus which is primarily a student apartment/dormitory area. The BTI was constructed in the Summer of 2001. The construction process for this BMP consisted of excavating the traffic island to a depth of approximately six feet. The excavated soil was then mixed at a 1:1 ratio with sand and placed back into the excavation to create a shallow depression. Due to the manageable size of the BMP, the entire excavation, soil mixing, and mixed soil placement process could be conducted without ever requiring that any equipment drive over either the excavated original soil surface (six foot depth) or the placed mixed soil. This process is illustrated in Figure 3.



Figure 3. Fully excavated original soil (left) and composite soil placement process (right).

The resulting topography of the basin was determined in a survey conducted by William Heasom in June of 2002. This topographic survey with 0.1 ft contours is shown in Figure 4.

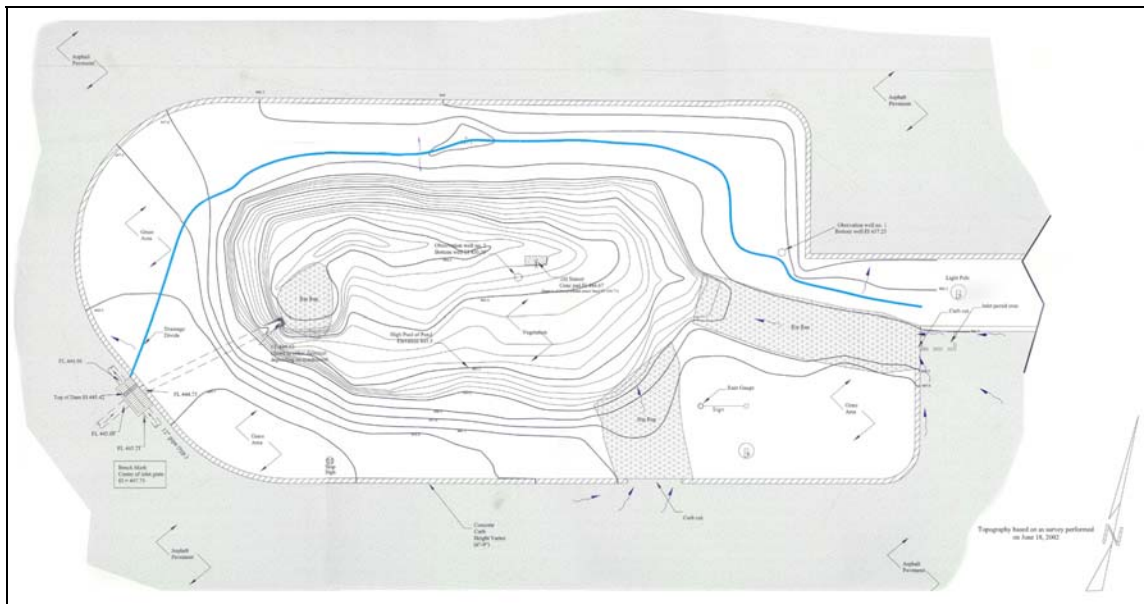


Figure 4. Contour view of BTI (based on survey conducted by William Heasom in June of 2002).

Soon after the BMP was completed, shredded hardwood mulch was placed over the soil surface and the vegetation was planted in the BMP. The plant selection was done by Villanova University's chief horticulturist, Chuck Leeds. The premise of the plant selection was to create an "inverted sand dune" (Chuck Leeds, personal communication). Therefore plants native to the New Jersey shoreline were selected for their ability to withstand periods of extremely wet soil moisture conditions (and ponding), as well as extremely dry conditions due to the sandy composite soil within the BMP. Consequently the plants selected were also naturally salt tolerant, which is advantageous due to the University's snow removal practices. The original plants have all flourished and there has only been a minimal amount of invasive weeds, which have been periodically hand pulled. The original plant list is provided in Table 1.

Table 1. Planting list for the BTI.

| Common Name | Scientific Name | Type |
|----------------------|--------------------------------|-------------|
| American Beach Grass | <i>Ammophila breviligulata</i> | Grass |
| Coastal Panic Grass | <i>Panicum amarum</i> | Grass |
| Switch Grass | <i>Panicum virgatum</i> | Grass |
| Little Bluestem | <i>Schizachyrium scoparium</i> | Grass |
| Seaside Goldenrod | <i>Solidago sempervirens</i> | Herbaceous |
| Black Chokeberry | <i>Photinia melanocarpa</i> | Woody |
| Groundsel Tree | <i>Baccharis halimifolia</i> | Woody |
| Winterberry | <i>Ilex verticillata</i> | Woody |
| Marsh Elder | <i>Iva frutescens</i> | Woody |
| Beach Plum | <i>Prunus maritima</i> | Woody |

Runoff can enter the BMP through three different locations. Two curb cuts were created along the eastern side of the BMP. The curb cuts are connected to the BMP via riprap lined swales, the longest of which is approximately 30 ft with a slope of 0.02 ft/ft. These swales are shown in grey in Figure 4. The third inlet to, and primary outlet of the BMP is

via a modified existing inlet box. The original 2×4 ft inlet box was connected to upstream inlets and an inlet across the roadway and had a single outlet conduit which ultimately drains to an existing detention basin also located on west campus. The modification entailed the addition of another conduit which slopes down and into the BMP as shown in Figure 5. The modification also included the construction of a weir which serves to divert the two inlet conduits into the BMP. During the course of a storm the BMP fills and will back water up into the pipe which connects the BMP and the inlet box. Ultimately water will begin to flow over the V-notch weir and thus bypass the BTI as illustrated in Figure 5.

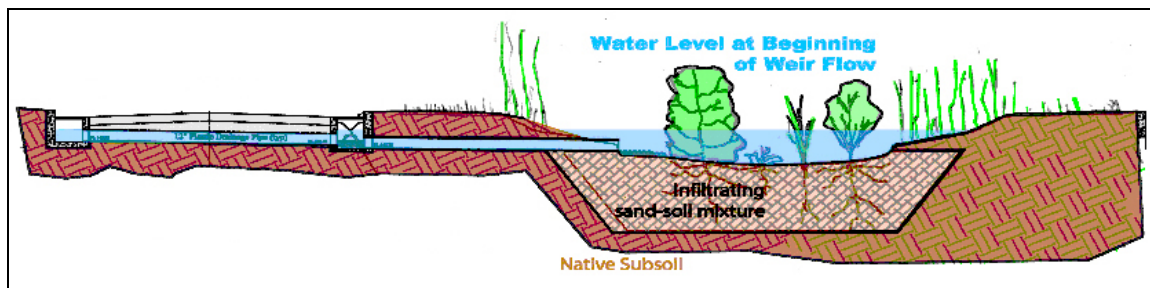


Figure 5. Cross section of outflow conditions via the modified 2×4 ft inlet box (image by William Heason).

The BTI collects runoff from approximately 1.3 acres, approximately 35% of which consists of directly connected impervious area. This results in a DCIA to BMP footprint loading ratio of ~10:1. The watershed consists of pervious turf areas and standard asphalt areas which include both parking and driving lane areas.

The instrumentation at the BMP has changed over its operation. Two specific parameters however, have been consistently monitored, namely rainfall and depth of ponded water in

the BMP. The rainfall is measured by a tipping bucket rain gauge and the depth is measured by an ultrasonic transducer. The ultrasonic transducer is located near the center of the BMP and at an elevation of 0.23 ft above the lowest elevation in the bed. Between August 2002 and August 2003 a pressure transducer was installed in an observation well which is located near the center of the BMP. The well is screened at the bottom and located at the original soil/composite soil interface. During this year of monitoring the pressure transducer never recorded any ponded depth at this layer. This information is crucial to understanding the subsurface flow dynamics of the BMP as is further discussed later. Due to the information provided by the pressure transducers they were removed and three soil moisture meters were installed at 2, 4, and 8 ft depths. The laboratory calibration of these meters was problematic and therefore they did not provide quantitative information on the soil moisture content but rather provided valuable qualitative information on the timing of the moisture front. In November of 2005 a pressure transducer was installed in a new well which was located just outside the storage basin. The transducer is located approximately 20.6 ft below the lowest point in the basin. The since the transducer is located below the water table it provides a time record of the groundwater elevation. More recently a temperature logger (Thermochron iButton DS1921G by Dallas Semiconductor) was installed beginning in March of 2005. The temperature logger was located in a shaded location near the low point of the storage bed. Finally in July of 2007 three more monitoring wells were drilled in the vicinity of the BMP to provide further research opportunities on the groundwater flow near the BMP. Another pressure transducer was installed directly in the modified inlet box to provide better measurement of the head on the outflow weir.



Figure 6. Completed BTI (August 28th 2007).

There has been essentially no maintenance conducted at the site in its six years of operation. Occasionally litter is removed from the BMP. The removal of invasive weeds accounts for less than one hour per year and to date the riprap swales have not been cleaned to remove sediment buildup. In the winter of some years the university has cut down and removed the tall grasses that line the perimeter of the BMP. Otherwise no maintenance has been done to the vegetation. Further information regarding the BTI can be found in Prokop (2003), Ermilio (2005), and Heasom, Traver et al. 2006.

1.3.3 Infiltration Trench (IT)

The IT is the newest of the three infiltration BMPs examined here. This retrofit was constructed in July of 2004. While both of the other two infiltration BMPs were retrofits that were required to be designed into an existing built environment, the IT is unique because it represents a truly urban retrofit. The size and location of the BMP were dictated by the physical constraints of the location. The BMP is located between an academic building and a two level parking garage. There are large electrical conduits which are encased in concrete along with an existing 2×2 ft inlet and a beech tree. The IT is located precisely in the relatively small area encompassed by these physical

constraints. Prior to the retrofit, the runoff from the downspouts from the majority of the adjacent parking garage was routed onto the street and into the existing stormwater conveyance system. The purpose of the retrofit was not only to improve the stormwater management at the site but also to improve the aesthetics of the area. The area was commonly used by students and university employees due partially to its proximity to the academic building and the presence of two picnic tables. However there was a steep slope coming from the second floor entranceway to the academic building. This slope was heavily eroded and there was no vegetation present. Furthermore the turf area where the picnic tables were located was poorly graded. Prior to the construction of the BMP a retaining wall was constructed to prevent further erosion. Following the construction of the retaining wall the BMP was excavated. The courtyard prior to construction and the excavation of the BMP are shown in Figure 7.



Figure 7. Preconstruction view of BMP location (left) and BMP excavation with retaining wall in place.

The site was excavated to a depth of six feet and a hand auger was used inside the excavation which revealed that there was no bed rock within four feet of the bottom of the BMP. Like the other sites the groundwater table is about 15 ft below the bottom of

the BMP. The excavation was lined with a nonwoven geotextile and filled with crushed stone to create a void space of approximately 40%. A smaller crushed aggregate was used at the surface to create a firm base course for the EP Henry Eco-Pavers which top off the BMP. The Eco-Pavers provide approximately 17% pervious area per square foot. This is accomplished by nubs that provide adequate spacing between the pavers.

The downspouts from the parking deck were connected via four inch PVC conduit. Nearly half of the parking deck area is collected by the downspouts which were diverted. This accounts for a total drainage area of approximately 20,400 ft² (0.47 acres). The inflow enters via a single 4 in pipe. The pipe empties into a monitoring bench. The bench was built to conceal various monitoring equipment including a V-notch weir and pressure transducer, while also providing a convenient location for students and employees to congregate. Additional monitoring at the BMP includes a pressure transducer in one of the monitoring wells installed in the BMP to determine the ponded depth of water within the storage bed and various devices to measure temperature including a stand-alone temperature logger (Thermochron iButton DS1921G by Dallas Semiconductor) and a Campbell Scientific thermistor. A tipping bucket rain gauge is also installed on the deck of the garage. Figure 8 shows the IT prior to the installation of the Eco-Pavers and the finished BMP.



Figure 8. IT prior to the installation of the Eco-Pavers (left) and the completed BMP (right).

The BMP has a 6 in overflow pipe which connects the storage bed to the existing 2×2 ft inlet. The storage bed begins to overflow at approximately 5.2 ft of depth. During periods of intense rainfall when the BMP is already full, the water will actually flow up and out of the pervious Eco-Pavers and become evenly distributed sheet flow which flows over approximately two feet of turf and into the same 2×2 inlet. When full the BMP stores only approximately 200 ft³ which represents 0.12 in over the drainage area. Since the drainage area for the IT is entirely impervious surfaces the BMP has a DCIA to BMP footprint ratio of ~130:1. The Pennsylvania Stormwater Best Management Practices Manual recommends a 5:1 ratio for this type of application (PADEP 2006). The BMP was intentionally designed with an exceedingly high loading ratio. This was an attempt to accelerate the aging process of the BMP. This concept is further detailed in Section 2.2.4.2.

1.3.4 Summary of Infiltration BMPs

The BMPs central to this study cover a wide range of the various applications of infiltration to manage stormwater runoff. While the individual BMPs have been

described in the previous sections, the purpose of this section is to highlight some of the main design differences among the BMPs.

The three BMPs are each unique in terms of their geometry and configuration. Most notably the PCIB and the IT use a crushed stone storage bed lined with a nonwoven geotextile while the BTI uses an open, heavily vegetated storage bed. Both of these design techniques offer their own advantages and disadvantages in relation to the actual infiltration process; this topic is later discussed in Chapter 2. However it is important to note that the choice of an open or underground storage/infiltration surface is often dictated by other factors including location and cost. For example for more urban applications like the IT where space is limited and the footprint of the BMP is required for other uses, a subsurface design is mandatory. Another major difference is the geometry of the IT compared to that of the other two BMPs. Figure 9 shows a typical cross section of the BMPs.

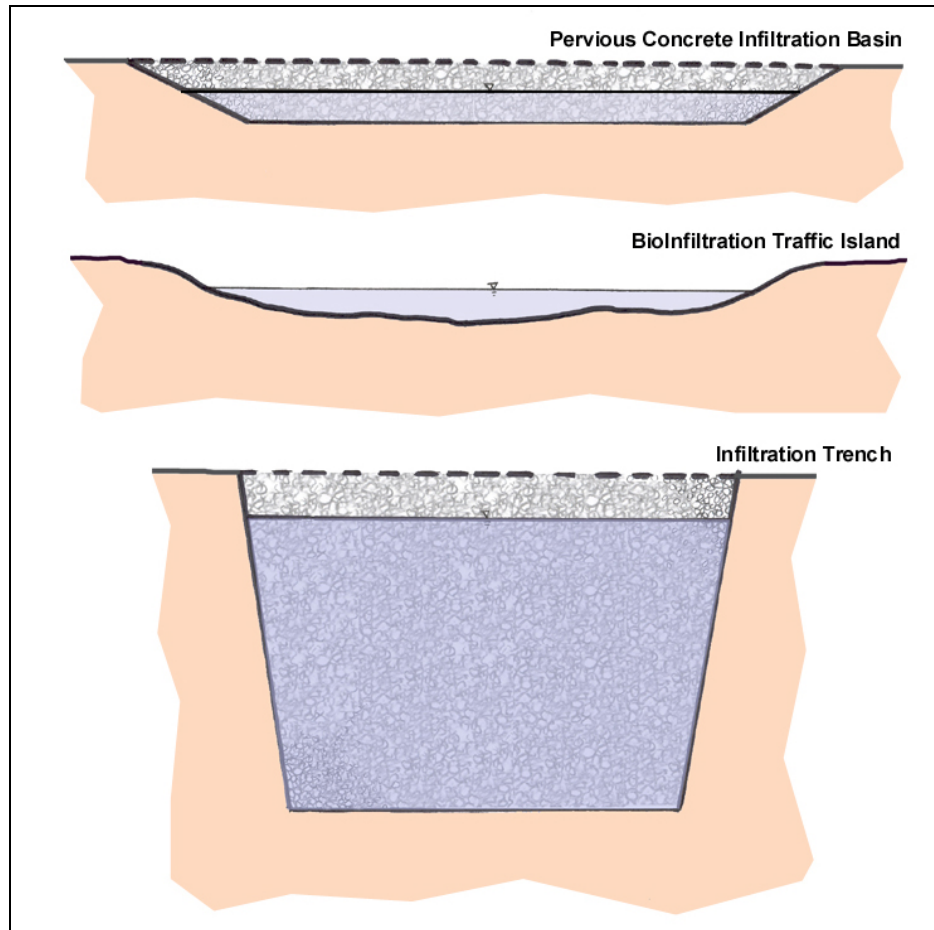


Figure 9. Representative cross sections of all three infiltration BMPs with crushed stone and overflow depth shown.

Figure 9 illustrates the differences between the geometry of the BMPs. This is important in understanding the details of the subsurface flow processes at each BMP. The importance of the storage bed geometry is further discussed in Chapter 2.

Another significant difference among the infiltration BMPs is the relative size and other characteristics of the BMPs' contributing areas. One commonly referenced metric of the contributing area to an infiltration BMP is the ratio of the Directly Connected Impervious Area (DCIA) to BMP footprint. DCIA, or sometimes total impervious area, is often used

in place of total area due to the high runoff potential of impervious surfaces. This is not meant to underestimate the runoff potential of the often highly disturbed “pervious” areas. Another commonly used measure of the loading of an infiltration feature is the annual loading rate. This metric is more commonly used in the effluent recharge field. For application to stormwater this loading rate can simply be estimated by multiplying the average annual rainfall by the DCIA and then dividing that by the footprint area of the infiltration BMP. In theory, this represents the equivalent depth of a column of water which represents the annual loading of the BMP. Clearly, this measure does not represent the actual annual infiltration volume as it does not consider the portion of the inflow that may become overflow. Another commonly used design metric is the total storage volume of the BMP at the onset of overflow. This storage is often expressed as inches of water over the contributing impervious surface area. Figure 10 shows an aerial view of the BMPs and their contributing areas, the images are all at the same scale. Table 2 summarizes the characteristics of the contributing areas for the three infiltration BMPs.

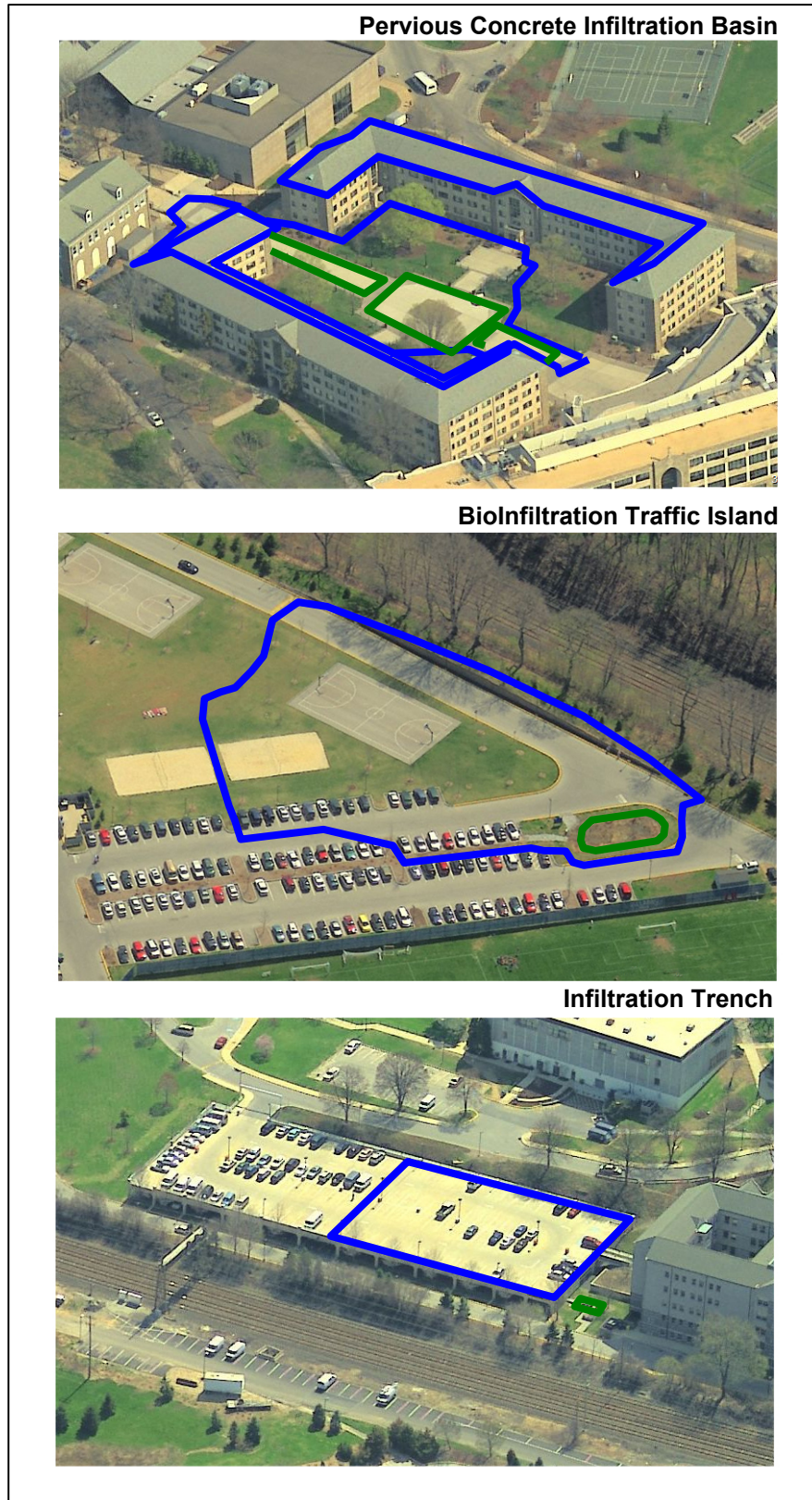


Figure 10. Aerial view of contributing areas (outlined in blue) to three infiltration BMPs (outlined in green).

Table 2. Summary of the contributing areas to the three infiltration BMPs.

| | Footprint [ft ²] | Drainage Area [ac.] | DCIA [ft ²] | DCIA:BMP ratio | Loading Rate [in/yr] | Storage [in] | Description |
|---------------------------------|---------------------------------|---------------------------|----------------------------|-------------------|----------------------------|-----------------|--|
| PCIB [lower bed] | 5,600 [1,800] | 1.3 [8,000] | 36,000 [6,000] | 6:1 [3:1] | 270 [140] | 2.2 [2.1] | Four-story rooftops, and walkway/courtyard |
| BTI | 1,600 | 1.3 | 20,000 | 10:1 | 410 | 0.59 | Parking and driving areas, and turf areas |
| IT | 130 | 0.47 | 20,000 | 130:1 | 5,700 | 0.12 | Heavily used parking deck |

Figure 10 and Table 2 illustrate the differences in the contributing areas of the BMPs. As a point of comparison the Pennsylvania Stormwater Best Management Practices Manual recommends a DCIA:BMP ratio of approximately 5:1 for most infiltration BMPs (PADEP 2006). In general from a loading perspective, the PCIB appears be well designed with a reasonable loading rate. The BTI has a moderate loading ratio although somewhat higher than is typically recommended. Finally, the IT has obviously been intentionally undersized for the large contributing area. This is compounded by the fact that the drainage area consists of a heavily trafficked parking deck and therefore produces runoff that has characteristically high solids concentrations. The solids loading at this site was further examined by Batrone (2008). The soil type at the three BMPs will be discussed in Chapter 3.

Chapter 2. Long-term and Seasonal Performance of the Infiltration Process in Stormwater Management BMPs

2.1 Introduction and Background

Infiltration BMPs has become a widely used tool in an effort to better manage stormwater runoff. Many new stormwater regulations require the implementation of stormwater BMPs to reduce the volume of stormwater runoff. Capture and reuse and evapotranspiration methods are sometimes used. However, the most widely implemented volume reduction BMPs are engineered infiltration practices such as infiltration basins, infiltration trenches among others. Some regulations specifically require the use of infiltration with an effort both to limit site runoff volume and to provide groundwater recharge (NJDEP 2004). However, questions remain about how infiltration BMPs will function over the course of a year and, more importantly, how long they can be expected to continue to meet their original design criteria.

One of the main lingering questions about infiltration BMPs is their longevity and potential lifespan (Lindsey, Roberts et al. 1992; Hilding 1996). This has been a major factor that has often explained engineers' and regulators' reluctance to implement infiltration BMPs (Schueler 1994; Livingston 2000).

In contrast, there has been little question or concern for lifespan and longevity of a detention basin designed for peak flow attenuation. Assuming that inlets, outlets, and embankments are designed and built to prevent excessive erosion, there is little that can occur to affect the lifespan or decrease the performance of a detention basin over time.

The design and process of locating a potential detention basin is not particularly sensitive to the underlying soil type and site geology. Generally speaking, any soil type, granular or fine textured, can be used to construct a basin that will retain water and release it at predetermined rates with the installation of concrete pipes and outlet structures. The lifespan and functionality of a detention basin does not rely heavily on the construction techniques, construction staging, grading, compaction, or the specific machinery used. Additionally, the function of a detention basin is not impacted by the land use and consequent water quality of incoming stormwater runoff. Typical sedimentation that can be observed in detention basins (see Figure 11) is not severe enough to decrease the surface storage by a significant amount.



Figure 11. Sedimentation occurring in two detention basins in Chester County, PA.

Unlike detention basins, there can be due cause for lifespan and longevity concerns for stormwater infiltration practices. Proper design, site investigation, construction, implementation, and potentially maintenance, are crucial factors to ensure that an

infiltration practice will continue to meet its design objectives over the long-term. Infiltration practices have specific, although as-yet poorly described, requirements for each of these crucial factors. For example, the infiltration capacity of soil can be severely compromised by the influx of suspended sediments or even simply the redistribution of existing soil particles caused by wetting and drying cycles (Hillel 1998). Therefore, the longevity of such an infiltration BMP can clearly be impacted by the solids content of incoming runoff. The clogging potential of solids-laden inflow has long been observed at the field-scale (Berend 1967; Behnke 1969; Schueler 1994; Assouline 2004). However it has only been experimentally explored at the laboratory scale using soil columns (Siriwardene, Deletic et al. 2007). The clogging process is dictated by many factors including inflow solids concentration, particle-size distribution, pore size distribution and other characteristics of the existing soil. The infiltration process will also be compromised by an increase in soil bulk density resulting from physical compaction. These are perceived to be two of the most significant causes of infiltration BMP failures.

In addition to the issue of lifespan, there remain other questions about the seasonal variation in the performance of infiltration BMPs. Generally, this topic is limited to speculation about the potential for frozen ground to impede infiltration and the seasonal contribution of vegetation due to evapotranspiration. While in some situations these may be relevant issues, it is proposed here that the seasonal variation of infiltration BMPs is primarily due to temperature-induced viscosity effects. The magnitude of the variation is often surprising to stormwater professionals, and it should be taken into account when designing, predicting, or assessing the performance of infiltration BMPs.

Continuous monitoring has been performed on three infiltration BMPs located on the campus of Villanova University. One of the major goals of this monitoring effort is to address the question of long-term performance of stormwater infiltration BMPs. The span of the continuous data record used in this analysis varies among sites and is a maximum of four years for the BTI. The following sections summarize these data records for each of the three infiltration BMPs. The data sets have been examined in an effort to answer the following two questions:

- 1) Are the BMPs showing signs of an overall decrease in performance?
- 2) Are the BMPs demonstrating a seasonal variation in performance? If so, what is the magnitude and origin of the variation?

2.2 Characterization of the Long-Term and Seasonal Performance of Infiltration BMPs

Before the performance of any system can be assessed it is necessary to define the criteria on which a measure of “performance” is based. An analysis of the “performance” of an infiltration BMP might often be focused on a hydrologic balance of the BMP. This could be represented in such quantities as annual runoff reduction or peak flow rate reduction, among many others. These types of typical performance indicators have been, and are currently being, examined for the BMPs studied here. All of these parameters are dependent on the characteristics of the specific BMP’s contributing area, including total drainage area, percent impervious, land use, and many others factors. These are

important factors to consider in the design process of any stormwater BMP. Therefore, the purpose of this examination is to focus on the infiltration process occurring at each BMP, not the hydrologic/hydraulic effectiveness of the BMP.

Infiltration is defined as “the movement of rain or melting snow into the soil at the Earth’s surface” (Hornberger, Raffensperger et al. 1998). More generally the term “infiltrate” is defined by the American Heritage Dictionary as “To permeate a porous substance with a liquid or gas”. This process is best characterized and quantified as a flux $[L/T]$ through a unit area or, more generally, a flow rate over a known area of soil.

At each infiltration BMP, the depth of ponded water above the soil surface is monitored. Unlike the case of a ring infiltrometer, a decrease in the measured depth over time does not represent a direct measurement of the infiltration or flux of water into a known soil area. To translate the time-series record of ponded depth following a storm event into a measurement of the rate of infiltration, many factors need to be known and taken into account. These factors include an accurate knowledge of the depth or stage vs. storage relationship for the storage basin, which may include the porosity of the storage bed itself. Also, the wetted or infiltrating area of the storage basin changes with depth and this relationship may also need to be established. Translating the observed depth record, even where the depth vs. storage and wetted area relationships are known, would only yield a time-series of the averaged infiltration per unit area of soil. While there is some merit to this approach, for the purpose of monitoring the long-term performance a more

straightforward approach is justified which does not incorporate any potential errors in the geometric relationships of the storage basin.

The observed recession rate of the ponded water surface, while not a direct measurement of infiltration, can be used as a performance indicator of the infiltration process. Clearly, the recession rate of ponded water has many design implications. Often infiltration BMPs are required to empty within a predetermined time span to prevent nuisance ponding and mosquito breeding habitat (MDE 2000; NJDEP 2004; PADEP 2006). Additionally, the recession rate is an easily measured parameter that can be observed at any infiltration BMP with relatively simple means.

This method assumes that the previously mentioned geometric characteristics of the storage basin remain reasonably constant over time. It also assumes that the storage volume occupied by vegetation is not significant enough to change the depth vs. storage relationship by a measurable amount over both the lifespan of the BMP and over the annual growing seasons. These assumptions are well justified for the three infiltration BMPs at the focus of this study. This approach cannot be used to compare the infiltration performance of one BMP to another unless the geometric relationships of depth, storage, and wetted area are identical.

Consider a simplified hypothetical case of two identical storage basins with perfectly flat bottoms and vertical side walls which prevent lateral infiltration. The only difference between them is that one uses an underground crushed stone bed and the other an open

surface storage basin. All other things being equal, including the rate of infiltration into the soil, the observed recession rate of the open storage bed basin would be expected to be slower than the observed recession rate of the stone bed by a factor of the stone storage basin porosity. This is explained by the conservation of mass principle, as follows.

First, if the rate of infiltration (mass flux) of both storage beds are the same:

$$Q_{open} = Q_{stone} \quad (2.1)$$

$$V_{open} \times A_{open} = V_{stone} \times A_{stone} \quad (2.2)$$

Where: Q = infiltration rate [L^3T^{-1}]
 V = observed recession rate [LT^{-1}]
 A_{open} = open portion of the storage basin cross sectional area [L^2]
 A_{stone} = effective cross sectional area of stone [L^2]

The cross sectional area within the crushed stone storage basin is:

$$A_{stone} = n_{stone} \times A_{open} \quad (2.3)$$

$$V_{open} = V_{stone} \times n_{stone} \quad (2.4)$$

Where: n_{stone} = porosity of the stone storage bed [-]

The three infiltration BMPs studied here are each unique in their design, storage bed geometries, overflow depths, and underlying soil properties. Therefore, each will exhibit very different characteristic recession limbs. This is shown in the following figure which compares the depth record for the same storm event for all three infiltration BMPs.

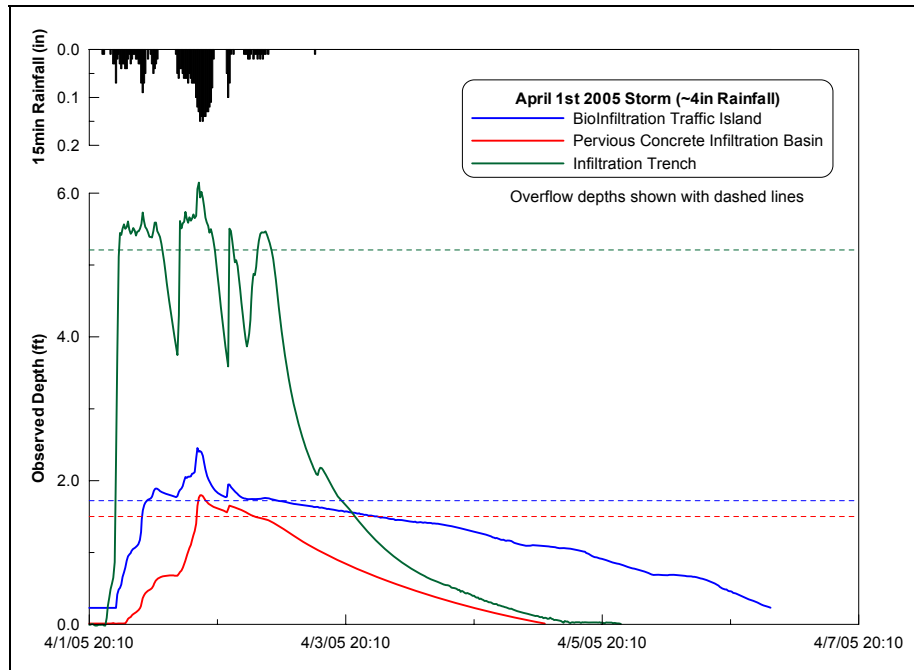


Figure 12. Depth records from all three infiltration BMPs for the April 1st 2005 storm event.

The April 1st 2005 storm was a large and intense storm with approximately four inches of rainfall measured over 36 hours, and a maximum one-hour intensity of 1.16 in/hr measured at the IT rain gauge. Figure 12 displays the depth record for each BMP along with the overflow depths marked with dashed lines. For this event, the storage capacity was exceeded and all three BMPs produced overflow. After the rainfall and consequent inflow ceased, each BMP emptied in a unique fashion. Most notably, the IT fills to a much higher depth than the other two BMPs and its recession limb was much more curvilinear. The BTI and the PCIB have similar overflow depths but exhibit different recession limbs, with the BTI showing a more linear slope. These differences are due to basic differences in storage bed geometry and porosity, and the underlying soil properties.

As different as the recession limbs are from one site to another, they exhibit the same general characteristic shape for different storms for each individual BMP. For example, recession limbs measured at the BTI are typically linear and those measured at the IT are typically nonlinear. Therefore it is possible to use quantifiable properties of the recession limbs, such as slope, to compare one recession limb to another over time for each BMP. A general decrease in the slope over time (years) would indicate a decrease in the infiltration performance of the BMP. Due to the aforementioned differences in the characteristic recession limbs among the BMPs, a slightly different method of comparing consequent recession limbs is needed for each BMP.

Figure 12 illustrates, the recession limbs cannot always be accurately described by a constant slope; this is especially true with the IT. It is necessary to consider the use of a piecewise approximation of the recession limb. This approximation is accomplished by subdividing the depth into incremental subsections. A linear approximation of the recession limb is then measured in each subsection. As the number of subsections increases and the incremental depth range approaches a single value, the slope measurement will approach the derivative, or true slope, of the recession limb at that depth. The number of subsections required for an accurate estimation of the incremental slope depends on the degree of curvature of the recession limb. It should be observed that this method of incremental slope measurement is sensitive to potential baseline shifts in the data. This is especially true with increasing curvature of the recession limb.

The use of an incremental slope method also enables the user to determine if the general shape of the recession limb is changing over time. For example, if it is determined that the incremental slopes towards the bottom of the recession limb, near empty, are decreasing over time, this may indicate that the infiltration through the wetted area at that depth, primarily the bottom, is also decreasing over time. This can be used to gain an understanding of potential changes in the infiltration over the depth of the basin. More precise descriptions of these changes over depth are only possible when the geometric relationships of the basin are known and assumptions are made to quantify the actual infiltration as a function of depth over the complete surface area of the basin.

In the case of the PCIB, the method can be graphically illustrated for a single storm by the following figure.

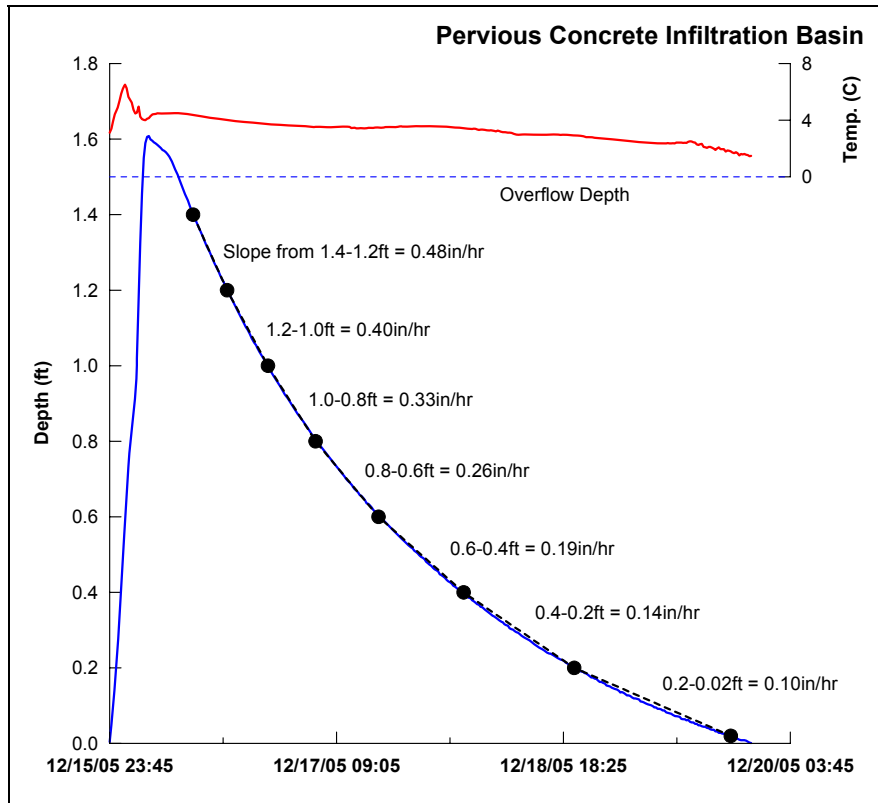


Figure 13. Incremental slope approximations for December 15th 2005 storm event at the PCIB.

Figure 13 shows the observed depth record for the December 15th 2005 storm event. This storm provided a total of 1.99 in of rainfall as measured by the site's rain gauge. For this storm event, the storage capacity of the lower storage bed was exceeded and the site produced some overflow over a period of approximately five hours. Once the overflow stopped, the depth continued to recede. This recession is solely due to infiltration. For the case of the PCIB, the depth has been broken into 0.2 ft incremental steps starting with an upper limit of 1.4 ft. This upper limit was chosen because it is a sufficient depth below the estimate of the overflow depth for the lower storage bed. The shallowest incremental slope is measured from 0.2 ft to 0.02 ft for the PCIB; this was chosen to prevent near-zero noise from interfering with the slope calculations. The specific depth

benchmarks and ranges vary for each site and will be summarized in the following sections.

Each incremental slope can be calculated graphically as shown in Figure 13 by dividing the change in depth of each incremental step by the time required for the water surface to pass from the upper limit of the step to the lower limit. This is further explained as follows:

$$\text{Slope} \frac{\text{in}}{\text{hr}} = \frac{(D_{\text{upper}} - D_{\text{lower}}) \text{ft} \times 12 \frac{\text{in}}{\text{ft}}}{(T_{\text{upper}} - T_{\text{lower}}) \text{hr}} \quad (2.5)$$

Where:

- D_{upper} = depth of the upper incremental step limit [ft]
- D_{lower} = depth of the lower incremental step limit [ft]
- T_{upper} = time that water surface passes upper depth limit
- T_{lower} = time that water surface passes lower depth limit

Continuous depth data has been collected at all three infiltration BMPs. This record spans from approximately two years for the PCIB to four years at the BTI. In total there is over nine years of data with hundreds of storm events and potentially thousands of individual incremental slopes that need to be calculated for this analysis. The large amount of data makes a graphical approach impractical. Further, it introduces additional opportunities for potential user error. This requires the development of a more robust, flexible, practical, and easily quantifiable method. A program was created using the visual basic programming capabilities within Microsoft Excel to find and calculate the slopes in an automated fashion. The program, named SlopeFinder, is summarized in Appendix A.

The SlopeFinder program, and its analysis of the recession limb, is the basis of the method used to observe changes in the long-term infiltration performance of the BMPs. Site-specific modifications are required for the analysis of each BMP. Additional methods have also been used on a site-specific basis to determine hydraulic conductivity estimates from the monitoring data record as are detailed in the following site-specific sections.

2.2.1 Long-Term and Seasonal Performance of the PCIB

Storage bed depth data from calendar years 2004 and 2005 are used to determine the long-term variability of the infiltration process within the BMP. The majority of the data, including the depth data, at the PCIB are recorded at five-minute intervals. It can be shown that for the purpose of this analysis, a five-minute time interval is unnecessarily short. Artificially lengthening the data interval by averaging the depths and temperatures and incrementally summing the rainfall data has two advantages. First, it effectively smoothes the depth data, and along with the minimum recession time, avoids the calculation of many small inconsequential slopes caused by noise in the depth data. It also makes the analysis less cumbersome by essentially cutting the amount of data to be processed by two thirds.

The time interval conversion is also accomplished through the use of Visual Basic Code in the form of a Microsoft Excel Macro. The code simply calls the Excel AVERAGE function for both the depth and temperature and it calls the SUM function for the

incremental rainfall data. The Visual Basic code for the time interval conversion macro is supplied in Appendix B. The following figure compares the depth record for a storm in both the original five-minute format and the derived 15-minute data. Figure 14 shows that the data conversion process does not have a significant impact on the slope, temperature and rainfall calculations performed by SlopeFinder.

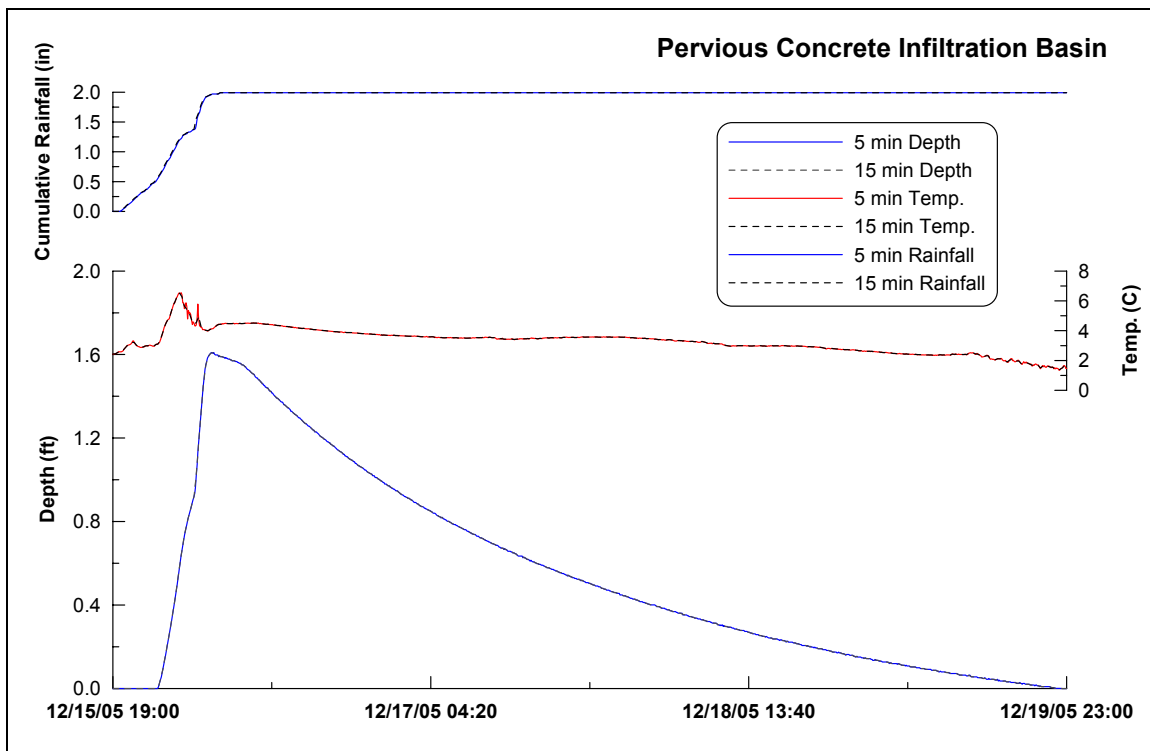


Figure 14. Comparison of recorded five-minute data to derived 15-minute data.

As previously mentioned, the incremental slope method is sensitive to baseline changes in the depth data. For this reason, the data had to be manually corrected for minor fluctuations in the baseline, or zero depth, for the depth record. The largest correction applied (< 2 in) was for a small period in the summer of 2005. Generally, the corrections

were less than a tenth of an inch. This correction ensured that the measured depths and consequent depth ranges for slope calculation from one year were directly comparable.

The PCIB has an overflow depth that is approximately 1.5 ft above the location of the pressure transducer that is used to measure depth in the lower storage bed. This depth was only exceeded eight times in two years (2004-2006). Generally speaking, a change in bed depth is only measured when there has been more than 0.1 in of rainfall. This may be due to the relatively small contributing area to the lower bed. Additionally, there is no positive evidence that the pressure transducer is located at the absolute lowest point in the storage bed. The result is that there are generally fewer recession limbs per year at the PCIB than either of the other two infiltration sites.

The data set used to examine the long-term infiltration performance of the PCIB spans from 1/1/2004 to 12/31/2005. Figure 15 shows the depth record for calendar years 2004 and 2005 along with the measured temperature recorded by the pressure transducer and the precipitation as measured by the rain gauge at the site.

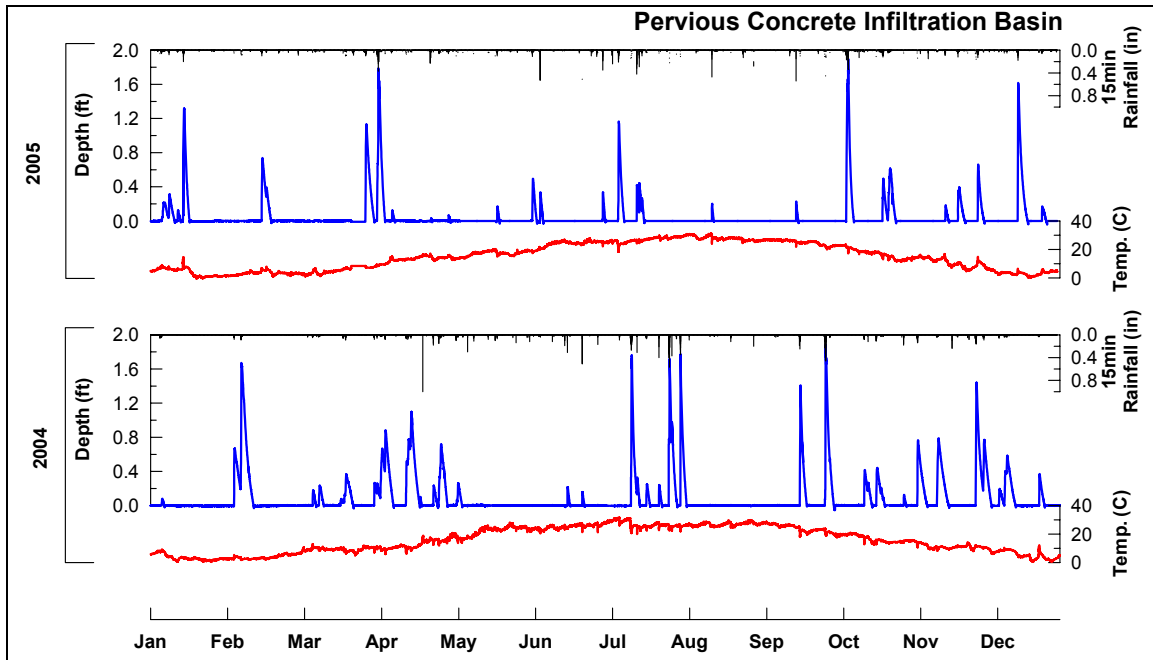


Figure 15. Calendar years 2004 and 2005 data for the PCIB.

The PCIB recession limbs were divided into seven incremental depth ranges for the purpose of this analysis. The overflow depth is estimated to be 1.5 ft above the pressure transducer. Therefore the first slope calculation was chosen to start at 1.4 ft and continue to 1.2 ft. The increment was kept constant at 0.2 ft all the way to empty with the exception of the last of 0.2 to 0.02 ft. This last increment was shortened to avoid the potential interference of near-zero noise in the data. The recession limb subdivision was shown graphically for the 12/15/2005 storm in Figure 13.

Examining the results for all the incremental slopes together illustrates the characteristic recession limb shape for the BMP. The slope is steeper at higher depths and decreases towards the empty condition. The measured slopes for the data record used here range from 0.83 in/hr for the 1.4 to 1.2 ft range to 0.12 in/hr for the 0.2 to 0.02 ft range. The

following figure summarizes the average slope found for each of the incremental depth ranges as well as the average temperature during each calculated slope.

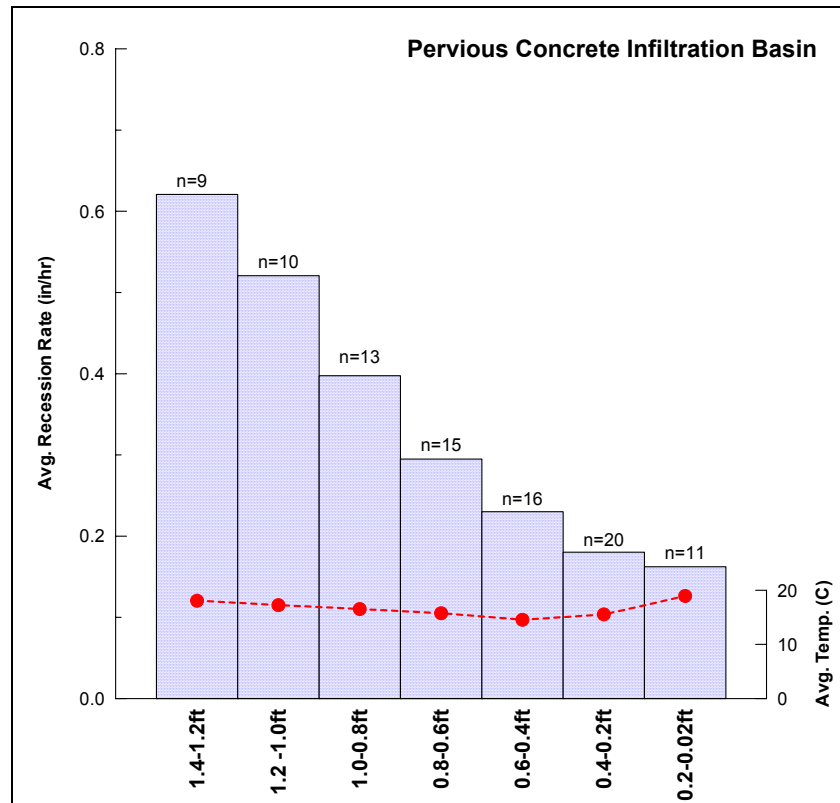


Figure 16. Average recession rates and temperature for each of the seven incremental depth ranges for the PCIB data record (2004-2005).

A first step in an effort to determine if the BMP is experiencing an overall decrease in infiltration performance is to compare the average incremental recession rates from 2004 to those found from the 2005 data. This is shown in Figure 17.

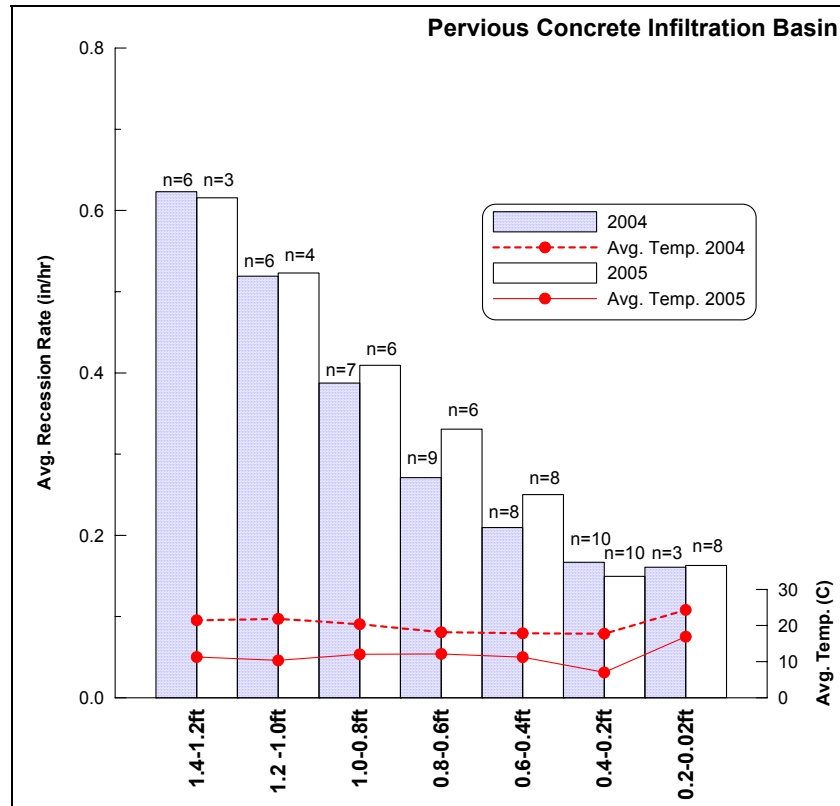


Figure 17. Comparison for averaged incremental slopes for data from calendar years 2004 and 2005.

Figure 17 shows that in general the incremental slopes were slightly steeper in 2005 than they were in 2004. However applying a Student's T-test (with unequal observations) to compare the means from 2004 and 2005 for each of the incremental slopes shows that none of the differences between the two years approach statistical significance at the 95% level ($\alpha = 0.05$). This is shown in the following table with the P value never approaching the 0.05 level. These results are summarized in Table 3.

Table 3. Student's T-test for incremental slopes from 2004 and 2005.

| Depth Range [ft] | 2004 | | | 2005 | | | P |
|---------------------|------|-----------------|---------------------|------|-----------------|---------------------|-------|
| | n | Avg. [in/hr] | σ [in/hr] | n | Avg. [in/hr] | σ [in/hr] | |
| 1.4 to 1.2 | 6 | 0.623 | 0.126 | 3 | 0.616 | 0.161 | 0.939 |
| 1.2 to 1.0 | 6 | 0.519 | 0.0882 | 4 | 0.523 | 0.128 | 0.954 |
| 1.0 to 0.8 | 7 | 0.387 | 0.0849 | 6 | 0.409 | 0.101 | 0.678 |
| 0.8 to 0.6 | 9 | 0.271 | 0.0835 | 6 | 0.331 | 0.0773 | 0.187 |
| 0.6 to 0.4 | 8 | 0.210 | 0.0643 | 8 | 0.250 | 0.0686 | 0.242 |
| 0.4 to 0.2 | 10 | 0.167 | 0.0417 | 10 | 0.194 | 0.0499 | 0.210 |
| 0.2 to 0.02 | 3 | 0.161 | 0.0398 | 8 | 0.163 | 0.0243 | 0.910 |

Analysis of the two years of data from the PCIB with the SlopeFinder program does not provide any clear indication that the infiltration performance is showing signs of a systematic decrease over time. It does, however, suggest that the infiltration process at the PCIB follows a seasonal trend with its highest rates in the late summer to early fall and lowest in winter.

Figure 18 shows the results for each of the seven incremental slopes examined for this BMP over time. In general, it can be seen that the higher rates correspond to higher temperatures measured on the bottom of the storage basin. It appears that the seasonal variation far outweighs any potential long-term decrease in performance (over the two-year window examined here). For simplification, the temperature represented on the plot is the average temperature calculated for the 0.4 to 0.2 ft increment. Generally the temperature is fairly constant during the entire recession limb (through all incremental slopes).

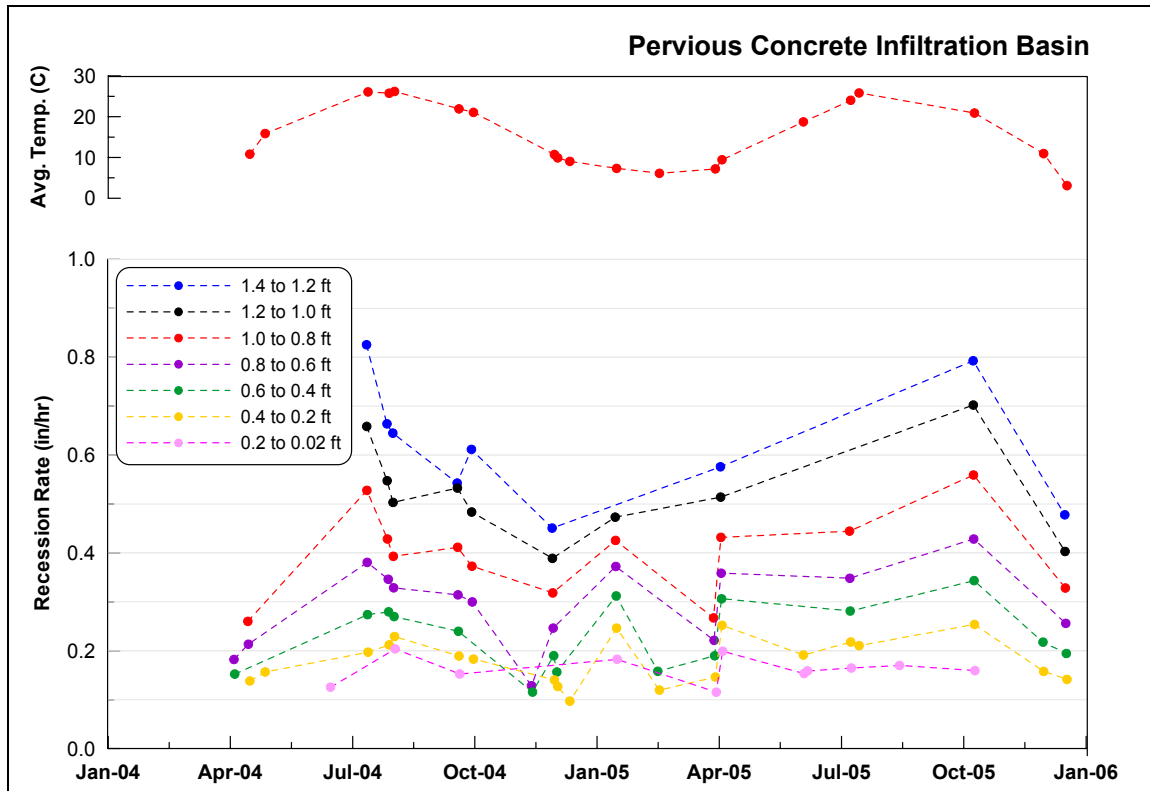


Figure 18. Incremental slopes found for the PCIB.

Figure 18 also illustrates the importance of continuous long-term monitoring. The incremental recession rates vary by a factor of two over the course of a year. Therefore, monitoring a single or only a few storms could give a misleading impression of how the BMP is performing.

Figure 18 indicates that a temperature dependency may have a greater effect on the recession rate than would any potential lifespan related decrease performance. A simple, less quantitative, but valuable method of illustrating this is to compare two different recession limbs from two different storms graphically. One event from October 2003 was chosen here to give the longest possible time span between events, almost two years.

Figure 19 compares the recession limbs of the October 29th 2003 and October 9th 2005 storm events.

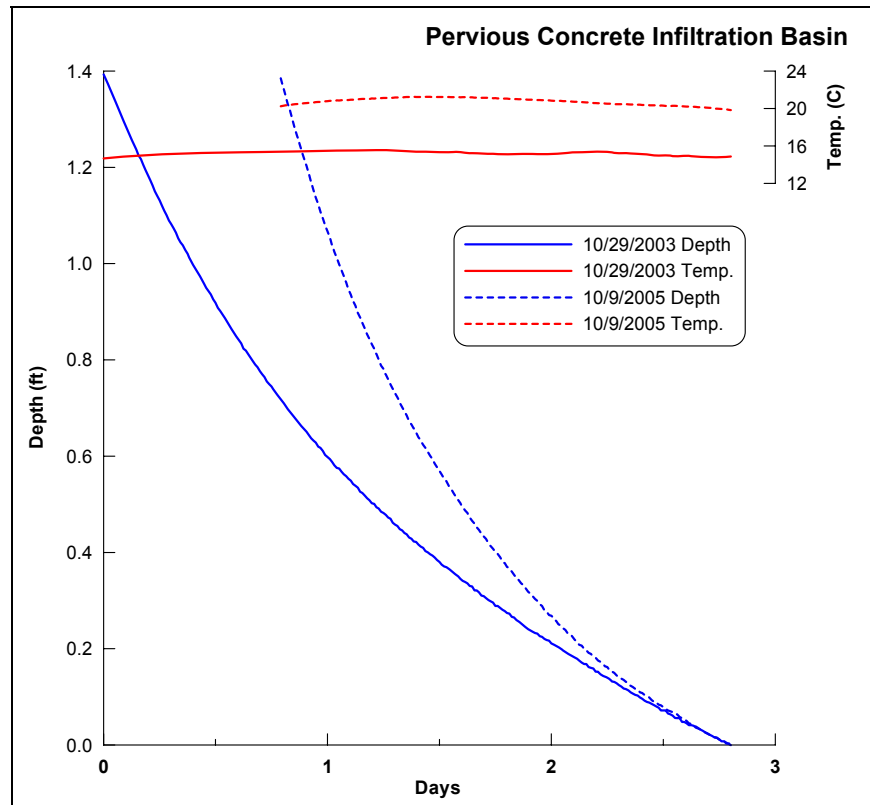


Figure 19. Recession limb comparison for October 29th 2003 and October 9th 2005.

The comparison clearly shows that the recession limb of the 2005 storm is markedly steeper than the storm nearly two years prior. Unfortunately two similar storms with similar temperatures could not be found for comparison. The temperature during the 2005 event was approximately 5.5°C warmer than the 2003 event. This illustrates how dominant the seasonal/temperature dependency of infiltration is compared with any potential lifespan related decreases in performance. If all other factors were equal, including temperature, and there was no degradation of the infiltration performance of the BMP, one would expect both recession limbs to be identical. Because the recession limb

of the 2005 storm is steeper than the 2003 storm, Figure 19 shows that the effect of a 5.5°C increase in temperature greatly exceeds a potential decrease in performance over a two-year period. The 2005 storm infiltrates so much faster than the 2003 storm that the total ponded time from 1.4 ft of depth to empty is decreased by 19 hours.

To define and quantify the observed seasonal variation further, a linear regression method is proposed. The purpose of the linear regression is to determine the magnitude and origin of the temperature dependency of the infiltration process occurring in the BMP. For the PCIB, the recession limb was broken into seven incremental slopes. For the purpose of the linear regression, only one depth range was chosen for analysis. The measured recession rates between 0.8 and 0.6 ft were used in this regression because they are in the middle of the depth range of the BMP and they most closely represent the average recession rate of the recession limbs. For this depth range there are a total of 15 data points during the 2004-2005 data record. Each of these slope measurements has a corresponding average temperature, as measured by the same pressure transducer that is used to measure depth. The temperature during the ponding event is typically stable as can be seen in Figure 19. The incremental slope measurements range from 0.13 to 0.43 in/hr. Because the objective is to relate the seasonal variation to the known phenomenon of the infiltration process, it is first necessary to attempt to relate the incremental slopes to an actual mass flux per unit area of infiltrating surface. This is accomplished for the PCIB by multiplying the slopes by an estimate of the storage bed void space (0.40). Therefore, the actual data used in the regression only ranges from 0.05 to 0.17 in/hr. The average temperature measurements during these slopes range from 3.5 to 26 C.

The linear regression is created by regressing the mass flux (in/hr) (dependent variable) with the measured temperature (°C) (independent variable). Figure 20 shows the results of the linear regression with $n = 15$.

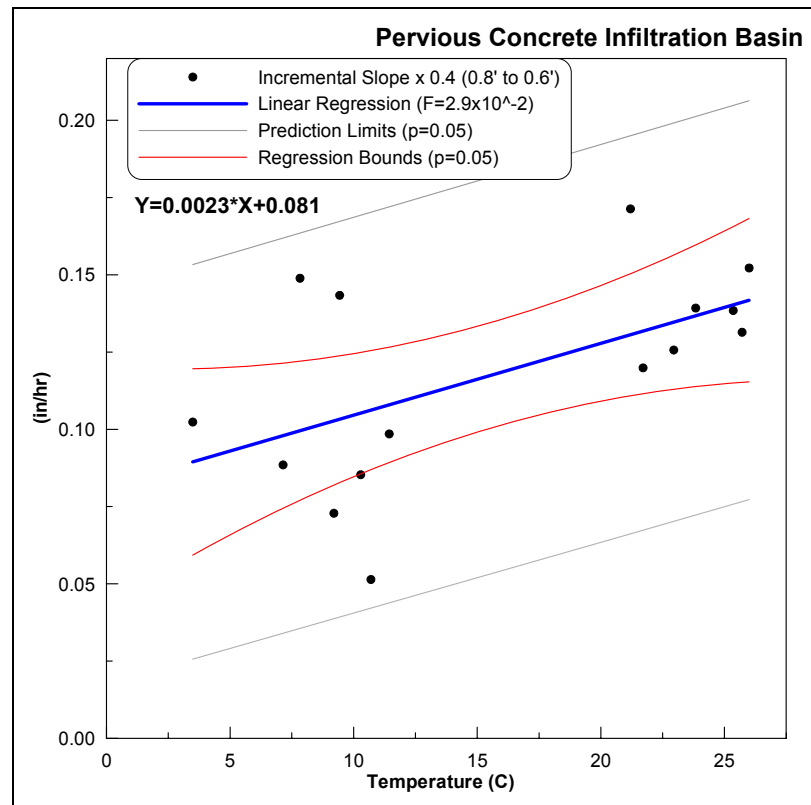


Figure 20. Temperature dependency linear regression for the PCIB.

Figure 20 shows the raw data for the 15 data points along with the linear regression (blue), the confidence interval for the regression ($\alpha = 0.05$, red), and the prediction interval (grey). The regression is significant at the $\alpha = 0.05$ level with a P value of 0.029. The necessary assumptions of the linear regression are met as follows. First the relationship between the two variables is expected to be somewhat linear, this is further discussed later in this section. Secondly the residuals appear to follow a fairly normal

distribution around the regression. This is illustrated by plotting a histogram of the residuals in Figure 21.

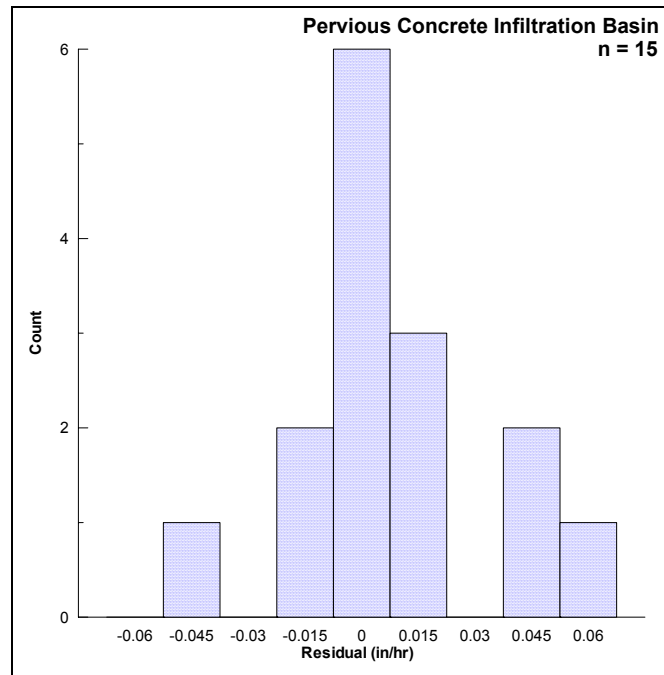


Figure 21. Histogram of regression residuals for PCIB.

The assumptions of the linear regression also include that the residuals must have a constant standard deviation, or that the data exhibit homoscedasticity. This assumption is checked by plotting the regression residuals versus the independent variable, temperature as shown in Figure 22.

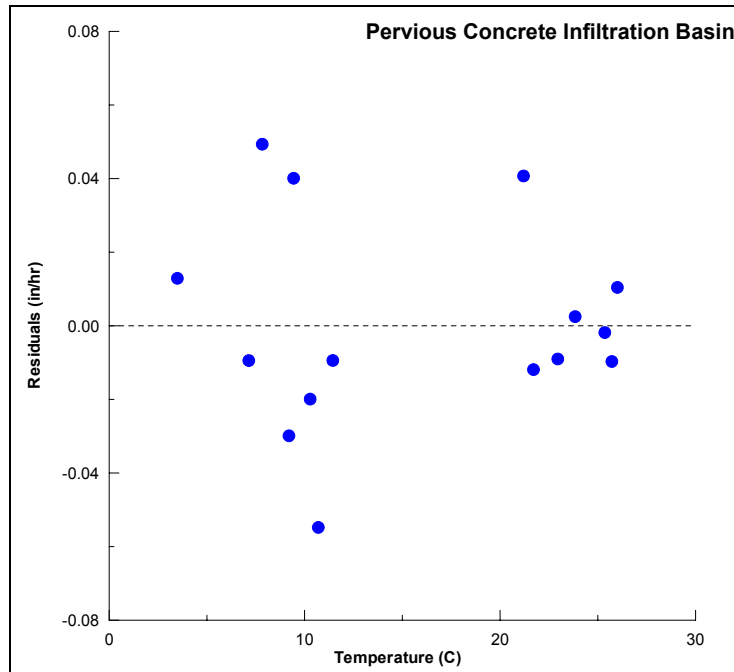


Figure 22. Check for homoscedasticity for PCIB regression.

Figure 22 indicates that there may be some slight indication of heteroscedasticity in the data. While it is difficult to determine with such a small sample size, there appears to be more variation in the recession rate at lower temperatures and slightly less at higher temperatures. Also the apparent lack of recession rates in the middle of the temperature range that can be seen in Figure 22 and the original regression adds to the uncertainty. Finally, the data must be checked for autocorrelation, this is accomplished by plotting the residuals versus time as shown in Figure 23.

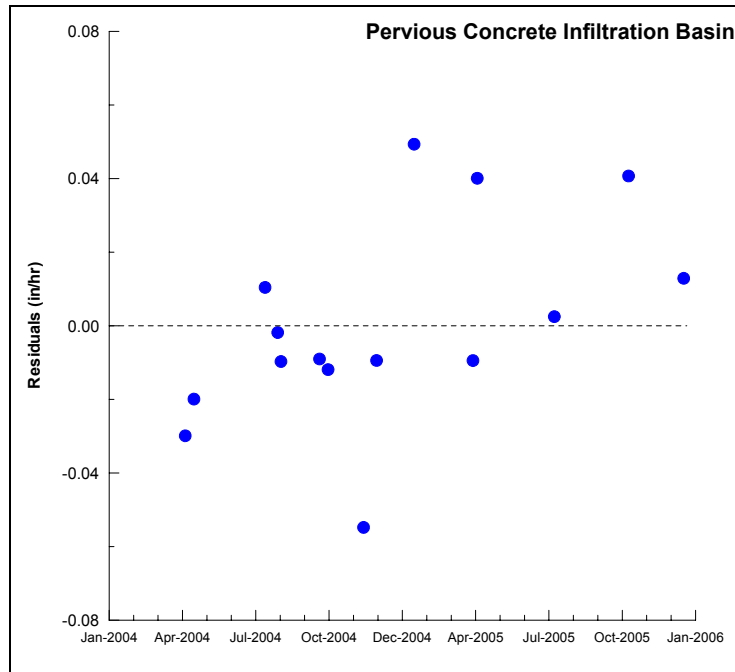


Figure 23. Check for autocorrelation of residuals for PCIB.

One potential cause for autocorrelation in this situation is if the infiltration BMP was forming a clogging layer that increased resistance to infiltration over time. This would result in autocorrelation with the residuals typically showing a general decrease over time. However, Figure 23 does not indicate that this is occurring at the PCIB. It may even suggest to some extent that the opposite is occurring, as there is some indication that the later data points tend to have incremental slopes higher than that predicted by the linear regression. This subject is revisited later in this section.

With the regression reasonably validated, it can be further examined for its potential implications. The regression is not particularly strong with a fair amount of scatter resulting in a coefficient of determination (r^2) of 0.32. The slope of the regression is 2.3×10^{-3} in/hr/ $^{\circ}\text{C}$. This slope implies that for the 22.5°C seasonal change in temperature

observed at the PCIB over the two year record, one could expect a 0.052 in/hr increase in the mass flux (rate) of ponded water into the soil at the site. The crushed stone storage bed at this site would tend to exaggerate the seasonal variation and one could expect a 0.13 in/hr increase in the observed recession rate of the ponded water surface for the same 22.5°C change. For the PCIB with a maximum depth of 1.5 ft this variation implies that the total ponded time from full capacity to empty would vary from approximately 50 hours at higher temperatures to over 80 hours at colder temperatures. Clearly this magnitude of variation could have considerable design implications.

The ponded water in the storage basin is not exposed to sunlight or wind and is covered by additional crushed stone, geotextile filter fabric, choker stone, and ~4 in of standard concrete. Further, there is no significant vegetation in close proximity to the BMP.

Evaporation and transpiration are not expected to contribute to the seasonal variation.

The hypothesis of this work is that the seasonal variation in the performance of the BMP is caused by temperature-induced viscosity changes of the ponded water. Regressing the performance indicator (here an estimate of the mass flux of water into the soil) against temperature is not enough evidence to claim that the variation is due to viscosity change alone, as there could be other temperature dependent processes that could have similar effects. To determine what portion of the variation could be attributed to viscosity changes, the properties of water must first be understood.

The viscosity of water more than doubles over the average range of temperature for the Mid-Atlantic region. The magnitude of this variation is not commonly recognized. More

commonly acknowledged is the variation of the density of water. Unlike viscosity, the density of water is not a monotonically decreasing function of temperature. The density of water reaches a maximum of 1.000 g/cm^3 at 3.98°C and decreases down to approximately 0.9922 g/cm^3 at 40°C . To compare the relative variation of these two properties, the density and viscosity of water as a function of temperature is normalized by its value just above freezing. This procedure is graphically summarized in Figure 24.

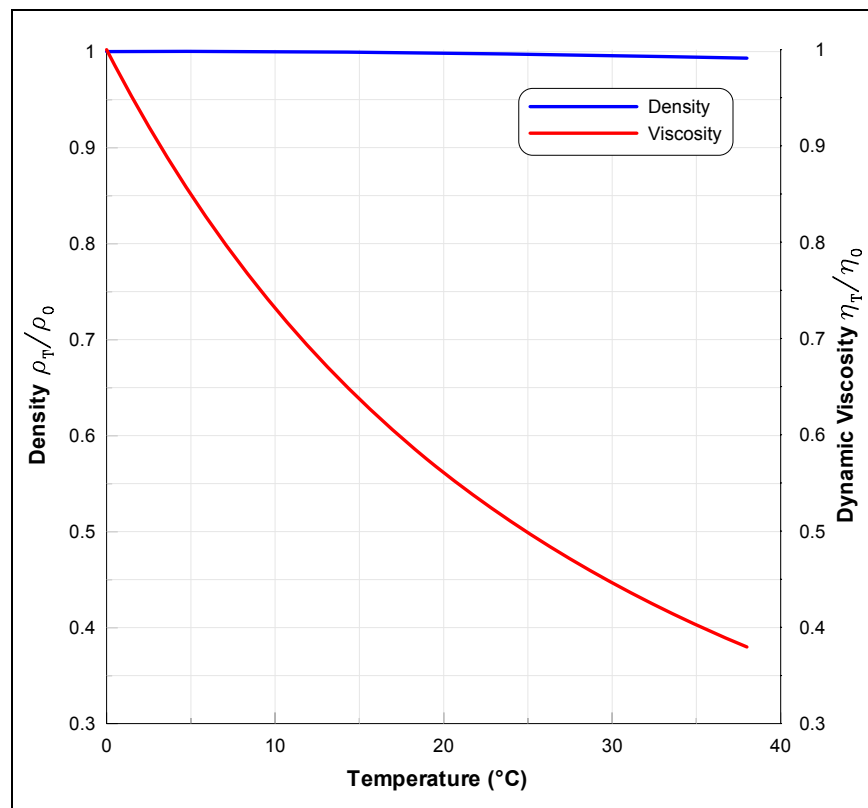


Figure 24. Relative variation of density and viscosity of water with temperature.

The magnitude of the variation of density is insignificant compared to that of the viscosity of water. Therefore, the temperature dependency of viscosity is far more important to consider than is the variation of density. However, for thoroughness both viscosity and density variation are considered in this examination.

Another factor that can affect the viscosity of water is its dissolved solids concentration. While the PCIB does occasionally receive high concentrations of dissolved salts from university snow melt operations, the concentrations found do not warrant viscosity change considerations.

To test the hypothesis that the observed seasonal variation, as indicated by the incremental slope measurements, is caused by temperature-induced viscosity effects, several assumptions must first be made about the infiltration process at the PCIB. First, the infiltrating soil surface is assumed to be an area-averaged homogeneous soil. Secondly, the infiltration process is assumed to be adequately described by a one-dimensional vertical approximation. Because the storage bed is relatively large, square and shallow, this is a valid assumption. Finally, the recession infiltration process is assumed to follow the physics of late-time, or steady-ponded infiltration, where the soil moisture potential no longer has a significant effect on flow, and the rate of infiltration (mass flux of water into soil) is primarily governed by gravimetric forces and the saturated hydraulic conductivity of the soil. This assumption can be validated by examining the soil moisture meter data recorded at the PCIB. Figure 25 shows monitoring data from one storm used in the linear regression analysis.

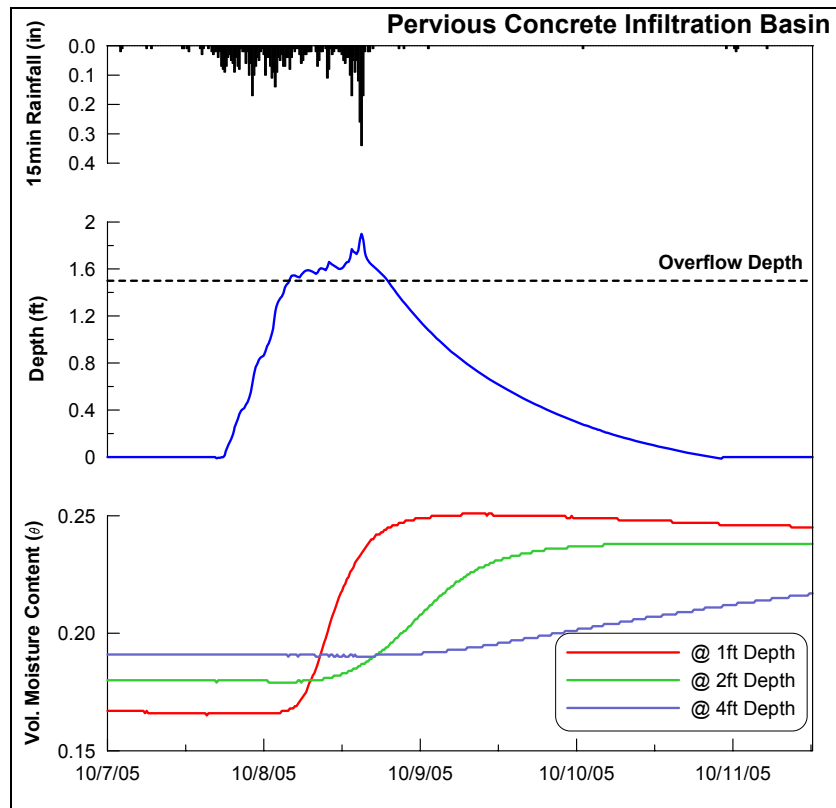


Figure 25. Rainfall, depth, and soil moisture reading for the October 7th, 2005 storm event at the PCIB.

The October 7th, 2005 storm was fairly large and produced overflow from the BMP. Approximately 0.25 in of precipitation was measured before any ponding was detected at the pressure transducer. By the time the ponded depth had receded below the overflow depth, as indicated by the dashed line and abrupt change in slope of the depth record, the moisture meter at one foot below the soil surface had essentially reached a plateau. This elevated, and relatively constant level, indicates that the soil at that depth (one foot) is near saturation or has reached its “field capacity” saturation (Hillel 1998). The moisture meters located at two and four foot depths are slower to respond and show a much more gradual increase. Therefore, the soil near the surface, shallower than the one foot moisture meter, would likely respond even sooner and with a faster (steeper slope)

increase. Therefore, the assumption of late-time infiltration (no significant soil moisture potential) is valid.

It is possible then to assume that the steady ponded recession rate of the water surface (corrected for the storage bed porosity) is a valid *estimate* of the hydraulic conductivity of the soil for the fluid it is conducting. This estimation does not account for the influence of the relatively shallow ponded depth of water. The potential influence of the ponded depth (and other factors) is further investigated using a Monte Carlo application of the Green and Ampt infiltration model, see Appendix C. Hydraulic conductivity is not a property of the soil alone; it is also dependent on the fluid of interest. Hydraulic conductivity is defined as follows:

$$K = \frac{k\rho g}{\eta} \quad (2.6)$$

Where:

- K = hydraulic conductivity [LT^{-1}]
- k = intrinsic permeability of soil [L^2]
- ρ = fluid density [ML^{-3}]
- g = gravimetric acceleration [LT^{-2}]
- η = fluid dynamic viscosity [$ML^{-1}T^{-1}$]

Therefore hydraulic conductivity can be broken into two parts, one part which describes properties associated with the soil structure, and one which is solely dependent on fluid properties (Hillel 1998). This is accomplished as follows:

$$K = k \times f \quad (2.7)$$

Where:

$$f = \frac{\rho g}{\eta} \quad (2.8)$$

Where: f = fluidity [$L^{-1}T^{-1}$]

The temperature dependency of the fluidity of water considering both viscosity and density variation is shown in the following figure.

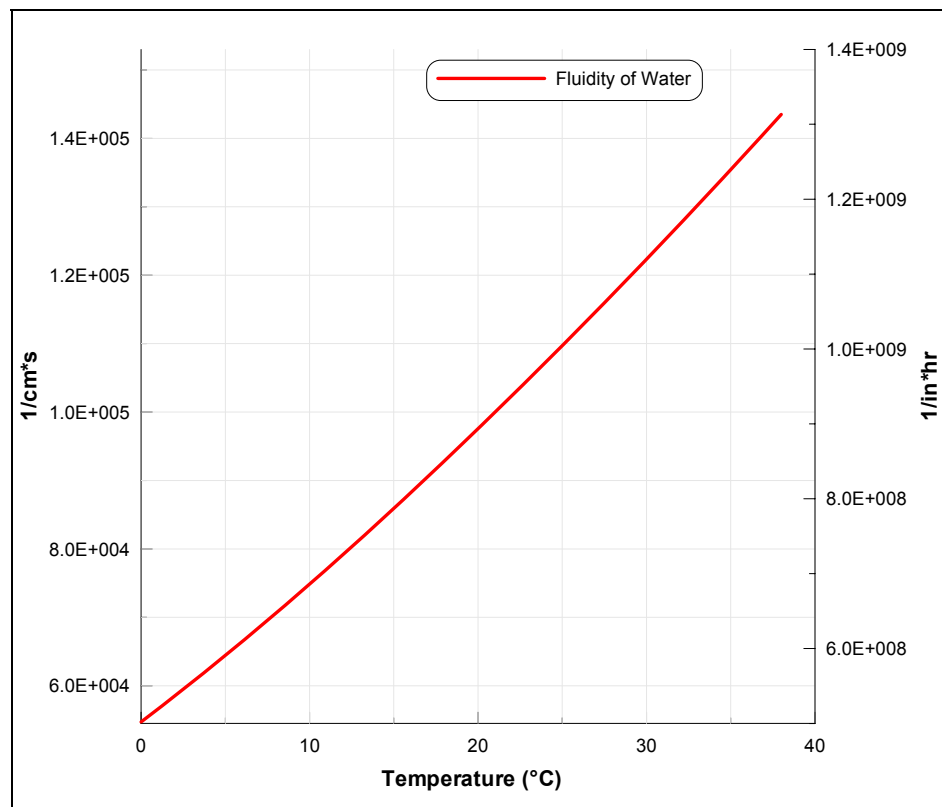


Figure 26. Fluidity of water as a function of temperature.

The observed recession rates (corrected for storage bed porosity) give estimates of the hydraulic conductivity, and the fluidity of water is known at any given temperature as

illustrated in Figure 26. Therefore, the only unknown quantity is the intrinsic permeability of the soil. Intrinsic permeability is a function of the size, shape, and connectivity of pore spaces within the soil matrix. Therefore, it is not possible to make a direct measurement of the intrinsic permeability of a soil sample. Typically, a controlled flow experiment is performed to determine the hydraulic conductivity. Then with the necessary fluid properties known, the intrinsic permeability can be determined.

The method used in this analysis is similar and is described as follows. First the average temperature for all the data points is determined. For the Pervious Concrete Infiltration the average temperature is found to be 15.8°C. Then the linear regression is used to determine the corresponding estimate of the hydraulic conductivity for that temperature.

This calculation is shown as follows:

$$K = 0.0023 \frac{\text{in/hr}}{^\circ\text{C}} \times T^\circ\text{C} + 0.081 \frac{\text{in}}{\text{hr}} = 0.0023 \frac{\text{in/hr}}{^\circ\text{C}} \times 16^\circ\text{C} + 0.081 \frac{\text{in}}{\text{hr}} = 0.12 \frac{\text{in}}{\text{hr}} \quad (2.9)$$

This value for hydraulic conductivity is within the range of typical values for a loam-like soil that is present at the PCIB. This value also corresponds well with a flexible wall hydraulic conductivity test that was run on a soil core from the site. The flexible wall test resulted in a hydraulic conductivity of 0.24 in/hr for the sample as is further described in Section 3.3.1. Considering the order of magnitude variation that is typical of this parameter and the fact that the soil core was not taken directly from the storage bed area, but from an adjacent borehole, the values are remarkably similar. Additionally, if the

laboratory value is corrected from the approximate laboratory temperature to the (lower) 15.6°C reference temperature used here, it would be even slightly closer (~0.21 in/hr).

Finally, by using the 0.12 in/hr estimate for hydraulic conductivity and the fluidity of water at the reference temperature, the intrinsic permeability can be found as 1.5×10^{-10} in² or 9.5×10^{-10} cm². This value corresponds well with published estimates for similar soils. The text *Applied Hydrogeology* states that for silt, sandy silts, clayey sands, and till the intrinsic permeability is expected to be in the range of 1×10^{-11} cm² and 1×10^{-9} cm² (Fetter 1994).

The estimate of the intrinsic permeability is assumed to be constant for all temperatures and over time. Each data point in the regression has an observed temperature associated with it. This temperature is used to calculate the corresponding fluidity for each data point. Then the fluidity is multiplied by the estimate for intrinsic permeability as is shown in Equation 2.7. This gives an estimate for hydraulic conductivity. This procedure can be used to create a plot of the predicted, or expected, hydraulic conductivity based on the fluidity correction for the range of temperatures observed at the BMP. This relationship, specifically its slope, can be compared to the observed temperature dependency of the hydraulic conductivity estimate to determine what portion of the variation could be caused by the viscosity change. For example, if the plots of both the observed and predicted hydraulic conductivity have similar slopes, then the variation is likely explained by the viscosity variation. It should be noted that the predicted variation will not be perfectly linear because the fluidity of water as shown in

Figure 27 is not truly linear. However, it can be seen that the line is adequately explained by a linear relationship and thus one of the main assumptions of the original regression method is valid. The results of this analysis are shown in Figure 27.

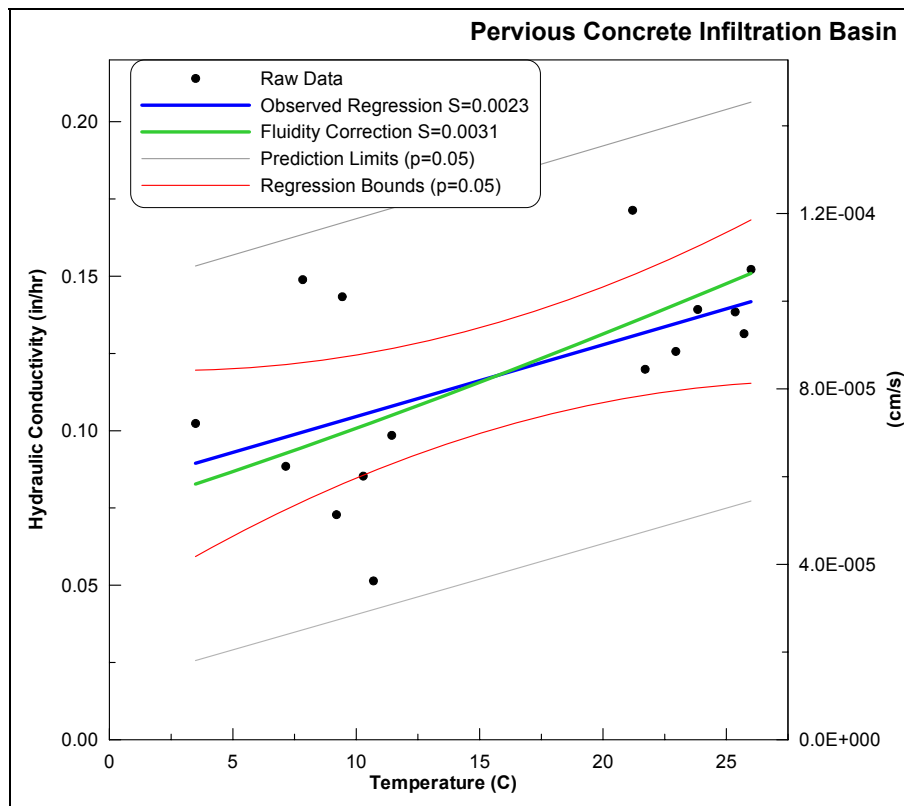


Figure 27. Temperature dependency of the predicted and observed estimates of hydraulic conductivity for the PCIB.

The predicted variation of hydraulic conductivity based on the fluidity correction (shown in green in Figure 27) can be represented by a straight line having a slope of 0.0031 in/hr/°C, only slightly higher than the observed dependency. This implies that the BMP is not showing as much seasonal variation as would be expected. However, the predicted variation is well within the 95% confidence interval for the regression. Therefore, due to the similarity of the two relationships and the amount of variation in the original

regression, it is reasonable to conclude that the fluidity correction, primarily the temperature dependency of the viscosity of water, is responsible for the seasonal variation of the infiltration performance at the PCIB.

Another method of further illustrating the seasonal variation and temperature dependency of the infiltration process is accomplished by plotting the hydraulic conductivities calculated from the original regression and those calculated with the fluidity correction versus time. This is done by using the measured ponded water temperature for each storm as the independent variable. An equation was fit to both the upper and lower 95% confidence intervals for the original regression to relate them to temperature. This enables the confidence intervals also to be plotted as a function of temperature and time. The results are shown in Figure 28.

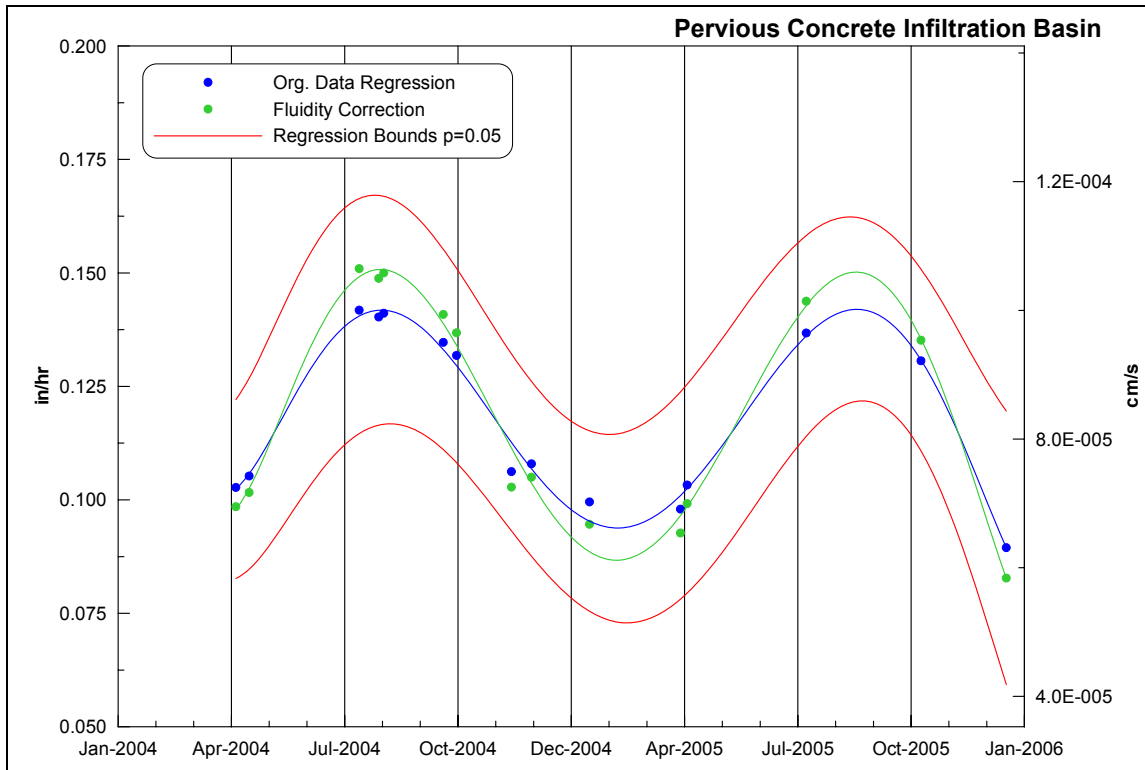


Figure 28. Original data regression and predicted fluidity correction for hydraulic conductivity as a function of measured temperature over the two year data record for the PCIB.

Significant seasonal variation has been observed even with the relatively sparse ponding events at the PCIB. However the recession rate does not seem to show any signs of a systematic change over the two year record. The check for autocorrelation among the residuals of the temperature dependency regression (Figure 23) suggests that if an overall (non-cyclic) trend exists over time, it may be one implying a general increase in performance. With the seasonal variation adequately explained based on the temperature dependency of the ponded water properties, this topic was reexamined by means of a multiple linear regression. The multiple linear regression uses *both* the measured temperature of ponded water and time (age of BMP) as the independent or explanatory variables.

The multiple linear regression results in a slightly higher slope with respect to temperature, 0.0028 in/hr/°C compared with 0.0023 in/hr/°C from the original regression without consideration of age. The slope with respect to age of the PCIB is 0.030 in/hr/yr with a 95% confidence interval of 0.00090 in/hr/yr to 0.060 in/hr/yr and a *P* value slightly significant at the 95% level (*P* = 0.044). However, a rule of thumb for multiple regressions to insure that the model is not prone to overspecification is that the number of observations should be equal to, or larger than, five times the number of independent variables plus two ($n \geq 5 \times (k + 2)$). This guidance is not satisfied in the presented multiple linear regression model with only 15 observations. Therefore, while the regression indicates that there may be a slight increase in performance over time, the model is not sufficiently strong to substantiate this finding.

In summary, the PCIB is not exhibiting signs of decreased infiltration performance. This conclusion is based on the analysis of two years of monitoring data from the lower storage bed of the BMP. The BMP has maintained its characteristic recession limb over the period of record. The temperature dependency is shown to outweigh any potential detrimental impact of two years of operation. The amount of seasonal variation observed in the performance of the BMP with respect to temperature is close to that which would be expected due to temperature-induced changes in the viscosity of water.

2.2.2 Long-Term and Seasonal Performance of the BTI

Constructed in the summer of 2001, the BTI is the oldest of the infiltration BMPs examined in this study. The depth record from this BMP spans more than a four-year period from 2003 into 2007. Temperature monitoring in the open storage basin began in March of 2005; the two-year period from March 2005 to March 2007 was used to examine the potential temperature dependency of the BMP. The four year period including calendar years 2003, 2004, 2005, and 2006 was used separately to investigate potential life-span related questions of the BTI's performance. Because this is the longest data span used in the study, it may represent the best opportunity to answer any lifespan related questions of infiltration BMP performance.

The dataset is fairly complete, although there are times where equipment failure resulted in a loss of data. For these times there is no storage basin depth record, but precipitation from another on-campus BMP rain gauge has been used. Additionally, there were time periods where vegetation interfered with the ultrasonic level detector and produced erratic readings, these data points have been removed from the data set to be analyzed. The four-year data record for the BTI is shown in Figure 29.

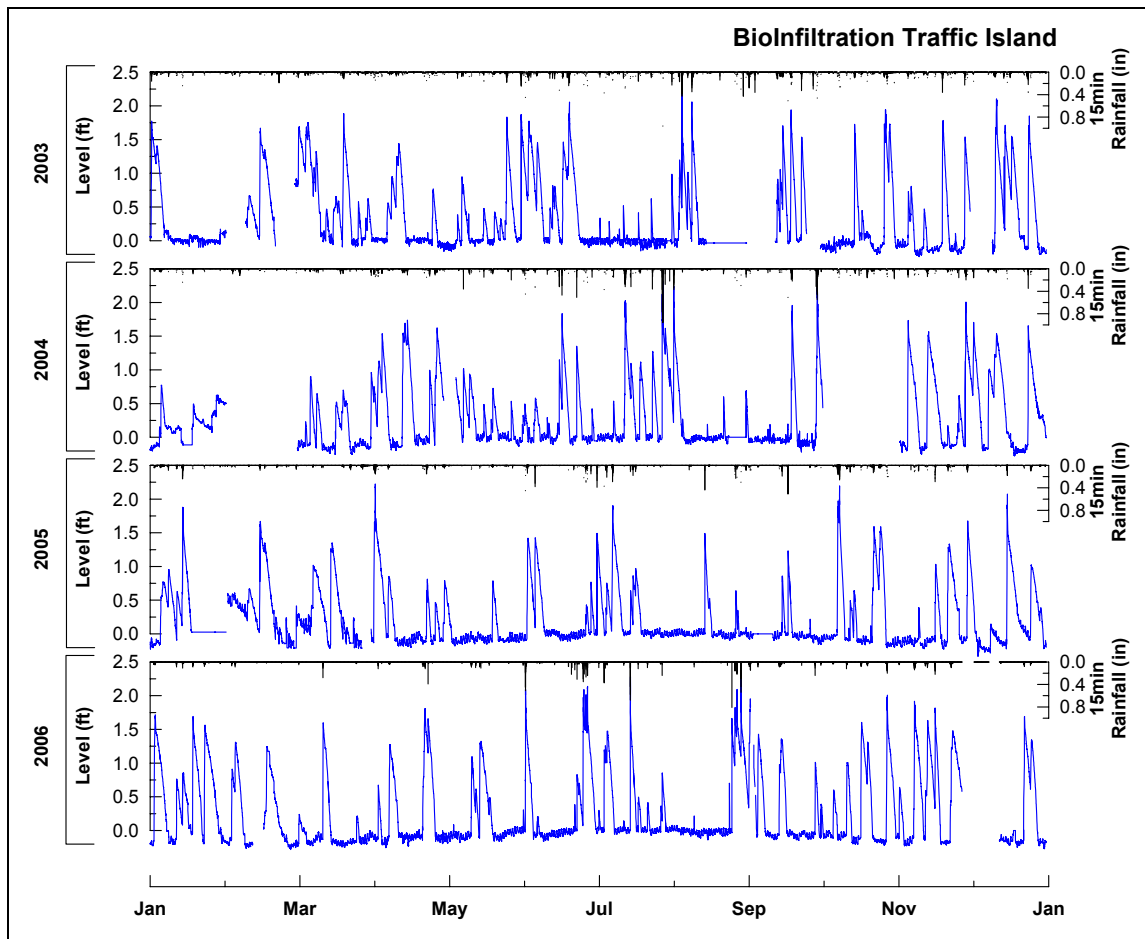


Figure 29. Data set used for analysis of the BTI.

As mentioned in Section 1.3.2 the ultrasonic level detector is not located at the lowest point in the storage basin. The detector will not begin to read a free water surface in the storage basin until the depth, measured from the lowest elevation in the basin, is 0.23 ft. To convert the level detector readings into actual depths, 0.23 ft must be added to the level reading. It should be noted that taking level readings starting at 0.23 ft only excludes 7.3 ft^3 , or 0.6%, of the total storage at overflow capacity. The data used in this analysis are the raw level data. The BMP overflows at a depth of 1.72 ft, which corresponds to a level reading of 1.49 ft. As can be seen in Figure 29, the storage capacity of the BMP is exceeded approximately 15 times per year. The depth record of

the BTI is much more responsive to rainfall than that of the lower bed of the PCIB. This is largely due to the differences in the ratio of drainage area to BMP footprint between the two sites with the BTI having nearly 10 ft² of directly connected impervious surface for every 1 ft² of BMP area.

The ponded depth is measured with an American Sigma 950 datalogger equipped with an ultrasonic transducer. The system records a depth measurement at five minute intervals. As in the case of the PCIB, it is advantageous to artificially increase the sample interval of the dataset from five minutes to an equivalent 15-minute time series. This was accomplished in the same fashion as was done for the PCIB.

Because the BTI uses an open storage bed, the storage volume of the bed does not need to be adjusted for the porosity of a crushed stone bed. Even though the PCIB and the BTI have similar overflow depths, they exhibit different characteristic recession limbs. One major factor for this is the difference in porosity of the storage bed as explained in Section 2.2. Because of its open storage bed and relatively flat and shallow geometry, the recession limb of the BTI is reasonably linear. Figure 30 compares the water surface level record for three different storm events, each approximately one year apart.

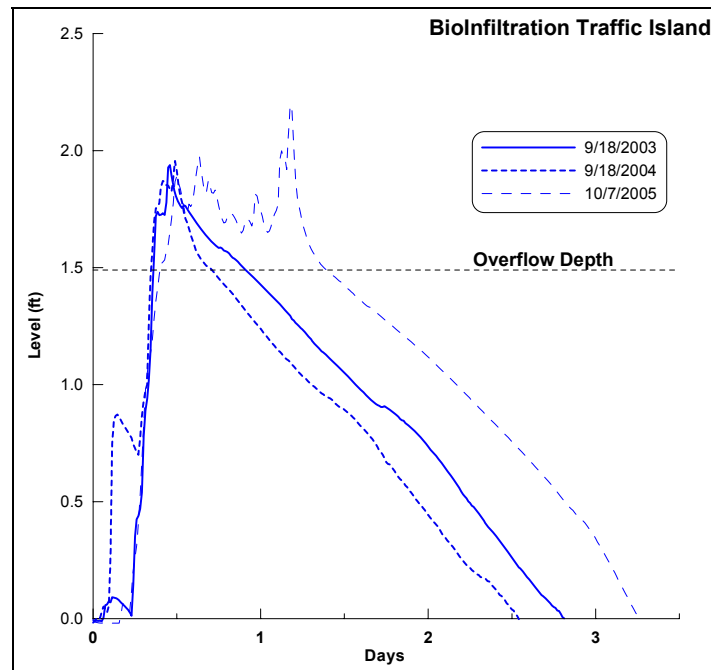


Figure 30. Comparison of three storm events at the BTI.

These three storms have recession limbs that are typical for the BMP. It should be noted that the deviations in the slope evident at the lower depths are an artifact of the ultrasonic transducer. However, staff gauge readings have confirmed that the actual depth does not deviate from the constant slope as is implied by the ultrasonic transducer readings at higher depths. Additionally, the oscillations occur when the basin is empty, which also implies that the oscillation is a result of the instrument and not an indication of the actual BMP operation. The oscillation is large enough to affect the measured slope of the recession limb significantly. Therefore, the slope measurement method explained for the PCIB was modified to prevent the instrument oscillations from obscuring the actual recession limb of the BMP. The level data record was resampled to a two-hour interval and the slope of a linear regression fit to that section of the recession limb was used in

place of the simple two-point method described previously. The details of the instrument oscillation and the details and verification of this method are provided in Appendix D.

The proper analysis and handling of the depth data for the BTI is especially important considering the potential for the instrument oscillations to significantly obscure any potential trends that may be present in the data. Therefore, additional data smoothing and two different methods for slope calculation were compared. The results from the linear regression slope calculation were chosen for the remainder of the analysis. Because of the nature of the oscillations, it was decided that this method might provide an improved measure of the recession rate. The full range (1.4 to 0.4 ft) results for the four-year period are shown in Figure 31.

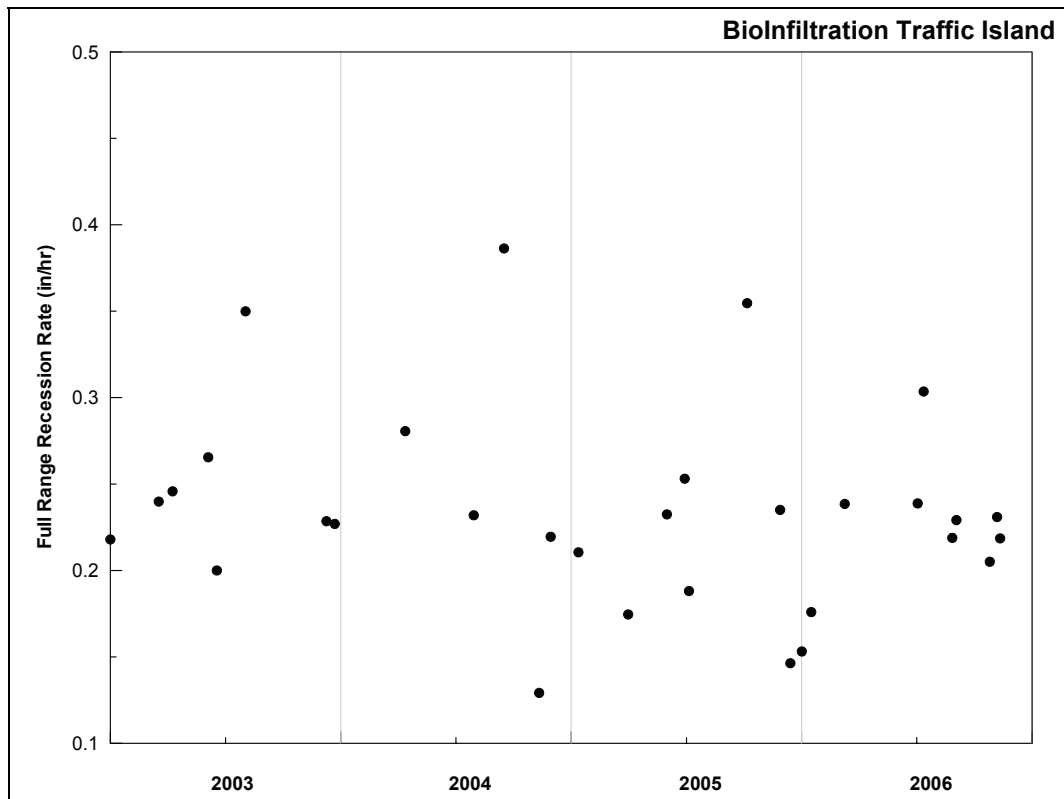


Figure 31. Full Range (1.4 to 0.4 ft) slopes for BTI.

The average slope found for the entire four-year dataset is 0.235 in/hr with a standard deviation of 0.0570 in/hr and a minimum and maximum of 0.129 in/hr and 0.386 in/hr, respectively. The data do not seem to exhibit a significant upward or downward trend. The most impressive characteristic of this data is its variability. The restrictions placed on the slope calculation (full range from 1.4 to 0.4 ft, >24 hr duration, < 0.02 in rainfall during) result in less than 8 slopes being calculated on average per year. When the full range constraint is removed and the minimum recession time decreased to 12 hr, the average number of slopes per year is increased to almost 30. An examination of these results, shown in Figure 32, indicates that the BTI, like the PCIB, exhibits a strong seasonal change in performance.

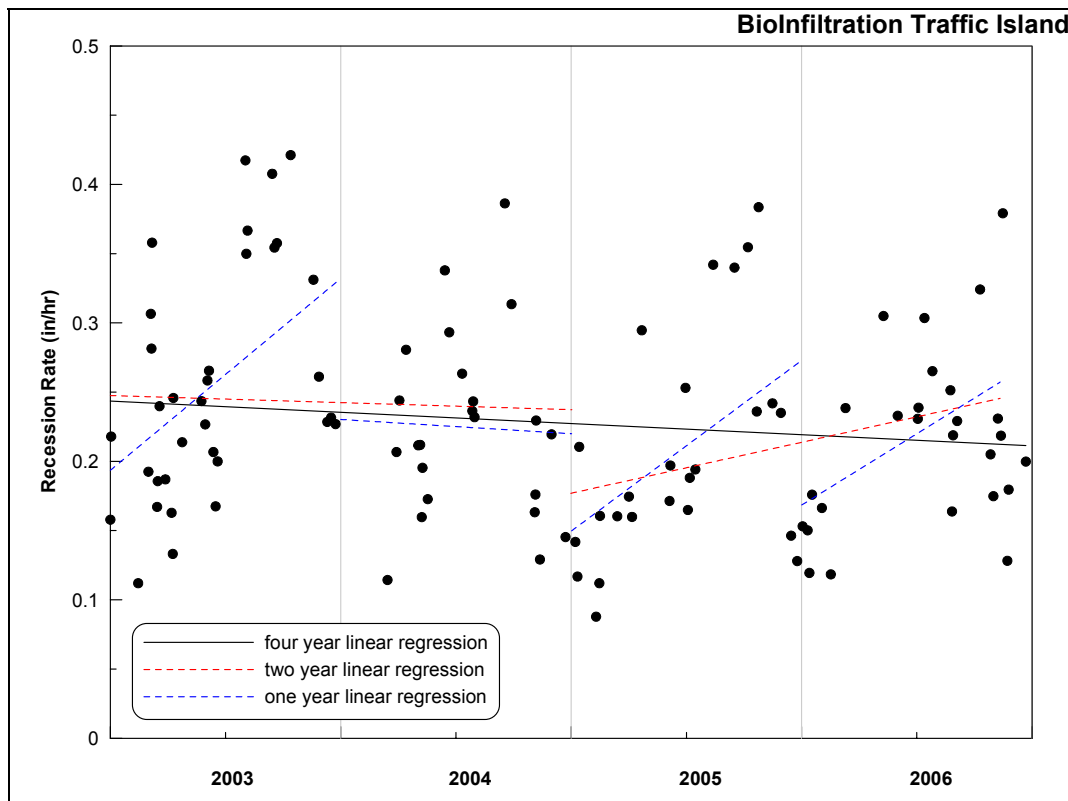


Figure 32. Measured recession rates between water levels of 1.4 and 0.4 ft with a minimum recession time of 12 hours for the BTI without full-range constraint, displayed with one, two and four year linear regressions.

In Figure 32, a four-year linear regression (shown in black) indicates a negative slope of 0.008 in/hr/yr. However, the regression is not significant with a P value of only 0.19. One- and two-year linear regressions are also shown in blue and red respectively. It can be seen from Figure 32 that the residuals around the four-year regression exhibit autocorrelation, typically being positive in the summer and fall and negative in the winter and spring. This indicates that regressing the measured recession rate versus the age of the BMP for the four-year dataset does not provide statistically significant evidence that the BMP's infiltration performance is decreasing and that such an analysis fails to satisfy the assumptions inherent to the linear regression method. Therefore, any lifespan related

analysis would likely have to account for the seasonal variation in such a BMP. This can be accomplished using a multiple linear regression as is later discussed. The smaller time period regressions (two- and one-year) are displayed simply to illustrate the importance of using long-term data, and to show how the recession rates are dependent on the time of year.

To better illustrate the seasonal variation, the same data from Figure 32 is plotted with both a seven-point moving average and a best-fit sinusoidal function.

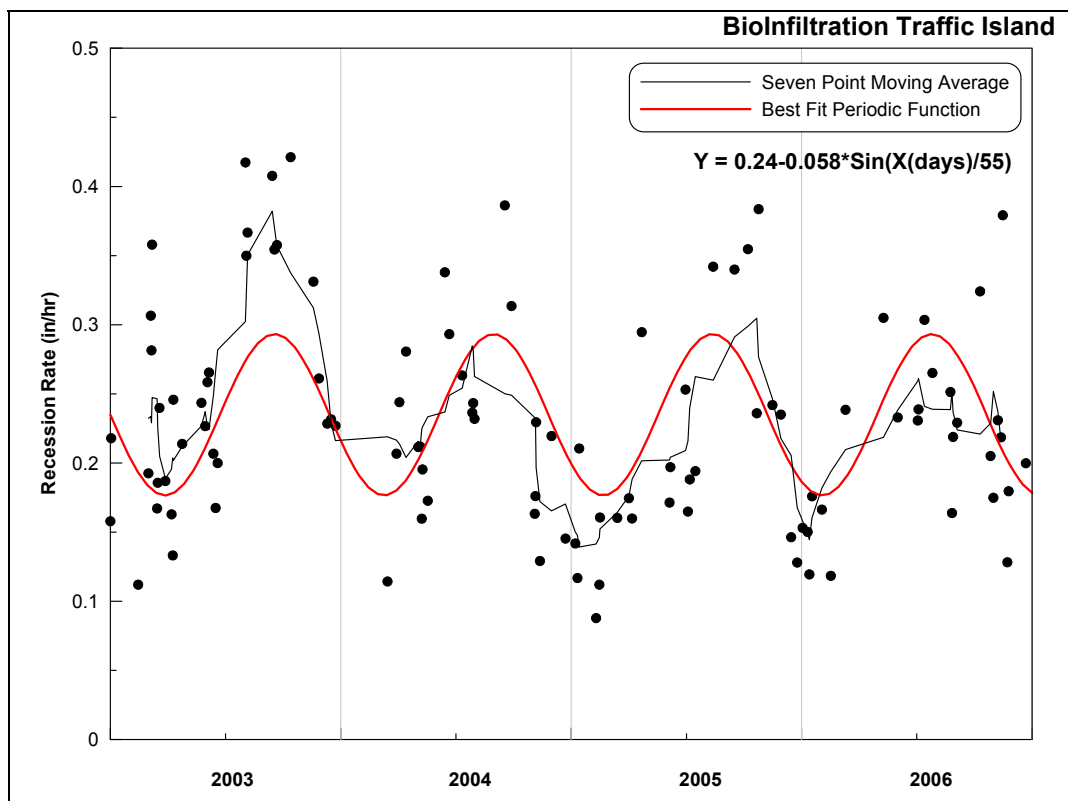


Figure 33. Recession rate data from the BTI fit with seven-point moving average and best-fit periodic function.

The periodic function was found using a simple least squares method. A true periodic regression is not possible because there is not a constant time span between storm events.

The observed seasonal variation at this infiltration BMP is slightly higher in magnitude than that found at the PCIB. The two BMPs differ in their basic design and underlying soil properties. Nevertheless, it is the hypothesis of this work that temperature-induced viscosity effects, not evaporation, transpiration, or increased biological activity are responsible for the majority of the seasonal variation. The depth and temperature record used in this analysis is shown in Figure 34.

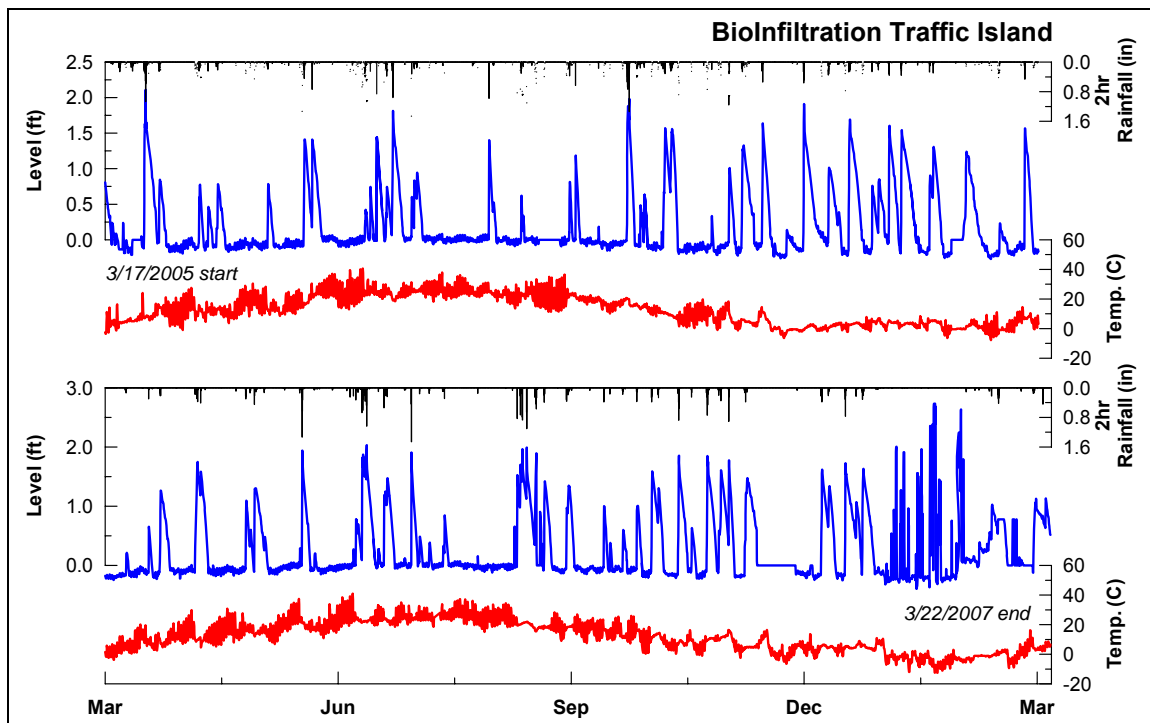


Figure 34. Two-year data record with measured temperature at the BTI.

The same method and results as described earlier were used to determine the temperature dependency of the BTI with an additional three months of data (January, February, and

March of 2007) to be processed. For this depth range (1.4 ft to 0.4 ft), there are a total of 53 data points during the two-year record. Each of these slope measurements has a corresponding average temperature as measured by the temperature logger at the bottom of the storage basin. Unlike the PCIB, the observed temperature during the recession limb showed a reasonable amount of diurnal variation. This is caused by the open storage bed, which is more susceptible to diurnal temperature fluctuations than a closed underground storage bed.

The recession limb slope measurements range from 0.12 to 0.38 in/hr. The average temperature measurements during these slopes range from 0.91 to 26 °C. The results of the linear regression with $n = 53$ are shown in Figure 35.

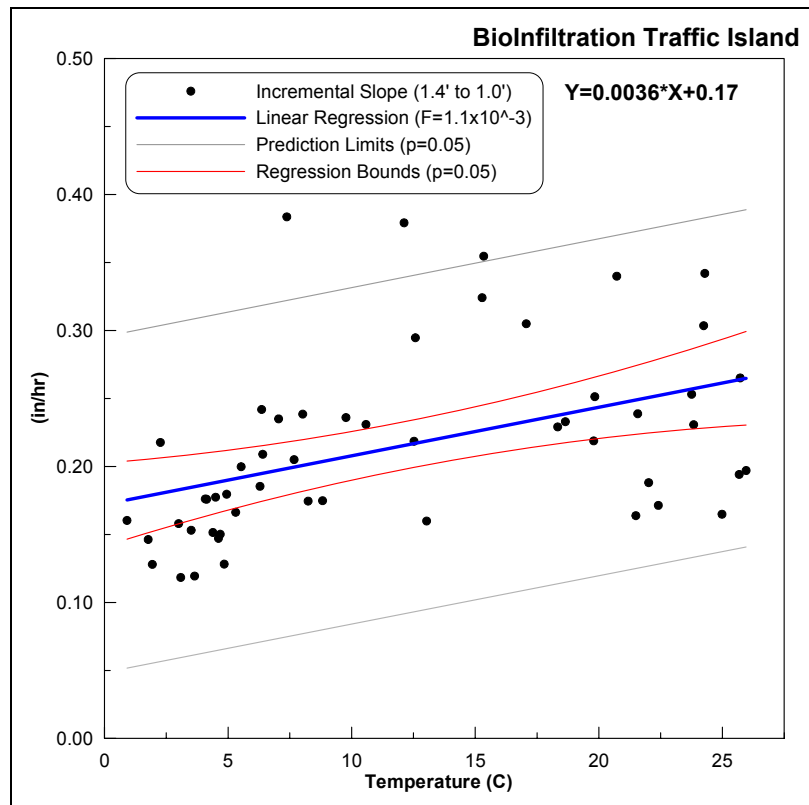


Figure 35. Temperature dependency linear regression for the BTI.

Figure 35 shows the raw data for the 53 data points along with the linear regression (blue), the confidence interval for the regression ($\alpha = 0.05$, red), and the prediction interval (grey). The regression is significant at the $\alpha = 0.05$ level with a P value of 0.0011.

Here again the necessary assumptions of the linear regression are validated. First, the relationship between the recession rate and the temperature is expected to be linear. Secondly, the residuals appear to be somewhat normally distributed around the regression, although the three data points that exceed the upper 95% prediction interval tend to create a longer tail toward the positive side of the residual distribution. These three data points that have the largest residual occur on the following dates: October 9th,

2005, October 26th, 2005, and November 17th, 2006. This is the time of year when the soil tends to be warmer than the ponded water. Therefore this may imply that a more representative temperature measurement might be made at a shallow depth into the soil at the BMP. The opposite may be true in the spring when the temperature of the ponded water might tend to be warmer than the temperature within the soil. The residuals are plotted in the following histogram shown in Figure 36.

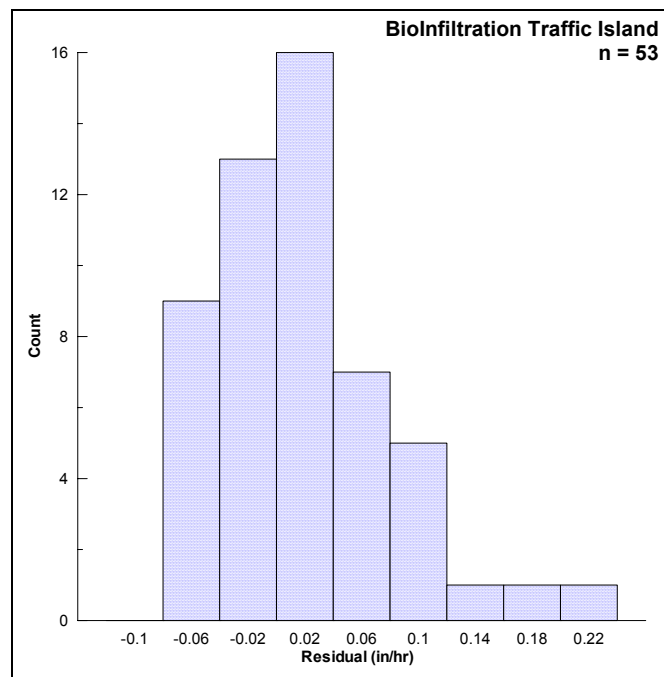


Figure 36. Histogram of regression residuals for BTI.

The residuals of the regression for the BioInfiltration Island seem to have a fairly constant variation when plotted versus temperature. This implies that the data meet the homoscedasticity assumption of the linear regression method. This validation is shown in Figure 37.

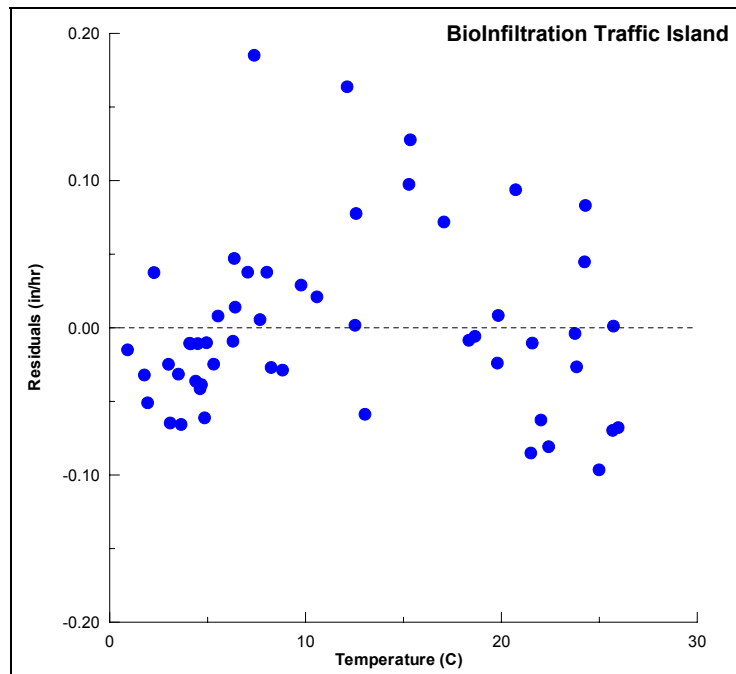


Figure 37. Check for homoscedasticity for BTI regression.

Finally, the data must be checked for autocorrelation this is accomplished by plotting the residuals versus time as shown in Figure 38.

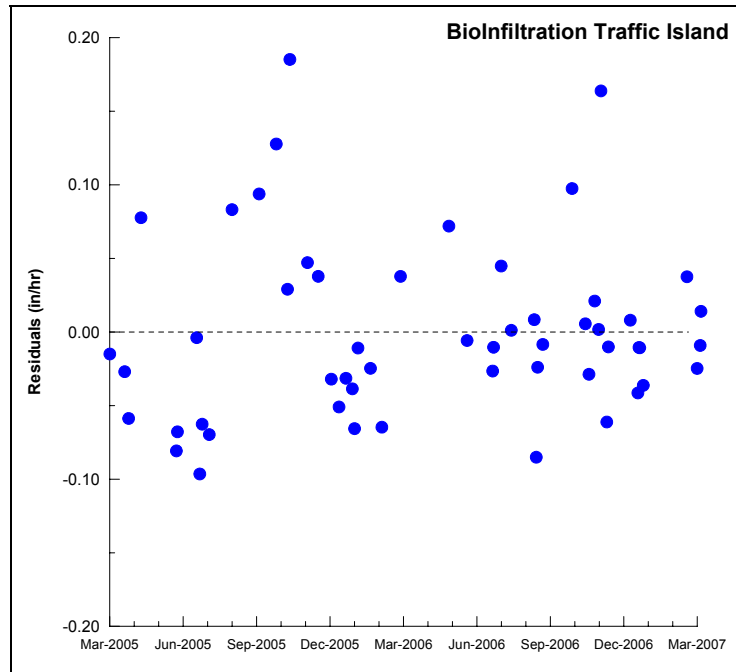


Figure 38. Check for autocorrelation of residuals for BTI.

The plot shows that the residuals do not appear to show any significant trend with respect to the date of occurrence. This is important because if the residuals showed signs of autocorrelation, and they were generally decreasing over the two-year data record, this would indicate that the BMP is experiencing a general decrease in performance along with the seasonal variation.

The regression for the BTI, while valid, is not particularly strong with a significant amount of scatter resulting in a coefficient of determination (r^2) of 0.19. The slope of the regression is 3.6×10^{-3} in/hr/ $^{\circ}\text{C}$, which implies that for the 25.05 $^{\circ}\text{C}$ seasonal change in temperature observed at the BTI over the two-year record, there is an expected 0.090 in/hr increase in the steady ponded recession of water at the BMP. On average, this increase would translate into approximately a 40 hr decrease in the total ponding time

from the overflow depth to empty with it taking on average about 80 hr at a warm condition and 120 hr in the cold condition.

Unlike the PCIB, the BTI is open to the atmosphere and is well-vegetated. Therefore, evaporation and transpiration cannot be immediately ruled out as potential sources of the seasonal variation. Both of these processes would tend to increase during warm weather and generally increase the slope of the recession rate versus temperature regression. First, the expected variation due to temperature-induced viscosity changes should be estimated before these additional two processes are examined. This is accomplished using the same method described for the PCIB.

To determine what portion of the observed seasonal variation is due to temperature-induced viscosity effects, several simplifying assumptions must be made about the infiltration process at the BTI. The area-averaged homogeneous soil assumption is necessary and the infiltration process is assumed to be adequately described by a one-dimensional, vertical approximation.

Finally, the recession infiltration process is assumed to follow the physics of late-time, or steady ponded infiltration, which is characterized by a negligible influence of soil moisture potential and a rate of infiltration that is governed by gravimetric forces and the saturated (or likely near saturated) hydraulic conductivity of the soil. The strength of this assumption can be substantiated by examining some of the soil moisture meter data recorded at the BTI. Figure 39 shows storm event monitoring data including rainfall,

depth within the storage bed, and soil moisture meter response from the shallowest meter (two feet).

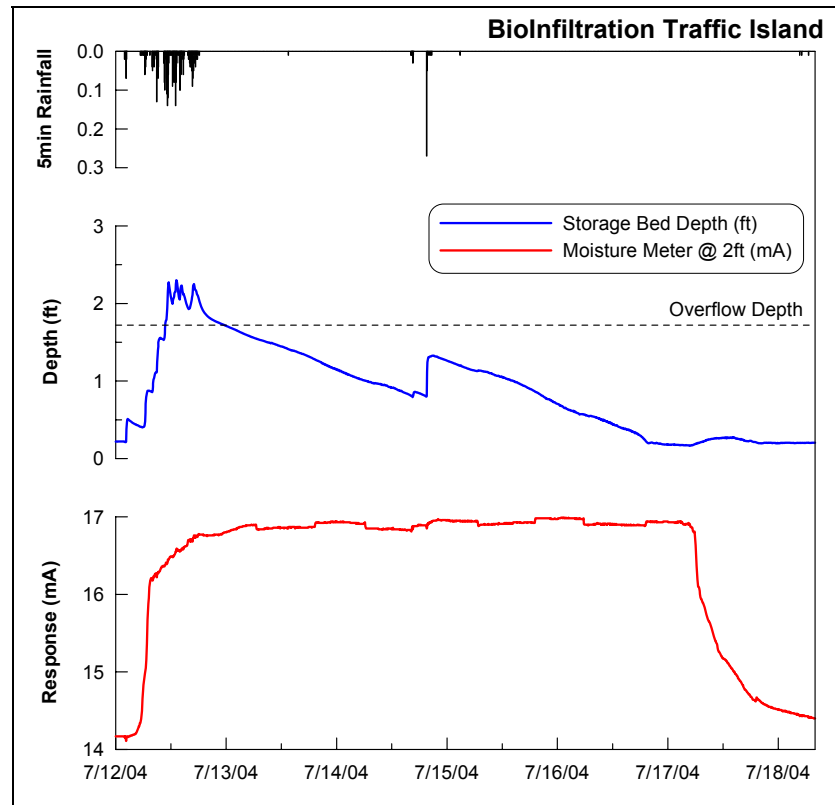


Figure 39. Rainfall, level, and soil moisture reading for the July 12th, 2004 storm event at the BTI.

The moisture meter located at a depth of approximately two feet shows that the moisture content quickly reaches a saturated or “field capacity” saturation level. This moisture content is sustained during the entire ponding duration. The level remains constant even after an additional rainfall and second peak on July 15th. This implies that the soil moisture potential of the near surface (to a depth of two feet or greater) is quickly dissipated. Therefore, the soil moisture potential of the wetting front has little effect on the recession rate of the ponded water. This is a definitive characteristic of late-time

infiltration. This method does not consider the influence of the ponding depths. A Monte Carlo sensitivity analysis using the Green and Ampt infiltration model has been performed to substantiate this assumption (see Appendix C).

The final assumption is that the observed recession rate is approximately equal to what would be an area-averaged unit flux between the level readings of 1.4 ft and 0.4 ft. The geometry of the BTI storage basin is reasonably flat. To validate this assumption, an observed recession limb was fit with a best-fit linear regression slope (0.24 in/hr) as calculated with the SlopeFinder program. The observed recession limb was then replaced with the straight line approximation to avoid complications due to noise. Each depth reading was used to interpolate what the corresponding storage in the basin would be for that depth. The same method was also applied to determine what the wetted area would be at each depth. This information was interpolated from tables created based on the topographic survey of the BMP. By subtracting the current storage from the previous storage an incremental change in storage is calculated. This value represents an infiltration, and potentially other losses, flow rate. By dividing this flow rate by the corresponding wetted area, a unit flux [in/hr] can be found. The average unit flux found with this method was only 0.01 in/hr higher than the slope found with the SlopeFinder program, providing confirmation that the SlopeFinder results are adequate for this analysis.

Therefore, it is possible to assume that the steady ponded recession rate, as determined by the SlopeFinder program, is a legitimate *estimate* of the hydraulic conductivity of the soil

surface and infiltrating water. The remaining analysis follows that as described for the PCIB. The average temperature for the BTI recession limbs was found to be 12.0°C. Based on the linear regression this temperature would correspond with an observed estimate of hydraulic conductivity of 0.21 in/hr. This is a reasonable estimate based on the sandy loam nature of the mixed fill soil installed at the BMP.

Solving for the intrinsic permeability at the BTI generates an estimate of $3.0 \times 10^{-10} \text{ in}^2$ or $1.9 \times 10^{-9} \text{ cm}^2$. This estimate puts the soil closer to a silty or fine sand which agrees well with the soil texture (Fetter 1994). Predicted hydraulic conductivities are then generated based on the known fluidity of water at each measured temperature. Finally, the predicted values based on the fluidity correction are compared to the observed values as shown in Figure 40.

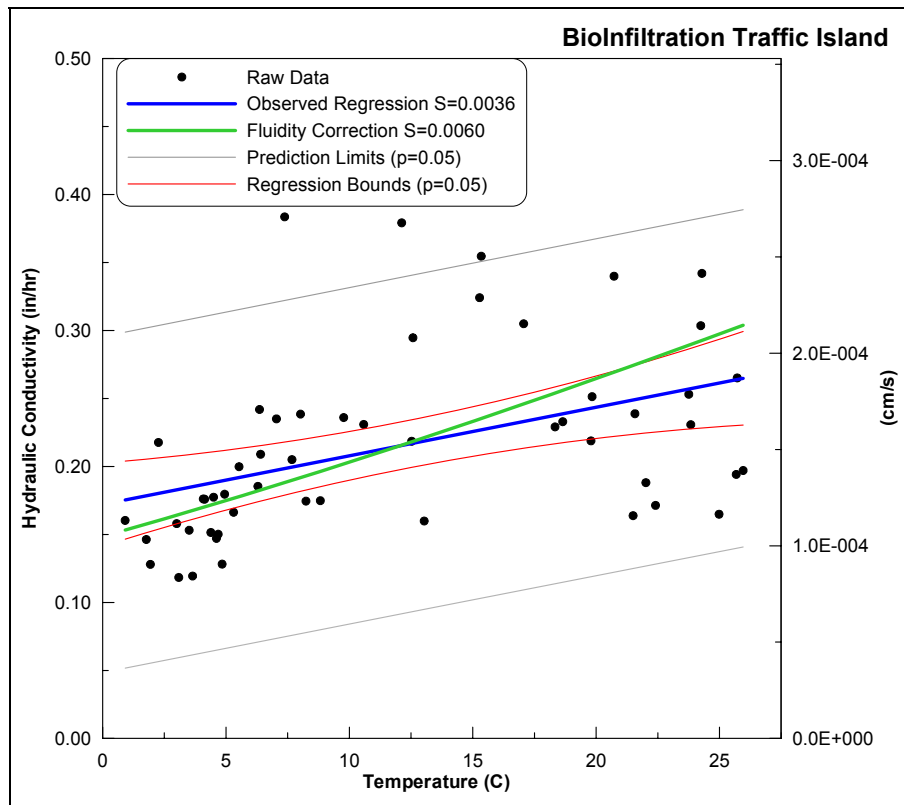


Figure 40. Temperature dependency of the predicted and observed estimates of hydraulic conductivity for the BTI.

The predicted variation of hydraulic conductivity (shown in green) can be represented with a straight line with a slope of $0.0060 \text{ in/hr/}^{\circ}\text{C}$. This is higher than the observed temperature dependency ($0.0036 \text{ in/hr/}^{\circ}\text{C}$) and slightly exceeds the upper 95% confidence boundary for the observed regression ($0.0056 \text{ in/hr/}^{\circ}\text{C}$). The fact that the predicted variation at the BTI is greater than the observed variation suggests that the BTI is not showing as much seasonal variation as would occur based on viscosity changes alone. Initially this result is somewhat unexpected. If evaporation and plant transpiration contributed a significant amount of losses during the recession limb, they would increase the overall observed temperature dependency, as both of these processes are more prominent with warmer conditions. However, the maximum potential rate of both of

these processes is generally much smaller (often by orders of magnitude) than the 0.23 in/hr average observed recession rate at the BMP (Berend 1967; Constantz, Thomas et al. 1994).

The vegetation at the BTI does not play a significant and direct role in the steady ponded recession rate at the site. The vegetation may enable the soil near the surface down to bottom of the root zone (~4 ft) to dry out quicker. The benefit of this would be experienced during early infiltration at the onset of the next storm. The drier soil conditions would create greater (negative) soil moisture potential which would increase the rate and volume of infiltration during early time infiltration. However, this process would not be significant during the ponding and recession period of the storm event. Consequently, the seasonal impact of vegetation is mainly found in the soil moisture recovery in the root zone. However, this effect may contribute significantly to the overall hydrologic performance of a given BMP. Its impact would be a function of the BMP drainage area to surface (infiltrating) area, with the effect being much more evident at lower ratios. In addition to the direct effect (transpiration) that the vegetation may have on the BMP's water budget, vegetation is also expected to have many advantageous indirect effects on the infiltration process. These effects concern the maintenance and protection of the soil surface structure and are further discussed in Section 2.3.

Ponded evaporation at the BTI is another process that has obvious seasonal variations. Improvised pan evaporation experiments have been conducted within the BMP storage basin when empty. These short-term (~two day) experiments have never produced a

measurable or even noticeable amount of evaporation. Based on data provided by the Pennsylvania State Climatologist Class A pan evaporation rates for South Eastern Pennsylvania rarely exceed 0.25 in/day. With some of the *slowest* recession rates being in the neighborhood of 0.10 in/hr, or 2.4 in/day, it is unlikely that direct ponded evaporation is a significant contributor to the seasonal variation observed at the BTI.

The measured temperature during a ponding event at the BTI does show some diurnal variation due to solar heating. However, the average temperature was used as the independent variable in this analysis. This simplification may be responsible for some of the scatter around the regression. There is another, more important simplification that may have more influence on the regression and may explain why the observed variation is less than the predicted variation. No temperature profiles into the soil surface were measured in this study. However, the diurnal and seasonal temperature variations are dampened and delayed with increasing depth (Hillel 1998; Ronan, Prudic et al. 1998; Constantz, Tyler et al. 2003; Cheviron, Guerin et al. 2005). The temperature of the ponded water as measured in this study (near the surface) may not be the best representation of the temperature that is responsible for the variation in hydraulic conductivity. It is possible that this temperature measurement should be made at a shallow depth in the soil (<1 ft). Measurements at this location will show a temperature variation that is delayed and more importantly dampened, with smaller both diurnal and seasonal temperature ranges. If the variation (range) of the measured temperatures used in this regression was smaller, it would increase the slope of the observed regression and bring it closer to that predicted based on the fluidity correction. This implies that the

controlling layer may not be directly at the soil surface but rather at some shallow depth just below the surface.

The temperature dependency of the BMP, both observed and predicted, can also be illustrated by plotting both regressions as a function of time. This is done by using the measured temperatures for each data as the independent variable. The results are shown in Figure 41.

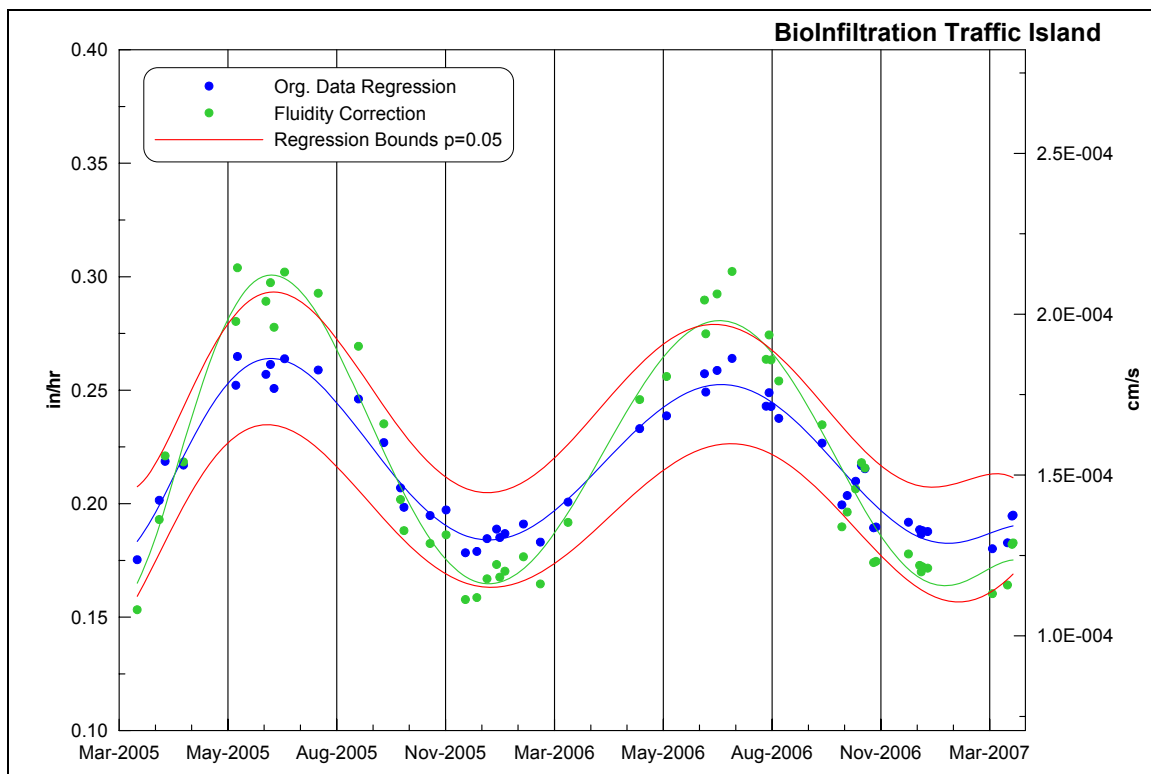


Figure 41. Original data regression and predicted fluidity correction for hydraulic conductivity as a function of measured temperature over the two-year data record for the BTI.

The seasonal variation makes it difficult to determine if the BMP is experiencing a general systematic (not cyclic) change in performance. Since the temperature

measurements were only taken for two years, it is only possible to use these two years of data in a multiple linear regression with temperature and time (age of BMP) as the independent (explanatory) variables. A multiple linear regression is necessary because of the already proven influence of temperature. The temperature variation must be considered when attempting to discern any potential longevity-related issues. Therefore, a multiple linear regression was performed on the data.

The slope of the multiple linear regression with respect to temperature, r^2 , and the standard error are basically unchanged from previous regression. The slope of the regression with respect to the age of the BTI is found to be 6.4×10^{-3} in/hr/yr. This positive slope would imply an *increase* in performance of 0.013 in/hr over the two year period. However, the 95% confidence interval for the slope ranges from $-23. \times 10^{-3}$ to $35. \times 10^{-3}$ in/hr/yr. Since the confidence interval for this partial regression coefficient includes, and is fairly well centered around, zero (no change), it is not possible to assume that the BTI is showing any statistically significant ($\alpha = 0.05$) evidence of a systematic change in performance.

In summary, the BTI is not exhibiting signs of decreased infiltration performance. This conclusion is based on the analysis of four years of monitoring data at the BMP (only two years used in multiple linear regression). The BMP has maintained its characteristic recession limb over the period of record. The BMP was in operation for approximately 16 months prior to the full instrumentation of the site. Therefore it is not known what, if any, change in performance may have occurred prior to the data record used in this

analysis. The results indicate that the infiltration process at the BTI varies significantly over the course of a year. The amount of seasonal variation observed with respect to temperature is less than would be expected due to temperature-induced changes in the viscosity of water. This discrepancy may be a result of the location at which the temperature measurements were taken. Additionally, it appears that plant transpiration and direct evaporation have an insignificant influence on the steady ponded recession rate of the BMP. Therefore, the seasonal variation at the BTI can be explained by temperature-induced viscosity changes.

2.2.3 Long-Term and Seasonal Performance of the IT

Constructed in 2004, the IT is the newest of the three infiltration BMPs examined in this study. One of the main objectives behind the design and construction of the IT was to specifically test the BMP's longevity (see Section 1.3.3). To exacerbate any longevity-related issues, the BMP was essentially overloaded with stormwater runoff. A typical application of this BMP would not be designed with such a high loading rate. For comparison, the BTI has approximately 0.5 acres of DCIA draining to the BMP. If it had the same loading ratio of the IT it would have 9 acres of DCIA. When full to the overflow pipe elevation, the crushed stone storage bed in the IT can only hold the equivalent of 0.12 in over the drainage area to the BMP.

Another design aspect of the IT that separates it from the other two BMPs is its depth. The overflow pipe is located at 5.21 ft above the storage basin bottom. During intense

periods of rainfall and overflow when the pavers are overflowing, the basin can experience ponding depths of over 6 ft.

Due to the focus on longevity for this BMP, special precautions were taken to prevent any runoff from entering the BMP until the monitoring equipment was fully installed, calibrated and tested. This ensured that the very first storm that the BMP experienced was recorded. This is the first known study where an infiltration BMP was monitored for the very first storm and a continuous record thereafter. This provides valuable information about the short-term or startup performance along with insight into the long-term performance.

Due to the size and drainage area characteristics of the IT, the data is logged at a one-minute time interval. For this study a one-minute time interval is not required. Therefore the dataset was resampled to a 15-minute time interval, with the exception that the first three months of the dataset, July, August and September of 2004, were analyzed using five-minute data. This was due to the extremely high recession rates observed at the higher depths during that time period. With 15-minute data and using one foot incremental sections, the fastest rate that can be measured is 48 in/hr. This method requires that at least two points lie within the depth range. Therefore it was necessary to use five-minute data during the first three months of operation.

The continuous data record used for the IT spans from July 2004 to March 2007 (33 months) with only a few short periods with no data due to instrumentation malfunction

and maintenance. Due to the large drainage area to BMP ratio, the capacity of the storage bed is frequently exceeded. Figure 42 shows the depth data record for the IT (approximately 2.75 years).

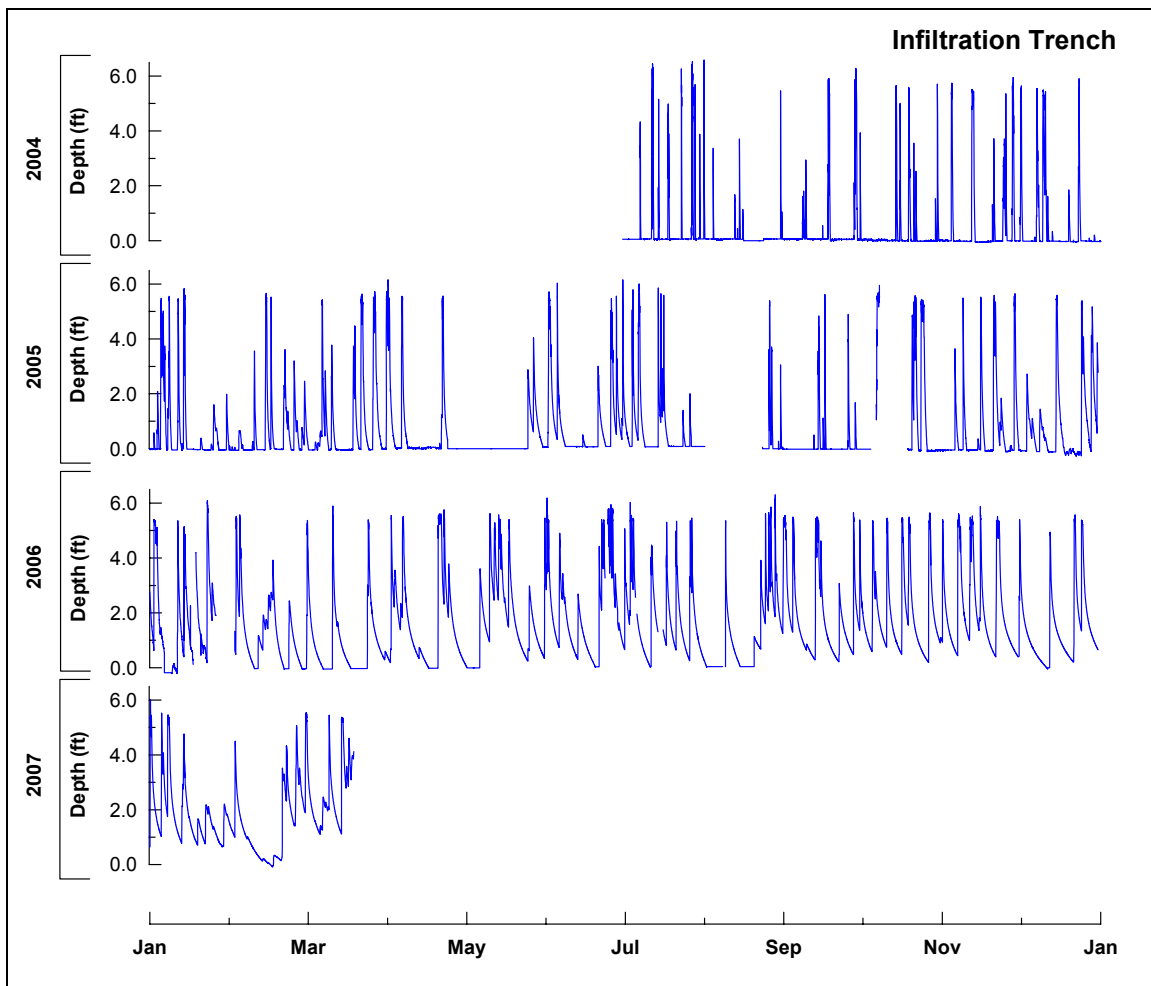


Figure 42. Depth data record for the IT.

Since the characteristic recession limb of the IT is curvilinear, the incremental slope method was used to calculate the slope between predefined depths. Given that the overflow depth is 5.21 ft, the first incremental slope was chosen to be measured between 5 and 4 ft. A one-foot span was used for each of the following incremental slopes with

the exception of the final span which was found between 1 and 0.1 ft. For the section of the recession limb between these depths, the slope was calculated with both the best-fit linear regression method and the original two-point method with the results from the linear regression method being used in the analysis. Both methods produced similar results. This method is graphically explained in Figure 43.

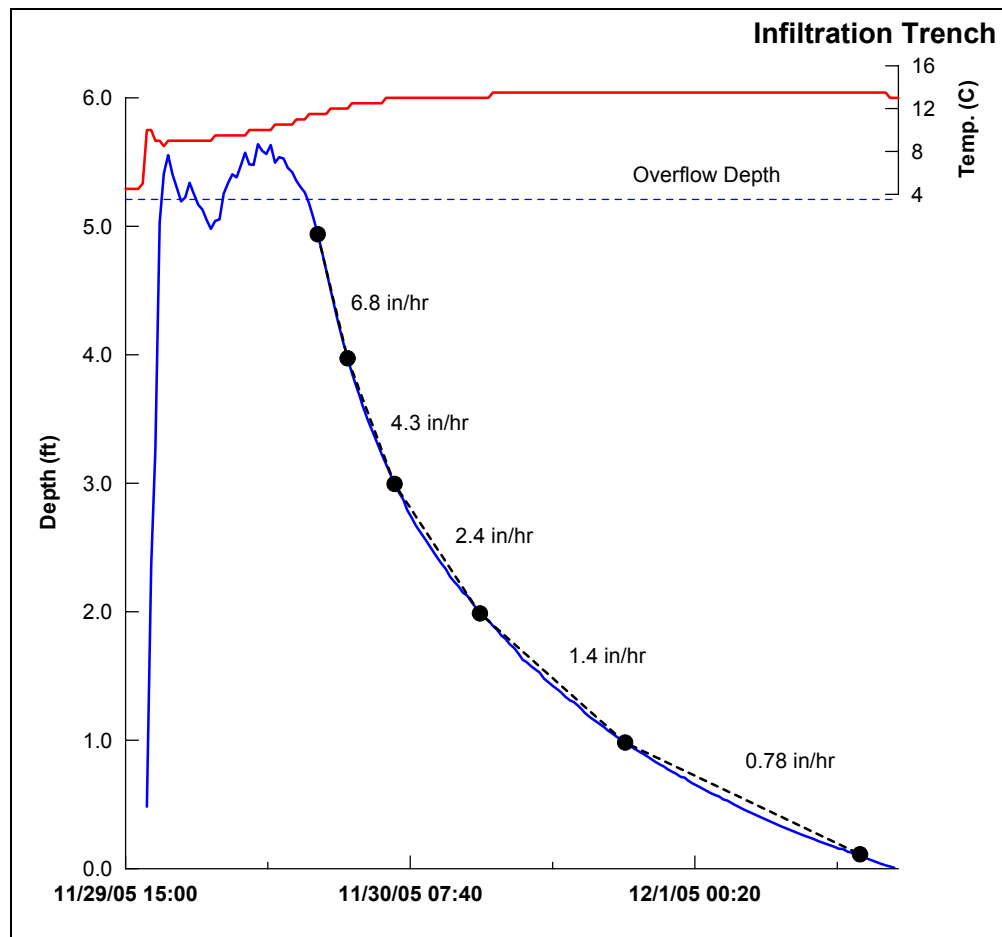


Figure 43. Incremental slope method for IT for the November 29th, 2005 storm.

Once each of the five depth ranges was run with the SlopeFinder program, the results were sorted to select only those that best represent the infiltration process. Even small rainfall depths (less than 0.25 in) produce full ponding (and overflow) conditions in the

BMP, because of the BMP's extremely high loading ratio. Consequently, there are more recession events recorded at the IT than there are at either the other two infiltration BMPs. At the highest depth range from five to four feet, the program identified 207 slopes in the less than three year data record. The sorting procedure included deleting any slopes that had measurable precipitation (>0.00 in) during part of the recession limb. Secondly, the slopes that were spanned less than 0.5 feet were also not included. For example, if the upper depth was found to be 4.4 ft and the water surface receded past 4.0 ft, this slope would not be included because it did not span more than 0.5 ft. After sorting, the number of slopes for the five to four foot level was decreased to 112. Graphically the data has a defined upper boundary with a large amount of scatter below the boundary. This scatter is due to continued inflow that is occurring during the beginning of the recession process. This inflow is less than the outflow (infiltration) resulting in the continued recession at a slower than expected rate. The sorting criteria had the effect of deleting slopes that lie farther away from the apparent upper limit of the data. Figure 44 compares the results before and after sorting for the upper-most depth range (five to four feet) with the recession rates presented on a log scale. The points along the upper boundary are the best indicators of the infiltration process.

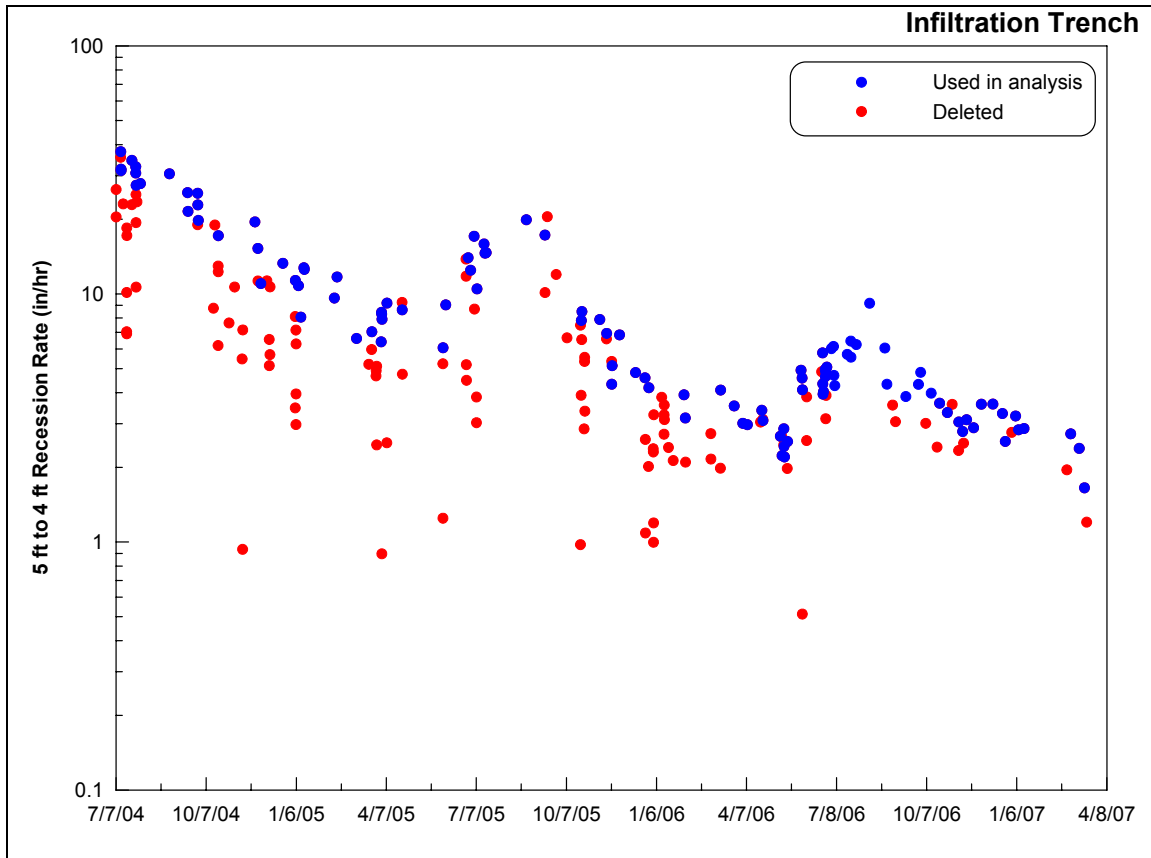


Figure 44. Incremental slopes between five and four feet for the IT before and after sorting.

The same sorting procedure was done for the other four incremental slopes. The results indicate that the IT has experienced a general and drastic decrease in infiltration performance along with marked seasonal variation in performance as shown in Figure 45.

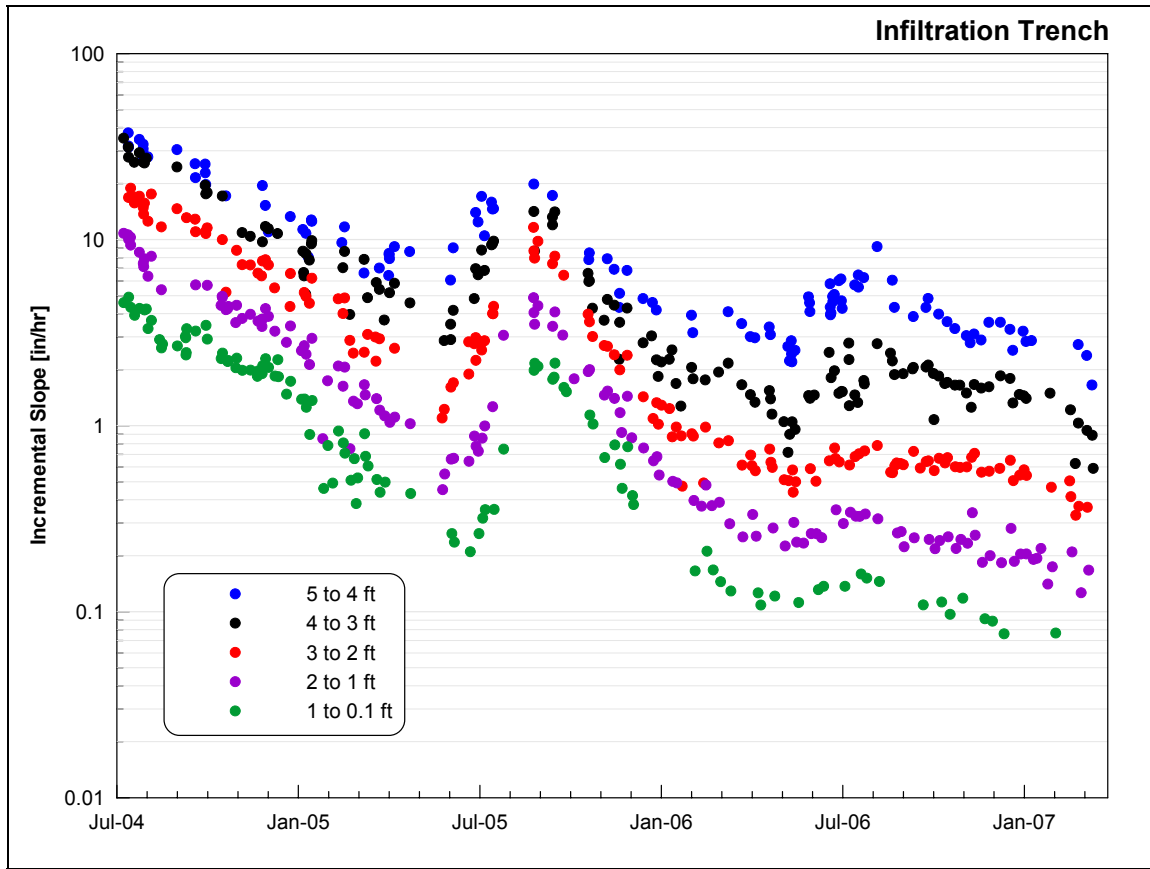


Figure 45. Incremental slopes for the IT from July 2004 to March 2007.

Figure 45 shows a strong general decrease in infiltration performance for all five incremental slopes with two periods (summer) of increasing performance. The decrease follows an exponential (non-linear) trend over time and is displayed in Figure 45 with a log scale y-axis. Plotting the data on a log scale also makes the seasonal variation at later times (August 2006) more apparent. The seasonal variation displayed in the first year is much more apparent in the first summer than in the second. This difference is expected based on the changing soil properties responsible for the drastic change in infiltration as is further discussed in the following section.

The change in performance is drastic enough to be detected by a visual examination of the raw depth data (Figure 42). The slower recession rates result in longer ponded times and in general an increase in the total ponding over the course of a year. The change has been large enough to substantially shift the depth duration curve from one year to the next (see Figure 46).

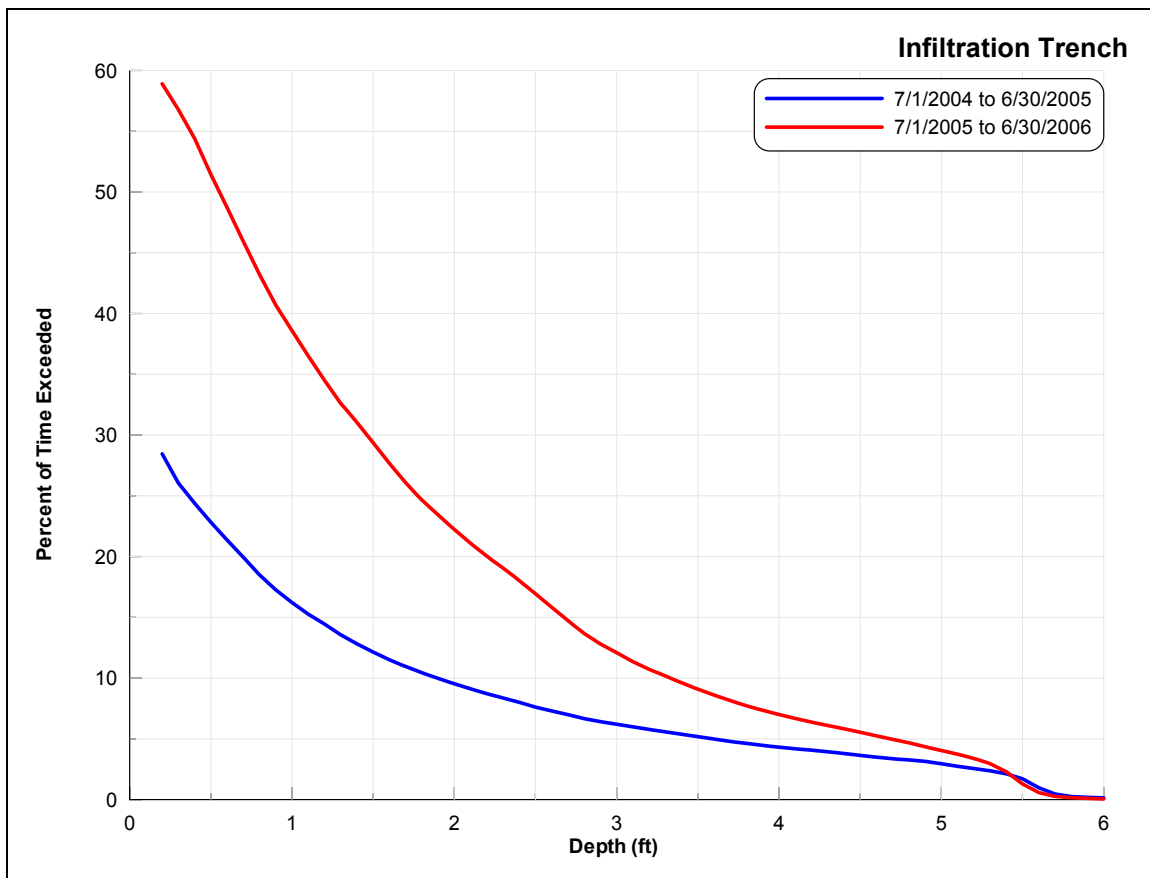


Figure 46. Depth duration curves for first two years of data at IT.

The curves in Figure 46 show that in the first year of operation the BMP experienced ponding depths greater than one foot only about 16% of the time (~58 days). Whereas in the second year of operation that percent increased to approximately 38% (~140 days).

Figure 45 clearly shows that the recession limb of the stage hydrograph for the IT is changing over time. However, the changes have not always been proportional among the incremental depth ranges. If the changes were proportional (recession limb maintaining its characteristic shape) then one recession limb would overlay with another by simply multiplying the x-axis (time) by a constant value. Figure 45 also indicates that the relation of one incremental slope to the other is not consistent over the dataset. To better illustrate this, a three-point moving average of each plot was first calculated to smooth out the short time variation in the data. Then the averaged data was interpolated to a one-week time interval, creating a plot similar to Figure 45 with the observed data points replaced by representative weekly points. For each weekly data point the incremental slope for each depth range is then divided (normalized) by that of the lowest depth range (1 to 0.1 ft) as shown in Figure 47.

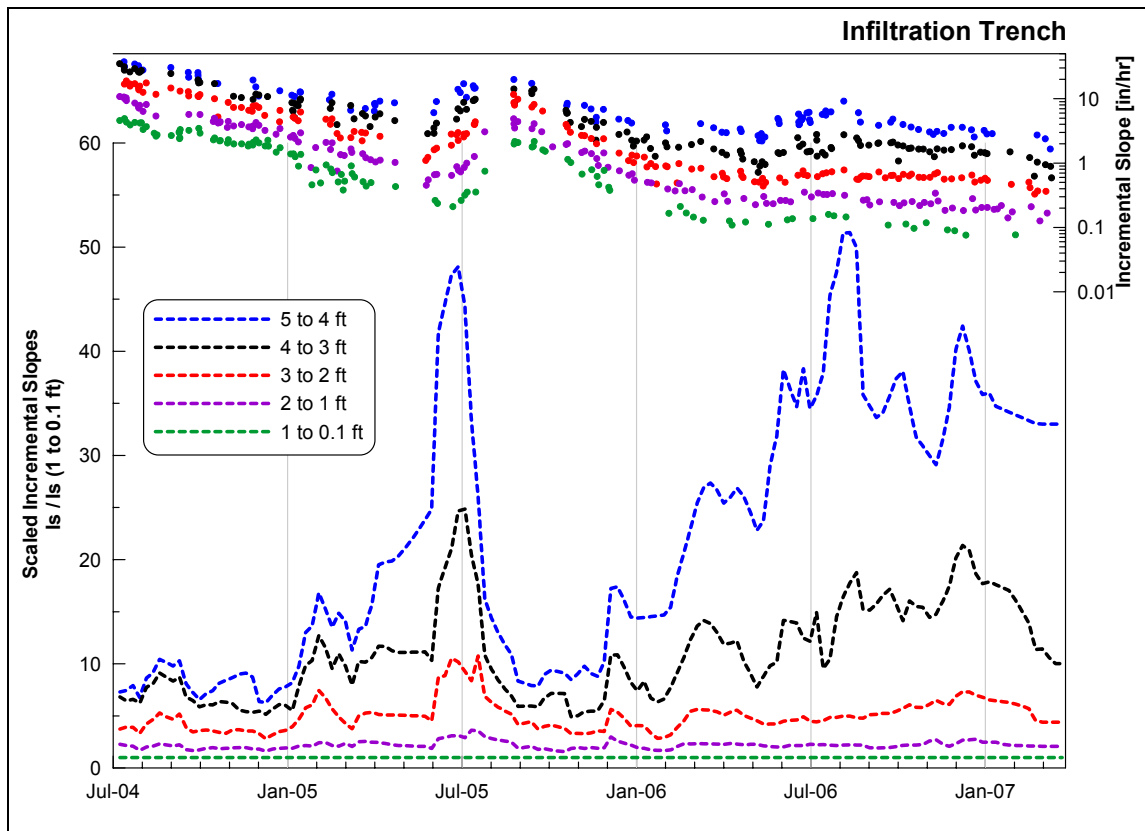


Figure 47. Scaled incremental slopes for the IT from July 2004 to March 2007.

This method shows that the original shape of the recession limb is reasonably constant, although decreasing proportionally, for the first six months of operation. The recession limb then begins to show more tailing reaching a maximum in July 2005. This date corresponds with the onset of a general increase in performance that begins in June and July of 2005 and reaches a maximum in September of 2005. In September when the incremental slopes reach their maximum values for 2005 the general shape of the recession limb is essentially back to its original state although slower by a factor of approximately three. This shape again holds constant for about four or five months before the shape again begins to show signs of increased tailing which occurs at roughly the same time of year as it did the prior year. The tailing again reaches a maximum

around July to August of 2006. The recession limb does not seem to recover to its original shape after this time as it did the prior year. Instead, it shows signs of extended tailing with the upper incremental slopes maintaining proportionally much higher slopes than the bottommost slope.

Because there is a significant amount of inter-event variation in the recession limb it is difficult and somewhat arbitrary to select individual recession limbs and make meaningful comparisons. Therefore, representative theoretical recession limbs were created. This was accomplished by first creating a five-point running average of the data in Figure 45 to further smooth out some of the inter-event variation that can still be seen in Figure 47. For every three-month period in the data record, a hypothetical recession limb was created by connecting each depth interval by a straight line with a slope corresponding to its average value at that time in the data record (see Figure 48).

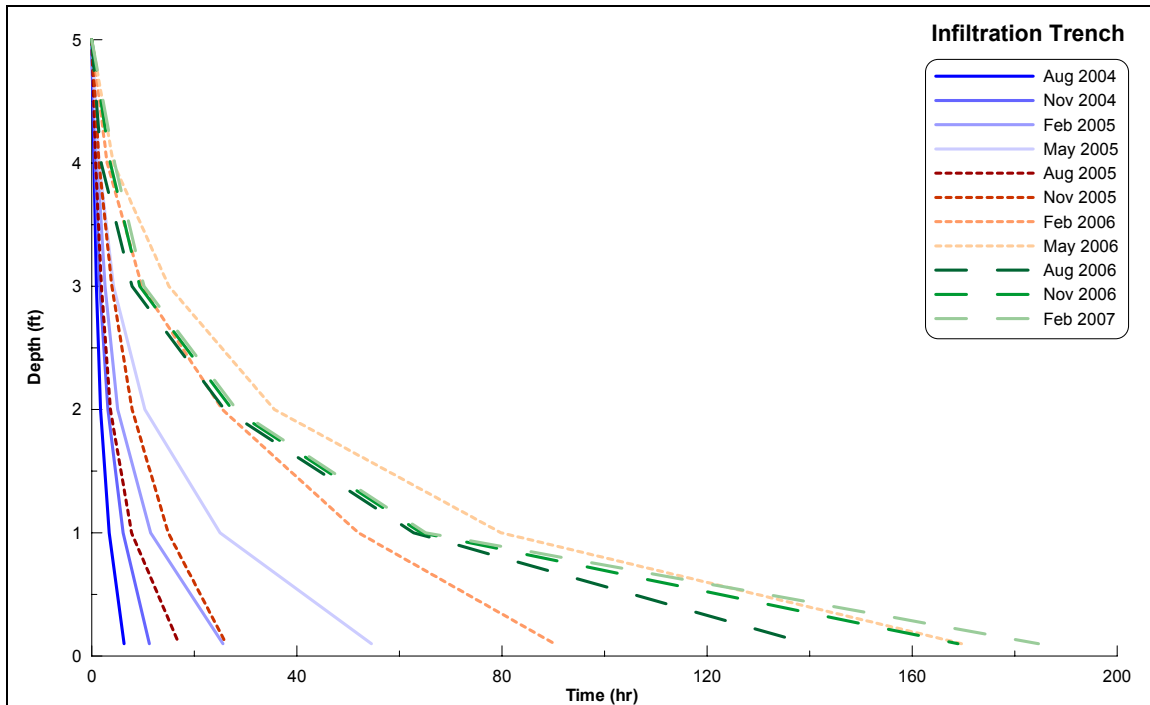


Figure 48. Representative theoretical recession limbs for the IT.

The first year of data is shown in shades of blue with the first representing the month of August. The later months November, February, and May are shown in increasingly lighter shades of blue. The second full year of data is displayed with reddish/orange tones, and the final year (not a complete year) in green. The first two years show similar patterns with August showing the fastest recession rates and May the slowest. Figure 48 also shows the effect of seasonal variation on the recession limb. The recession limb for August 2006 is almost back to what it was in November of 2005. Figure 48 also shows that the average time to empty has gone from less than 10 hours in the beginning to almost 200 hours in February of 2007. However, one of the most significant findings shown in Figure 48 is the fact that the recession limb changed very little over the last seven months of the data record (August 2006 to February 2007).

The fact that the recession limb of the IT has changed in a manner that is not proportional implies that the changes to the infiltrating surface within the BMP are also not proportional. This was somewhat expected as processes that degrade the infiltration performance of the BMP (suspended solids loading) are likely to impact the infiltrating area in a non-proportional fashion (bottom more than sides).

This analysis of the recession limb of the IT has so far just dealt with the shape of the recession limb itself and has not been related to any physical properties of the BMP.

While both the PCIB and the BTI were able to be approximated by a one-dimensional infiltration model, the IT with its extremely small footprint, deep ponding depths and nearly vertical side walls makes a one-dimensional assumption unrealistic.

Consequently, a model was developed to explicitly account for the IT's geometry. The rationale of the model (called McKsat) was that the relative contribution of infiltration through the sides and the bottom must be expressed in the shape of the recession limb. The model is an attempt to quantify basic physical parameters (hydraulic conductivity) to provide the best approximation of the observed infiltration from the BMP on a storm by storm basis.

Conceptually, McKsat divides the IT into two distinct parts, the bottom area and the sum of the side wall areas. In order to implement the model, several simplifying assumptions were made. First, infiltration from the BMP was broken into two distinct areas and flow is assumed to be perpendicular to their surfaces. The bottom area of the BMP is assumed to be homogeneous with respect to its hydraulic conductivity (K_{bottom}) and the hydraulic

conductivity of the sides is assumed to vary linearly from a value equal to that defined for the bottom to a separately defined value (K_{top}) for the sides at a depth of 5.21 ft (overflow depth). Because the side areas are effectively lumped together, no distinction is made among sides. As a result of the BMP's elevation above the water table and its extended periods of ponding, the BMP is assumed to have a limiting layer at the soil interface. For this type of application the development of a limiting layer is the rule rather than the exception (Bouwer 1989; Hillel 1998; Assouline 2004). This limiting layer is at or near saturation while the soil underneath or adjacent (in the case of the sides) is assumed to maintain relatively constant unsaturated conditions. Ponded infiltration through such a layer can be explained by a formulation of Darcy's law as follows (Bouwer 1978).

$$q = K_{layer} \frac{H_w + L_{layer} - \Psi}{L_{layer}} \quad (2.10)$$

Where:

- q = infiltration flux into soil [LT^{-1}]
- K_{layer} = hydraulic conductivity of limiting layer [LT^{-1}]
- H_w = depth of ponded water [L]
- L_{layer} = thickness of limiting layer [L]
- Ψ = constant soil moisture potential of unsaturated soil [L]

The thickness of the limiting layer is an idealized and largely hypothetical parameter.

Additionally, the soil moisture potential of the unsaturated subsoil is unknown.

However, the depth of ponded water is measured and the rate of infiltration will increase with ponded depth. The infiltration process was further simplified and the infiltration flux is simply estimated as the product of the hydraulic conductivity of the bottom (K_{bottom}) and the depth of ponded water, the equivalent of assuming the soil moisture

potential and thickness of limiting layer are both 1 ft in Equation 2.10. The flow rate of infiltration from the bottom is simply the product of the infiltration flux and the bottom area which is a constant (69 ft^2). At any given depth the averaged value for the hydraulic conductivity of the sides is found by interpolating between the two specified hydraulic conductivity values at a depth equal to half the current depth of ponded water. This averaged value for the hydraulic conductivity of the sides is multiplied by the averaged depth of water on the sides in order to estimate the infiltration flux from the sides. The assumptions and geometric relationships are shown in the following conceptual diagram.

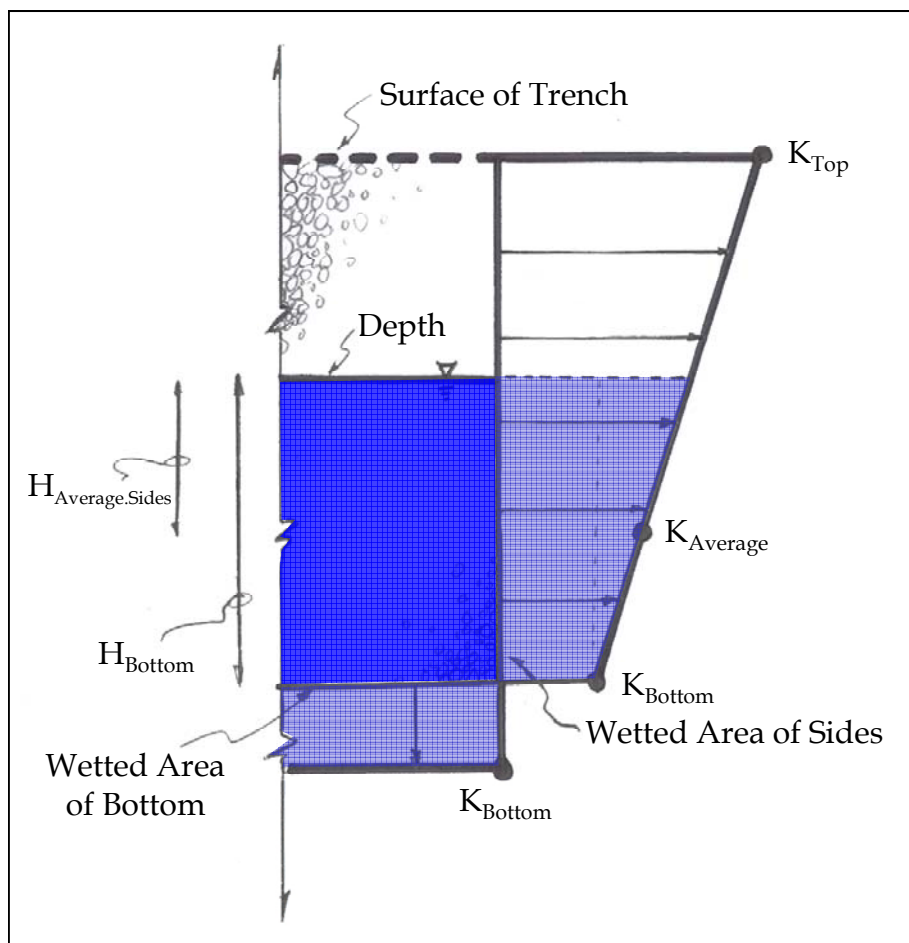


Figure 49. Conceptual diagram of hydraulic conductivity for McKsat model of the IT.

For each given depth there is a corresponding wetted area of the side walls, based on measurements taken during construction of the storage bed at the IT. The area is multiplied by the infiltration flux to calculate the total infiltration flow rate from the sides of the BMP for that time step. The two infiltration flow rates (bottom and sides) are summed to determine the total infiltration flow rate for each time step. The model assumes a 35 percent void space is provided by the crushed stone storage bed. Figure 50 summarizes the geometric data associated with the IT.

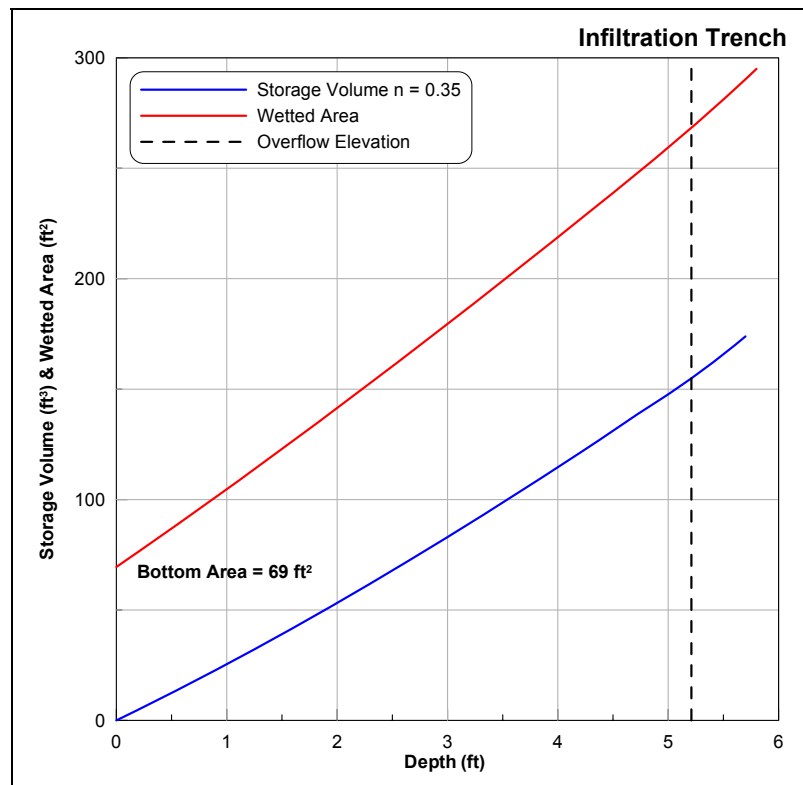


Figure 50. Geometric relationships for the IT BMP.

Figure 50 can be used to convert an observed recession limb into an infiltration hydrograph by calculating the change in storage for each time step during the recession

limb. With values specified (guessed) for the two unknowns, K_{bottom} and K_{top} , the same observed recession limb can be used with the aforementioned assumptions to calculate a predicted infiltration hydrograph. The closer the two infiltration hydrographs match, the better are the estimates of the hydraulic conductivities. This is the basis of the McKsat model. The match, or goodness-of-fit, of the observed and predicted hydrographs is quantified using a flow-weighted sum of squares method in an effort to provide an optimal and near-perfect mass balance.

$$Error = Q_{obs} \times (Q_{obs} - Q_{predicted})^2 \quad (2.11)$$

Where: Q_{obs} = observed infiltration flow rate for current time step [L^3T^{-1}]
 $Q_{predicted}$ = calculated infiltration flow rate for current time step [L^3T^{-1}]

These errors are calculated for each time step and then summed to represent the total error for the storm event. This allows estimates of hydraulic conductivity (bottom and sides) to be compared to one another based on their ability to predict the observed infiltration hydrograph.

An automated procedure is necessary to efficiently guess multiple values for the two unknowns and compare each to the observed infiltration hydrograph. This portion of the model is accomplished using the Visual Basic capabilities available in Excel. The program uses a Monte Carlo method where values within some input range are chosen (from a random distribution) for the hydraulic conductivities. Then the worksheet calculates the predicted infiltration hydrograph and determines its deviation from the

observed hydrograph. The program repeats this process a user-specified number of times and reports each combination of hydraulic conductivities and the goodness-of-fit measure. After the program has completed the iterations, the minimum error value is found and the corresponding hydraulic conductivities are reported. More details on the method along with the Visual Basic code and screenshot of the worksheet are provided in Appendix E.

To demonstrate the sensitivity of the model, the results (optimal values for K_{bottom} and K_{top}) from the April 8th, 2005 storm were increased and decreased by both twenty and fifty percent. For this storm event the best-fit hydraulic conductivities found for the recession limb were 0.24 and 1.3 in/hr for the bottom and top (sides) conductivities respectively. The results of the sensitivity check are shown in the form of infiltration hydrographs in Figure 51.

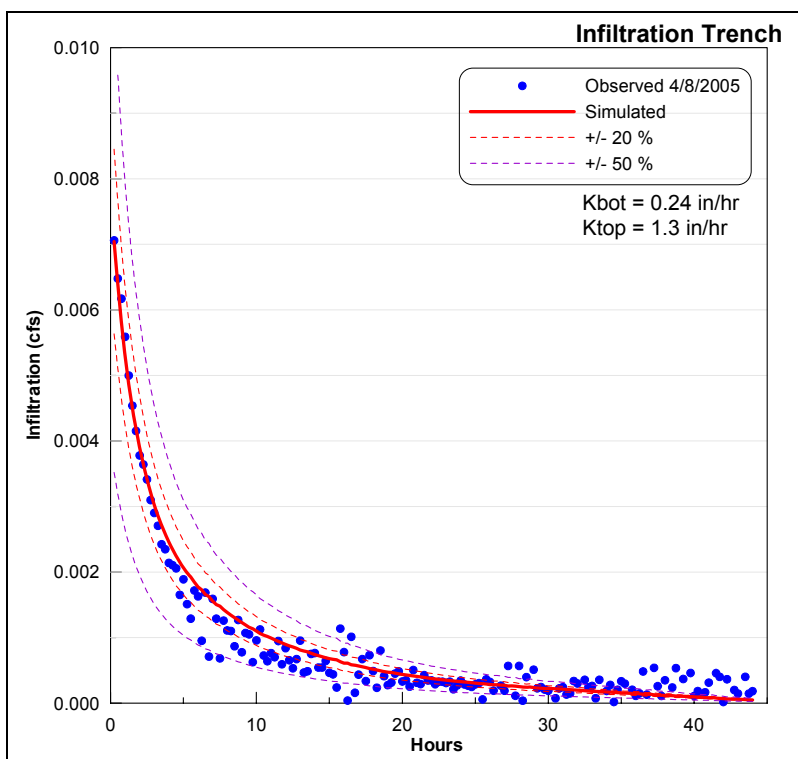


Figure 51. Sensitivity of the McKsat model for the April 8th, 2005 storm event.

All recession limbs that spanned from near-full to near-empty were used with the McKsat model. In total, the model was run for 72 different storm events between July of 2004 and March of 2007. For those storms with temperature data available, the average temperature was also calculated for each recession limb. The results (infiltration hydrographs) of this analysis for four selected storms are shown in Figure 52 and a summary of the results from all 72 storms is provided in Figure 53. The noise in the observed data that can be seen in the April 8th, 2006 storm event is caused by the extremely mild slope of the recession limb for this storm.

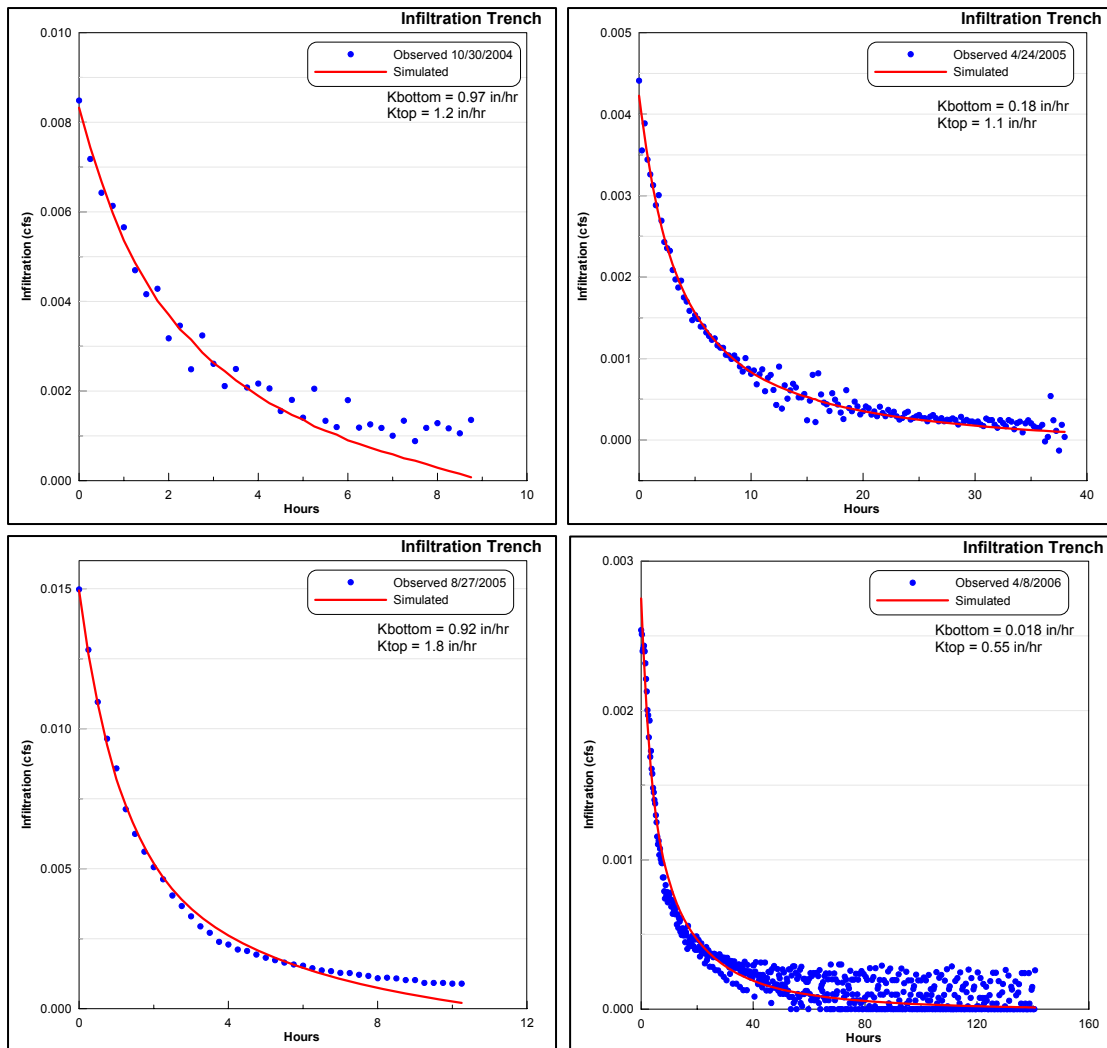


Figure 52. Observed and simulated (McKsat) infiltration hydrographs for four selected storms at the IT.

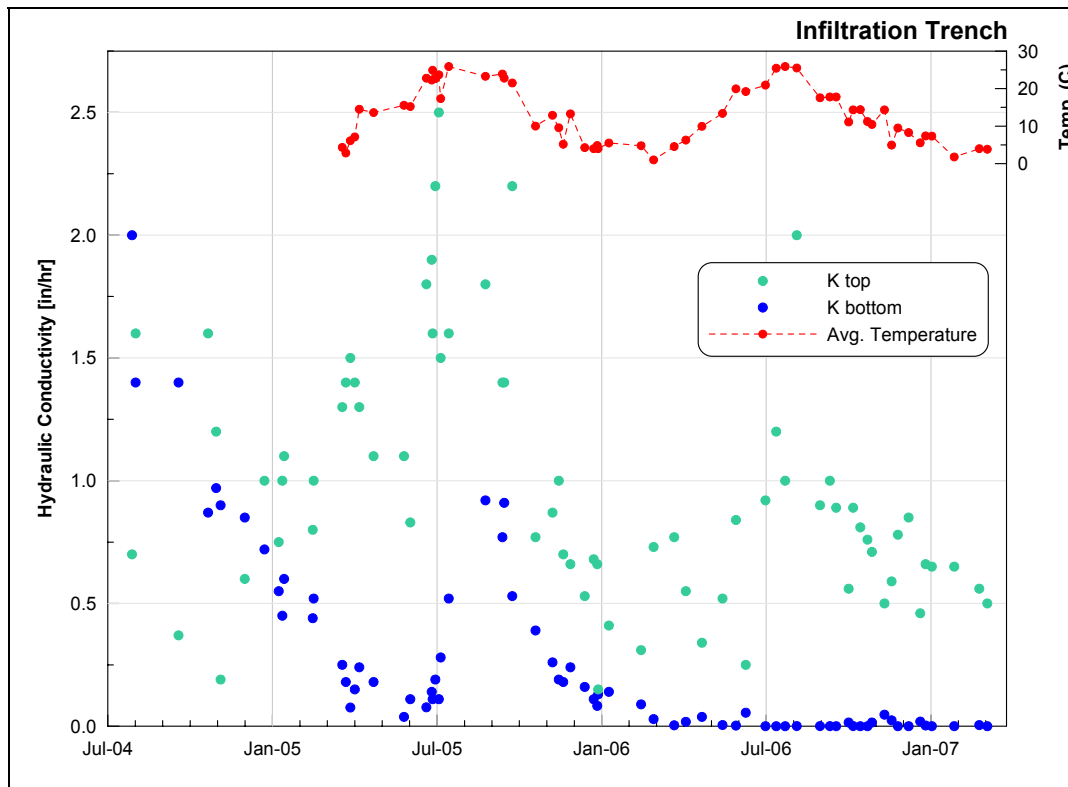


Figure 53. Results for all 72 storms from McKsat for the IT.

With the exception of only four storms early in the data record, the hydraulic conductivity of the bottom was found to be less than the value for the top of the side walls. Both values show a general decrease along with significant seasonal variation with higher values corresponding to higher measured temperatures inside the crushed stone storage bed. The K_{top} values show much more variation than the K_{bottom} values. This may be an indication that there is some influence of soil moisture potential at early ponding times or the influence of changes in soil temperature with depth. After July of 2006 the model predicts extremely low values for K_{bottom} . This coincides with the time in the data record when the characteristic shape of the recession limb shows extended tailing. During this time the K_{bottom} values essentially approach zero, indicating that the bottom of the IT is currently contributing little to the overall performance of the BMP.

Because both K_{top} and K_{bottom} have significant impact on the infiltration process from the BMP, it was chosen to examine an average value for hydraulic conductivity instead of looking individually at either K_{top} or K_{bottom} . Additionally, the average hydraulic conductivity of the sides is a function of both values $((K_{\text{top}}+K_{\text{bottom}})/2)$. A linear regression is again used to determine the portion of the seasonal variation that can be attributed to temperature-induced viscosity effects. As a result of overall decrease in performance of the IT, the residuals will show evidence of autocorrelation as is shown in Figure 54.

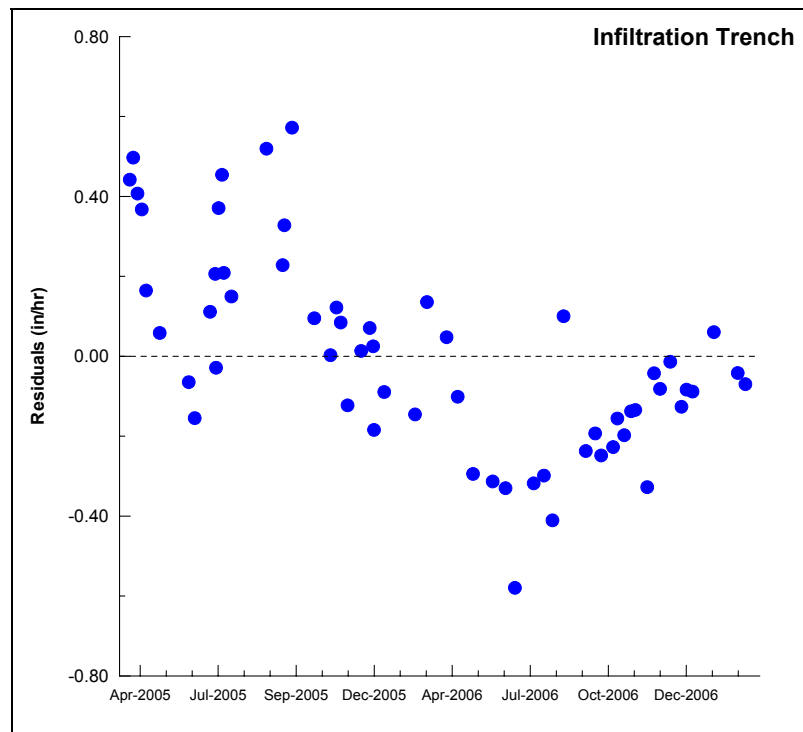


Figure 54. Autocorrelation check for average hydraulic conductivity vs. temperature regression for the IT for two-year data record.

The plot shows obvious signs of autocorrelation with early data points generally above the regression and later points below. This plot would show even more autocorrelation if the temperature data record started at the same time of the depth record, (July 2004) as the decrease was much more drastic at that time. Multiple linear regression with two dependent variables (temperature and age) was also not relevant due to the non-linear decrease exhibited by the data. An attempt was made to determine if the decrease would become linear when plotted against the cumulative days of prior ponding. This variable was chosen because it is a readily-calculated variable that characterizes the age of the BMP with relation to its loading. This was not successful in creating a linear relationship.

The decrease in performance of the IT has followed an exponential trend over the near three-year data record. However, over the last full year of record the performance of the BMP has not changed significantly. Only this part of the depth record was used in a linear regression to determine how the performance of the IT varies with temperature and the proportion of this variation that may be attributed to viscosity-related effects. The data spans from March 20th, 2006 to March 20th, 2007 and contains 28 storms that were analyzed with the McKsat model. Two of these storms, August 10th, 2006 and June 16th, 2006 were removed from the analysis because they are outliers with fairly high leverage on the final regression statistics as can be seen in Figure 54. The temperature in the IT, like the PCIB, was reasonably constant (usually only varying within 1°C of the average). The resulting linear regression of the average hydraulic conductivity found by McKsat vs. temperature is shown in Figure 55.

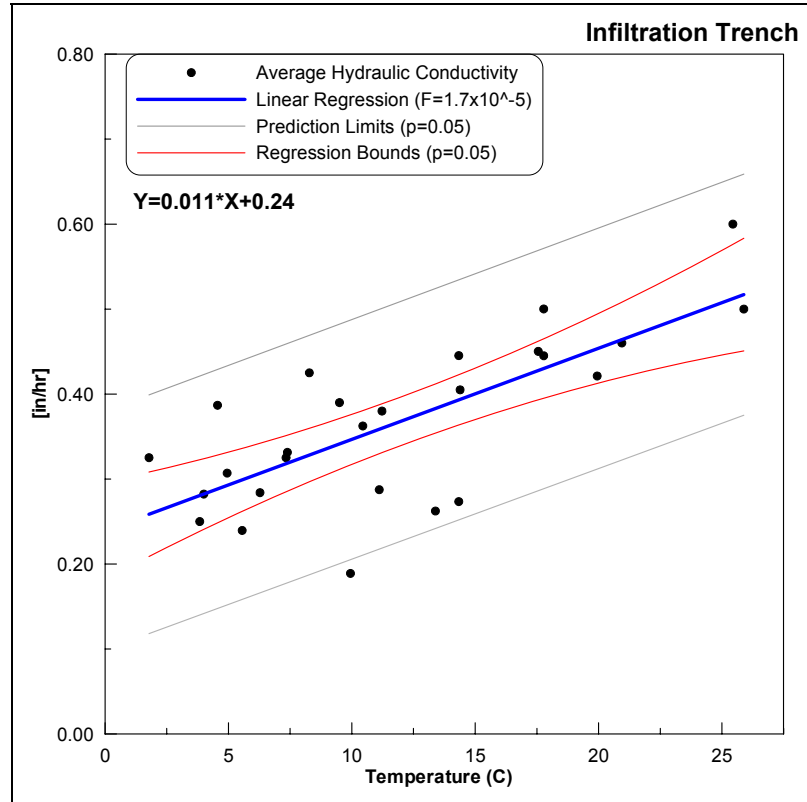


Figure 55. Temperature dependency linear regression for the IT for the last full year of data.

This linear regression is stronger than for either of the other BMPs ($r^2 = 0.54$, $P = 1.7 \times 10^{-5}$). The IT data indicates that the BMP shows an average hydraulic conductivity that varies by $0.011 \text{ in/hr/}^\circ\text{C}$, much more than either other BMP. By only using the last year of data, the autocorrelation assumption now appears to be met, as is shown in Figure 56.

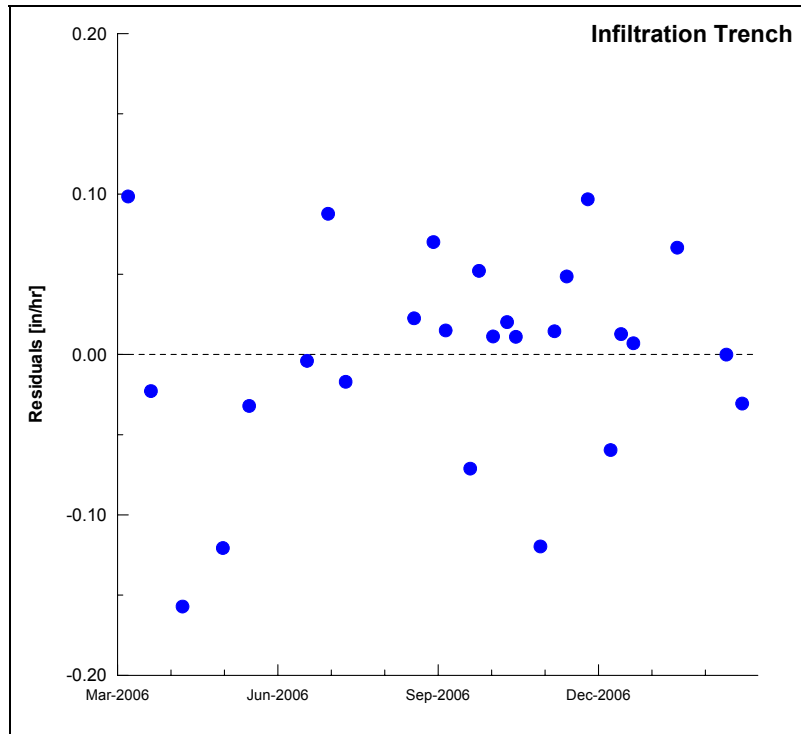


Figure 56. Check for autocorrelation of residuals for IT (last full year of data only).

To determine what portion of the variation can be attributed to temperature-based viscosity effects, the same procedure as was completed for the other BMPs was applied to the IT data. Based on the average temperature of 11.9°C the soil was estimated to have an intrinsic permeability of $5.1 \times 10^{-10} \text{ in}^2$ or $3.3 \times 10^{-9} \text{ cm}^2$. This estimate puts the soil closer to a silty sand or fine sand which are reported to range from approximately 1×10^{-10} to $1 \times 10^{-8} \text{ cm}^2$ (Fetter 1994). However, it is important to note that these values were derived from the average hydraulic conductivity $((K_{\text{bottom}} + K_{\text{top}}) / 2)$ found with the McKsat program. The results clearly show that although they remain fairly constant over the one-year period, the properties of the interfacial soil layer (namely intrinsic permeability) vary widely depending on the location in the BMP. The bottom likely has an intrinsic permeability that is an order of magnitude less than that of the soil near the

top of one of the side walls. The complete fluidity correction method is fully described in Section 2.2.1. The results for the IT are shown in Figure 57.

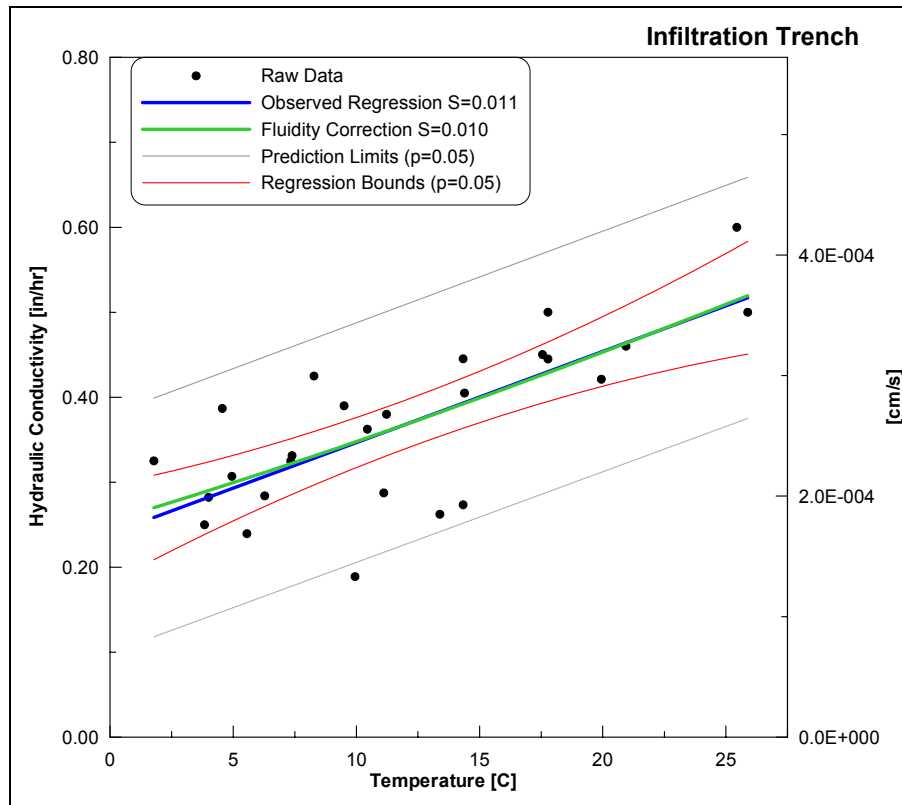


Figure 57. Temperature dependency of the predicted and observed average hydraulic conductivity for the IT (last full year of data record).

Remarkably the fluidity correction and observed variation are nearly collinear. The temperature variation (slopes) of both plots are so close that the slight nonlinear nature of the fluidity of water can be seen. Fitting a straight line to the fluidity correction (green) results in a slope of 0.010 in/hr/°C compared to the 0.011 in/hr/°C found in the observed McKsat results (blue). This indicates that the seasonal variation of the IT may be fully accounted for by temperature-induced viscosity effects. Finally, to illustrate this variation over the one-year data set, both graphs are plotted as shown in Figure 58.

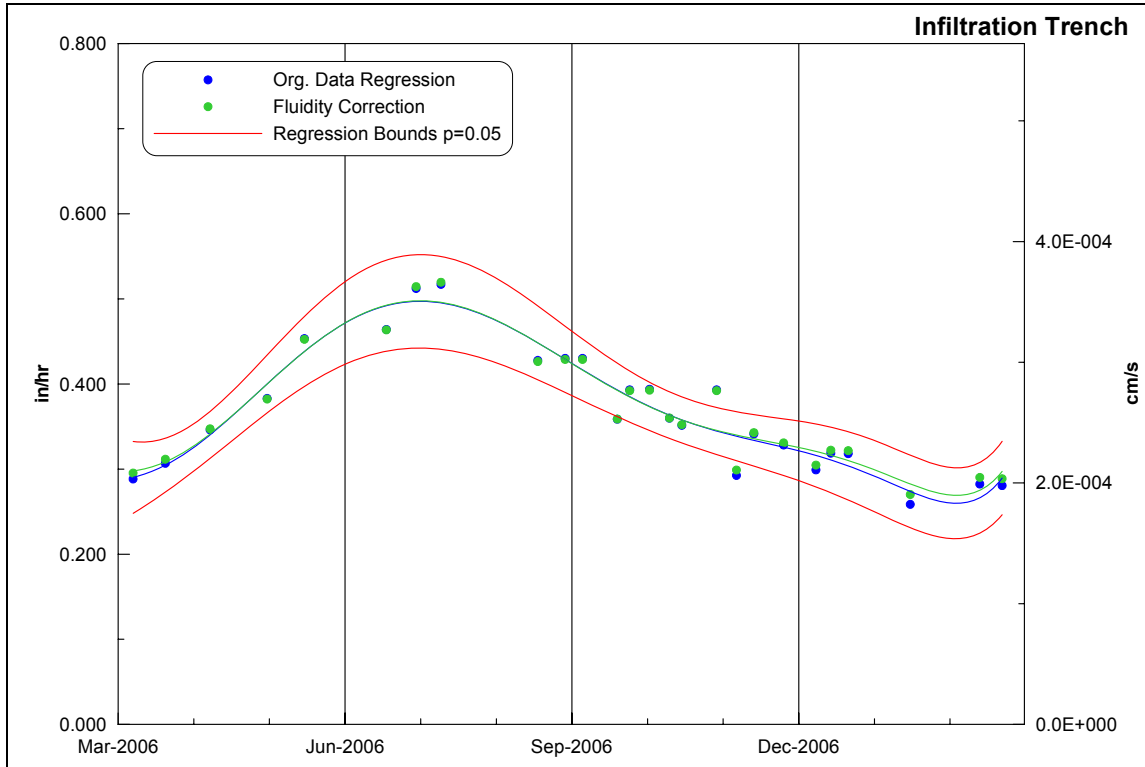


Figure 58. Observed data (McKsat) regression and predicted fluidity correction for hydraulic conductivity as a function of measured temperature over a one year data record for the IT.

In summary, the IT in less than its first three years of operation has shown significant signs of decreased infiltration performance. Early in the data record the BMP required less than one day to empty completely from overflow depth. Towards the end of the nearly three-year data record the IT requires nearly eight days to empty. Due to this extended recession period the BMP now rarely empties completely because of insufficient time between storms. The rate of the infiltration process at the BMP has followed an exponential decay, with the last third of the record showing only a slight decrease. Possible causes of this decrease are further discussed in Section 2.3. Even with such drastic signs of decreased performance, significant seasonal variation is present.

The seasonal variation was significant enough to reverse the downward trend for both full summer seasons in the data record. These two periods of increasing performance do not achieve full recovery to the rates of the prior year and therefore the IT exhibits an overall decreasing trend of infiltration capacity. The magnitude of the seasonal variation is nearly identical to that predicted from the temperature dependency of the viscosity of water and showed a drastic decrease from the first summer to the second. This is indicative of a decrease in the intrinsic permeability of the soil interface. This concept is further explained in the following section which further compares the temperature dependency of the IT to that of the other two BMPs.

2.2.4 Summary of Long-Term and Seasonal Performance of BMPs

Over nine years of hydrologic monitoring data was collected at three infiltration BMPs located on the campus of Villanova University. Analysis of this data has provided valuable insight into the characteristics of long-term concentrated infiltration of stormwater runoff. The BMPs all show significant seasonal variation and one demonstrates a systematic decrease in performance. In the following two sections the findings about temperature dependency and longevity for each infiltration BMP are compared and contrasted.

2.2.4.1 Temperature Dependency

All three infiltration BMPs exhibit substantial variation over the course of the year. The variation corresponds with the measured temperature of ponded water within the BMP,

with faster rates observed during higher temperatures. Generally, the magnitude of the variation is not significantly different from that expected from viscosity changes alone.

The timing of the variation is consistent for all three sites. The variation seems to be only slightly out of phase (delayed) from the variation of ambient temperatures in the northeast. This is not surprising considering the dampened and delayed temperature regime of the subsurface. The temperature measurements taken for this study were at the soil surface/ponded water interface and no subsurface temperature profiles were measured. Averaged one-foot depth temperature readings were taken as part of the in-situ infiltration testing conducted at the BTI, see Section 3.4. These temperature readings provided evidence that the near surface soil in the BMP typically lags behind both the diurnal and to a lesser degree seasonal surface temperatures. This effect is probably more dramatic at the other two BMPs which use a covered crushed stone storage bed which would provide more insulation. The low frequency of ponding events at the PCIB and the significant general decrease found at the IT make this comparison difficult to quantify.

Temperature data from each infiltration BMP was collected and analyzed to determine how much of the seasonal variation is associated with the temperature dependency of the properties of water. Linear regressions were used to relate the performance variable (estimate of hydraulic conductivity) to temperature. The three regressions are overlaid in Figure 59 for comparative purposes. The relevant statistics of both the observed data

regression and the fluidity correction are summarized in Table 4 and Table 5. The slope and y-intercept of the regressions are reported as ‘m’ and ‘b’ respectively.

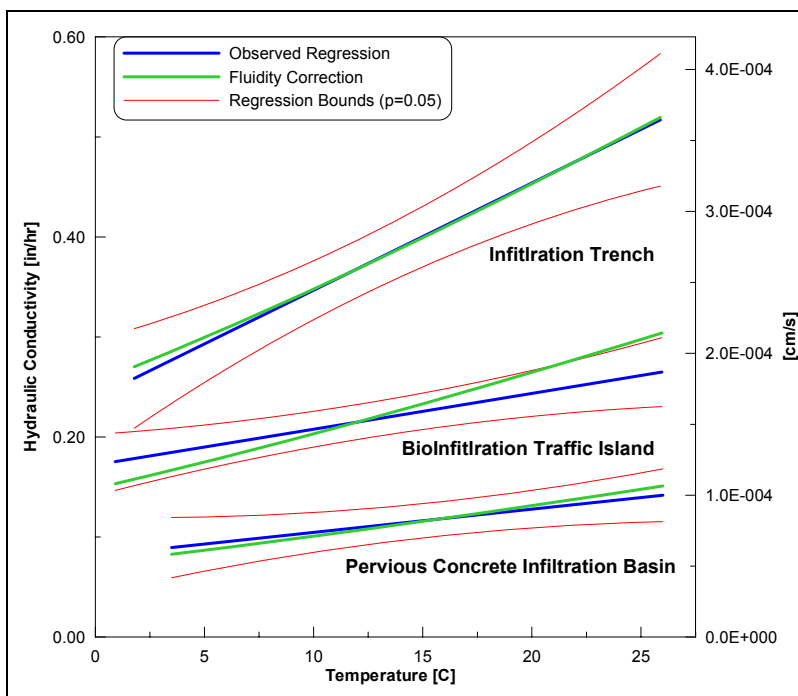


Figure 59. Overlay of linear regressions for all three infiltration BMPs.

Table 4. Summary of the observed temperature dependency for all three BMPs (blue lines).

| | m [in/hr/°C] | - 95 % | + 95 % | b [in/hr] | r² | P[*] |
|-------------|------------------------|---------|--------|---------------------|----------------------|----------------------|
| PCIB | 0.0023 | 0.00028 | 0.0044 | 0.081 | 0.32 | 2.9×10^{-2} |
| BTI | 0.0036 | 0.0015 | 0.0056 | 0.17 | 0.19 | 1.1×10^{-3} |
| IT | 0.011 | 0.0066 | 0.015 | 0.24 | 0.54 | 1.7×10^{-5} |

* *P* values less than 0.05 indicate significance at the 95% level ($\alpha = 0.05$)

Table 5. Summary of the fluidity corrections for all three BMPs (green lines).

| | k [$\times 10^{-10}$ in ²] | k [$\times 10^{-9}$ cm ²] | m [in/hr/°C] | b [in/hr] |
|-------------|---|--|------------------------|---------------------|
| PCIB | 1.5 | 0.95 | 0.0031 | 0.071 |
| BTI | 3.0 | 1.9 | 0.0060 | 0.14 |
| IT | 5.1 | 3.3 | 0.010 | 0.25 |

Two main conclusions can be taken from Figure 59. First, the IT has a higher hydraulic conductivity on average followed by the BTI and PCIB. Secondly, the same pattern applies to the variability, or slope of the regressions, with the IT showing the most variation and the PCIB showing the least. Although the slopes of both the PCIB and the BTI fall within the confidence intervals of one another (Table 4) and therefore cannot be assumed to be statistically different.

The magnitude of the seasonal variation is roughly a factor of two at the BMPs. This difference has a similar effect on the event ponding time over the course of a year. The amount that the recession rate is expected to vary (on average) over the annual temperature range at the BTI (0.090 in/hr) is greater than the 0.052 in/hr range in the mass flux that might occur at the PCIB. The presence of a crushed stone storage bed at the PCIB magnifies the temperature dependency and results in more seasonal variation at the PCIB (0.13 in/hr) than at the BTI. Additionally, the range of temperature measured at the BTI varied by an additional 2.54°C, compared to the PCIB. This is not surprising considering the insulating effect provided by a subsurface crushed stone storage bed.

The observed (blue) and predicted slopes (green) are similar for each of the three infiltration BMPs. The P values summarized in Table 4 are the result of a null hypothesis that the slope 'm' is equal to 0. In all cases the null hypothesis is rejected with all the P values being less than 0.05. A similar test can be conducted with the null hypothesis being that the slope of the observed regression (blue) is equal to the predicted slope (green). In the case of both the PCIB and the IT, the P statistic is greater than 0.05 (0.42 and 0.89 respectively), therefore the null hypothesis cannot be rejected. However, for the BTI the same procedure results in a P statistic of 0.023. It is likely that these two slopes are indeed statistically different from one another. This may be a result of the location that the temperature measurement was taken, as was discussed in Section 2.2.2.

The BTI exhibits the most scatter as indicated by an r^2 of 0.19, the lowest of all three regressions. This may be a result of the BMP's open storage bed, which is exposed to solar heating, while the other two BMPs have a subsurface storage bed. The temperature during the ponding event at the BTI is not constant and is only represented here by an average from the single measurement location. Other physical processes at the BTI (freeze-thaw, plant activity) may also contribute to this scatter.

The effect of shifting a hypothetical particle-size distribution towards larger diameter would tend to raise the hydraulic conductivity (increase y-intercept) and to increase the temperature dependency (slope) of the plots in Figure 59. This phenomenon has been documented in laboratory studies on repacked columns which compared two different textured soils (loam and sand) (Constantz and Murphy 1991). This same shift in the

particle-size distribution (of a well graded soil) would also increase the intrinsic permeability of the soil. Estimates for intrinsic permeability were made for the three BMPs and all are in the range reported for a silt to a silty sand, as displayed in Table 5 (Freeze and Cherry 1979). The intrinsic permeability estimate is largest for the IT ($5.1 \times 10^{-10} \text{ in}^2$) and smallest for the PCIB ($1.5 \times 10^{-10} \text{ in}^2$). The order of these estimates corresponds with what would be predicted independently, based solely on the particle-size distributions found in the subsoil of each BMP. While it is difficult and highly imprecise to make estimates of the intrinsic permeability based solely on particle-size distributions, it is expected that more granular (less fines) soils will have a higher intrinsic permeability. The particle-size distributions (mechanical sieve analysis only) provide an independent confirmation of the relative order of the intrinsic permeability estimates (see Figure 60).

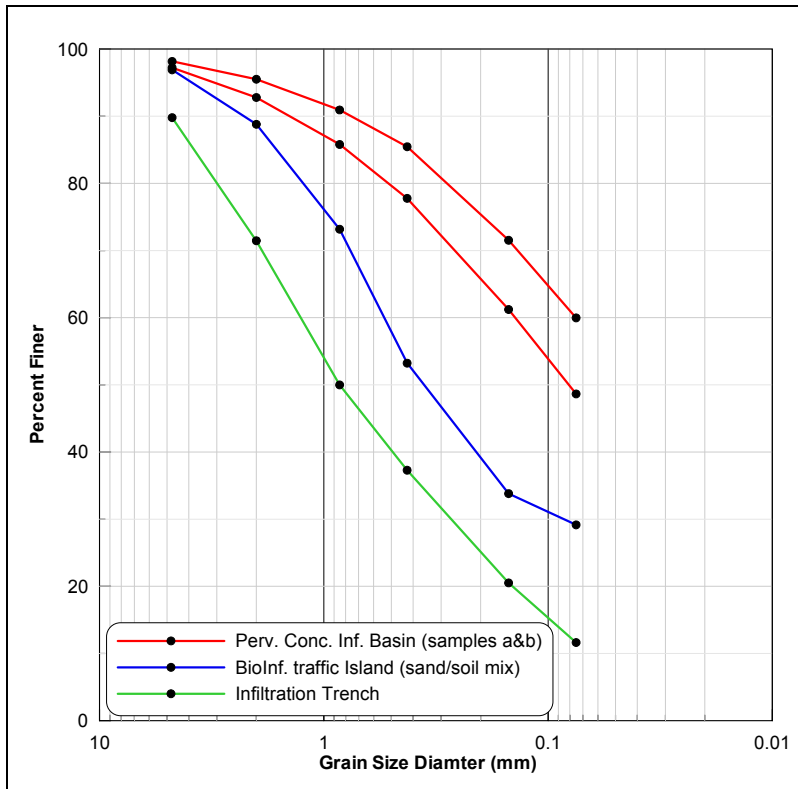


Figure 60. Particle-size distributions for the three infiltration BMPs.

The distributions show that the PCIB has approximately 55% of fines (passing no. 200 sieve) while the BTI has 30% and the IT has only about 10% fines. This is consistent with the linear regressions summarized in Figure 59 and Table 4 and consequently compatible with the intrinsic permeability estimates.

A distinction should be made between the terms “seasonal variation” and “temperature dependency”. Seasonal variation is the observed variation in performance expressed here as change in hydraulic conductivity or recession rate over the course of a year.

Temperature dependency refers specifically to the variation in performance as a function of temperature. The amount of seasonal variation for any infiltration BMP will depend on the regional climate of the location of the BMP (latitude, elevation), as these factors

influence the average annual temperature variation at the BMP. Secondly, the local climate of the BMP (open vs. underground bed, volumetric heat capacity of the soil, and in the case of an open bed, the albedo of soil surface) also affects the observed seasonal variation. Another factor that influences the seasonal variation of an infiltration BMP is thermal characteristics of the contributing area and their direct influence on the temperature of the stormwater runoff they produce. Finally, the soil properties, specifically intrinsic permeability will affect the seasonal variation. Soils characterized by more granular particle-size distributions (higher intrinsic permeability) will show more seasonal variation in addition to generally higher recession rates than those found in finer soils.

The temperature dependency of a BMP, as shown in Figure 59, directly accounts for the variation in temperature. It is not influenced by any temperature related attributes of the site, including location, orientation (open or below ground), drainage area characteristics and others. The temperature dependency is only influenced by the soil's intrinsic permeability, with a higher intrinsic permeability leading to an increase in the variation (slope) of hydraulic conductivity with temperature.

In summary, all three of the infiltration BMPs exhibit strong cyclical changes in performance over the course of the year. It has been demonstrated for two BMPs that the magnitude of the temperature dependency is not statistically different than the variation that would be expected based on the temperature dependency of the fluidity of the ponded water.

2.2.4.2 Longevity

One of the main concerns about infiltration BMPs is their expected lifespan (Schueler 1994). The three infiltration BMPs were examined for evidence of a systematic decrease in performance. The ponded recession rates for individual storms were calculated over the entire data set for each infiltration BMP. The data from the PCIB and the BTI were evaluated with multiple linear regressions which included both the measured temperature and age of the BMP. The results of these multiple linear regressions are shown in Table 6.

Table 6. Summary of multiple linear regressions.

| | n | Slope (Temp.) | | | | Slope (Age) | | | | r ² |
|------|----|---------------|---------|--------|--------|-------------|----------|--------|-------|----------------|
| | | in/hr/C | -95% | +95% | P | in/hr/yr | -95% | +95% | P | |
| PCIB | 15 | 0.0029 | 0.00093 | 0.0046 | 0.0067 | +0.030 | +0.00090 | +0.060 | 0.044 | 0.52 |
| BTI | 53 | 0.0037 | 0.0015 | 0.0059 | 0.0012 | +0.0064 | -0.023 | +0.035 | 0.66 | 0.19 |

A general rule of thumb for multiple linear regressions is that the number of observations should be at least the number of independent variable plus two multiplied by five ($n \geq 5 \times (k + 2) = 20$). Therefore, the PCIB multiple linear regression may be prone to overspecification with only 15 observations. The increase in the r^2 from 0.32 for the original regression to 0.52 here indicates that the model is overspecified. The slope with respect to temperature is slightly increased from 0.0023 to 0.0029 in/hr/°C, and the slope with respect to age is 0.030 in/hr/yr. This positive slope implies that the BMP may actually be experiencing improved performance over time. Due to the relatively small sample size, little significance should be placed on the results of the multiple linear regression.

For the BTI there are 53 observations, enough to ensure that there is little risk of overspecification with only two independent variables. The slope with respect to temperature is almost completely unchanged from that found in the original regression (0.0036 in/hr/°C), and the r^2 is also unchanged. Like the PCIB, the slope with respect to age is positive, indicating a general increase over time. Note that the 95% confidence interval for the slope includes zero and the P value for the slope with respect age is 0.66, much higher than the typically used acceptance criteria of 0.05 ($H_0: \beta=0$). The data indicate that the BTI is not displaying a statistically significant systematic change in performance over the two-year dataset examined here.

The analysis of the monitoring data from the IT shows an obvious change in performance. The decrease found in all of the incremental slopes is an exponential. The decrease appears to be present throughout the data record although it is interlaced with significant seasonal variation that has been attributed to the temperature dependency of the fluid properties of water. This temperature dependency is responsible for two periods in the data set when the incremental slopes actually increase in spite of the systematic ongoing decrease. The magnitude of the seasonal variation decreases from the first year to the second. This is expected based on the apparent decrease in the intrinsic permeability of the soil surface of the IT. Less permeable soils will exhibit a weaker (absolute) dependency on the temperature of the ponded water. In the case of the IT the change in the magnitude of the temperature dependency is another indication of the change in soil properties at the BMP. The processes that may be responsible for the

decrease at the IT and the sustained performance of the other two BMPs are discussed in Section 2.3.

Unlike the temperature dependency, it is difficult to make direct comparisons of the lifespan-related performances of the three infiltration BMPs. As described in Chapter 1, there are many major differences in the design of the BMPs, particularly in their watershed size and land use characteristics that play major roles in the longevity of the BMPs. The potential roles of these factors are explained in Section 2.3.

The IT was intentionally undersized to accelerate the aging process of the BMP. The span of the data record examined in this study is 2.75 years. It is difficult to estimate what type of a reduction in performance would be expected had the BMP been properly sized. However, there is a simple approach to estimate the “equivalent age” of the BMP based on suggested design guidelines. The Pennsylvania Stormwater Best Management Practices Manual recommends a 5:1 DCIA to BMP area ratio for this type of infiltration BMP (PADEP 2006). The IT has more than 25 times this recommended ratio.

Therefore, in the mere three years of its operation the IT has received an amount of runoff and potentially the suspended solids load equal to roughly 80 years of an equivalent properly-sized BMP.

Another important consideration is the timing of the data used in this analysis. The IT was the only BMP that showed an unquestionable decrease in performance. It is also the only site where the span of the data record went back to the first storm experienced by the

BMP. The PCIB experienced ponded infiltration events even prior to the end of construction in the Summer of 2002. The span of depth-monitoring data used in the PCIB analysis did not begin until almost a year and a half later. Any changes that may have taken place prior to data collection are not known. Construction began on the BTI in August of 2001, and the monitoring data began in January of 2003, again almost a year and a half later. While the decrease in performance found at the IT is drastic; very different conclusions would have been drawn had the first year and a half of data not been recorded. In order to illustrate this, the incremental slopes from the IT are plotted with the first one and a half years of the dataset removed. This results in data that span about 1.25 years and is shown in Figure 61.

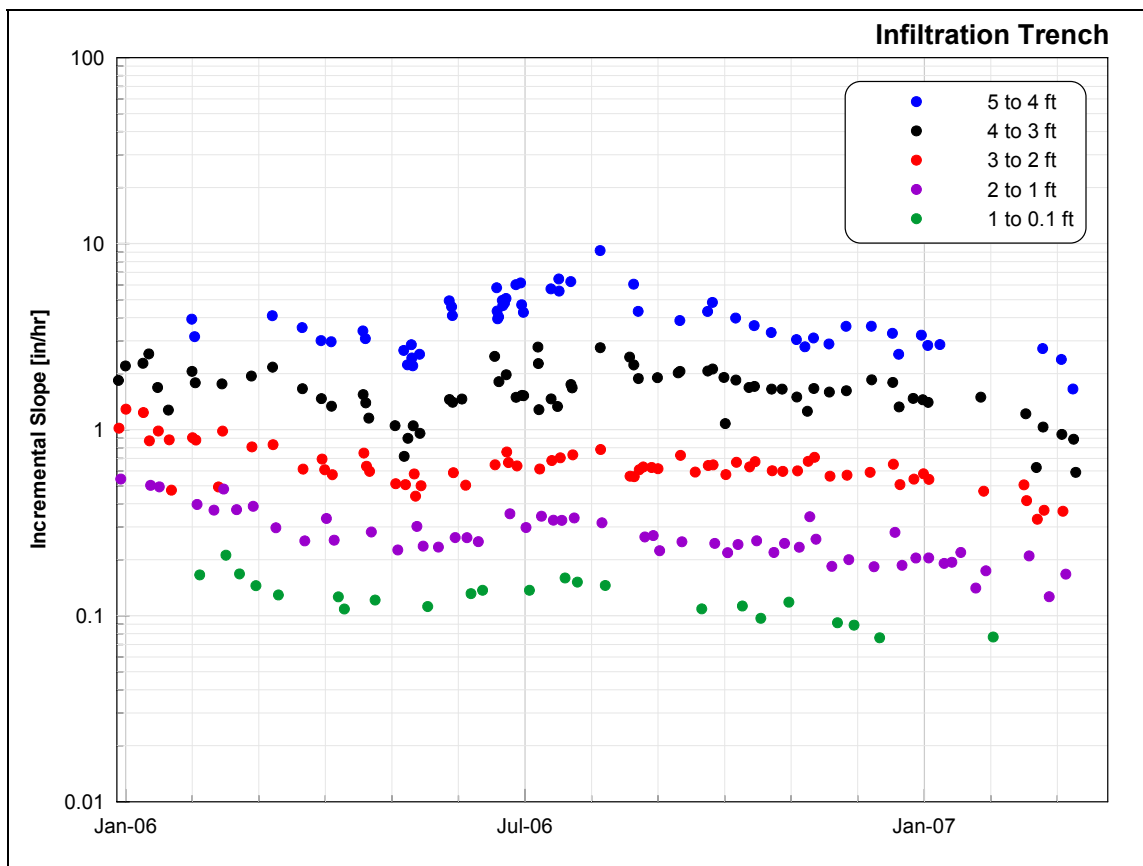


Figure 61. Incremental slopes found for a hypothetically shortened data span for the IT.

A visual examination of Figure 61 would indicate that the BMP is experiencing only a mild decrease in performance at lower depths. However, the previous year and a half of data clearly indicates that the infiltration process at the BMP has changed drastically over time. The early exponential decay in the performance of the BMP stopped, and the last year of data indicates that the performance of the IT is continuing at a fairly constant level.

The significance of this is that the results from the PCIB and the BTI should not be implied to be able to be extrapolated back (approximately one and a half years) to when the BMPs were first constructed. Both of these BMPs may have experienced a similar

(although likely not as drastic) start-up period of decreasing performance before arriving at the cyclic but constant level of performance. The processes that may be responsible for this behavior are discussed in the following section.

Table 7 displays the ages of the three infiltration BMPs and attempts to normalize their age based on the 5:1 ratio recommended by Pennsylvania Stormwater Best Management Practices Manual (PADEP 2006). This equivalent age comparison does not account for known differences in water quality and land use (parking area vs. rooftop, level of pretreatment among others).

Table 7. Relevant dates including the start and end of the data record used in this study along with equivalent age comparisons for the three infiltration BMPs.

| | Built | Start of data record | End of data record | Age at end of data record [yr] | Loading ratio [DCIA:BMP] | Equivalent age at end of data record [yr] |
|-------------|--------------|-----------------------------|---------------------------|---------------------------------------|---------------------------------|--|
| PCIB | 8/2002 | 1/2004 | 1/2006 | 3.4 | 3:1 | 2.1 |
| BTI | 8/2001 | 1/2003 | 3/2007 | 5.7 | 10:1 | 11 |
| IT | 7/2004 | 7/2004 | 3/2007 | 2.8 | 130:1 | 80 |

The length of the span of data is also important. The longest continuous data record studied here was four years for the BTI. While this is an unsurpassed length of time for the level of monitoring that has been carried out at the BMP, it is short of the desired lifespan of such a BMP. Longer time spans are needed to further determine what lifespan infiltration BMPs have. However, if the data span examined here is long enough to investigate potential failure mechanisms and exceeds the timing of many BMP failures

that have been reported, as will be detailed in the following section (Lindsey, Roberts et al. 1992; Schueler 1994).

2.3 Discussion and Review of Processes that Influence Infiltration

The objective of this section is to further explain and understand the long-term observations of infiltration (seasonal and longevity) found at the three infiltration BMPs using existing examples from published literature. Many of the processes and phenomena described in this section are highly dependent on many factors including drainage area size and characteristics, level of pretreatment, storage bed configuration, and others.

2.3.1 Temperature Dependency

The first objective of this section is to summarize examples from literature that focus on the temperature dependency of the infiltration process. Secondly, this section aims to relate the findings and knowledge gained from these previous researchers to the temperature dependency and seasonal variation found in the current investigation.

Hydraulic conductivity varies over thirteen orders of magnitude in commonly found sediments. Very few other physical properties exhibit such a wide range of variation (Freeze and Cherry 1979). Often values for hydraulic conductivity are referred to on an order of magnitude basis. Additionally, hydraulic conductivity values are typically found to be strongly heterogeneous; often with orders of magnitude variation over relatively small distances (Fuentes, Flury et al. 2004; Neurath, Sadeghi et al. 2005; Wuest 2005).

Different measurement techniques also yield very different estimates of hydraulic conductivity for a given soil, although estimates are typically on the same order of magnitude (Gribb, Kodesova et al. 2004). Temperature-induced variations in hydraulic conductivity (with water as the permeate) are roughly two-fold over typical annual temperature ranges. Considering the wide variability, extreme heterogeneity, difficulty and variability in measurement, along with the generally assumed isothermal groundwater conditions, the temperature-induced variation of hydraulic conductivity for many groundwater-related circumstances is not significant and therefore, not considered. However, there are specific applications where the temperature dependency of hydraulic conductivity can be a significant factor.

Large scale groundwater recharge applications, such as wastewater effluent recharge and stormwater infiltration, are usually not directly concerned with the variability (heterogeneity) of the infiltrating soil area. The average hydraulic conductivity of the surficial soil is what determines their ability to meet design criteria. The steady recession rate of the ponded water in a large recharge basin is representative of this average hydraulic conductivity. In these large scale infiltration (recharge) applications with loading rates sometimes approaching 300 ft/yr (3,600 in/yr) a change in the hydraulic conductivity of a factor of two can have major operational implications (Lin, Greenwald et al. 2003). Often these infiltration applications, specifically stormwater infiltration, collect water from areas which may drastically influence its temperature (asphalt for example) and concentrate it into areas exposed to ambient air temperatures and solar radiation. This enables the temperature of the ponded water to vary with the same

magnitude as the ambient air temperature as has been found at the BTI. Consequently, this allows the hydraulic conductivity to vary in the same manner. In summary, temperature effects on hydraulic conductivity are typically ignored. In specific applications the temperature dependency of hydraulic conductivity can be significant. In these situations it is important to consider the effect of temperature when attempting to describe the long-term performance of any infiltration/recharge application.

2.3.1.1 Examples from Literature

There has been little research published that deals with the continuous monitoring of infiltration BMPs. This is due to their relatively recent widespread regulation and implementation and to the considerable cost and time associated with continuous monitoring. One exception is the paper titled “Hydrologic Modeling of a Bioinfiltration Best Management Practice” which dealt with the same infiltration BMP in the current study (Heasom, Traver et al. 2006). Without long-term continuous monitoring, seasonal variation is difficult to discern. Few other studies have monitored over a long enough period to observe seasonal variation, and the few that have often attribute it to changes in biological activity, specifically changes in evapotranspiration. This study has shown that the majority of the seasonal variation observed in the recession limb can be attributed to the temperature dependency of the fluid properties of water. The temperature dependency of the infiltration process has been observed at all three infiltration BMPs. The observed magnitude and impact on the total event time of ponding is often surprisingly large. The purpose of this section is to further explain the temperature dependency by summarizing related studies which also focused on the temperature

dependency of the infiltration process. Previous research on this topic can mainly be found in journals focused on soil science and soil physics with a few other related sources.

The aforementioned study which also dealt with the BTI found that accurate hydrologic simulation of the BMP required so-called “seasonal parameters”. The study focused on a method to accurately simulate the hydrology and hydraulics of the BMP and its drainage area. The Army Corps of Engineers HEC-HMS was used to construct the hydrologic model. The infiltration process within the BMP was simulated with the use of a diversion element and storage-outflow relationship. Based on calibration to observed data, seasonal parameters were found for both the diversion (initial diversion volume) and the stage-outflow relationship (steady infiltration). The steady recession rate of the ponded surface was found to vary from 0.15 to 0.50 in/hr (Heasom, Traver et al. 2006). The model was able to achieve exceptional agreement with the observed level data collected at the BMP. This work demonstrates that seasonal variation of infiltration BMPs should be taken into consideration for any long-term or continuous simulation of infiltration BMPs. This is the only work that directly mentions changes in the viscosity of water as cause for the seasonal variation of a stormwater BMP.

In a study on the hydrology and nutrient removal of bioretention, the authors found statistically significant differences in the ratio of bioretention outflow to inflow between different seasons. While this comparison did not account for differences in storm characteristics between seasons, it represents a significant finding on the potential

seasonal variation of stormwater infiltration BMPs. The authors associated these variations with two potential causes. The first potential source of the variation was identified as seasonal changes in evapotranspiration. The second was the seasonal impact of shallow groundwater. While it was noted that the study area typically has shallow depths to groundwater, groundwater levels were not monitored as part of the study (Hunt, Jarrett et al. 2006).

Research has been done on the temperature dependency of infiltration for many years. The earliest obtained here was published in 1943 which includes references related to the temperature dependency of infiltration dating back to the late 1800s (Duley and Domingo 1943). There has been a significant amount of laboratory studies (packed columns) performed to quantify and further explore the temperature dependency of infiltration. One of the most widely referenced studies was performed on columns with two different soil types, Aiken Loam and Olympic Sand. The researchers ran controlled infiltration tests on the two columns at temperatures of 5, 25 and 60°C. The authors reported increases in the intake rates of both materials of three to four-fold for both soil types over the range of temperatures they examined. The study also successfully simulated the column infiltration experiments with a “simple temperature-sensitive modification to the Green and Ampt infiltration equation” (Constantz and Murphy 1991). The modification simply assumes that the hydraulic conductivity varies with the reciprocal of the viscosity of water for a given reference temperature as shown below.

$$K(\theta)_T = K(\theta)_{20} \times \left(\frac{\mu_{20}}{\mu_T} \right) \quad (2.12)$$

Where: K_T = hydraulic conductivity at input temperature [LT⁻¹]
 K_{20} = hydraulic conductivity at 20°C [LT⁻¹]
 μ_T = viscosity of water at the input temperature [ML⁻¹T⁻¹]
 μ_{20} = viscosity of water at 20°C [ML⁻¹T⁻¹]

This method assumes that the saturation of the wetted zone does not change with temperature and that the matric potential gradient also is not affected by changes in temperature. Other researchers have determined that soil moisture potential, $\psi(\theta)$ is somewhat affected by temperature. This effect has been found to be primarily due to the temperature dependency of the surface tension of water (Hopmans and Dane 1985; Hopmans and Dane 1986). However, these changes are minor and would appear to be “negligible compared to the change in $K(\theta)$ with temperature”, especially under late-time or ponded infiltration (Constantz and Murphy 1991).

In addition to laboratory studies some research has been performed on temperature-induced variation at the field-scale. The temperature-induced influence on infiltration is often noticed, and consequently studied by chance. For example, perhaps one of the most thorough and controlled examinations of field-scale temperature variations on infiltration was performed by D.B. Jaynes (1990). This work was especially important because the author observed drastic temperature-induced diurnal variations in infiltration and proposed a conceptual mathematical model which included a temperature-dependent hydraulic conductivity term. The author also suggested that the presence of a surficial limiting layer was prerequisite for the observed diurnal variation. The author and others

were in the process of conducting a Bromide “solute-leaching” experiment using a continuously flooded enclosed area. The investigators were surprised to notice that the water required to maintain a constant ponded depth varied considerably over the course of a day, with the highest flow required in the late afternoon. According to the author, “The cyclic variation of infiltration rate after a prolonged period of continuous ponding (>30d) was totally unexpected” (Jaynes 1990). The author also states that although they had assumed that there would be temperature variations in the shallow ponded water due to solar radiation, he thought that the repercussions of these temperature variations would be “negligible”. The experimental setup consisted of a 6.1 × 6.1 m (20 × 20 ft) sheet metal border which was driven 0.2 m (8 in) into the ground. Surrounding the centermost 3.66 × 3.66 m (12 × 12 ft) area was a similar sheet metal enclosure. Both enclosures were maintained with approximately 40 mm (1.9 in) of ponded water. The amount of water required to maintain the specified depth was measured with two independent flow meters and additionally the exact depth of water was measured. The combination of these measurements enabled the researchers to accurately monitor the infiltration flux [LT⁻¹] with the following conservation of mass-based equation:

$$q = \frac{Q}{A} + \frac{dH}{dt} \quad (2.13)$$

Where: Q = the measured flow rate of supply water [L³T⁻¹]
 A = the area of the flooded area [L²]
 H = depth of ponded water [L]

In addition to flow and depth, the temperature beneath the basin was also measured at depths of 0, 100, 200, 600 mm (0 - 2 ft).

The researchers found that the infiltration flux varied from 15 to 27 mm/hr (0.57 to 1.1 in/hr) over the course of one day. The variation of the infiltration flux followed the variation of the measured temperatures. The ponded soil surface was exposed to direct solar radiation (experiment was located in Arizona) which resulted in temperatures ranging from 15 to 32°C over the course of one day. No attempt was made to prevent or control evaporation from the ponded water surface. This was justified with Class A pan evaporation measurements at a nearby location. The maximum daily evaporation measurement never exceeded 15.4 mm/day (Jaynes 1990). This corresponds to an averaged hourly rate of 0.025 in/hr which at best only “represents about 3% of the average flow rate and is not significant when compared to the $\pm 25\%$ daily variation...” (Jaynes 1990).

Due to the long period of continuous ponding prior to the five-day experimental period, the author assumes that the infiltration was dictated by a unit hydraulic gradient and had also established a one-dimensional flow pattern. The author did not expect to see significant temperature-induced variation in the rate of infiltration. The author explains this original theory as follows:

Although the temperature of the infiltrating water was varying throughout the day due to solar heating, we expected this variation to cause only negligible effects. Temperature fluctuations in the soil were expected to penetrate, at most, only a meter below the surface in response to the daily temperature cycle. We also assumed that a unit gradient and a nearly one-dimensional flow regime had been established in this deep profile due to the continuous ponding. Under these conditions, a simple thought experiment would lead us to believe that any change in the hydraulic properties in the surface 1 m would be dominated by the

unchanging hydraulic properties of the much thicker lower profile and, therefore, little change in infiltration rate would be seen. That is, since the average hydraulic conductivity of the profile is equal to the harmonic average of the hydraulic conductivity of each layer, the effect of a changing conductivity in the relatively thin surface layers would have little effect on the overall conductivity.

However, when water is ponded on a soil, the soil profile will generally create a thin surficial limiting layer of lower hydraulic conductivity (Jaynes 1990; Fox, Bissonnais et al. 1998; Hillel 1998; Assouline 2004; Lado, Paz et al. 2004). This topic is further addressed in Section 2.3.2. Due to the large amount of observed diurnal variation in the mass flux rate of infiltration, the author asserts that a restricting surface layer must be present. The author explains how this condition would impact the infiltration process and its temperature dependency as follows:

If the soil profile consists of a layer near the surface having even a slightly lower permeability than the underlying layers, then this near-surface layer may act as a restricting barrier to flow. During infiltration, the restricting layer would be saturated while the underlying soil was unsaturated. Restricting layers at or near the surface are common in soils due to crusting from rain, slaking of the surface during irrigation, or compaction due to traffic. Any changes in the permeability of the restricting layer would propagate down through the unsaturated profile. Thus, changes in near-surface soil temperature have the potential of greatly altering the infiltration rate in these soils.

In an effort to model and further explain the theory behind the observed diurnal variation, the author proposed a theoretical model. The objective of the model was to conceptualize and reproduce the magnitude of the diurnal variation. Therefore, no effort was made to precisely fit the simulated and observed data. Instead, typical soil parameters were taken from literature to represent the system. The model used a combination of the one-dimensional heat-transfer equation and a one-dimensional version of the Richards

equation, written with the viscosity-based temperature correction for hydraulic conductivity (Hopmans and Dane 1985; Constantz and Murphy 1991). With this simplified model the author was able to achieve an adequate representation of the observed variation in the mass flux rate of infiltration.

Another example of field-scale observation of temperature-related effects comes from a large scale effluent recharge and recovery study, often referred to as soil aquifer treatment or SAT. The temperature dependency was also not originally the focus of the study. The magnitude of the variation and its close dependency to temperature was a surprise to the researchers and therefore warranted further investigation. This study focused on depth and temperature data from four different recharge basins over an intermittent four-year period (Lin, Greenwald et al. 2003). The purpose of the research was to attempt to explain the observed seasonal variation to temperature-induced viscosity changes of water. The researchers used similar methods as those employed in this study. The steady (linear) recession rate of the ponded water was calculated for each flooding (loading) and recharge cycle. The authors refer to this slope as the “infiltration rate”, a term which is otherwise avoided in this document due to its ambiguous nature. The authors also assume one-dimensional flow and the late-time infiltration assumption with the hydraulic conductivity being the dominant factor. The recession rates for the recharge basins ranged on average from 0.2 in/hr to 3.0 in/hr. To determine the contribution of the viscosity effects the authors normalized averaged infiltration rate values to their averaged value near 25°C. They did the same normalization process to a measure of the fluidity of water. The normalized infiltration rates were plotted versus the

measured temperatures and the slope of linear regressions fit through these plots for each recharge basin were compared to the slope of the normalized measure of the fluidity of water versus temperature. This method showed that the temperature dependency of the normalized infiltration rates was approximately ~1.5 - 2.5 times that of the fluidity of water (Lin, Greenwald et al. 2003).

Another field-scale example of the temperature impact on the infiltration process is the paper titled “Influence of Irrigation Water Properties on Furrow Infiltration: Temperature Effects” (Lentz and Bjorneberg 1999). In this investigation the authors conducted full-scale furrow irrigation experiments where they were able to control the irrigation water temperature and measure the rate of furrow infiltration. In addition to the field testing they performed column tests and found increased intake rates with temperature in both experiments. In fact, the increase in mass flux of infiltration between the furrow and column were 2.3%/°C and 2.0%/°C, respectively, and were not significantly ($P = 0.24$) different from one another (Lentz and Bjorneberg 1999).

The temperature dependency of hydraulic conductivity has also been used to explain diurnal variation in stream flow (Constantz, Thomas et al. 1994; Ronan, Prudic et al. 1998). In the study by Constantz et al. (1994) the researchers measured stream flow losses in two streams. Both streams were located well above the water table. The variation of the diurnal stream flow losses for one 160 m (520 ft) reach was on the order of 6%. For example, on one day of the four-day experiment, the stream flow loss in the reach went from 26 % at approximately 18:00 to 20% the following morning (~6:00).

Corresponding diurnal stream temperatures ranged from 4 to 18°C. The second studied reach was longer at 655 m (2,150 ft) long. The researchers made estimates and took some direct measurements of the evapotranspiration rates over the length of the reach and adjacent bank areas. This was accomplished using a hemispherical evaporation chamber which “was used to estimate water vapor flux densities from dawn to dusk at hourly intervals.” (Constantz, Thomas et al. 1994). This measurement was taken over the exposed unsaturated soil alongside the stream, over the small shrubs and grasses, and over the stream itself. Evapotranspiration from trees (only 20% coverage of study floodplain) was estimated using the Penman approach with locally measure meteorological data for the study period (Penman 1948). Over the course of one full day the stream reach lost 1,555 m³/day (54,870 ft³) of water as measured by the upstream and downstream Parshall flumes. During this same time a total evapotranspiration rate for the area was estimated at only 65.8 m³/day (2,320 ft³). This represents less than 5% of the stream flow loss in the reach. The experimental location was the Tijeras Arroyo in New Mexico, and the experiment was carried out in the middle of May with stream flow temperatures ranging from 12 to 22°C (Constantz, Thomas et al. 1994). Relating the stream flow loss to an equivalent infiltration flux along the reach was accomplished by developing a relationship for the wetted area of the streambed. The aforementioned 10°C temperature range should result in an increase of the hydraulic conductivity of the streambed of 29%. The stream flow loss data indicated that the infiltration flux out of the stream varied by 27% on average over the entire reach. This confirmed the hypothesis that the stream flow losses in losing streams is dominated by the temperature-induced

changes in stream bed hydraulic conductivity and not by evapotranspiration, as has often been assumed.

In a similar study by Ronan et al. (1998) the researchers collected temperature data and stream flow in an ephemeral stream in Nevada. The authors used the same method to translate stream losses into an equivalent infiltration flux over the ~1,000 m (3,000 ft) study reach. Evapotranspiration was measured and estimated by the same methods as the previous study. The diurnal change in evapotranspiration was found to explain only 6% of the diurnal variation in stream flow. Again the stream flow variation was found to be primarily a function of the diurnal changes in stream water viscosity. The infiltration fluxes in the reach were found to vary from approximately 1.0 to 2.0 in/hr over the course of a typical day in the study. Experimental data (~four days) was collected on two separate occasions approximately a year apart. The first set of experimental data was used to calibrate a variably saturated groundwater model with heat transport (VS2DH). The model was calibrated to both the temperature data and the infiltration flux estimates. The following set of data was used to determine whether the calibrated model and the current measured temperature data could be used to successfully predict the infiltration flux in the reach. The stream bed was modeled with a thin 3 mm (0.1 in) limiting surficial layer. The sediment underneath the surface layer was represented with a hydraulic conductivity that was forty times higher than that of the surface layer. The authors note that “this lower hydraulic conductivity layer at the surface greatly accentuates the magnitude of temperature driven viscosity effects” (Ronan, Prudic et al. 1998). The model was able to accurately predict diurnal temperature variations beneath

the stream bed. The calibrated model was relatively successful in predicting the infiltration flux of the second set of experimental data based solely on temperature measurements. This indicates that there is promise in the ability to estimate stream flow losses based on temperature data once a model is calibrated to the specific stream reach. Other studies have also attempted to use temperature profiles to estimate recharge (Constantz, Tyler et al. 2003; Doman, Ferre et al. 2003; Cheviron, Guerin et al. 2005).

In summary, the temperature dependency of the infiltration process has been studied at both a laboratory scale and discovered and consequently studied at a field-scale. These studies have related the temperature dependency of hydraulic conductivity to temperature-induced changes in the viscosity of water. The variation and magnitude of evapotranspiration rates are generally insignificant compared to the variation and magnitude of infiltration losses. While the temperature dependency of hydraulic conductivity is often not necessary to consider at the field-scale, in some applications it can be a significant factor. These applications include any surface infiltration operation, especially when the infiltrating water is susceptible to seasonal and diurnal changes in temperature. Some examples of such situations include soil aquifer treatment and wastewater recharge, small/shallow losing stream reaches, and stormwater infiltration. All of these situations tend to create a limiting surface layer of lower hydraulic conductivity, as further detailed in the following section. This ensures unsaturated conditions lower in the soil profile. This shallow thin layer will tend to accentuate the effect of temperature-induced changes in hydraulic conductivity.

2.3.1.2 Relation to Villanova Infiltration BMPs

The temperature dependency of the infiltration process has been demonstrated and studied at both the laboratory and field-scale. Practical applications of the temperature dependency have been explained at large-scale soil aquifer treatment operations and used to explain the diurnal variation of small losing stream. While seasonal variations in stormwater BMPs have been observed, the origin of the variation has not been previously examined (Heasom, Traver et al. 2006; Hunt, Jarrett et al. 2006). The same processes and characteristics of the previously mentioned studies make the temperature dependency of hydraulic conductivity applicable to the infiltration of stormwater runoff.

In the study by Lin et al. (2003), which focused on the temperature dependency of soil aquifer treatment recharge basins, the author found slightly more variation than could be explained by temperature-induced viscosity changes alone. The authors reported that the variation was found to be between ~1.5 and ~2.5 times what would be expected from viscosity changes alone. In the current study a slightly different method was used to determine the potential influence of the viscosity changes (see Section 2.2). However, the same ratio (viscosity dependency/observed dependency) can be calculated and used as a rough comparison for the three infiltration BMPs. The values in Table 8 are smaller and closer to one (perfect agreement) than those (~1.5 to 2.5) reported by Lin et al. (2003).

Table 8. Summary of the observed and predicted temperature dependencies for the three BMPs.

| | Observed [in/hr/°C] | Predicted [in/hr/°C] | Pred./Obs. [-] |
|-------------|--------------------------------|---------------------------------|---------------------------|
| PCIB | 0.0023 | 0.0031 | 0.74 |
| BTI | 0.0036 | 0.0060 | 0.60 |
| IT | 0.011 | 0.010 | 1.1 |

A commonly found theme among the literature is the comparatively insignificant effect of evaporation and transpiration. Pondered evaporation is typically considered to be negligible in effluent recharge operations and has been cited as being two orders of magnitude lower than “average” infiltration fluxes (Berend 1967). Evaporation was also found to be insignificant during the shallow pondered infiltration experiment conducted by Jaynes (1990) in Arizona. In the stream flow loss study by Constantz et al. (1994) the infiltration fluxes calculated in one reach ranged from 0.1 to 0.3 in/hr. These are well within the ranges of those found in the current study. For example, the steady pondered recession rates at the BTI typically range from 0.2 to 0.4 in/hr over the course of the year. The study by Constantz et al. (1994) indicates that the observed recession rates and their seasonal variation are dominated by infiltration and not evapotranspiration, with evapotranspiration accounting for only ~5% of the variation. The significance of evaporation is related to the absolute rate of infiltration. In other words, if the infiltration rate is extremely slow (orders of magnitude lower than those described here) then evaporation will be a more significant process.

The evaporation rates reported in these studies would probably be very conservative estimates for evaporation in the Northeastern US, while the infiltration fluxes reported in these studies are in the same range as those found at the three infiltration BMPs.

Therefore, evaporation is an insignificant process compared with infiltration, especially for the two BMPs with underground storage beds.

Another significant conclusion of these studies is the theory proposed by Jaynes (1990) that the temperature dependency of the infiltration process implies the presence of limiting surface layer. The author asserts that a restricting surface layer must be present, due to the diurnal variation in the rate of infiltration. This limiting layer type of flow condition is expected at the three infiltration BMPs studied here.

In summary, these studies have shown that temperature-induced changes in the hydraulic conductivity are adequately explained by changes in the viscosity of water. Additionally, these studies have highlighted specific applications where this effect becomes significant. The examples have also shown that while evaporation and transpiration were not measured as a part of this study, they are likely to be insignificant compared to the variation in hydraulic conductivity and infiltration.

2.3.2 Soil Surface Evolution and BMP Longevity

The purpose of this section is to examine the various processes that can occur at the soil interface of a stormwater infiltration BMP. The objective is to relate the observations on the longevity of the three infiltration BMPs to well-documented physical processes.

These processes often have a drastic influence on the ability of a soil surface to infiltrate water. Generally, there are multiple soil evolutionary processes at work. The degree to which these processes will either decrease or increase the soil's ability to infiltrate water will depend on the relative contribution of each process. The relative contribution of these processes is dependent on many design-related aspects of the infiltration BMP itself. These include the quantity and quality of the incoming runoff, level of pretreatment, existing soil characteristics, storage bed geometry, soil surface treatment, inter-event ponding time, among many others. The three infiltration BMPs provide a wide variety of these design variables. The purpose here is not to quantify the proportional influence of different processes, but rather to provide qualitative explanations based on existing literature, monitoring data observations, and the design characteristics of the BMPs.

All three infiltration BMPs display seasonal variation but only the IT has displayed a systematic decrease in infiltration performance. The tendency of almost any soil surface undergoing concentrated ponded infiltration is the formation of a limiting surface layer of a decreased hydraulic conductivity, decreased porosity and pore size, and a consequent increase in bulk density (Bouwer 1988; Bouwer 1989; Hillel 1998; Houston, Duryea et al. 1999; Assouline 2004). The characteristics and formation of such surficial layers are varied and highly dependent on a multitude of parameters and complex processes including TSS loading.

Typically, limiting surface layers are broken down into two main distinctions based on their origin (Hillel 1998; Assouline 2004). Structural seals are those that are created due to the mechanical destruction of soil aggregates. As the soil aggregates are destroyed, the soil particles are allowed to redistribute into soil pores resulting in an increased bulk density and decreased porosity and hydraulic conductivity. This breakdown of the soil structure is a result of some combination of the following three processes. First, and most often recognized, is the aggregate breakdown (slaking) that can occur from the erosive forces of raindrop impact. Secondly, sudden wetting from rainfall or flooding can cause soil aggregates to create a wetted perimeter thus encasing and compressing air. When the compressed air suddenly escapes after continued wetting, the aggregate's structural integrity is lost and it collapses (Hillel 1998). This process is also referred to as "entrapped air implosion" (Assouline 2004). Finally, mechanical compaction due to equipment or foot traffic will also create a limiting surface layer. The second main type of limiting layer is the depositional seal. Depositional seals are formed when suspended solids are washed onto the soil surface and settle or are filtered out of solution by the soil profile. The main distinction is that the soil particles responsible for clogging in structural seals are native to the soil surface. In addition to these two types of processes biological clogging of porous media has also been well-documented (Lozada, Vandevivere et al. 1994; Rowe, Armstrong et al. 2000; Rodgers, Mulqueen et al. 2004; Lado, Paz et al. 2005). Biological clogging however is usually limited to situations where the infiltrating water has higher concentrations of organic matter and low turnover. Typically these situations include prolonged waste water recharge and landfill leachate collection systems.

2.3.2.1 Examples from Literature

Examples of soil surface evolution from published literature can be roughly divided amongst the following general topics. First, soil science and agronomy sources contain a multitude of research related to soil surface evolution and its influence on the infiltration process. Secondly, the engineered recharge of waste water effluent is also concerned with the evolution of the soil surface and the maintenance of satisfactory recession rates under these highly specific conditions. Similarly, geotechnical engineering also has similar concerns over the evolution of soil surfaces whether its goal is to maintain or restrict the flow of water or leachate. Finally, there has been research that focused on soil surface evolution as it relates to stormwater infiltration. As diverse as these topics are, they all share many of the same physical processes and characteristics that control the ability of soil to infiltrate water.

Published experiences with the soil surface evolution and longevity of stormwater infiltration BMPs are few. This lack of research may be explained by the fact that this type of research is difficult to conduct in a relatively uncontrolled field-scale setting. Additionally, stormwater infiltration is still a recent advancement in the engineering field and has only recently been proposed as a requirement for land development. However, there have been a few studies which focused on site inspections of existing infiltration BMPs in an effort to determine how the BMPs are performing over time. The most widely recognized of these studies was conducted in Prince George's County Maryland (Galli 1993). Prince George's County has been a "regional leader in infiltration design

standards, plan review, and construction inspection” (Schueler 1994). The study by Galli (1993) included over 60 infiltration BMPs (primarily infiltration trenches) of various ages from recently-built to approximately six years old. The author found that less than half of the infiltration trenches were working as designed (Schueler 1994). The majority of these underground BMPs were collecting runoff from commercial developments. The author also examined pretreatment techniques used with the BMPs (sump pits or filter strips). Sediment accumulation was prevalent with a median sediment volume of 10 ft³ found in sump pits. Many of the BMPs surveyed failed due to improper design or siting (poor soils, depth to groundwater) while others were likely the result of poor maintenance. In summary, the author suggests that with improved preliminary geotechnical/groundwater investigations, specification of clean washed crushed stone for storage beds, and regular clean out of pretreatment devices, the longevity of infiltration trenches can be improved (Schueler 1994). While both broad and qualitative this is a valuable study that has provided insight into the potential longevity of infiltration BMPs, the majority of which were either poorly designed, constructed, or poorly maintained.

Another similar study was conducted in suburban Maryland. The objective of this study was to compare the results of a field inspection of 207 stormwater infiltration facilities conducted in 1986 to a repeat study of the same facilities in 1990. Eighty two percent (177) of the originally surveyed facilities were included in the 1990 survey (Lindsey, Roberts et al. 1992). The main criterion to determine whether the facility was functioning as designed was whether or not the storage basin was empty within 72 hours. This 72 hour ponding time limit is somewhat standard and was set in 1984 by the

Maryland Dept. of the Environment's *Standards and Specifications for Infiltration Practices* (Lindsey, Roberts et al. 1992). The specific methods by which this was determined (inspection after storms or controlled flooding) was not described in the paper. Additionally, the time of year in which the surveys were conducted was not stated. This could have a major impact on the findings of such surveys as seasonal variations can have significant impact on the total time of ponding. Some of the factors that were found to be partially responsible for failure included "poor design, inappropriate soils, and compaction of soils resulting from poor or careless construction practices" (Lindsey, Roberts et al. 1992). Approximately one third of all facilities surveyed showed signs of sediment buildup. In summary, this research provides little information on the potential lifespan of a properly designed and constructed infiltration BMP.

A third study also focused on the use of field inspections to estimate the condition of 23 infiltration basins surveyed in the Puget Sound Basin in Washington State. The infiltration basins in the study were an average of 10.6 years old. The survey indicated that the majority of the basins were still working, although the basis of this judgment was not detailed. Excess sediment buildup was found at 35% of the BMPs. The author implies that the prevalent gravelly and sandy soils with low clay content (< 13%) typical of the region may play a role in their relative success when compared to those in the suburban Maryland studies. Additionally, many of the basins received maintenance over their lifetime. The author estimates that the "average cost to maintain the basin ranged from \$500 to \$1,000 per year" (Hilding 1996). The maintenance included sediment

removal, soil surface scarification, and vegetation maintenance (primarily mowed grass). The results indicate that “infiltration basins can still be an attractive stormwater option in regions with a high infiltration rate and stringent design [and maintenance] guidelines” (Hilding 1996).

More recently, a study was conducted to determine the failure rate of infiltration basins in southern New Jersey. The study was based on a visual assessment of 47 infiltration basins located in the Mullica River watershed. The visual assessment indicated that 70% of the basins (33 of 47) had standing water indicating a failure to meet the 72 hour drawdown guidance. Almost half of the assessed basins had ponded water over more than 75% of the basin bottom (New Jersey Pinelands Commission 2005). While the visual assessment was not detailed enough to determine the cause of individual basin failures, the study suggested that “background research for [the] report revealed severe deficiencies in the site selection and soil assessment methodologies, construction practices, post construction performance verification and long-term basin infiltration surface maintenance.” (New Jersey Pinelands Commission 2005). A detailed investigation of two of the basins was conducted by a geotechnical engineer contracted by the Pinelands Commission. This further investigation indicated two main reasons for the failure of the two infiltration basins. The original designs did not account for the existence of hydraulically restrictive layers below the basins and the lack of maintenance of both the basins (Princeton Hydro, LLC 2005).

These field investigations provide valuable information about the typical status of infiltration BMPs as built and maintained in the field. The results they highlight are probably typical of what could be found throughout the country. The common theme of these reports is that if an infiltration BMP is poorly designed and has inadequate pretreatment and maintenance, it is likely to fail. These studies provide little quantitative information about the longevity of infiltration BMPs to be applied to other applications.

A recent laboratory study that focused on the clogging of gravel based infiltration BMPs provides insight and quantitative data that help describe the clogging process. The experimental setup consisted of a 20 cm diameter column packed with a 90 cm gravel filter overlaying a 70 cm soil column (Siriwardene, Deletic et al. 2007). Unlike many infiltration BMPs there was no geotextile filter fabric used to separate the gravel from the soil. The gravel used in this study is much smaller ($d_{50} = 10.5$ mm) than the gravel that is typically used in storage beds with an average diameter of 50 – 80 mm (PADEP 2006). The soil used was described as fine sand with a d_{50} of 0.22 mm. While the d_{50} of the experimental soil was similar to the soil at the Villanova BMPs, it was a much more uniformly graded soil and contained very few fines. The gravel/aggregate typically used in the United States is larger and therefore is not considered or intended to function as a filter. Generally, the function of the aggregate is to provide structural support and adequate void space for temporary storage. The purpose of the study was to provide quantitative information about the clogging process of the gravel filter and underlying soil interface. The experiments were carried out with two different flow scenarios. The first was with a constant ponded water surface above the soil interface. The second was a

variable water surface where the level was filled to 75 cm and allowed to drain down to 5 cm before refilling. The column was run with simulated stormwater runoff which was created by collecting and continuously mixing actual stormwater sediment with water to create a concentration of between 80 and 300 mg/L TSS (Siriwardene, Deletic et al. 2007). Water samples were taken at various depths along the gravel filter and at the soil surface interface. Hydraulic head measurements were taken through the length of the column and outflow was measured over time. The experiments were run until the outflow reached approximately 25% of its initial value. The results showed that in all cases a clogging layer formed at the soil surface. This layer resulted in a consistent decrease in the hydraulic head of the underlying soil which eventually became negative (unsaturated). The gravel filter was more effective under the constant level condition than it was with the variable depth. The variable water level experiments showed much smaller percentages of sediment held in the filter, with the majority collecting at the soil interface. This indicates that the variable water surface, typical in subsurface infiltration beds, will clog the soil surface faster than if a constant level was maintained. The authors suggest that this is a result of the increased turbulence expected under the variable conditions. The variable water surface experiments reached 25% of the original outflow after only about 100 filter pore volumes of the simulated runoff had passed, whereas some of the constant level runs lasted to over 500 filter pore volumes. For this setup 100 filter pore volumes is the equivalent of approximately 4,000 cm (~1,700 in) of water. The authors tested five different cumulative inflow variables (volume of water input to system, mass of sediment input to system, mass of sediment reaching clogging layer, and the mass of sediment reaching the clogging layer that was less than 2 & 6 μm). Based on

the variable depth runs the cumulative mass of sediment less than 6 μm reaching the clogging layer, the cumulative volume of water, total cumulative mass of sediment reaching the clogging layer, and the cumulative mass of sediment input to the system were all adequate predictors of the decreasing outflow with r^2 values of 0.77, 0.69, 0.59, 0.53 respectively (Siriwardene, Deletic et al. 2007).

Other studies focused on depositional surface layer formations have shown similar results. Reddi, Ming et al. (2000) conducted column tests and found that the hydraulic conductivity of a sandy soil decreased by more than an order of magnitude after only approximately 300 to 600 pore volumes of a 500 and 1,000 mg/L kaolinite clay and polystyrene solutions. This was found even though the solution particles were smaller than the majority of soil pores (Reddi, Ming et al. 2000).

In arid regions where much of the annual rainfall occurs in short-duration high-intensity storms, much of the rainfall is lost to runoff. Groundwater resources are especially limited and depleted in these areas. Therefore, recharge of these flood waters is desired. In the past, these applications have been referred to as artificial groundwater recharge and not stormwater management. However, functionally the recharge areas are large scale stormwater infiltration BMPs. The same soil surface evolutionary processes that affect them are the same as those that may apply to a smaller scale infiltration BMP.

Additionally, they receive similar quality water typified by high suspended solids concentrations and low organic content. This research indicates that suspended solids contained in the inflow can quickly create clogging surface layers (depositional seals)

which compromise the effectiveness of the recharge facility (Berend 1967; Behnke 1969; Bouwer 1978). These studies indicate that “even a few tens of mg/L [suspended solids] usually has a greater influence than other clogging factors”. The author explains the evolution as follows “The usual consequence of this process is that seepage rates, which were initially determined by an array of geometric conditions and hydraulic conductivities, tend to become a function of the hydraulic resistance of the clogged surface and of the hydraulic head due to the water column above it” (Berend 1967). This creates unsaturated conditions just below the clogged surface layer which, without the influence of a deeper limiting layer, would tend to remain fairly constant with depth resulting in a gravity controlled unit hydraulic gradient (Behnke 1969).

The formation of a depositional layer results in an exponential decay of the infiltration process. This has been observed at both the laboratory and field-scale. The physical pore clogging is clearly dependent on the particle-size distributions of the suspended particles and the original infiltrating soil. Based on column studies, Behnke (1969) found that larger pore size soil clogs faster with larger particle size solids in the inflow, and smaller pore size soils clog faster with smaller particles. Experience in this field has shown that clogging is a surface phenomenon with “tensions [unsaturated conditions] registered at points only 0.50 cm below the sand surface for suspensions as dilute as 50 ppm” (Behnke 1969). Since the depositional clogging is a surface feature often as thin as a few millimeters, it can be easily remedied. Mechanical disturbance of the layer, especially when wet, provides little, and only short-lived, improvement. However, “thorough drying of the surface has been found extremely effective” (Berend 1967). The author

continues and explains that the thorough drying of the surface may only be effective if the layer is no thicker than a few millimeters. Remediation of thicker layers may require thorough drying and removal.

Another similar application is the recharge of waste water effluent. This is also important in areas where groundwater supplies are limited or of ecological importance. Although the characteristics of the effluent is different than stormwater, many of the same processes are in effect. The effluent typically contains higher nutrient and organic matter contents and lower nonvolatile suspended solids concentrations. Therefore, algae and other biological processes are of greater concern. Research from this field also indicates a strong tendency for the development of a depositional limiting layer. The surface layer effectively becomes a filter which filters material (suspended algae and other organic material) out of the water, further decreasing the soil's hydraulic conductivity (Bouwer 1988; Bouwer 1990; Houston, Duryea et al. 1999). These recharge basins also form an unsaturated zone beneath the surface layer. Field-scale infiltration tests conducted, even with clean pumped groundwater as the permeate, showed that after only 30 days of continuous ponding, direct water content measurements beneath the ponds showed that the degree of saturation was only 60% (Houston, Duryea et al. 1999). These waste water effluent recharge experiences have shown that total ponding and inter-event (drying) time are critical design factors for recharge basins. Longer ponding times tend to create an increase in the growth of suspended algae, which then forms a filter crust on the soil surface. Substantial drying time is required to break up the crust and maintain seepage rates (Bouwer 1989; Houston, Duryea et al. 1999).

Often, a combination of processes is responsible for the reduced performance of an infiltration BMP. One such combination is the formation and consequent compaction of a depositional seal. While mechanical compaction is considered a structural seal-forming process, there are some situations where a depositional seal must exist in order for the compaction to take place. This hybrid process relates to the designed maximum depth of ponded water. Effective stress is the stress experienced by the soil particles. Particle rearrangement and consequent reduction of pore space (consolidation) is dictated by changes in the effective stress. Changes in the total stress alone do not affect the structure of the soil matrix (Freeze and Cherry 1979; Das 1998). The relationship between these variables is described by the following equation.

$$\sigma_e = \sigma_T - u \quad (2.14)$$

Where:

- σ_e = effective stress
- σ_T = total stress
- u = pore water pressure

When water is ponded over a saturated soil profile, both the total stress and the pore water pressure increase equally, resulting in no increase in the effective stress. This means that for a saturated profile the ponded depth of water, regardless of the depth, is not capable of compacting the soil because the pore water pressure increases proportionally to the depth and the effective stress remains unchanged. However, under concentrated infiltration a limiting surface layer develops. This results in unsaturated conditions just below the limiting layer. These unsaturated conditions result in negative

pore water pressures (soil moisture potential). The pore water pressure must go from being equal to the depth of ponded water at the water/soil interface, to negative values possibly only millimeters into the soil/limiting layer surface. This rapid change in pore water pressure along with the relatively constant increase in total stress across the thin limiting layer results in an increase of the effective stress in the limiting layer. An increase in ponded depth increases the hydraulic gradient across a limiting layer and the flow through such a layer increases as a function of the ponded depth (Bouwer 1978). The net result of such a situation is that the ponded depth can increase the effective stress and further compact the layer which further reduces its hydraulic conductivity. This may result in recession rates that are ultimately less than what would otherwise be predicted with the increases in ponded depth (Bouwer 1989). In fact, this process has been shown experimentally to actually produce a net decrease in the recession rate (Houston, Duryea et al. 1999). The influence of this process is dependent on many factors including the depth of ponded water, limiting layer thickness and compressibility, and how the hydraulic conductivity of the layer changes as a function of its bulk density.

The literature indicates that the tendency is for concentrated infiltration applications to become less effective over time, although many examples have focused on infiltration/recharge applications with extremely high loading rates ($> 1,000$ in/yr) as compared with those typically designed for stormwater infiltration. The examples have shown that numerous processes are often involved in the highly variable clogging process. This experience first emphasizes the importance of proper design. It has also shown, especially in the case of stormwater infiltration, the importance of proper

construction techniques and maintenance. While the commonly expected tendency is for such infiltration practices to decrease in performance over time and eventually to fail to meet design criteria (Livingston 2000), there are other processes that can maintain and increase the infiltration performance over time. The goal is to design, construct, and maintain an infiltration BMP such that the processes that decrease infiltration and those that serve to maintain and increase infiltration balance so the BMP continues to meet its original design criteria.

In engineering, soil has traditionally been considered a sterile matrix of solid particles that possesses quantifiable structural and hydraulic properties. Soil, especially near the surface (A horizon), is a complex biological system. Surficial soil often contains significant amounts of organic matter. This zone is home to a diverse population of microorganisms including bacteria, protozoa and fungi. Often billions of organisms can be found in just a handful of soil (Hillel 1998). In addition to microorganisms there are often numerous species of burrowing insects and earth worms that inhabit this part of the soil profile. The abundance and diversity of subsurface life often far exceeds that which can be found on the surface. Plants also inhabit the near-surface soil layers. The roots of plants are continuously dying and growing. These roots exist in a complex symbiotic relationship with microorganisms and the soil structure. Together these elements cycle organic matter within the soil profile. This combination of processes and relationships ultimately helps maintain and improve the soil's ability to infiltrate water. Nowhere are these processes more important than in the agricultural field. Therefore, research has been performed to determine how biological activity (both vegetation and

microorganisms) and organic matter function to maintain the soil's ability to infiltrate water.

Soil organic matter “influences soil compactibility, friability, and soil water-holding capacity while aggregated soil organic matter has implications for the functioning of soil in regulating air and water infiltration...” (Carter 2002). Different types and sizes of organic matter determine the extent to which the organic matter will influence the various properties and processes. Numerous studies have focused on quantifying the relative influence that soil organic matter has on infiltration. Some of these studies have focused solely on the influence of organic matter and others have examined the effect organic matter has in combination with the increased plant growth that can be supported with increasing levels of organic matter. Soil organic matter is known to increase soil aggregate stability due to numerous biological, physical, and chemical processes. This increase in aggregate stability makes soil less susceptible to aggregate breakdown and redistribution, a process which can be caused by raindrop impact and rapid wetting. Additionally, soils with high levels of organic matter have a lower particle dispersivity and are less likely to redistribute. Therefore, soil organic matter acts to prevent the formation of surface seals (Lado, Paz et al. 2004). This has been demonstrated in controlled settings where soils with different levels of organic material were subjected to simulated rainfall. Surface intake rates (infiltration) were monitored and resulting surface seal formation was analyzed with scanning electron micrographs (Lado, Paz et al. 2004). The results showed more aggregate breakdown, higher dispersivity, denser and deeper surface seals, and lower intake rates (infiltration) in the soil with lower organic matter

content. In this study the soil samples contained no vegetation as the focus was on the direct impact of organic matter.

Other studies focus on the combined influence of organic matter and vegetation. One such study focused on the organic matter content and hydraulic properties of soil under various agricultural management practices including conventional till, no-till, and natural prairie (Fuentes, Flury et al. 2004). The authors found that the natural prairie soil maintained the highest, and generally increasing, hydraulic conductivity over the two-year study period. The hydraulic conductivity of the prairie soil was typically at least one order of magnitude greater than the other two treatments. The natural prairie soil had nearly twice the organic matter content as the other two soils. The 27-year no-till soil displayed a significantly greater saturated hydraulic conductivity over the conventional till soil. However, it appears that even after 27 years of no till agriculture (primarily wheat, lentil, barley, and peas), the soil's hydraulic properties did not reach the natural prairie condition (Fuentes, Flury et al. 2004). All three soils had relatively similar particle-size distributions. This study illustrates the importance of organic matter and natural vegetation in maintaining and improving the hydraulic properties of soil.

A similar study focused on the application of different types and amounts of organic matter. The experiments investigated 0, 5, 10, and 15 Mg ha⁻¹ of three different types of organic matter (wheat straw, a composted agricultural waste, and manure). One year after application the soil's yield (wheat), aggregate stability, bulk density, unsaturated hydraulic characteristics, and ability to infiltrate water were compared for each treatment.

The authors found that the low bulk density of organic matter has the “ability to increase soil aggregate stability” and result in “lower soil bulk density and soil compactability” (Barzegar, Yousefi et al. 2002). As was expected, the higher application rates of organic matter resulted in statistically significant lower bulk densities, higher porosities and consequent increases in infiltration. Also not surprisingly, the average yield of wheat grain and stubble increased with each increased application. A similar study compared the organic matter content, structural stability, and infiltration characteristics of soils that had been cropped various times with legumes (soybean and siratro) (Yaacob and Blair 1981). Legumes are unique due to their ability to fix atmospheric nitrogen through a symbiotic relationship with bacteria (rhizobia) on their root systems. Therefore, the nitrogen level, and consequently the organic matter content of a soil, can be improved over successive crops of legumes. The results of the study found that with increasing numbers of legume crops (1 to 6), the nitrogen content of the soil increased significantly as did the aggregate stability and infiltration. This was attributed to the increase in organic matter that was observed with successive crops (Yaacob and Blair 1981).

Another study controlled the nitrogen content directly with the addition of three levels of nitrogen fertilizer application including a control (no application). The objective of the study was to determine the ability of a perennial grass crop (based on different levels of fertilizer) to alter the structural attributes of a compact clay loam soil. “It has long been established that the presence of grass roots increases soil structure stability...” and consequently, maintains a soil’s ability to infiltrate water (Douglas, Koppi et al. 1992). Roots increase “volume fraction of continuous macropores...due to the formation of

channels by growing roots” (Douglas, Koppi et al. 1992). The authors used a complex system of epoxy resin casting and digital binary photography to measure the total volume and shape/connectivity of pore spaces for the three treatments. The study found first that the biomass yield increased with increasing levels of fertilizer. With each increased nitrogen application, there was also a resulting increase in organic matter content and aggregate stability. The pore structures of the three different treatments showed “significant differences”. The zero nitrogen application images showed the largest area of no pores and showed a significant decrease in the pore space with increased depth of 10 cm. At 5 cm the porosity of the soil with the heaviest nitrogen application was three times that of the control (Douglas, Koppi et al. 1992). This study showed that increased root growth (as a function of fertilizer application) promotes deeper increased porosity and pore connectivity. “It is well established that biologically created macropores display large degrees of continuity through the soil and, therefore, such pores usually enhance soil aeration and drainage [infiltration]” (Douglas, Koppi et al. 1992). Many other researchers have reported on the ability of roots to improve compacted soils and increase the soil’s ability to infiltrate water. One study measured the ability of the soil with and without plants to infiltrate water. The results indicated that planted soil (various agricultural crops) increased the infiltration capacity of the soils. Of the eight different types of crops examined “safflower produced higher infiltration of water through the compact layer” (Douglas, Koppi et al. 1992). This was observed even though the safflower was found to produce fewer “biopores” (biologically created macropores). This apparent contradiction was attributed to the larger size of the biopores created by the safflower roots.

Another process that can have a significant effect on the near-surface hydraulic soil properties is the freeze-thaw process. Research into this topic has produced varied results. The hydraulic impact of the freeze-thaw process is highly dependent on “soil texture, compaction, soilwater regime and rates of freezing and thawing” (Asare, Rudra et al. 1999). In one study three common soil types (silt loam, clay loam, and loamy sand) were used to determine the influence of freeze-thaw cycles on the hydraulic properties of soil (saturated hydraulic conductivity, air-entry pressure, and porosity). The hydraulic parameters were measured on each of the soil types with three different initial bulk densities and three different saturation levels prior to the freeze-thaw cycle(s). The parameters were measured after 0, 1, 3, and 6 freeze-thaw cycles (Asare, Rudra et al. 1999). The authors found that the hydraulic conductivity of all three soil samples increased with increasing numbers of freeze-thaw cycles, with one exception of a slight decrease for the clay loam at the medium saturation level and bulk density values of 1,300 and 1,500 kg/m³ (Asare, Rudra et al. 1999). Porosity was only minimally and generally positively affected by the number of freeze-thaw cycles. The effects of freeze-thaw cycles on the air-entry pressure was found not to be significant ($\alpha = 0.05$). The authors noted that surface heave was observed in the samples. This heave created continuous channels and macropores that accounted for the increase in saturated hydraulic conductivity (Asare, Rudra et al. 1999).

Improvement of the hydraulic properties of soil is desired in most agricultural applications. However, there are some instances where this process is not desirable. One

example of this is in water balance cover soils. These cover soils are designed with specific hydraulic parameters (hydraulic conductivity and soil water characteristic curve) to prevent flow through the layer by balancing the soil profile's water budget. Often the original properties of these cover soils change over time due to processes such as "freezing and thawing, wetting and drying, root growth and death, and burrowing of worms and insects" (Benson, Sawangsuriya et al. 2007). The purpose of one study was to monitor how the hydraulic properties of various water balance cover soils located in different climates change over time (~5 years maximum). The study found significant increases in the saturated hydraulic conductivity; only one soil experienced a slight decrease. Some of the increases approached values 10,000 times greater than the original conductivity. Generally, the lower conductivity soils increased more than the coarser grainer soils. Increases for coarser grained soils were less drastic and usually less than 10 times their original values. The authors also observed changes in the soil-moisture characteristic curve ($\Psi(\theta)$). Typically the van Genuchten 'n [-]' parameter, used to fit the experimentally determined soil-moisture characteristic curve, decreased over time. This represents a general broadening of the pore-size distribution and graphically a soil-moisture characteristic curve with decreased slope. The study illustrated that natural processes can improve the hydraulic properties of soil (from an infiltration standpoint).

In conclusion, many sources highlight the processes that deteriorate the hydraulic properties of near-surface soils over time, and many of the stormwater-related field-scale examples focused more on the fact that failed infiltration practices were often improperly designed, constructed, or maintained. There is also an abundance of literature that

documents the ability of soil to maintain and improve its hydraulic properties through natural/biological processes. These examples focused on agricultural studies where the soil is only required to infiltrate the rainfall (and irrigation) that lands directly on its surface. Therefore, concentrating runoff onto soils, as in the case of stormwater infiltration BMPs, will further stress the soil's ability to maintain its hydraulic functions. This creates a tradeoff between the ratio of contributing area, specifically directly connected impervious area, to BMP soil surface area. This highlights the importance of an appropriately designed contributing area ratio. The aspiration is to design, construct, and maintain a stormwater infiltration BMP so the BMP will indefinitely continue to meet its design criteria. To accomplish this, the BMP must be designed, constructed, and maintained such that deteriorating processes are balanced by those processes that maintain and increase the soil's hydraulic properties. In the following section the impact of these potentially balancing processes are related to the design, construction and maintenance of the three infiltration BMPs on the Villanova University campus.

2.3.2.2 Relation to Villanova Infiltration BMPs

The objective of this section is to associate the longevity-related findings from the three infiltration BMPs to the documented physical processes summarized in the previous section. The PCIB and the BTI have maintained their level of performance, while the IT has experienced a systematic decrease in performance.

The PCIB uses underground crushed-stone storage beds. Located approximately three feet below ground level, the storage beds are not affected by freeze-thaw processes as

confirmed by the temperature record from the BMP. Additionally, the beds were constructed in a soil that has a low organic matter content. The soil had the appearance of a B to C soil profile. As a retrofit of a paved area, the soil had been previously covered by asphalt and there was no vegetation present. Therefore, many of the soil properties and physical processes that have been documented to maintain and improve the hydraulic properties of soil are not present at the BMP. Nevertheless, data from the PCIB indicates that the BMP is not experiencing a decrease in performance. This implies that the processes that would tend to decrease infiltration at the BMP are not sufficient enough to affect the infiltration process at the BMP. This is not surprising considering the low DCIA to BMP area ratio of the lower bed (~3:1). The advantage of this low loading ratio is compounded by the fact that most of runoff received by the BMP originates from four-story slate rooftops of the adjacent dormitories. This runoff is characterized by low suspended solids concentrations. Therefore, even without any pretreatment, the BMP is continuing to function as an effective infiltration BMP almost five years after construction. This is accredited to good design and proper siting.

The BTI uses a fully vegetated, open, infiltration bed. The selection and placement of the vegetation at the BMP was superior. With the exception of a minimal amount (~30 min/yr) of removal of invasive vegetation, no maintenance has been done to maintain, replace or augment the vegetation at the BMP. The plantings have flourished under the unique soil conditions present at the BMP. Two to three inches of hardwood mulch, placed after construction, has protected the soil surface from the structural degrading processes associated with rain drop impact and rapid wetting. This initial mulch layer

also helps to assure the continued success of the plantings. The mulch layer at the BMP has not been replenished (or augmented) at the site (scarified, tilled, or significantly disturbed) in its six years of operation. The seasonal die-off of the vegetation has maintained a mulch-like surficial layer within the BMP. With the exception of a few years when the tall grasses around the perimeter of the basin (American Beach Grass, Coastal Panic Grass, Switch Grass, and Little Bluestem) were cut down seasonally, no vegetation (decomposing leaves, and stalks) has been removed from the site. Figure 62 shows the seasonal changes in vegetation that occur over the course of a year at the BTI.



Figure 62. Seasonal changes in vegetation, April 2006 (left) and September 2006 (right).

The root structure of the annual and perennial vegetation at the BMP is constantly growing and dying off. This has been documented to maintain and improve the hydraulic properties of soil through the creation of highly connected macropores. As a result of the ponded nature of the infiltration process at the BMP, these near-surface macropores may account for a large portion of the total infiltration.

The soil surface at the BTI is also exposed to freezing conditions. Significant frost heave is commonly observed during winter at the BMP. This process can also maintain and improve a soil structure conducive to infiltration. Earthworms and burrowing insects also create macropores that, only under ponded conditions, can account for a significant portion of the total infiltration (Hillel 1998; Neurath, Sadeghi et al. 2005; Wuest 2005). During instrumentation installation/maintenance and other minor disturbances to the soil surface, earthworms have not been found in the basin of the BMP. Some earthworms small in size and number have been seen in the perimeter of the basin in areas that do not experience frequent inundation. Therefore, it is surmised that earthworm activity is not a significant process in the natural maintenance of the soil structure at the BMP. This is expected to be a result of the frequency and duration of ponding in the basin which would tend to suffocate earthworms.

The BTI has some pretreatment provided by the two riprap swales. No maintenance has been performed on these swales to date. The swales are providing TSS removal as indicated by the sediment build-up present at both swales. The longest swale is 30 ft long with an average slope of approximately 0.02 ft/ft. This sediment build-up in this swale is shown in Figure 63.



Figure 63. Approximately six years of sediment build-up in a riprap swale at the BTI (photo taken on May 16th 2007).

Suspended algae growth is occasionally noticed at the BTI during summer months after periods of ponding. The algae and fine suspended material collect at the soil surface as the ponded water recedes. However, due to the sufficient inter-event dry time, the thin crust desiccates and is broken up. Emergent vegetation also appears to help maintain a loose surface layer as shown in Figure 64.



Figure 64. Desiccated surface crust with emerging vegetation at the BTI (photo taken on May 16th 2007).

The BTI is built with a DCIA to BMP area ratio of approximately 10:1, twice the recommendation of the Pennsylvania Stormwater Best Management Practices Manual (PADEP 2006). Additionally, the impervious area is an asphalt roadway and parking area which have displayed high levels of suspended solids (>500 mg/L during the onset of inflow). Even considering the moderate to high area loading ratio and the corresponding suspended solids of the incoming runoff, the combination of natural processes (vegetation, soil organic matter, freeze-thaw) and limited pretreatment has created an infiltration BMP that to date is maintaining its level of performance.

In addition to being the only BMP to show a significant decrease in performance, the IT is the only BMP to have been monitored from the very first storm to have filled the storage bed. Changes that may have occurred at the other two BMPs in their initial 1.5 years of operation are unknown. The IT showed a significant difference even between consecutive storm events during its initial operation. The incremental slope data calculated from the first six months of operation at the IT are shown in Figure 65.

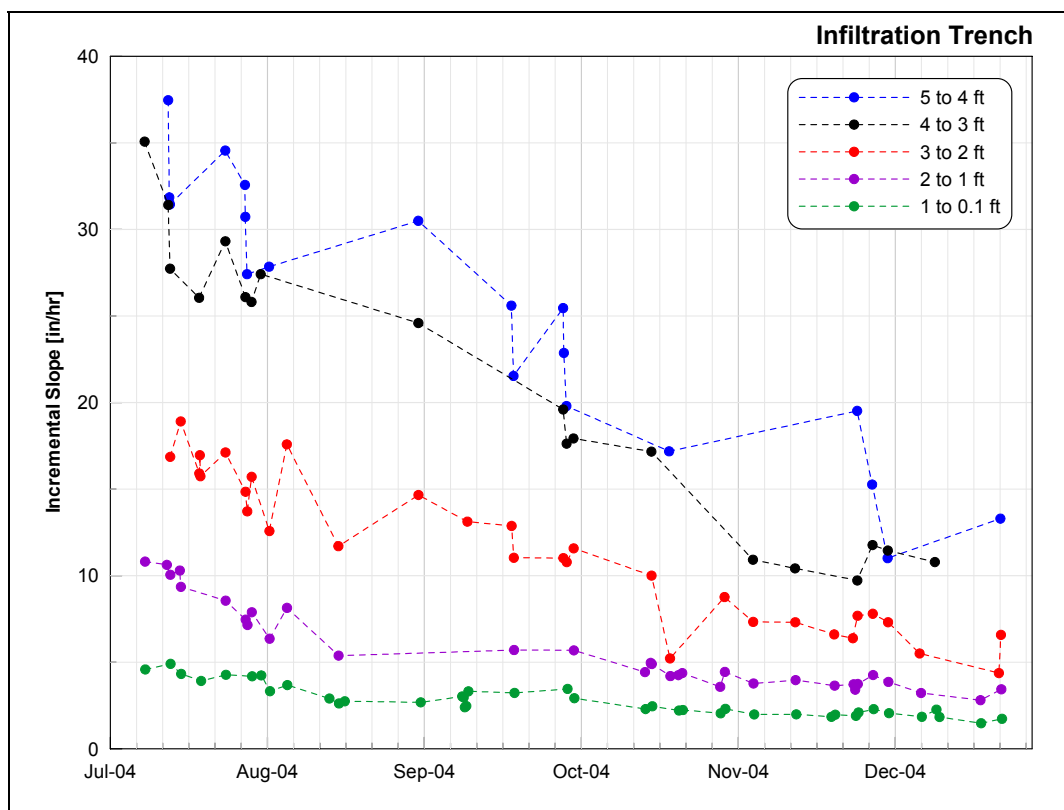


Figure 65. Incremental slopes from initial six months of operation at the IT.

Temperature data was not recorded at the onset of monitoring at the IT and some portion of the decreasing performance shown in Figure 65 is a result of the decreasing temperature expected during the period of record shown. The underground storage bed at the IT is approximately six feet deep with an overflow pipe located at 5.2 feet.

Therefore, like the PCIB, the soil surface in the IT does not have the advantage of vegetation, organic matter, and freeze-thaw processes to help maintain soil surface conditions that are conducive to infiltration. Furthermore, the BMP receives runoff from nearly one half acre of the top floor of a highly trafficked parking garage. The large 100% impervious drainage area and the relatively small footprint of the BMP create a DCIA to BMP area ratio of 130:1. With average precipitation conditions the BMP would receive the equivalent of almost 6,000 in of runoff (over the BMP area) over the course of a year. Much of this inflow is in excess of the storage capacity of the BMP and becomes overflow. However, based on flow weighted sampling collected from the inflow and outflow, the suspended solids loading and capture is not proportional to the water quantity balance of the BMP, with a disproportional amount of suspended solids being captured within the BMP. This work is further explained in Batrone (2008).

The McKsat model provides a simple method to estimate physical properties of the surrounding soil based solely on the depth record and geometry/storage characteristics of the BMP. With the exception of only four storms early in the data record, the hydraulic conductivity of the bottom was found to be less than that found for the top of the side walls. Both values show a general decrease along with seasonal variation. The K_{top} values show much more variation than do the K_{bottom} values. After July of 2006 the model predicts extremely low values for K_{bottom} . This coincides with the time in the data record when the characteristic shape of the recession limb shows extended periods of tailing. During this time the K_{bottom} values approach zero, indicating that the bottom of the IT contributes little to the overall performance of the BMP. The changes at the IT

have followed an exponential decrease. Clogging due to suspended solids loading has been shown to be an exponential process (Berend 1967; Bouwer 1978; Reddi, Ming et al. 2000). As a result of the exponential decrease, the final year of data indicate only minimal change. This implies that the bottom of the IT may be clogged to the point where additional suspended solids make little or no difference. The K_{top} values have decreased to some extent; however their decrease is not near as drastic as that found for K_{bottom} . This implies that suspended solids loading has a greater effect on the bottom than it does on the sides of the IT. This is expected for two reasons.

First, settling due to gravitational forces will take place in the vertical direction. The suspended particles will settle out on the bottom and not onto the near-vertical side walls of the BMP. Secondly, depositional seals are susceptible to compaction from increases in effective stress. This increase is a result of the ponded depth of water in conjunction with the rapid decrease in pore water pressure at shallow depths when soil surface seals are present. This phenomenon is accentuated by the design of the IT. The IT has a large ratio of impervious area to BMP area (130:1) and collects runoff from a heavily trafficked parking area. This, along with no significant pretreatment, results in high suspended solids loading to the BMP. During intense periods of rainfall and overflow the depth in the bed can exceed 6 ft. This combination of solids loading and deep ponded depths will worsen the impacts of a depositional seal within the BMP. The extent to which the ponded depth will compact the seal, thereby further decreasing its hydraulic conductivity, is a function of many unknown factors including physical properties of the seal and the actual change in effective stress (Bouwer 1989; Das 1998).

In summary, the physical processes that contribute to the degradation of the infiltration process are found at the three infiltration BMPs. The design and contributing area of the three BMPs make the IT the most susceptible to clogging due to excessive loading of suspended solids laden runoff. The relatively deep ponded depth within the storage bed of the BMP exacerbates the degradation process. Consequently, the BMP has shown a significant decrease in performance. The PCIB which also uses an underground storage bed (although shallow) has not shown the same degradation. This is a result of the PCIB's low loading ratio, and the characteristically low suspended solids concentrations from the rooftop leaders. The BTI is the only site where many of the processes that resist degradation and can improve the soil's hydraulic function are observed. Even with its moderate loading ratio, the BTI has not shown any evidence of a systematic decrease in performance. It is important to note that the loading ratio of the BTI is more than three times that of the PCIB, and the suspended solids loading is higher considering the heavily used driving and parking areas within the drainage area. Finally, this investigation has illustrated the importance of proper construction techniques. The entire construction process of all three infiltration BMPs was carefully supervised and no equipment was permitted to operate on the infiltrating soil surface. This was accomplished either by the design of small BMPs which can be entirely excavated from the perimeter of the BMP or through proper construction sequencing.

Chapter 3. Soil Testing for Infiltration BMPs

3.1 Introduction

The purpose of this chapter is to summarize and relate the results of various soil testing methods and measured soil properties to the observations on the BMPs' performance.

Predicting as-built infiltration BMP performance based solely on soil type and infiltration tests has been problematic. Many current stormwater BMP guidelines recommend very different methods of infiltration testing; often subjective correction factors are applied to relate the small-scale infiltration tests to the final BMP infiltration characteristics.

Currently no single, widely accepted, physically-based method exists to accurately predict the performance of an infiltration BMP from soil type and small-scale infiltration tests.

While the development of such a unified method is outside the scope of this work, this chapter provides three examples of infiltration BMPs where different investigative soil testing was performed prior to and after the construction. This represents an opportunity to compare the test results with the BMPs' as-built performance. Additionally, permanently installed constant head single-ring infiltration tests were run over a nine-month period on the surface of the BTI to determine the temporal variability of infiltration tests and how they compare to the BMP's performance.

3.2 Particle-size distribution and Soil Classification

A sieve analysis was conducted on soil samples taken from the three infiltration BMPs. The soil from the PCIB was determined to be a silt (ML) according to the Unified Soil

Classification System (USCS) (Kwiatkowski 2004). During construction of the BTI samples were taken of both the original soil and added sand. At the time of construction, sieve analyses were conducted on both samples, but not on the composite soil. The results of the two sieve analyses were hypothetically combined at a 1:1 ratio to produce the particle-size distribution of the sand/soil mixture assuming the approximate 1:1 mixing ratio conducted in the field. The composite soil mixture is classified as a silty sand (SM) according to the USCS (Heasom, Traver et al. 2006). A soil sample was also taken from a test pit located only a few feet from the IT. The depth of the soil sample location was similar to the depth of the bottom of the IT. Both sieve and hydrometer analyses were performed on this soil sample. Figure 66 summarizes sieve analyses for all three infiltration BMPs.

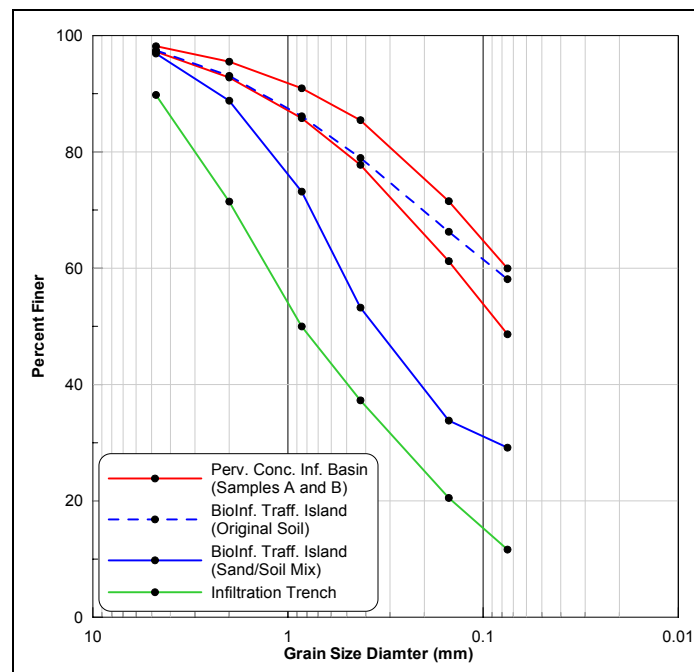
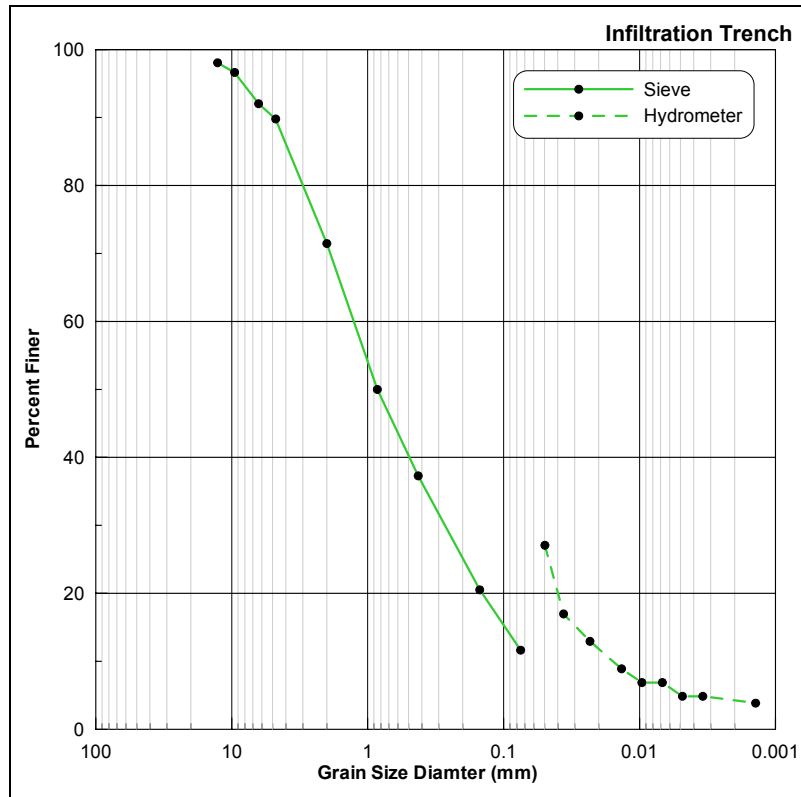


Figure 66. Sieve analyses for three infiltration BMPs.

The particle-size distributions show how similar the soil at the PCIB is to the original soil at the BTI. Both appear to have between 50% and 60% passing the No. 200 sieve (fines). However, the soil from the IT is much coarser with only about 10% fines. Even the 1:1 original soil and sand (poorly graded sand (SP)) mixture at the BTI is not as coarse textured as the original soil at the IT.

The particle-size distribution for the IT, including the hydrometer data, is shown in Figure 67. Note that the hydrometer data and sieve data have not been adjusted to provide a more continuous curve. The particle-size distribution for the IT implies that the original soil at that location is approximately 80% sand, 15% silt, and 5% clay. According to the USDA soil classification triangle, a soil with these proportions would be considered loamy sand.



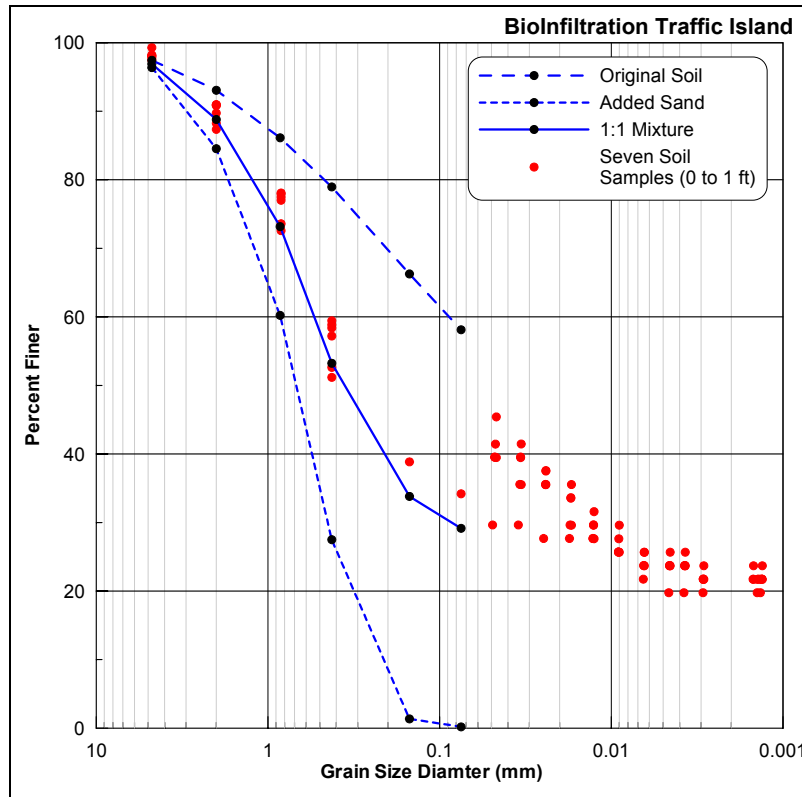


Figure 68. Complete particle-size distributions for the BTI.

The recent sieve data (shown in red) provides an excellent match for the hypothetically derived sieve data, indicating that the soil was mixed at a near 1:1 ratio. This data also enables classification of the soil using the USDA textural triangle which indicates that the composite soil is sandy loam.

A hydrometer analysis was not done for the PCIB. However, the sieve analysis and USCS classifications can be used to approximate the classification of the soil according to the USDA method (loam). These USDA textural triangle classifications are summarized in Table 9.

Table 9. Summary of approximate textural breakdown and USDA soil classifications for the three infiltration BMPs.

| | % Sand | % Silt | % Clay | USDA Classification |
|--------------------|---------------|---------------|---------------|----------------------------|
| PCIB | 50 | 30 | 20 | Loam |
| BTI (mixed) | 70 | 10 | 20 | Sandy Loam |
| BTI (org.) | 50 | 30 | 20 | Loam |
| IT | 80 | 15 | 5 | Loamy Sand |

3.3 Preconstruction Investigative Infiltration Testing

Preliminary infiltration tests were conducted at each of the three infiltration BMPs prior to or during construction. Although the methods varied from one site to another, the results from the infiltration tests and the actual infiltration characteristics of the built BMPs offers a valuable opportunity to observe how the tests relate to the as-built performance of the BMPs. The following section discusses the various infiltration testing methods used and summarizes the results for each of the three infiltration BMPs.

3.3.1 Pervious Concrete Infiltration Basin

The infiltration testing at the PCIB was conducted in 2001 by Cahill and Associates who provided the design engineer services for the retrofit. Prior to the reconstruction, two test pits were excavated in the standard asphalt paved courtyard. The test pits were each excavated to a depth of approximately three feet. An infiltration test was performed on the bottom of each test pit. The infiltration test performed is often referred to as a percolation test. This test requires that a six inch diameter hole be excavated in the soil and filled with water. It should be noted that the sidewalls of the small excavation for the test are not lined, and therefore flow is permitted to leave both through the bottom of the

hole and the sides. The results of the two infiltration tests showed recession rates of 6 and 8 in/hr. The temperature of the supply water was not measured during these field tests.



Figure 69. Location of two test pits (left) and an ongoing infiltration test in one of the test pits (right).

Independent of the infiltration tests by Cahill and Associates, an undisturbed soil core was taken alongside the BMP to a depth corresponding to that of the bed bottom to retrieve the most representative sample possible. A core was driven into the undisturbed soil at the base of the augured hole. The soil core was then extruded in the geotechnical lab at Villanova University; the hydraulic conductivity of the soil core was determined by the flexible wall method. The test followed the ASTM “Standard Test Method for Measurement of Hydraulic Conductivity of Saturated Porous Materials Using a Flexible Wall Permeameter (ASTM D 5084-90)” and was previously described by Kwiatkowski (2004) (ASTM 2000). The test apparatus is shown in Figure 70.

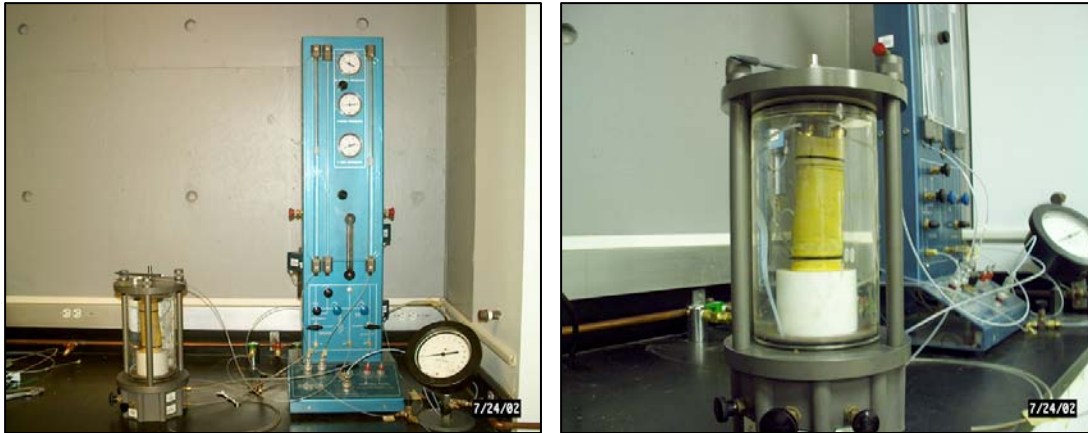


Figure 70. Ongoing flexible wall hydraulic conductivity test.

Four consecutive runs were conducted over a three hour period. The results for the four trials were 0.24, 0.25, 0.25, 0.20 in/hr which results in an average of 0.24 in/hr (1.7×10^{-4} cm/s). The temperature of the supply water was not measured during this experiment, however it was likely close to 20°C.

3.3.2 BioInfiltration Traffic Island

The infiltration testing at the BTI was performed in a fashion similar to that recommended by the 2000 Maryland Stormwater Design Manual (MDE 2000). A six inch diameter pipe was installed instead of the five inch pipe as recommended in the Maryland manual. The test was conducted after the BMP was excavated but prior to the placement of the sand/soil mixture. The test location was inside the excavation. The pipe was installed to a depth of approximately three feet below interface of the original soil and composite soil mixture. Three separate trials were conducted over a three hour period. The well was initially presoaked and then filled with 36 in of water and allowed to infiltrate into the soil while the depth of water was recorded at 30 minute intervals.

The test is shown in Figure 71 and results from the infiltration tests are plotted in Figure 72.



Figure 71. Ongoing infiltration test at the BTI.

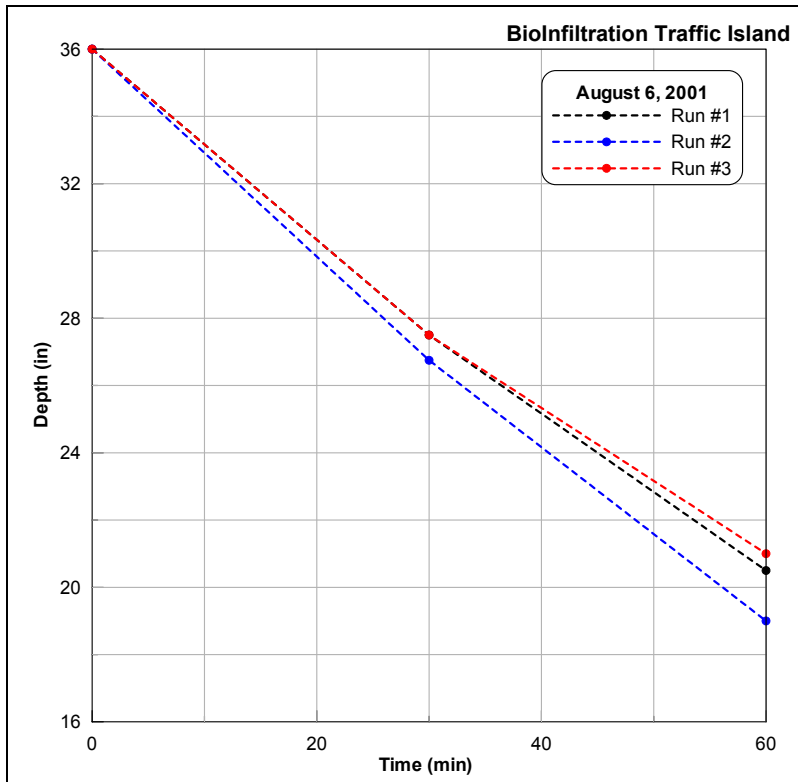


Figure 72. Depth versus time for three trials at the BTI.

The three test runs using the six inch well resulted in an average recession rate of 16 in/hr. The temperature of the ponded water was not recorded.

3.3.3 Infiltration Trench

Prior to the construction of the IT a test pit was excavated in an area adjacent the BMP location. At the time of the excavation the location of the BMP had not been finalized. The purpose of the test pit was to determine the depth to bedrock, soil type, and potential infiltration capacity of the soil. The test pit was located approximately 15 ft from the final BMP location. The six foot deep excavation revealed approximately 18 in of topsoil and mixed construction debris near the surface. The following two feet of soil were generally composed of weathered schist. Below this weathered schist was tan colored

sand for which the particle-size analysis was conducted. This was later determined to be a Loamy Sand as discussed in Section 3.2. At the base of the excavation (depth of six feet) was fractured schist. This material was firm enough to prevent further excavation by both a shovel and the backhoe bucket. However, during the excavation of the actual BMP, a hand auger used to excavate to a total depth of ten feet below grade found similar sandy material at depth and no indication of fractured rock at that location of the BMP. In one section of the test pit excavation a two foot undisturbed shelf was created above the base of the pit (four feet below grade). On this shelf of undisturbed Loamy Sand, two infiltration tests were performed. Figure 73 shows the excavation of the test pit and the pit during one of the infiltration tests.



Figure 73. Test pit location and fully excavated pit during constant head infiltrometer test.

The infiltration tests performed in the test pit at the IT include a constant head single-ring infiltrometer and a variation of the infiltration test described in the Maryland Stormwater Design Manual (MDE 2000). The constant head infiltrometer used a six inch diameter ring which was inserted approximately three inches into the ground. A constant depth of approximately six inches was maintained above the soil surface with a vertical Mariotte

standpipe. The temperature of the supply water was not monitored but was likely close to 20°C based on the ambient temperature on the day of the test. The constant head test resulted in a steady intake rate of 8.1 in/hr. This infiltration test was modeled using the VS2D variably saturated groundwater program (as further described in Section 3.4.3). This simulation assumed the default unsaturated hydraulic parameters for a Sandy Loam (Section 3.4.3) and used the saturated hydraulic conductivity to best match the observed intake rate of 8.1 in/hr. The simulation assumed a homogenous, isotropic, and isothermal (20°C) system. This process resulted in an estimated saturated hydraulic conductivity of 2.8 in/hr (1.9×10^{-3} cm/s). Figure 74 shows a volumetric moisture content plot of the axisymmetric simulation at one hour into the simulation.

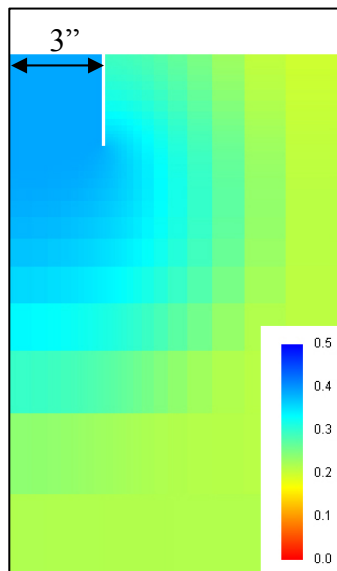


Figure 74. Simulated moisture content at one hour of the single-ring constant head infiltrometer test at the IT ($K = 2.8$ in/hr).

The second infiltration test was a variation of the method described in Appendix D.1 of the 2000 Maryland Stormwater Design Manual (MDE 2000). This method requires that a

five inch diameter pipe be installed two feet below the proposed bottom of the infiltrating feature. Water is then ponded and allowed to presoak for 24 hours. After the presoak the pipe is filled to a depth of 24 in and the ponded depth is monitored to determine if the recession rate is adequate (0.52 in/hr according to the Maryland Stormwater Design Manual). A five inch auger was not available therefore a three inch auger was used to auger 24 in into the undisturbed bench in the excavated pit. The auger never hit any rock and all the removed material was consistent with the Loamy Sand material. Figure 75 shows the three inch pipe installed in the undisturbed bench. The location of the constant head test can be seen in front of the PVC pipe. A small layer of pea gravel was added inside the pipe to help prevent erosion of the soil surface when water is supplied.



Figure 75. Three inch PVC pipe installed for Maryland infiltration test.

After the installation of the pipe the test pit was backfilled and lightly compacted in separate lifts. The following week the well was presoaked for 24 hours and four infiltration tests were performed in accordance with the Maryland method. The results from the four trials are summarized in Figure 76.

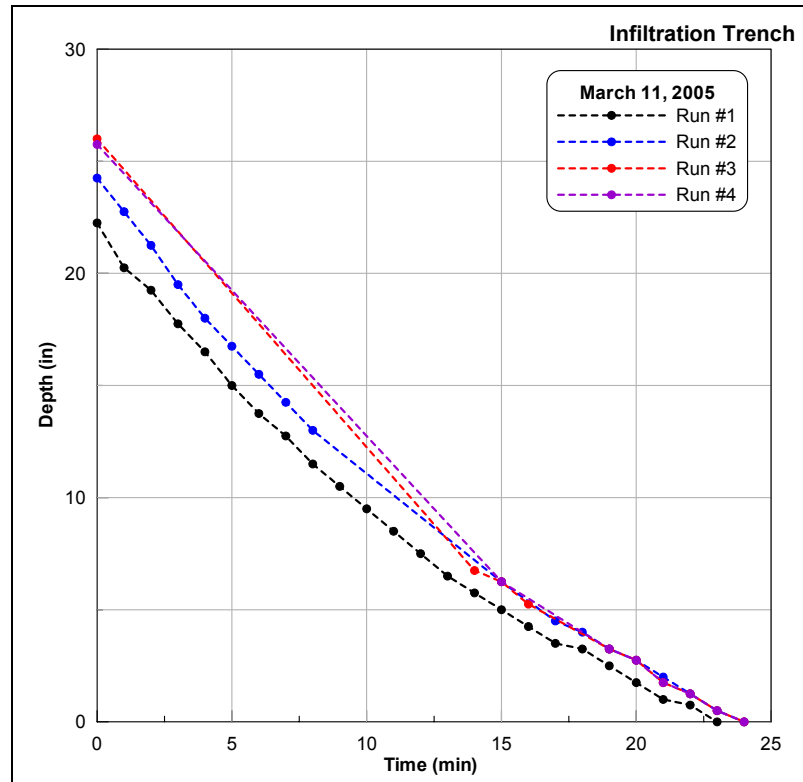


Figure 76. Results from the Maryland infiltration test using a three inch pipe at the IT.

The initial fill depths varied from 22.25 to 26 in and the well emptied within 24 minutes for all the experimental runs. This translates into a recession rate of 60 in/hr. This result is well in excess of the Maryland requirement of 0.52 in/hr, although not directly comparable due the different pipe diameters. A larger size pipe would tend to result in slower readings due to the diminished influence of three-dimensional flow with increases in diameter. However, the drastic difference between the measured and required rates gave an indication that the soil was a good candidate for infiltration.

3.3.4 Summary

The infiltration capabilities of the three infiltration BMPs were all investigated using different test methods. This, along with differences in soil texture, produced results that

varied drastically among the tests. One of the infiltration tests at the IT was easily adaptable to a variably saturated groundwater simulation. This enabled the results from the infiltrometer to be translated into an actual physical property which can be directly used in the design process. Without this type of analysis the results would only be comparable to results from similar tests (diameter, ponded depth, etc.). Table 10 summarizes the various tests and their corresponding results.

Table 10. Summary of preconstruction infiltration test at the three infiltration BMPs.

| Site | Test Description | Results |
|-------------|--|--|
| PCIB | Two open pit “percolation” tests, and flexible wall hydraulic conductivity test | Average of 7.0 in/hr for the “percolation” tests, and an average hydraulic conductivity of 0.24 in/hr for the soil core flexible wall test |
| BTI | Three runs with a modified Maryland method (6” diameter well) | Average of 16 in/hr |
| IT | 6” diameter constant head single-ring infiltrometer installed 3” deep with 6” of ponded head and modified Maryland method (3” diameter well) | 8.1 in/hr (VS2D simulations suggest $K = 2.8$ in/hr) for the infiltrometer, and 60 in/hr for the modified Maryland method |

As a result of the differences in geometry between the infiltration tests and the actual BMPs, most of the tests did not provide a good prediction of the actual performance (hydraulic conductivity estimate) of the BMPs. For comparison, the PCIB displayed an average recession rate (after correcting for the storage bed porosity) of 0.12 in/hr and for the BTI an average of 0.21 in/hr. The exceptions include the flexible wall hydraulic conductivity test at the PCIB and the constant head infiltrometer at the IT. The results from the flexible wall hydraulic conductivity test (0.24 in/hr) were only less than two times greater than the average rates observed at the PCIB and only slightly higher than

the maximum observed rate of 0.17 in/hr. The hydraulic conductivity estimate provided from the modeling of the constant head infiltrometer at the IT (2.8 in/hr) compares well with the estimates for K_{top} (maximum of 2.5 in/hr) based on the McKsat modeling (Section 2.2.3). The infiltration tests, which were either a direct measurement of the hydraulic conductivity of an undisturbed soil core or an in-situ test adaptable to a numerical model, show promise in being able to accurately predict the performance of an infiltration BMP. One method to use the hydraulic conductivity estimate in the design of an infiltration BMP is application of the Green and Ampt infiltration model (discussed in Appendix F). The direct results from the Maryland type test and the “percolation” infiltration test are not representative of the observed performance.

The analysis and comparison of the infiltration tests illustrate three important concepts regarding investigative infiltration tests.

- 1) Infiltration tests should be performed in a consistent manner to facilitate direct comparisons among various soil types and locations. This includes the general type of test (test well, single-ring, or others), the detailed dimensions of the test, and the ponded head used in the test.
- 2) Infiltration tests should be conducted such that they are adaptable to a variably saturated groundwater model or other physically based model. This enables the engineer to determine the magnitude of soil hydraulic properties such as the saturated hydraulic conductivity, thereby enabling the infiltration test to provide relevant information on the physical process that dictates the performance of an infiltration BMP.
- 3) The temperature of the infiltrating water should be a standard measurement taken during any infiltration test.

3.4 In-situ Infiltration Testing at the BTI

3.4.1 Introduction

In addition to the preconstruction tests, the BTI was also the subject of post construction infiltration tests with three main objectives. The first objective of the in-situ single-ring infiltration tests at the BTI was to determine the hydraulic conductivity of the soil surface within the BMP and provide some estimate of the spatial variability within the BMP.

Secondly, the in-situ infiltration testing was conducted to determine if the same seasonal variations observed in the monitoring data could also be detected through a simple infiltration test. Temperature was monitored during the tests. The final objective of the tests was to investigate how the results of the in-situ tests relate to both the preconstruction tests and the as-built performance of the BTI.

Spatial variability of infiltration in surficial soil has been well-documented (Fuentes, Flury et al. 2004; Neurath, Sadeghi et al. 2005; Wuest 2005). Therefore, large sample sizes (numbers of experimental locations) would be required to obtain reliable estimates of infiltration for each sample time. In other words, any potential seasonal changes in infiltration found from infiltration tests run in one or only a few locations would be overshadowed by the spatial variability encountered from running the tests in different locations. To eliminate spatial variability the tests were designed to be run in a constant location. However, due to difficulty of marking an exact location and primarily due to the high potential for soil disturbance during consequent experimental setup and take-down, permanently installed rings were installed.

The use of permanently installed rings is advantageous because it allows the sample (the soil within and beneath the ring) to experience the same seasonal conditions as the rest of the soil surface in the BMP without disturbing the sample. To further reduce the impacts of the permanently installed rings, two (2.5 in) holes were drilled in the above ground sides of the rings. These holes allow ponded water to enter and leave the soil surface inside the rings as it would if the rings were not there. The holes could be temporarily plugged with large rubber stoppers in order to conduct the infiltration test.

The single-ring method was chosen because it is a widely used and well-documented approach. “Single-ring infiltrometers are probably the most widely used device for measuring infiltration...” (Wu, Pan et al. 1997). The double-ring infiltrometer has become widely popular, based on the assumption that the outer ring guarantees one-dimensional flow from the inner ring. However, this assumption is not necessarily valid and the double-ring adds unnecessary experimental complications. Additionally, any difference in the water levels between the inner and outer ring can create erroneous results (Wu, Pan et al. 1997).

The single-ring infiltrometers were constructed from twelve inch diameter 24 gauge (0.025 in thick) galvanized steel cylindrical snap lock pipe. The snap lock pipe has a seam with a locking groove. This seam was locked and sealed with aquarium sealant to prevent any leakage from the seam. Two 12 inch long sections were created with the previously mentioned holes in the sides. The 12 inch diameter was chosen because it is a relatively large size but not so big that it would be inconvenient to leave permanently

installed at the site. Both rings were spray painted with a white paint specifically designed for weather proofing galvanized steel. The rings were driven into the soil surface using a large hammer and a piece of wood to evenly distribute the force. The rings were driven with small blows from the hammer and were checked to insure they were level between blows. The relatively thin material was able to penetrate the soil easily without any significant damage to the ring. This success was likely due in part to the relatively uncompacted nature of the soil in the BMP. Both rings were driven five inches into the soil, leaving seven inches exposed above ground. The rings were installed approximately one month prior to any experimental tests.

The locations of the rings were chosen in an effort to represent the extreme conditions (with regard to infiltration) within the BMP. Therefore, one (west ring) was installed in what visually appears to be the most compacted area. This is an area which receives a higher level of foot traffic and contains a noticeably lower plant density than the remainder of the BMP. This area had previously displayed lower infiltration values from tests with a small diameter hand-held Turf-Tec double-ring infiltrometer. The second location is in an area that receives little foot traffic and is more densely vegetated. The east ring is located at a slightly higher elevation but is still submerged during typical storm events. The rings are shown in Figure 77 and their approximate locations of the rings are shown in green in Figure 78.



Figure 77. Photographs of the west ring (left) and east ring (right) taken on November 21, 2006.

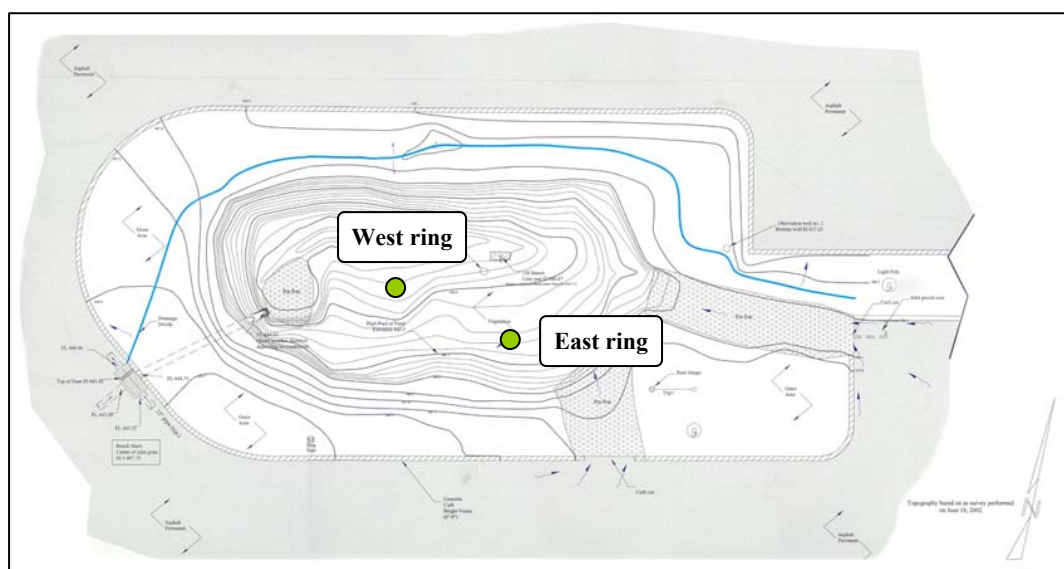


Figure 78. Approximate locations of single-ring infiltrometers in the BTI.

The purpose of the infiltration testing was to replicate post-storm ponded infiltration within the BMP as accurately as possible within the rings. Therefore, it was necessary to use a constant-head approach instead of a falling-head method to ensure that a quasi steady-state flux was obtained with the moisture content in the surrounding soil reaching

a semi-constant field capacity saturation level. The constant-head approach simply requires maintaining a constant ponded water surface above the soil surface in the ring. For accuracy and convenience a custom Mariotte tube assembly was constructed. The Mariotte tube assembly was built using two three foot long six inch inner diameter PVC pipes. The adjustable vent pipe and outlet were both located in the same pipe. The vent pipe is used to set the desired elevation of the ponded water surface. The second pipe was simply connected with half-inch flexible tubing at both the bottom and top to double the storage provided by just one vertical pipe. The total available storage within the Mariotte assembly is 1.2 ft³ or 8.8 gal. A clear plastic tube was installed on the side of one of the pipes and tapped into the main pipe at both the top and bottom to provide a visual representation of the level within the reservoirs. With every two inches of drop in the reservoir level there is an equivalent one inch drop in the 12 in single ring. A constant-head depth of 5 in was maintained. This depth was chosen because it is representative of typical ponding depths experienced by much of the BMP's soils surface.

Prior to the day of testing, tap water was stored in open air containers to equilibrate the temperature of the water and remove any residue chlorine. A 12 in long digital readout Wahl thermometer was inserted in a consistent location adjacent (~12 in) to the ring being tested. An additional 4.5 inch digital readout thermometer was also inserted adjacent to the larger thermometer. A standard mercury thermometer was used to measure the temperature of the ponded water in the ring. An attempt was made to ensure that the supply water was kept close to the ambient air temperature.

To begin the test a previously measured volume of water was held in a container separate from the Mariotte assembly. The separate container held enough water to fill the twelve inch ring to the prescribed constant-head depth of 5 in. Immediately after starting the stopwatch, the container was carefully poured into the ring. A large piece of flat rubber was placed on the soil surface to prevent the water from eroding or disturbing the soil surface during the process. The Mariotte supply line was then submerged in the ponded water to maintain the 5 in depth. The water level in the reservoir was then marked at various time intervals with a dry-erase marker on the water level indicator tube. The drawdown in the Mariotte assembly and the various temperatures were recorded until at least 30 minutes after the soil surface intake rate reached a steady state. The experiments were conducted at a consistent time of day over the course of the study. The complete experimental setup is shown in Figure 79 and a photograph of the submerged soil surface of the east ring during an experimental run is shown in Figure 80.



Figure 79. Single-ring infiltrometer experimental setup for the west ring on August 3rd, 2006.



Figure 80. Submerged soil surface within the east ring during an experimental run.

Unfortunately, as part of an unrelated experiment two soil core samples were taken from within 4-6 in of the west ring. The soil cores were taken within the week prior to the first experimental run. The soil cores left holes which were approximately one foot deep and 0.75 inch diameter as shown in Figure 81. Once discovered the decision was made not to disturb the soil further by filling the holes. Observing these holes during experimental runs provided valuable insight into the subsurface flow characteristics of the test, as the holes served as fully screened observation wells. Increasing levels of ponded water could be observed in the holes as the experiment progressed (usually within the first 30 minutes). This implied that the soil surrounding the hole was saturated or potentially that a macropore extending to a saturated area was intercepted by the holes. As time progressed one hole appeared to have been temporarily used by a mouse or some other small animal. It is assumed that during subsequent experiments on the west ring the holes became increasingly used as a preferential flow path. The time required before ponding in the holes was observed became shorter until finally during the December 19th, 2006 run the holes filled up and there was surface runoff emanating from the holes. Furthermore, the ring became significantly out of level in the direction of the two holes, implying that there was some particle migration and consequential settlement.



Figure 81. Excavations left by two soil cores taken from soil adjacent to the west ring.

Another complication to the west ring was that when the initial fill volume was added to the ring during the December 19th, 2006 run, a large portion of the surface layer detached from the soil surface and partially floated. This has not been observed during natural operation at the BMP and was simply a result of the rapid filling of the ring which enabled a significant volume of air to be temporarily trapped by leaves and other organic matter. This constituted a significant soil disturbance. This along with the surface flow from the holes provided a steady infiltration flux much higher than any previous run. As a result of the disturbance of the soil in the vicinity of the west ring, the following discussion will be focused on the east ring results.

3.4.2 Results

The single-ring infiltrometers were run on nine different occasions from July 27th, 2006 to March 27th, 2007. One run was conducted on February 8th, 2007 with ambient air temperature below freezing. Near freezing water was ponded within the east ring and no infiltration was observed, indicating that the near surface soil water was frozen and had effectively clogged the soil pores. All of the other experimental runs provided satisfactory results. Since identical experimental methods were used during each run, intake curves from all the runs can be directly compared. Intake curves are represented here as the cumulative volume of water provided to the ring over time. The intake volume, not including the initial fill volume, is divided by the ring cross-sectional area and expressed in inches. The results for the east ring and west ring are shown in Figure 82 and Figure 83, respectively.

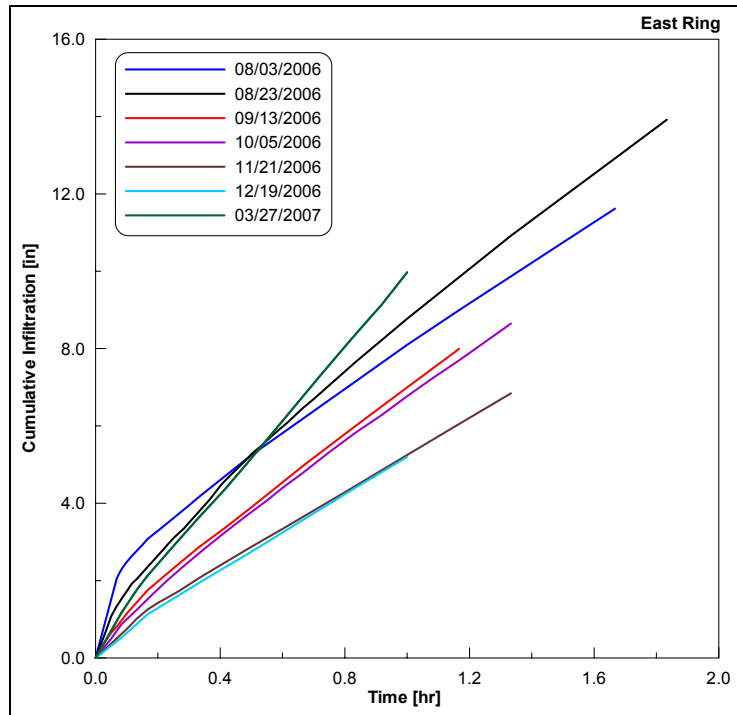


Figure 82. Intake curve from eight separate infiltration tests on the east ring infiltrrometer located in the BTI.

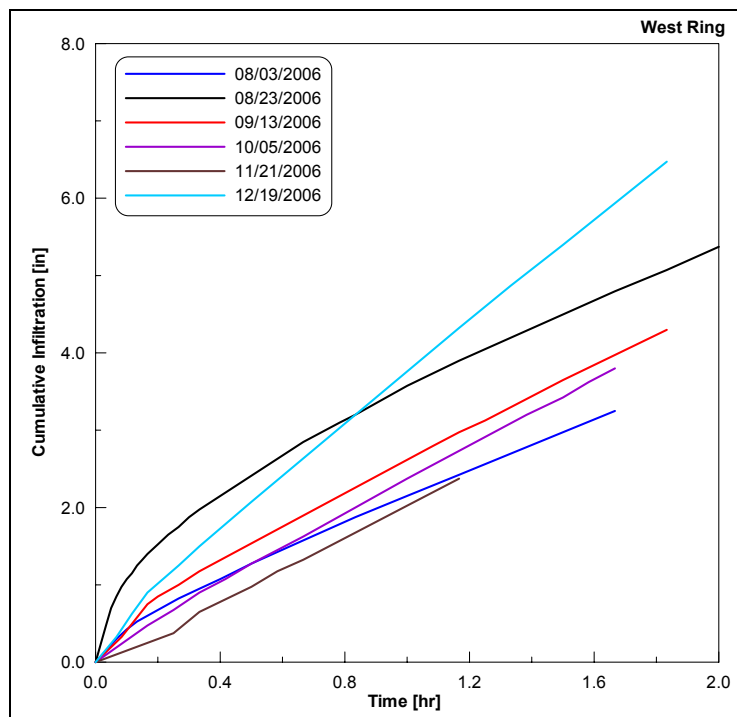


Figure 83. Six intake curves from the west ring infiltrrometer in the BTI.

The rings required between one and two hours to reach a quasi steady-state flux. The individual ring intake volumes are connected by straight line segments in both figures. No data smoothing operations have been performed on the data in Figure 82 and Figure 83.

The general shape of the intake curve is dictated at early time by the antecedent moisture content of the soil. The initial rate is fastest and decreases to approach a quasi steady rate. This steady rate is represented by the slope of the intake curve at late-time. Often this is termed the “infiltration rate” as measured by a single-ring infiltrometer. The steady intake rate is primarily dictated by near-saturated flow with unsaturated soil moisture potential gradients being sufficiently small. While there are substantial differences among the intake curves during early time (based on the antecedent conditions), the slope of the curves for late times are all relatively similar.

An attempt was made to quantify the antecedent moisture content of the surrounding soil with the use of a hand-held TDR soil moisture meter, however the readings proved to be too inconsistent to provide reliable estimates. The soil surface prior to the August 23rd, 2006 infiltration tests was extremely dry, with three weeks since the last significant ponding event. The soil surface prior to the November 21st, 2006 infiltration test was visibly moist but without any ponded areas. This test was run only three days since the last ponding event in the BMP. These differences are obvious in the intake curves for both rings. The August 23rd, 2006 curves show a significant time period of high intake rates due to high soil moisture potential gradients in the near-surface area. While the

November 21st 2006 results show that the initial intake rates were close to the final rates found at late times.

By measuring the slope created by the last few data points in the intake curves a value for the quasi steady-state intake rate can be calculated. These results along with the water temperature and initial soil temperature measured over the first foot of soil depth are shown in Figure 84.

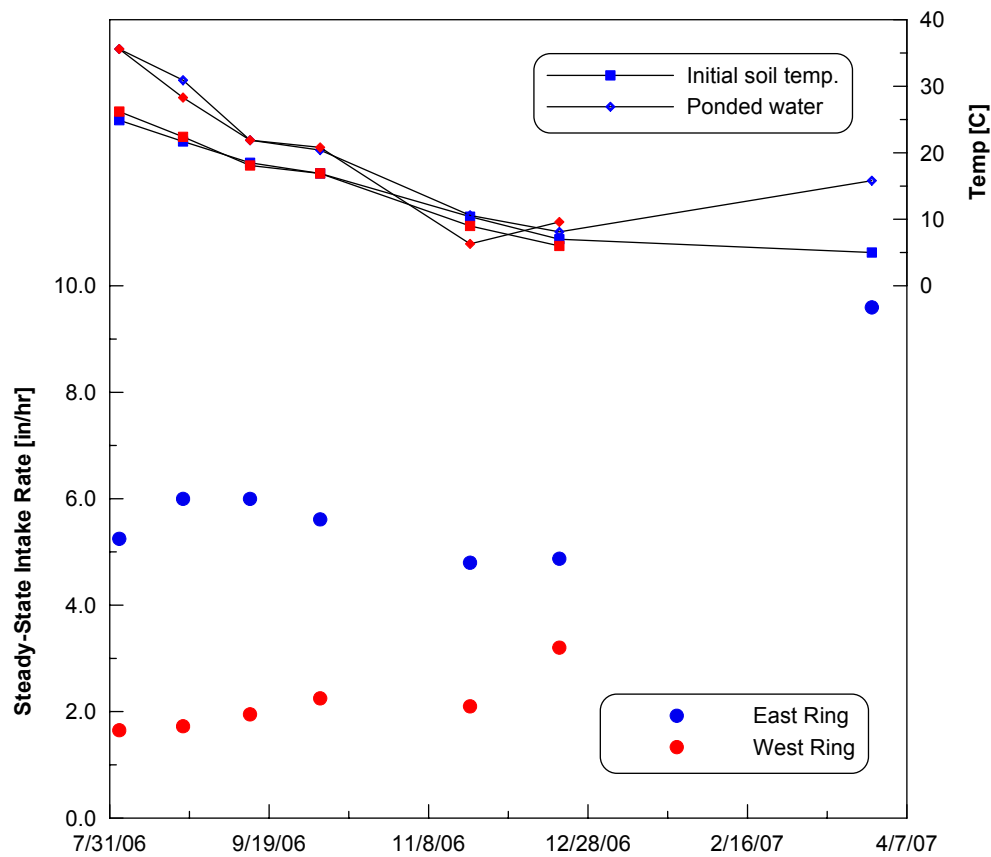


Figure 84. Steady-state intake rate and temperatures from single-ring infiltrometer runs at the BTI.

The intake rate at the east ring was generally more than twice as fast as the west ring. By visual inspection alone it was assumed that the west ring would be slower. The west ring data appears to be steadily increasing until the December 19th, 2006 run during which there was significant surface disturbance and water was observed flowing out of the holes left by the soil cores. The increase in intake rate corresponds with decreasing temperatures which was unexpected. This gradual increase may be a result of the development of preferential flow paths towards the holes. The east ring data shows a trend with the timing of a high point similar to that found from the BMP monitoring data (late summer). However, the final run on March 27th, 2007 found a much higher steady-state intake rate. The reason for this is not known. An attempt was made to conduct an infiltration test on the east ring in early February. However, due to a frozen soil surface and ponded water that was icing over, there was no infiltration observed. This ponding and freezing could have potentially disturbed the soil similar to typical freeze-thaw processes that occur at the BMP but in a more drastic and concentrated fashion. Without considering the last data point, the data from the east ring seems to correspond well with the temperature data; however it would be difficult to distinguish what portion of the variability could be attributed to viscosity effects and other physical soil structure changes with such a small sample size. The temperature variation for the east ring is shown in Figure 85.

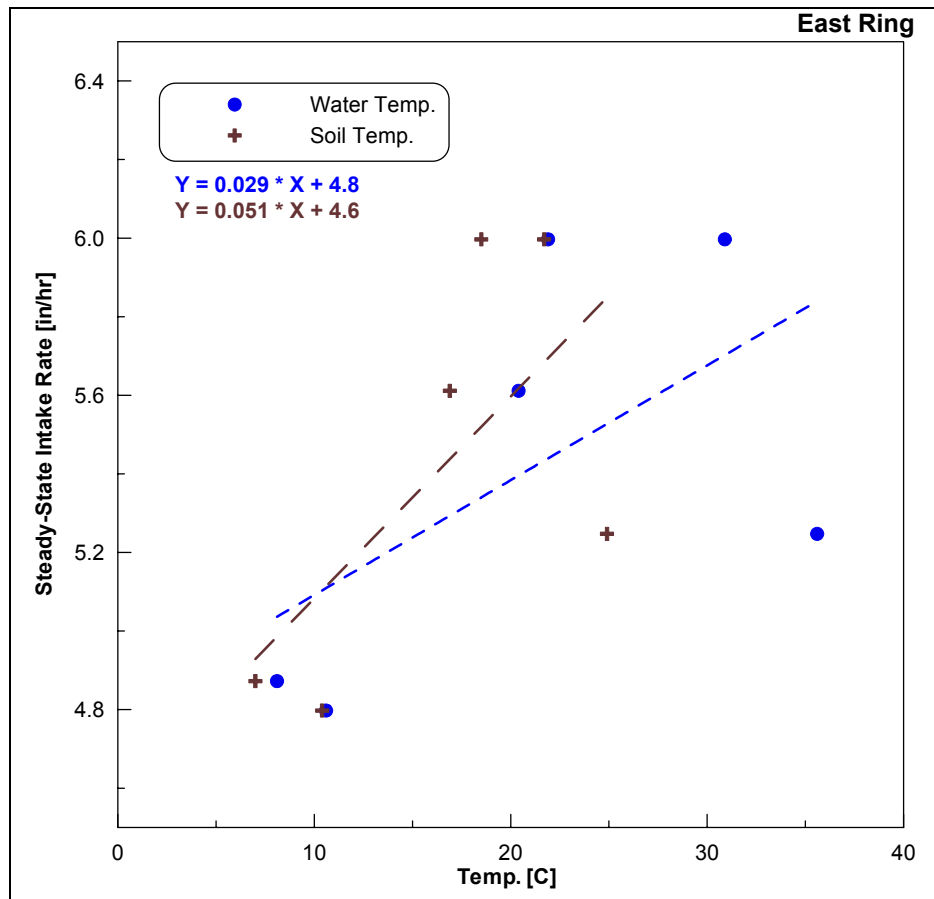


Figure 85. Steady-state intake rates vs. temperature for the east ring.

The data indicates that the infiltration within the basin is expected to vary spatially by at least a factor of two. The steady-state rates from both rings, roughly 2 to 6 in/hr, are well in excess of the average observed steady recession rate of the ponded water following storm events (~ 0.21 in/hr). This is expected due to the differences in flow geometry. The steady-state flow achieved from a single-ring infiltrometer cannot be expected to maintain a one-dimensional flow pattern after the moisture front has passed the extent of the ring in the soil. Even in this situation, with relatively deeply installed infiltrometers, the flow exceeds the ring depth and diverges within a few minutes. Another variable that could impact this difference is air entrapment. Air bubbles were observed to be released

from the soil surface during the first couple of minutes of all the infiltration tests. The specific impacts and variation of air entrapment are unknown.

Results from single-ring infiltrometers cannot be used to estimate the hydraulic conductivity directly unless considerations are made to account for soil moisture potential gradients and the three-dimensional nature of the flow pattern. The steady-state intake rate approached during a single-ring infiltration experiment is largely governed by the saturated hydraulic conductivity of the soil. In order to determine the relative contributions of saturated hydraulic conductivity and unsaturated soil properties on the experimental intake curves, the experiment must be modeled using a non-linear (variably saturated) version of Darcy's law coupled with the equation for conservation of mass. The unsteady, variably saturated version of Darcy's law combined with conservation of mass is typically referred to as the Richards or combined flow equation.

3.4.3 VS2D Simulations

3.4.3.1 Introduction

The purpose of this section is to explain how the finite difference numerical model VS2D was used to simulate single-ring infiltrometer data. Subsurface flow from infiltrometers is a three-dimensional process (Youngs 1987; Wu, Pan et al. 1997). Direct comparison of intake curves from one location to another provides insight into the relative differences between the two locations. The purpose of such experiments is to determine some quantifiable physical property of the soil (typically the saturated hydraulic conductivity) which can be used in the design and sizing of a BMP. Infiltration or other infiltration

test intake rates are often directly used in the design of stormwater infiltration BMPs, with the infiltrating surface area of the BMP assumed to demonstrate the same intake rate as the test soil surface. This will significantly overestimate the infiltration capacity of the BMP and will have a considerable influence on the design storage volume of the BMP. Other times semi-empirical methods like the Green and Ampt method are fit to infiltrometer intake curves in an attempt to determine the hydraulic conductivity. These methods frequently provide an exceptional fit of the infiltrometer data as shown in Figure 86.

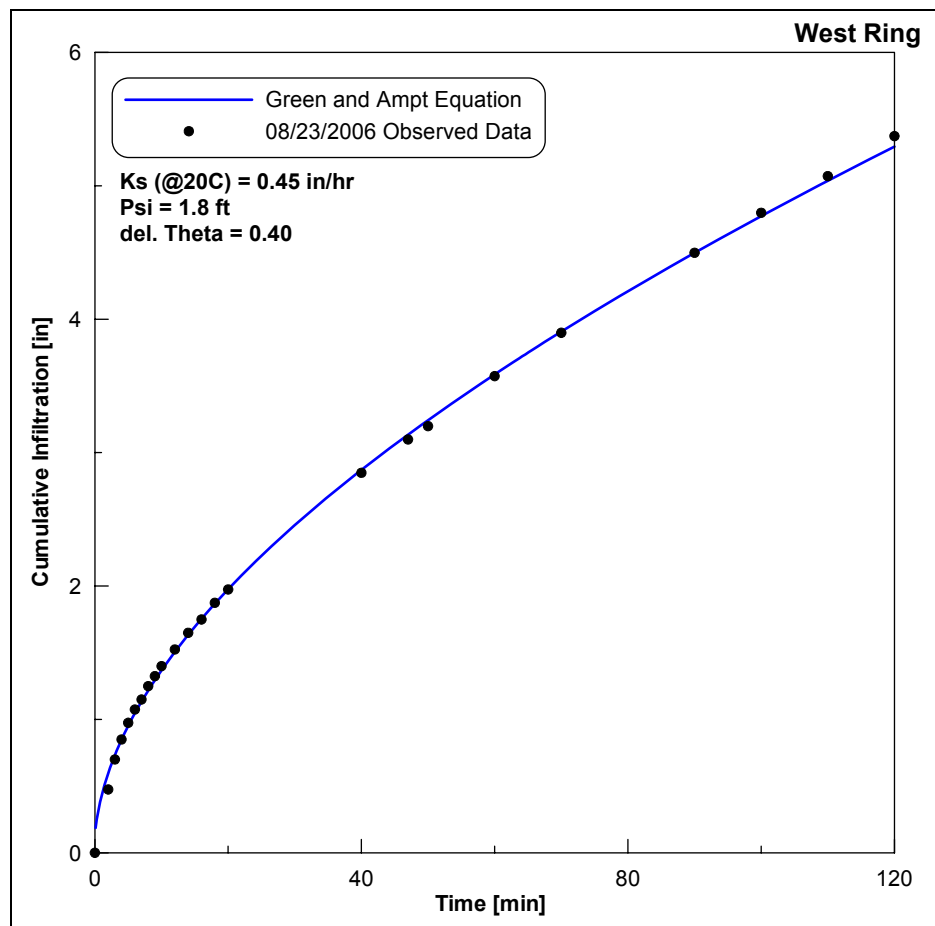


Figure 86. Green and Ampt approximation of August 23rd, 2006 west ring infiltrometer data.

The Green and Ampt equation makes many simplifying assumptions of the infiltration process. One of the most important assumptions with regard to infiltration tests is that infiltration occurs solely in the vertical direction (one dimension). As expected, the single-ring infiltrometer experiments conducted in the BTI showed evidence of lateral and upward flow, with the soil surface near the rings becoming visibly moist during the experiment. Therefore, along with the ambiguity and high influence of terms such as the wetting from suction, estimates for hydraulic conductivity from these one-dimensional methods will be an over prediction. Using the Green and Ampt infiltration model for a full-scale infiltration BMP is more realistic due to the increased validity of the one-dimensional assumption as is shown in the Green and Ampt adaptation to an infiltration BMP provided in Appendix F. There is no universal correction factor to convert these estimates. Other authors have provided methods to obtain hydraulic conductivity estimates from ring infiltration experiments. These methods are not universal and are only relevant to a specific experimental setup and dimensions (Youngs 1987; Jury and Horton 2004).

The most appropriate and robust method to account for the three-dimensional and unsteady nature of infiltrometer data is to use a three-dimensional form of the Richards equation. The general form of the Richards equation in three dimensions is as follows:

$$\frac{\partial \theta}{\partial t} = \nabla \cdot [K(\psi) \nabla H] \quad (3.1)$$

Where: θ = volumetric moisture content [-]
 $K(\psi)$ = hydraulic conductivity; function of soil moisture potential [LT^{-1}]
 H = hydraulic head [L]

Except for special cases there is no closed-form solution to this nonlinear partial differential equation. Finite-difference numerical methods are used to solve the equation with given soil characteristics and boundary conditions.

3.4.3.2 VS2D Background

The current version of VS2D was released in 2004 and packaged as VS2DHI version 1.2. The program is a two dimensional variably saturated finite-difference groundwater model. The program can also account for heat or contaminant transport (Healy and Ronan 1996). In addition to accounting for heat transport, VS2D uses a temperature dependent correction for hydraulic conductivity. The correction uses the simple viscosity correction as described previously in Section 3.3.1, where the input hydraulic conductivity is assumed to be given at 20°C (Healy and Ronan 1996). In addition to a standard two-dimensional simulation, VS2D can also use a radial coordinate system which is ideal for single-ring infiltrometers or any other axisymmetric infiltration test.

3.4.3.3 Model Development

First, the VS2D project options must be set; these include the model units and specification of a radial coordinate system. VS2D uses the total hydraulic head as the “principal independent variable”, therefore initial conditions must be set so that the

hydraulic head is specified throughout the entire domain (Lappala and Healy 1987). This can be done by directly specifying the head or by specifying the initial moisture content and allowing VS2D to calculate the corresponding head based on the soil properties and unsaturated hydraulic characteristic function. For this simulation the initial moisture content method was chosen to determine the influence of initial moisture content. Since this does not represent an equilibrium status there are slight transient effects which are far outweighed by the infiltrometer flow. VS2D can use three methods to describe the variably saturated soil hydraulic properties. These include the van Genuchten, Haverkamp, and Brooks-Corey methods. The van Genuchten method was chosen for this work because of its widespread usage (Genuchten 1980). Other model options include six different variables which deal with solver stability and numerical convergence. The model uses an implicit time-discretization scheme which is not necessarily stable due to the nonlinear nature of the combined flow equation (Lappala and Healy 1987). These variables, which are described in the program documentation, provide control over the time discretization and iteration methods used in an attempt to provide computational convergence. Proper specification of these variables is crucial to model convergence and computation time. The following table summarizes the values specified for the single-ring infiltrometer simulations. Finally, the desired output options can be set.

Table 11. Summary of VS2D solver options for single-ring infiltrometer simulations.

| Description | Parameter | Value |
|--|------------------|--------------|
| Relaxation parameter | HMAX | 0.3 |
| Minimum iterations per time step | MINIT | 2 |
| Maximum iteration per time step | MAXIT | 5000 |
| Stop simulation at convergence failure | ITSTOP | TRUE |
| Maximum number of time steps | NUMT | 10000 |
| Closure criteria for head | EPS | 0.0010 |

The model domain for the infiltrometer simulation was created with the intention of being sufficiently large enough to ensure that the boundaries have no effect on the active flow region. The domain simulates an axisymmetric area (cylinder) that has a three foot radius and a length of 15 feet. The depth was chosen because it is the approximate average depth of the groundwater table. The five inch depth of the ring was cut out of the domain to specify that there is no flow across the ring boundary.

The development of the computational grid is an important part of the model development process. A good computational grid is one that has adequate resolution where needed, but is not so dense as to unnecessarily lengthen the computational effort. Therefore, a grid was created so that the dimensions of the individual cells vary in relation to the cells' proximity to a domain boundary with the smallest grid cells located adjacent to the boundaries. For example, the first 0.025 ft of depth contains five rows of grid cells increasing in size with depth. The total domain for the single-ring infiltrometer simulations contains 47 columns and 61 rows for a total of 2,867 cells. The stability and convergence of the model is dependent on both the time step/program iteration parameters and the computational grid. The computational grid is shown in Figure 87.

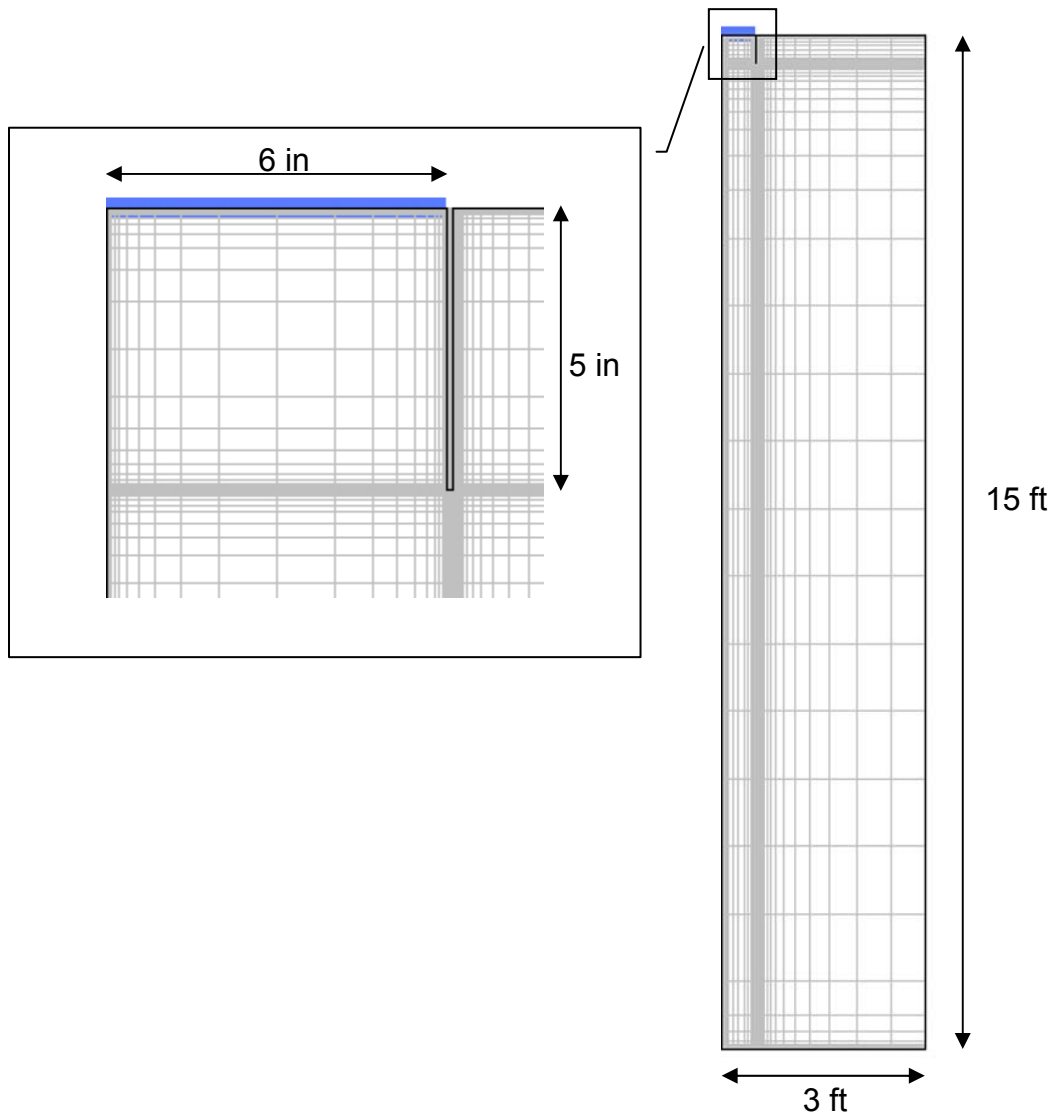


Figure 87. Full scale and ring close-up of axisymmetric VS2D single-ring infiltrometer simulation.

Boundary conditions must be specified for each segment comprising the domain. For the infiltrometer simulations all boundaries except the soil surface within the ring are specified as no-flow boundaries. The six inch radius representing the soil surface within the ring is specified as a constant total head boundary with a head of 0.398 ft or 4.77 in (~5 in) which is the depth of water provided over the soil surface during the tests.

Finally, the soil properties are specified. As part of a sensitivity analysis, the USDA soil classifications for the soil found at the three infiltration BMPs were input to the USDA Rosetta soil hydraulic property database program. Rosetta Lite v.1.1 is packaged as part of the HYDRUS-1D groundwater model (Simunek, Genuchten et al. 2005). The Rosetta model provides estimates for soil hydraulic information, including the van Genuchten curve fitting parameters, based on various levels of input data. The van Genuchten parameters for the three soil types found at the infiltration BMPs are summarized in Table 12. Each soil was considered to be homogeneous, isotropic, and isothermal.

Table 12. Summary of van Genuchten parameters for the three infiltration BMPs.

| | USDA Text. Class | Sat. K [ft/hr] | Sat. K [in/hr] | Porosity [-] | θ_r [-] | α [ft⁻¹] | β [-] |
|-------------|-------------------------|-----------------------|-----------------------|---------------------|----------------------------------|--|-------------------------------|
| PCIB | Loam | 0.01646 | 0.1975 | 0.3991 | 0.0609 | 0.3383 | 1.4737 |
| BTI | Sandy Loam | 0.05229 | 0.6275 | 0.3870 | 0.0387 | 0.8138 | 1.4484 |
| IT | Loamy Sand | 0.14370 | 1.7244 | 0.3904 | 0.0485 | 1.0577 | 1.7466 |

3.4.3.4 Sensitivity Analysis

A basic sensitivity analysis was performed to determine the relative importance of unsaturated soil parameters, initial moisture content, and saturated hydraulic conductivity on the intake curves from a standard one foot diameter single-ring infiltrometer.

Specifically, the sensitivity analysis aims to determine the relative influence that these parameters have on the quasi steady-state intake rate achieved during an infiltration test.

First, simulations were run with the three soil types using all the default parameters provided in Table 12 with initial moisture content of the surficial soil set at 0.10 (dry initial conditions). Next, the same simulations were rerun with the initial moisture content set to 0.30 (wet initial conditions). The results from these simulation runs are summarized in Figure 88.

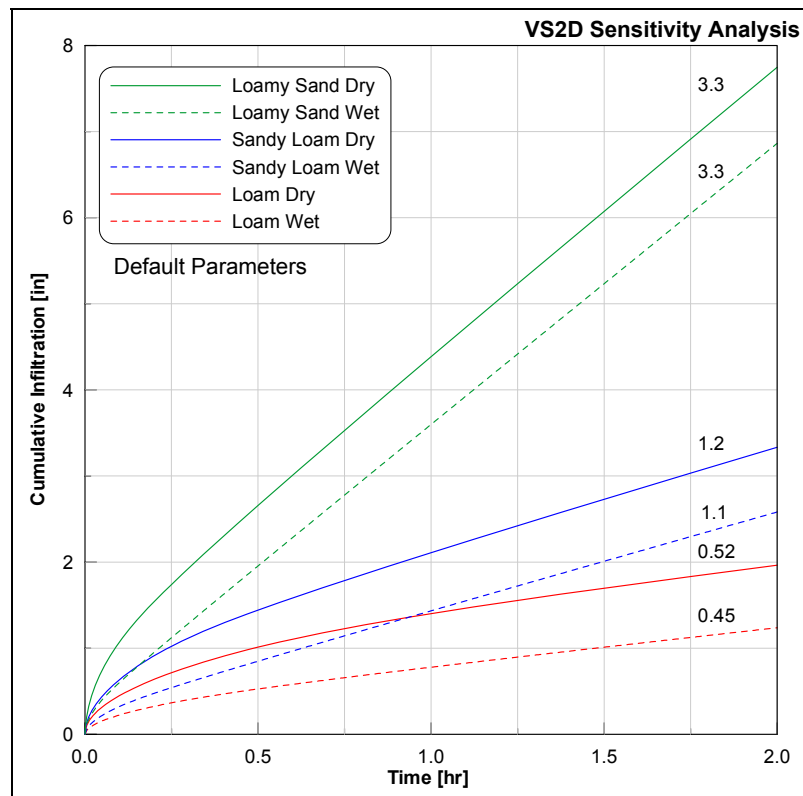


Figure 88. VS2D intake curves for the single-ring infiltrometer using the soil hydraulic parameters for three soil types at both a dry ($\theta = 0.10$) and wet ($\theta = 0.30$) initial condition. Intake rate at two hours labeled on plots [in/hr].

These results show that the textural soil class, or soil type, has a major impact on the intake curve from an infiltrometer experiment. They also illustrate the small effect that the large change in initial moisture content has on the final steady-state intake rate.

The second round of simulations was focused on the influence of the unsaturated soil properties. For these simulations each soil type was run with their original hydraulic parameters except the saturated hydraulic conductivity was set to a common 0.052 ft/hr (0.63 in/hr), the original value for the sandy loam. The runs were conducted under both the same wet and dry initial conditions. The simulation results for the sandy loam are the same as previously summarized in Figure 88. These results are shown in Figure 89.

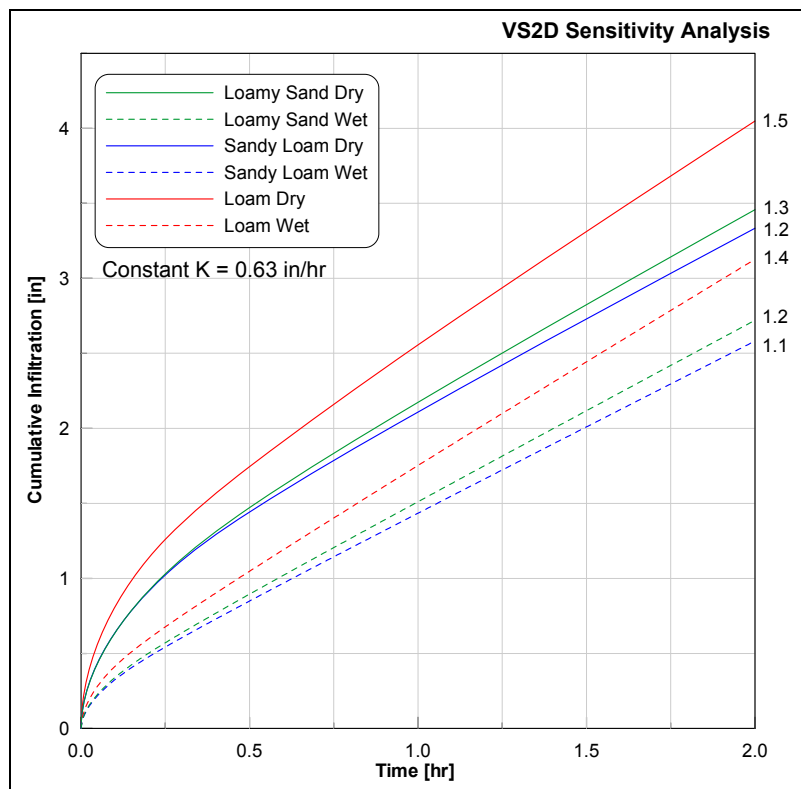


Figure 89. VS2D intake curves using the soil hydraulic parameters for three soil types with a constant saturated hydraulic conductivity at both a dry ($\theta = 0.10$) and wet ($\theta = 0.30$) initial condition. Intake rate at two hours labeled on plots [in/hr].

These simulations show how similar the intake curves from the three soil types are when they have the same saturated hydraulic conductivity. The steady-state intake rates are very similar, ranging only from 1.1 to 1.5 in/hr.

The next two sets of simulations were focused on the sandy loam soil type because this is the textural soil type found at the BTI. The first of these two runs focuses on the influence of initial moisture content, with runs being conducted at $\theta = 0.10$, 0.20 , and 0.30 . The three hypothetical intake curves are shown in Figure 90.

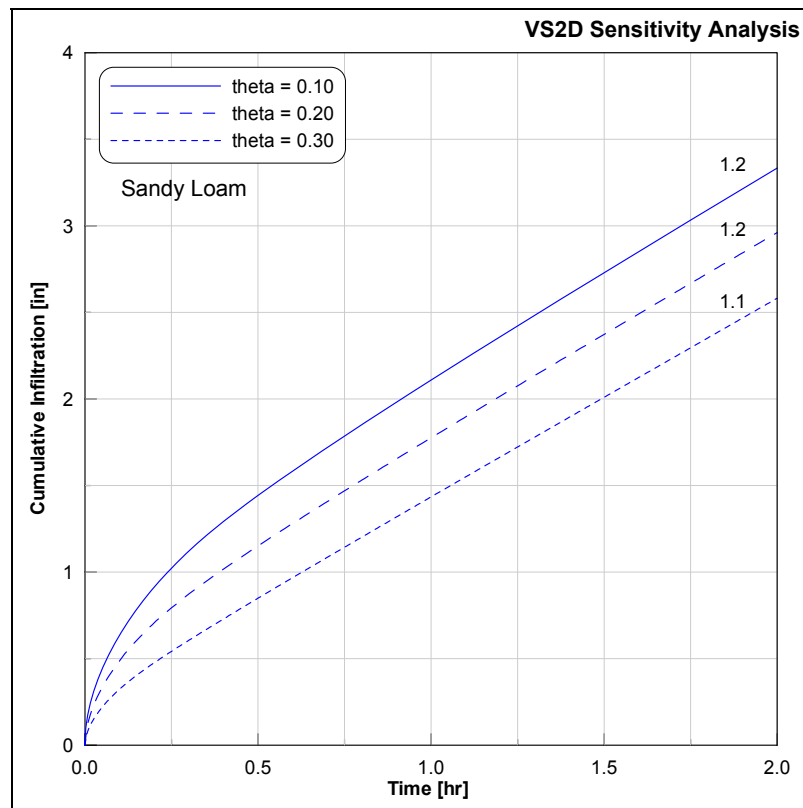


Figure 90. VS2D intake curves using the soil hydraulic parameters for sandy loam at three different initial moisture contents ($\theta = 0.10$, 0.20 , and 0.30). Intake rate at two hours labeled on plots [in/hr].

These three simulations with the initial moisture content varying from near θ_r to near θ_s result in a steady-state intake rate (at two hours) that only vary by only 0.055 in/hr from the highest moisture content to the lowest. This illustrates the minor effect that drastic changes in initial moisture content have on the final intake rate. It also confirms the early

time influence of dry initial moisture conditions, characterized by increasing early-time curvature.

The final set of simulations was run to further quantify the influence the saturated hydraulic conductivity has on the steady-state intake rate for the sandy loam. Three simulations were run with the initial moisture content equal to 0.20. Saturated hydraulic conductivity was set at 0.31, 0.63, and 1.3 in/hr for the three runs, as shown in Figure 91.

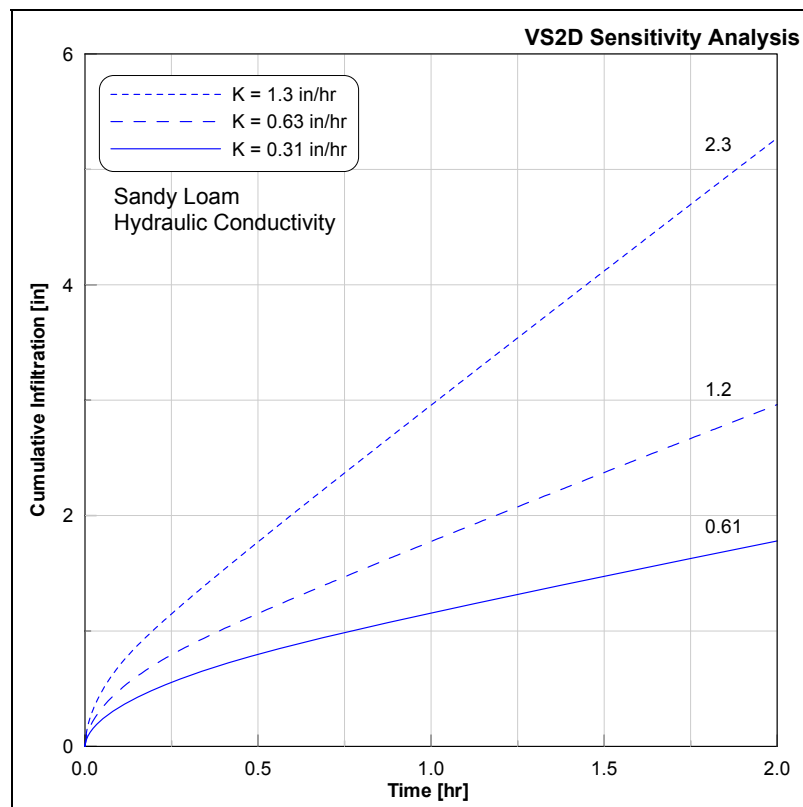


Figure 91. VS2D intake curves using the soil hydraulic parameters for sandy loam at a constant moisture content ($\theta = 0.20$) and three saturated hydraulic conductivities ($K = 0.31, 0.63,$ and 1.3 in/hr). Intake rate at two hours labeled on plots [in/hr].

The results for the sandy loam, for both initial moisture content and hydraulic conductivity tests, are further summarized in two scatter plots shown in Figure 92. These

scatter plots and the linear regressions fit to them are only valid for the unsaturated soil hydraulic characteristics entered for this soil type, and they are only relevant to a 1 ft single-ring infiltrometer driven to a depth of 5 in with a ponded head of ~5 in.

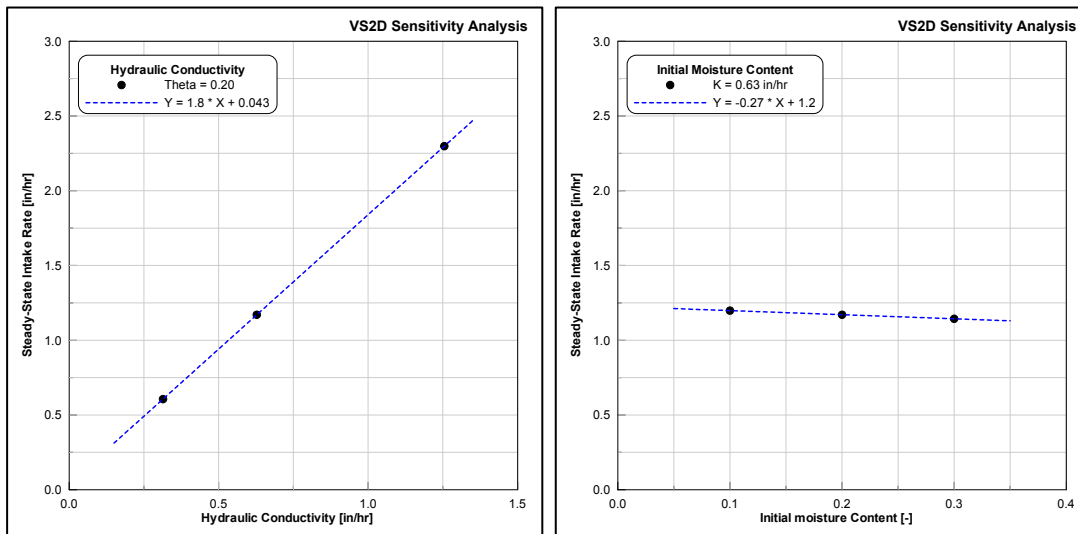


Figure 92. Steady-state intake rate for sandy loam as a function of saturated hydraulic conductivity (left) and initial moisture content (right).

In summary, the sensitivity analysis has illustrated the relative influence of the van Genuchten parameters, initial moisture content, and saturated hydraulic conductivity. As expected, the van Genuchten parameters and the initial moisture content have their greatest influence during early times when there are still significant soil moisture potential gradients. At later times, when the moisture front has propagated deeper into the soil profile, the soil moisture potential gradients are small and the surface intake is largely dictated by the saturated hydraulic conductivity. The variably saturated groundwater model enables the experimental late-time intake rate to be used as a predictor of the soil's saturated hydraulic conductivity.

3.4.3.5 Energy Transport

The temperature data taken during the infiltrometer runs show that none of the infiltrometer runs were conducted on an isothermal system. The heat transport version of VS2D (VS2DH) was used to account for temperature distributions and their influence on the saturated hydraulic conductivity. Energy transport is simulated with VS2DH by use of a modified version of the advection-dispersion equation as follows.

$$\frac{\partial}{\partial t} [\theta C_w + (1 - n) C_s] T = [\nabla \cdot K_T(\theta) \nabla T] + [\nabla \cdot C_w D_H \nabla T] - [\nabla \theta C_w v T] + [q C_w T^*] \quad (3.2)$$

Where:

- C_w = heat capacity of water [$\text{MT}^{-2}\text{L}^{-1}\text{C}^{-1}$]
- n = porosity of soil [-]
- C_s = heat capacity of dry soil [$\text{MT}^{-2}\text{L}^{-1}\text{C}^{-1}$]
- K_T = thermal conductivity of the soil/water matrix tensor [$\text{ML}^{\circ}\text{C}^{-1}$]
- D_H = hydrodynamic dispersion tensor [L^2T^{-1}]
- v = water velocity [LT^{-1}]
- q = rate of fluid source (input to domain) [T^{-1}]
- T^* = temperature of input source water [$^{\circ}\text{C}$]

This equation states that the “change in energy stored in a volume over time” (left hand side), is equal to (from left to right) the energy transport due to thermal conductivity, plus the energy transport due to thermo-mechanical dispersion, minus the advective transport of energy, plus any energy sources. The authors point out that this representation does not account for the heat capacity of air in the soil matrix but that this is generally insignificant compared to that of the water (Healy and Ronan 1996). Table 13 summarizes the energy transport parameters used for these simulations. The parameter values have been input from various literature sources (Healy 1990; Jaynes 1990; Hillel 1998; Ronan, Prudic et al. 1998; Jury and Horton 2004).

Table 13. Summary of energy transport parameters used in VS2DH simulations.

| Parameter | Description | Value | Units |
|--------------|----------------------------------|---------|---------------------|
| Long. Disp. | Longitudinal dispersion | 0.03281 | ft |
| Trans. Disp. | Transverse dispersion | 0.03281 | ft |
| C_s | Heat capacity of dry soil | 56630 | $J ft^{-3} °C^{-1}$ |
| K_{TR} | Thermal conductivity of dry soil | 0.4572 | $W ft °C^{-1}$ |
| K_{TS} | Thermal conductivity of wet soil | 0.5486 | $W ft °C^{-1}$ |
| C_w | Heat capacity of water | 118300 | $J ft^{-3} °C^{-1}$ |

Prior to any simulations the model's temperature correction for hydraulic conductivity was validated. This was accomplished by creating a run where the temperature distribution of the domain was isothermal and greater than 20°C, with the supply water specified at the same temperature as the domain. A second run was then created but with the isothermal conditions and supply water set to 20°C. However, in the second run the input hydraulic conductivity (assumed by the program to be specified at 20 °C) was corrected external from the program (using the viscosity ratio of the two temperatures) to the higher temperature of the first run. These two runs produced identical results, indicating the validation of the temperature compensation for hydraulic conductivity in VS2DH.

3.4.3.6 Results

The sensitivity analysis has shown that steady-state intake rate is primarily influenced by the saturated hydraulic conductivity. Therefore, the saturated hydraulic conductivity can be adjusted until the modeled steady-state intake rate matches the observed rate. This yields an estimate of the saturated hydraulic conductivity at the test location. To this point the model simulations have assumed that soil is homogeneous, isotropic, and

isothermal. The temperature measurements have shown that the infiltrometer experiments were conducted on a system that was not isothermal.

The soil underneath the rings is likely heterogeneous and due to the ponded conditions, a large portion of the near-surface flow may occur through macropores and other preferential flow paths. Direct determination of the presence of macropore and preferential flow (heterogeneity) is only possible through techniques that are destructive to the soil structure and would prevent future testing at the location. Typically, a conservative dye is introduced to the supply water near the end of the infiltration test and at the conclusion of the test the soil surface is excavated in layers and the dye concentrations are observed (Neurath, Sadeghi et al. 2005; Wuest 2005). Areas of concentrated flow will contain higher concentrations of dye while other areas will not. This procedure has not been conducted at the BTI; although the experimental intake curves provide evidence of heterogeneity as is discussed later in this section.

The simulation of the infiltrometer experiments was accomplished as follows. The only addition to the previous model used in the sensitivity analysis was the inclusion of the initial temperature distribution, based on on-site measurements, and the specification of the energy transport parameters. The subsurface temperature was input as a contour at a depth of six inches, which is the center of the one foot long temperature probe. The temperature at the water table (15 ft below) was input as 13°C for all simulations. The temperature was interpolated between these two points as shown for the west ring

simulation for the August 23rd, 2006 in Figure 93. The temperature of the supply water as measured in the ring was also input to the model.

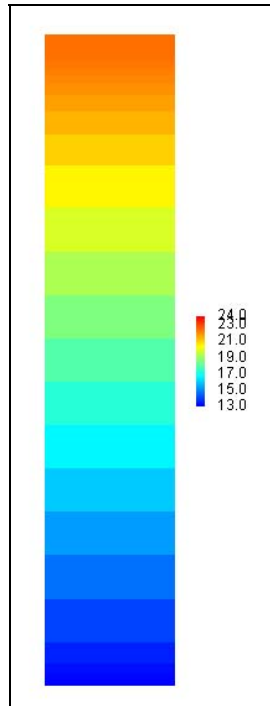


Figure 93. Initial temperature profile for the west ring infiltrometer experiment conducted on August 23rd, 2006.

One of the main objectives of the single-ring infiltrometer was to determine the saturated hydraulic conductivity of the soil at the BTI. Each east ring infiltrometer run (with the exception of the March 27th, 2007 run) was simulated by entering the measured temperatures (soil and supply water), specifying an initial surficial moisture content (0.10, 0.20, or 0.30 based on soil observations and observed intake curve), and using an iterative method to find the saturated hydraulic conductivity that best matches the observed steady-state intake rate. For the west ring, only the August 23rd, 2006 run was simulated. An initial moisture content of 0.10 was specified for the August 23rd, 2006

run at the west ring, due to the dry conditions in the BMP. Simulation runs with different hydraulic conductivities are shown in Figure 94 for the west ring data on August 23rd, 2006.

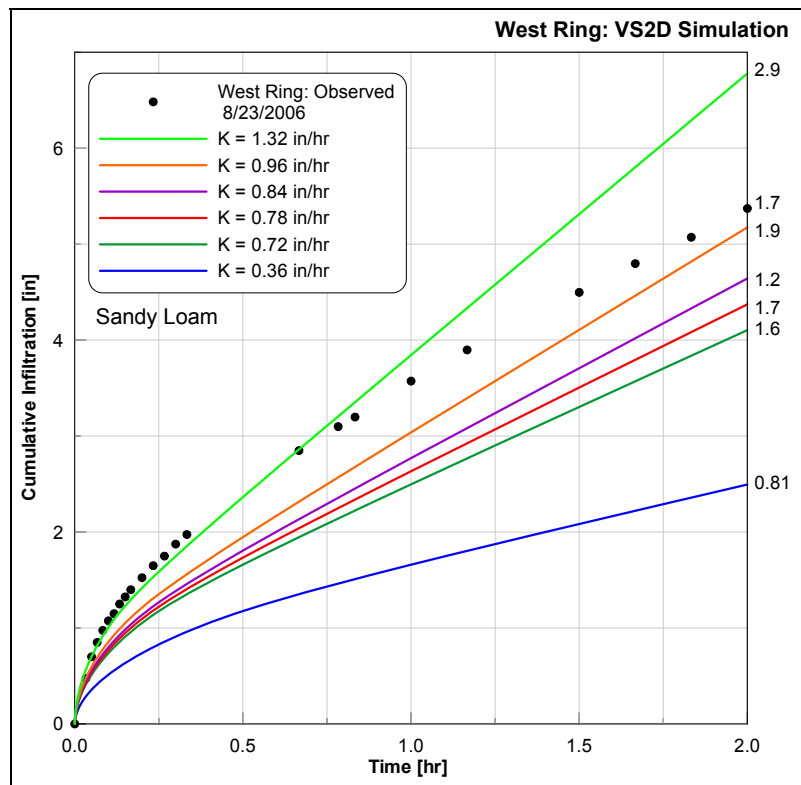


Figure 94. Observed and VS2DH intake curves with various hydraulic conductivities for the west ring infiltrometer on the August 23rd, 2007 run. Intake rate at two hours labeled on plots [in/hr].

For the west ring the model indicates that a saturated hydraulic conductivity (referenced to 20°C) of 0.78 in/hr (shown in red) provides a steady-state intake rate that best represents the observed data. While the final intake rate for the simulated run at 0.78 in/hr matches the observed rate, the cumulative infiltration at that time is 1.0 in less than the observed. Almost all of this difference accumulates during the first hour of the run with the majority in the first half hour. This discrepancy may result from inaccuracies in

the unsaturated soil hydraulic characteristics, or it could be a result of simulating a heterogeneous soil as an equivalent homogeneous soil. This phenomenon has been previously described, “In general, accounting for areal heterogeneity leads to shorter ponding times and to a more gradual decrease of the infiltration flux with time.”

(Assouline 2004). Therefore this discrepancy could be an indication of the heterogeneity of the soil being tested. This can be seen in Figure 94 with the observed (heterogeneous) intake curve maintaining a higher intake rate at early times and being slower to reach a steady-state rate than the intake curve from the homogeneous representation.

The east ring infiltrometer had higher final intake rates than the west ring for all experimental runs as was expected based on visual inspection of the soil surface. An iterative process was used for each experimental run data set to determine the best-fit hydraulic conductivity referenced at 20°C. The observed and best fit simulated intake curves (based solely on the final intake rate) for all six infiltrometer runs are shown in Figure 95. The temperatures, observed final intake rates, initial moisture contents, and saturated hydraulic conductivities are summarized in Table 14.

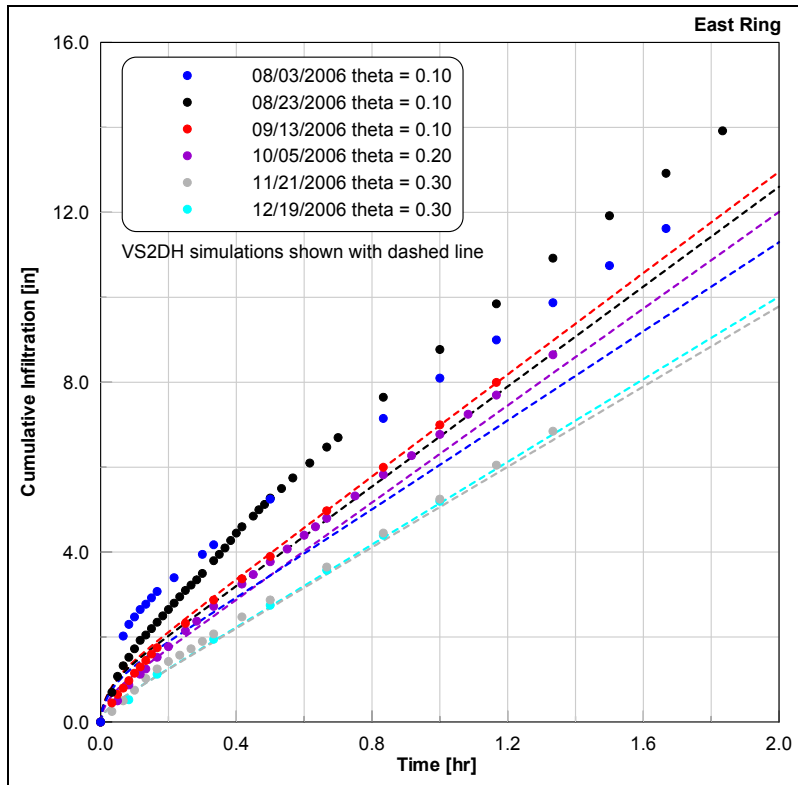


Figure 95. Observed and VS2DH intake curves for the six east ring infiltrometer runs.

Table 14. Summary of single-ring infiltrometer data and VS2DH simulations for the east ring infiltrometer.

| Run Date | Intake Rate [in/hr] | Soil Temp. [°C] | Water Temp. [°C] | θ [-] | K [in/hr at 20°C] |
|------------|------------------------|--------------------|---------------------|-----------------|----------------------|
| 08/03/2006 | 5.2 | 24.9 | 35.6 | 0.10 | 2.0 |
| 08/23/2006 | 6.0 | 21.7 | 30.9 | 0.10 | 2.5 |
| 09/13/2006 | 6.0 | 18.5 | 21.9 | 0.10 | 3.1 |
| 10/05/2006 | 5.6 | 16.9 | 20.4 | 0.20 | 3.1 |
| 11/21/2006 | 4.8 | 10.4 | 10.6 | 0.30 | 3.4 |
| 12/19/2006 | 4.9 | 7.0 | 8.1 | 0.30 | 3.7 |

The simulated intake curves from the two infiltrometer runs from August 2006 both show discrepancies in the final cumulative volume similar to the west ring data from the same time. Given that the analysis is focused on the intake rate, it may be advantageous to compare the observed and simulated intake rates in a graphical context. This illustrates

the early time discrepancies for some of the runs. Figure 96 also shows how well the simulated final intake rates correspond with the observed measurements for all six runs.

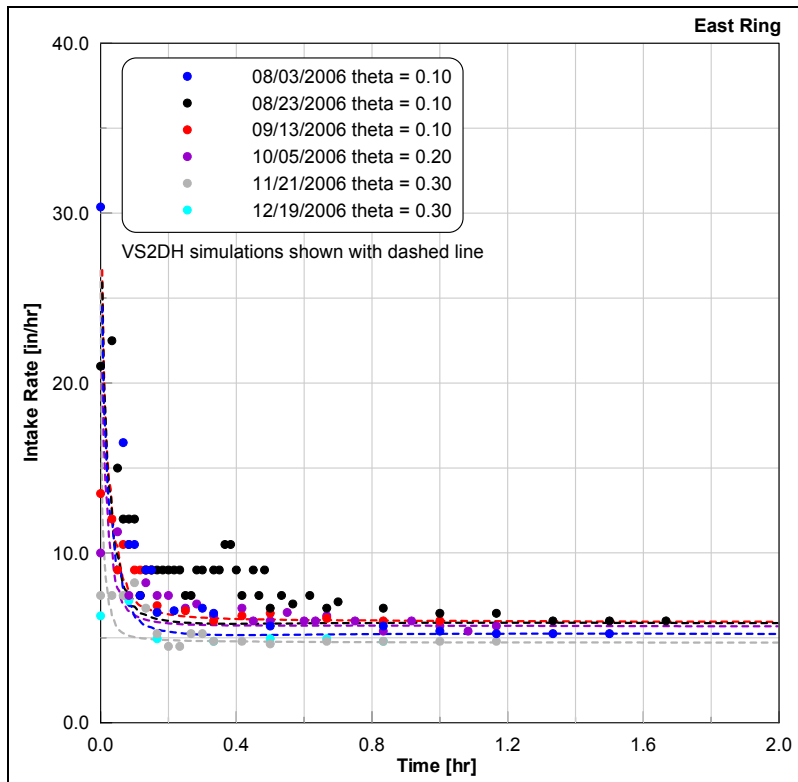


Figure 96. Observed and simulated intake rates for all six east ring runs.

Except for the first two runs with low initial moisture levels, all the simulated intake curves match the observed intake curves well. The average hydraulic conductivity found for the six infiltrometer simulations was 3.0 in/hr at 20°C, with a standard deviation of 0.62 in/hr. In general, the faster observed intake rates yielded lower estimates for saturated hydraulic conductivity. In an isothermal system faster intake rates would correspond with higher hydraulic conductivities; this highlights the importance of monitoring temperature. To illustrate this point the August 23rd, 2006 and November 21st, 2006 east ring runs were simulated as isothermal systems with no temperature

variation considered. These two runs were chosen because they displayed the fastest and slowest observed intake rate. Simulating these runs without any temperature dependence or references is the equivalent of running the two tests without measuring or considering temperature (a common practice). This method yields an estimate for saturated hydraulic conductivity of 3.2 in/hr for the August 23rd, 2006 run and 2.6 in/hr for the November 21st, 2006 run. These estimates are almost a perfect reversal of the estimates found when temperature is considered (2.5 in/hr and 3.4 in/hr respectively). If there were no physical changes to the soil sample over time, and all other factors remained equal except temperature, and the temperature distribution was perfectly represented, the runs which considered temperature should provide equal estimates of the saturated hydraulic conductivity referenced to 20°C. Since the hydraulic conductivity estimates varied, it can be assumed that either the soil underwent some physical changes or there were errors in the temperature measurements and heat transport properties. A more detailed near-surface temperature profile would have been more representative than the single one foot averaged value used here.

Finally, to illustrate the three-dimensional nature of the ring infiltrometer test, moisture content plots of the near-surface computational domain for the east ring August 23rd, 2006 run are shown in Figure 97. The plots are taken from VS2D at 0.25 hr increments. The August 23rd, 2006 date was chosen because it had dry initial moisture content (0.10) and therefore shows more three-dimensional flow. The plots in Figure 97 are axisymmetric views with volumetric moisture content shown in color.

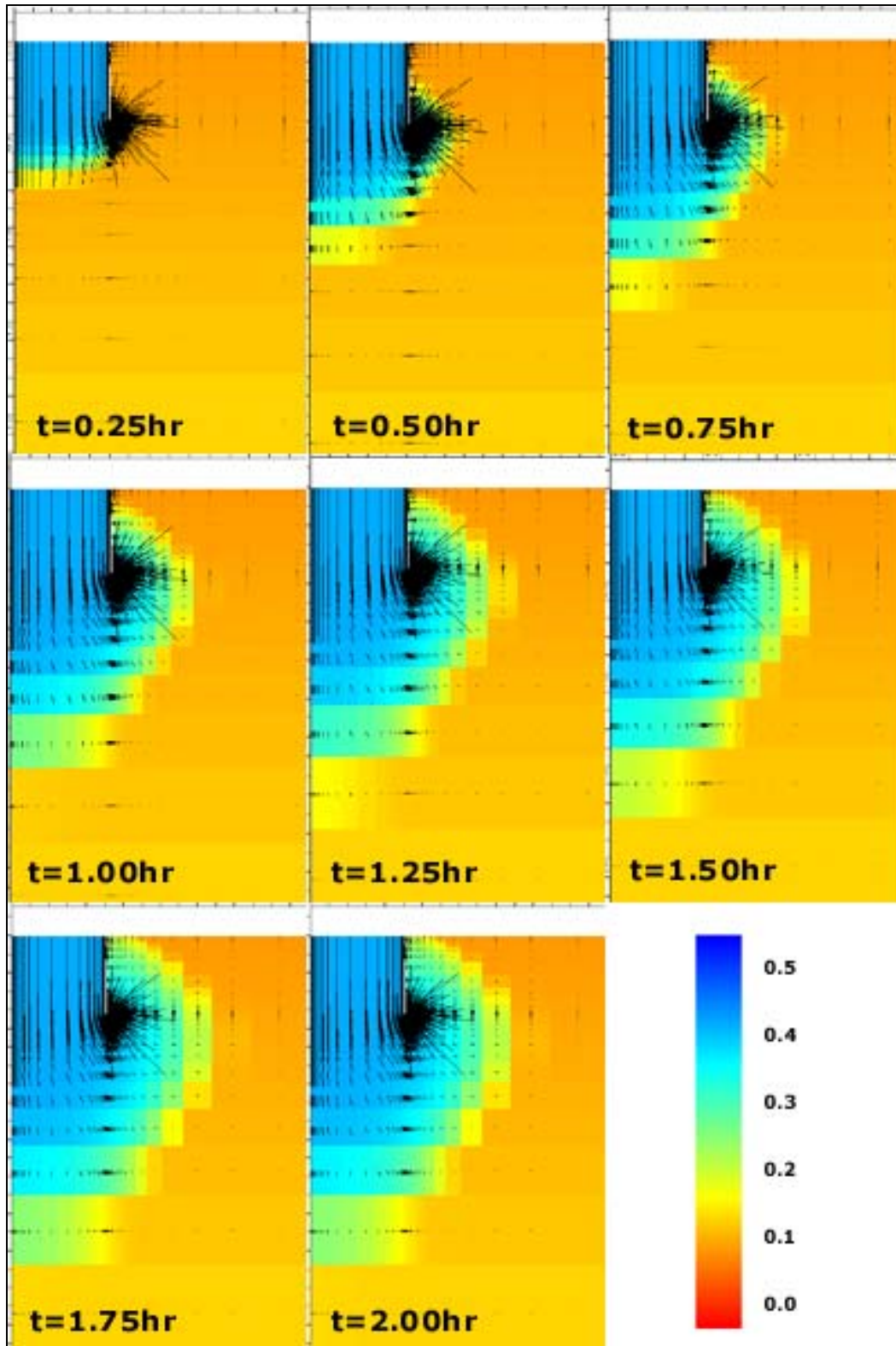


Figure 97. Axisymmetric view of volumetric moisture content from VS2D at 0.25 hr increments for the August 23rd, 2006 east ring infiltrometer simulation. Black lines represent grid cell flow velocity vectors.

3.4.3.7 Summary and Implications

In summary, the permanently installed single-ring infiltrometers provided insight into the spatial and temporal variations of infiltration in the BTI. The VS2D simulations provide a quantitative and physically based method to translate results from an infiltration test into estimates of saturated hydraulic conductivity. Additionally, the model can account for temperature variations and provide estimates for hydraulic conductivity that are not biased due to temperature differences.

On average, the east ring produced a steady-state intake rate that was more than twice that found for the west ring. This was expected based on visual observations of the soil surface at the two locations. However, it is unlikely that the two ring locations represent the absolute slowest and fastest locations within the BMP. The resulting hydraulic conductivity estimates for the rings, 0.78 in/hr for the west ring and 3.0 in/hr for the east ring, give some indication of variability expected within the BMP. It is important to remember that the combined area tested by the two rings is only 1.5 ft², representing only 0.1% of the total wetted surface area when the BMP is full. Therefore, due to spatial heterogeneity, it is unrealistic to expect a realistic estimate for the hydraulic conductivity based on such a small sample size. Based on the temperature dependency of the BMP, the effective (area-averaged) hydraulic conductivity of the BTI is 0.24 in/hr at 20°C. The estimate provided by the slower west ring is more than three times this estimate at 0.78 in/hr. With only two locations it is not possible to determine if this discrepancy is a result of spatial heterogeneity or if the infiltrometer estimates are providing estimates of something other than the area-averaged effective hydraulic conductivity. In other words,

if infiltrometer runs were conducted on a larger portion of the soil surface, would the mean approach 0.24 in/hr at 20°C? The current analysis cannot answer this question. One potential reason the mean might not approach this value is the potential for differences in air entrapment between the point source type of flow field of the infiltrometer and entire surface flooding that occurs during a storm event. Air entrapment would provide a more significant reduction in the hydraulic conductivity estimate when the entire surface is rapidly flooded as this would provide less area for air to escape.

3.5 Conclusion

In summary, soil testing for the infiltration of stormwater runoff is a critical topic. In addition to determining whether a site is a candidate for infiltration, this testing is used to determine the infiltration capacity of a potential infiltration BMP. Consequently, these test results have a strong influence on the design of the BMP, including its size and required storage volume. No unified method exists to dictate proper test methods nor to translate test results into predicted as-built BMP performance.

This chapter has summarized the soil testing at the three infiltration BMPs. The particle-size distribution is a commonly used and standardized test. These distributions are helpful in qualitatively comparing soils and they enable the soil to be classified using the USDA Soil Classification Triangle. The particle-size distributions for the soil at the three infiltration BMPs are consistent with the as-built BMP performance observations.

However, this data alone is not sufficient to provide quantitative information on soil hydraulic properties relevant to the infiltration process (hydraulic conductivity). Various

empirical methods to estimate the hydraulic conductivity from particle-size distributions have been reported in literature. Some of the most commonly used methods include the Hazen and Kozeny-Carmen equations (Freeze and Cherry 1979). However, these methods provide an order of magnitude estimate, which is not accurate enough to be capable of being used in the design of infiltration BMPs.

Various test methods were used in the preconstruction infiltration testing at the three infiltration BMPs. These various techniques provided a wide range of intake rates, some as high as 60 in/hr and as low as 0.24 in/hr among the various methods and sites. The tests that were a direct measure of the hydraulic conductivity (undisturbed core flexible wall hydraulic conductivity test) or an in-situ test adaptable to a variably saturated groundwater model provided useful information that was consistent with the observed BMP performance. These methods show they are capable of predicting the performance of a proposed BMP and, therefore, should be used in the design and sizing of such BMP. Because of its widespread use and experimental simplicity, the constant head single-ring infiltrometer with temperature measurements appears to be a robust and accurate method. The experimentally determined intake rate can be translated into an estimate of hydraulic conductivity when the experiment is simulated in a variably saturated model like VS2D. The observed intake rates from many other commonly used infiltration tests can be used to make comparisons among different soils/locations but are not directly representative of any physical properties of the soil. The intake rates reported for these experiments greatly overestimates the observed performance of the BMPs and should not be used in the design and sizing of an infiltration BMP.

The in-situ infiltration test conducted at the BTI provided valuable information on the hydraulic characteristics of the soil within the BMP. The results gave insight on the spatial and temporal variability within the BMP. The experiments were modeled using a temperature dependent simulation in VS2D. These simulations provided hydraulic conductivity estimates of 0.78 in/hr for the west ring and an average 3.0 in/hr (at 20°C) for the east ring. Both of these estimates are larger than the average 0.24 in/hr (at 20°C) that is observed from the BMP monitoring data. This may be a result of the spatial variability and the small sample area of the two ring installations. Conversely, this discrepancy could be a indication of the variation of the influence of air entrapment between the ring infiltration experiments and the areal flooding of the entire basin during a storm event. The numerical modeling of the infiltrometer data has further illustrated the importance of temperature measurements during such experiments.

Chapter 4. Groundwater Modeling of Infiltration BMPs

4.1 Introduction and Purpose

The variably saturated groundwater model, VS2D was used to simulate a hypothetical profile of the PCIB and BTI. The IT was not included in this analysis, because of the one-dimensional nature of the modeling. In general, infiltration BMPs are specified to be located at some distance above the local groundwater table (MDE 2000; NJDEP 2004; PADEP 2006). Therefore, a complete understanding of the infiltration process requires knowledge of unsaturated groundwater hydraulics. Numerical modeling is typically used to analyze flow in unsaturated soils, due to the nonlinear nature of the unsaturated flow equation. Simpler, empirical methods like the Green and Ampt model are also often employed (see Appendix F).

The purpose of this modeling was to provide a conceptual explanation of the infiltration process and create a reasonable, hypothetical profile that performs in a fashion similar to that observed at the BMPs. Some actual observed data from the BMPs was used as an input to the model. However, there was no calibration procedure undertaken to match other observed data from the BMPs. The observed depth data from both sites was used as the basis of the model input for both sites. The observed soil moisture meter data, the total profile intake volume, along with other knowledge of the subsurface flow process were used as a basis to judge the adequacy of each model. For each BMP a single representative storm was simulated. The models were first created and run under isothermal conditions (20°C). Then the same model was run under a hypothetical cold and warm condition. For the cold condition both the soil surface and the inflow were

specified at 0.9°C and 26°C for the warm condition. This temperature range is representative of the temperature extremes found at the BMPs. For both simulations the groundwater table was 15 feet below the soil surface and its temperature was specified at 13°C. The model domain for all simulations was a one foot wide by 15 ft deep section. The model domain was split into a single column (one-dimensional) and approximately 2,000 rows.

4.2 Pervious Concrete Infiltration Basin

The October 7th, 2005 storm was chosen to be modeled at the PCIB. This was a large storm with approximately 5.5 in of rainfall. The storm filled the lower storage bed and the BMP produced overflow for 14 hours. The bed depth data was used as a total head boundary condition set at the soil surface. VS2D allows a unique boundary condition for each specified recharge period in the simulation. Numerous 15-minute recharge periods were specified with the total head condition for each being set to the corresponding bed depth for that time. A total of 288 15-minute recharge periods were created with an additional 228 hour recharge period at the end in which the boundary condition for the soil surface was specified as a “no flow” condition to allow for the simulation of moisture redistribution in the subsurface after the cessation of surface infiltration. The text file-based automated input feature was used to efficiently import the bed depth and inflow temperature data.

The soil profile at the PCIB was modeled as a two-layer system. There was a 0.2 ft thick lower conductivity layer (one tenth the underlying hydraulic conductivity) underlain by

the remaining 14.8 ft layer of a higher conductivity soil layer. The VS2D model profile is shown in Figure 98 and the soil parameter details are summarized in Table 15.

Observation points are shown with small open circles (1, 2, and 4 ft). Note that heat transport properties of the soil were set the same as those detailed in Section 3.4.3.5.

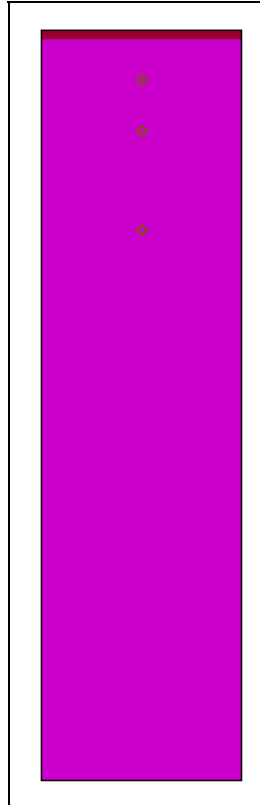


Figure 98. PCB model profile diagram.

Table 15. Model soil profile properties for the PCB.

| Layer | Depth [ft] | Sat. K [ft/hr] | Sat. K [in/hr] | Porosity [-] | θ_r [-] | α [ft ⁻¹] | β [-] |
|-------|---------------|-------------------|-------------------|-----------------|-------------------|---------------------------------|----------------|
| 1 | 0.20 | 0.002 | 0.024 | 0.43 | 0.15 | 1.10 | 1.56 |
| 2 | 14.8 | 0.02 | 0.24 | 0.43 | 0.078 | 0.154 | 7.00 |

A lower conductivity surficial layer was simulated because the formation of such a layer is certain (Hillel 1998; Assouline 2004). The properties and thickness of such layer are unknown and were estimated for the model.

The initial conditions of the simulations were specified using the initial moisture content option. The volumetric moisture content of the soil was set to that as measured by the moisture meters at their respective depths (1, 2, and 4 ft). The one foot moisture content was also specified at the soil surface, and the volumetric moisture content at a depth of 15 feet was set at the saturation level for that soil (0.43). The ponded depth and intake volume for the three simulations (isothermal conditions (20°C) and low and high temperatures) are summarized in Figure 99. The simulated intake volumes are reasonable estimates considering the observed total ponded depth, time of ponding, and storage bed porosity.

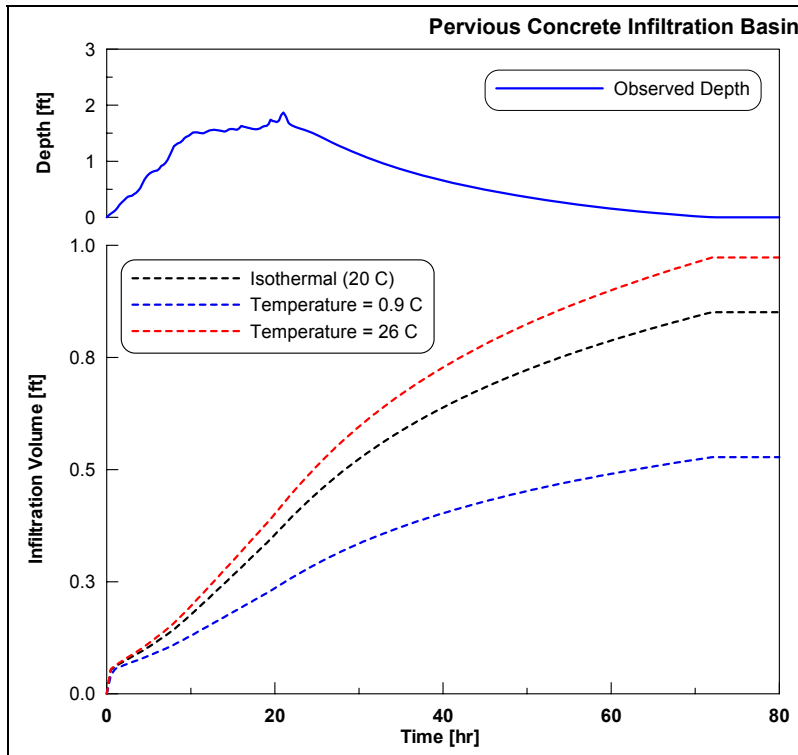


Figure 99. Total head condition (bed depth) and resulting soil profile intake curves for three VS2D simulations at the PCIB.

The program can write simulation output data relative to the user input observations points in a separate output file. The observation points were located to correspond with the observed soil moisture meter data. For this storm event the moisture meters reach maximum values of 0.25, 0.24, and 0.23 from initial values of 0.17, 0.18, and 0.19 respectively for the 1, 2, and 4 ft meters. From a mass balance perspective, the observed change in storage within the soil profile is too small. This may be a result of the calibration of the moisture meters or of heterogeneity and preferential flow in the soil beneath the BMP. Therefore, the observed results are scaled so that their maximum and minimum values correspond with that obtained in the modeling. Only the first 100 hours of observed moisture meter data are shown because after that time there was additional rainfall. The ponded head, observation point output, and scaled observed moisture meter

data are summarized in Figure 100. The observed ponded water temperature for this storm was 21°C.

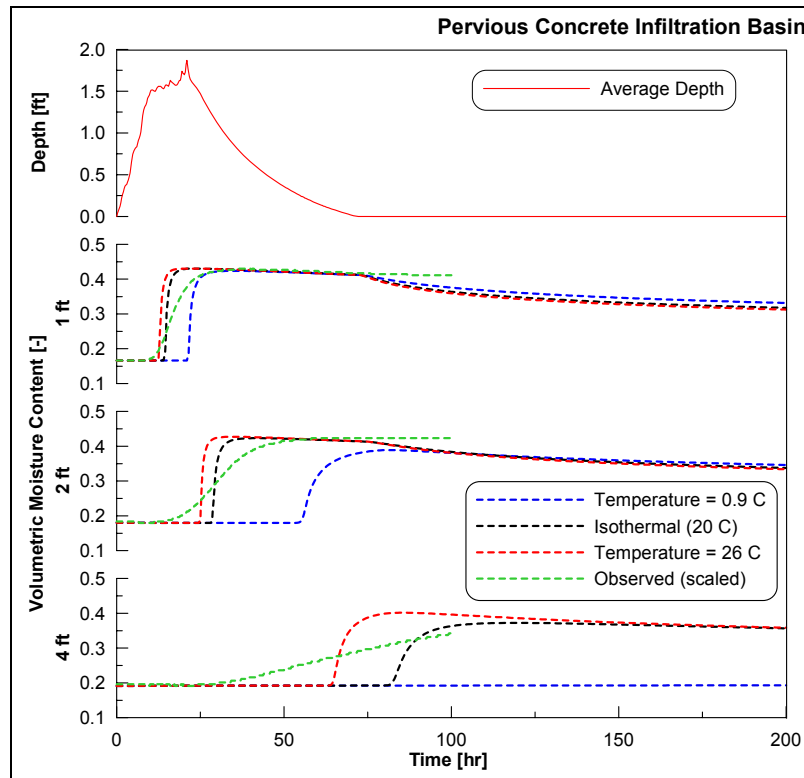


Figure 100. Total head condition (bed depth) and resulting volumetric moisture content output for three depths in soil profile at the PCIB.

The model results confirm that the lower conductivity surficial layer prevents the soil profile from becoming saturated at all three of the observation points. The moisture content levels approach full saturation (non-negative hydraulic head) but never attain it. The timing of the moisture front is fairly well represented by the simulation, although the observed moisture front is more gradual than that from the model, a typical artifact of heterogeneity. The timing of the moisture front is considerably changed between the different temperatures. The inflow and surface temperature of the domain was set at the

specified temperature (0.9°C, 20°C, 26°C) and the bottom of the domain was held constant at 13°C for both simulations. The domain temperature between those two depths is interpolated by the program since there were no other known temperatures between those locations. This assumption may result in initial subsurface temperature profiles that represent extremely warm and cold worst-case scenarios. It is possible that a constant temperature is attained at a shallower depth. This may explain why there is such a substantial difference in the timing of the moisture front at the different temperatures. Figure 100 illustrates that for the cold simulation the moisture front is just beginning to arrive at the 4 ft depth at 200 hours while in the warm simulation it arrives at only 70 hours.

4.3 BioInfiltration Traffic Island

The moisture meter data at the BTI is sparse and intermittent. The September 18th, 2003 storm was chosen for the groundwater modeling effort because it is a relatively large single peaking storm during which the moisture meters were in operation. There was approximately 1.5 in of rainfall for this storm event which produced six hours of overflow conditions from the BMP. The storage bed depth data was used to develop a total head boundary on the soil surface in the model. Unlike the PCIB, the detailed geometry of the storage bed at the BTI is known. Therefore, the measured depth data is converted to an average depth value for the entire stage hydrograph. This averaged depth was used as the total head boundary in VS2D, as it is a better representation of the conditions experienced over the entire surface of the BMP. 306 individual 15-minute recharge periods were created, each with its own total head value. A final 123.5 hr

recharge period with a no-flow specification for the soil surface was added at the end to allow for subsurface moisture distribution.

The soil profile at the BTI was modeled as a three layer system. The profile consists of the composite sand/soil mixture to a depth of 4 ft with the undisturbed original soil below. As in the case of the PCIB, a shallow layer (0.25 ft) of lower conductivity was added at the soil surface. The soil profile is shown in Figure 101 and its properties are summarized in Table 16. Observation points are shown with small open circles. Heat transport properties of all the soil types were set the same as those detailed in Section 3.4.3.5.

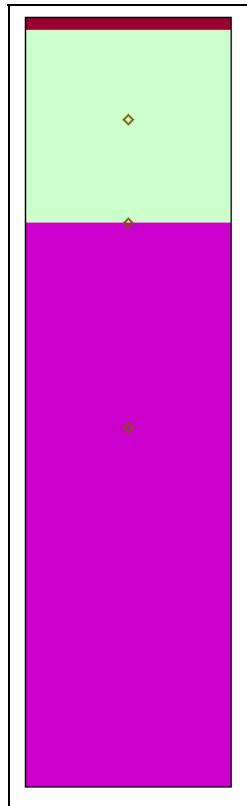


Figure 101. BTI model profile diagram.

Table 16. Model soil profile properties for the BTI.

| Layer | Depth [ft] | Sat. K [ft/hr] | Sat. K [in/hr] | Porosity [-] | θ_r [-] | α [ft ⁻¹] | β [-] |
|-------|---------------|-------------------|-------------------|-----------------|-------------------|---------------------------------|----------------|
| 1 | 0.25 | 0.005 | 0.06 | 0.41 | 0.0095 | 0.58 | 1.31 |
| 2 | 3.75 | 0.3 | 3.6 | 0.41 | 0.0650 | 0.80 | 1.89 |
| 3 | 11.0 | 0.03 | 0.36 | 0.43 | 0.0780 | 1.1 | 1.56 |

One of the main observations on the subsurface flow comes from the monitoring well within the basin which is located and screened at a depth equal to the sand/soil mixture and original soil interface (4 ft below surface). From September 2002 until September 2003 a pressure transducer was installed in the bottom of the well. During the entire year the pressure transducer never measured any ponded depth. This implies that the composite sand/soil mixture at the soil layer interface never reaches saturation and that there is no ponding at this interface. Therefore, the surface intake rate of the BMP is not influenced by the lower conductivity lower layer (original soil). Whether or not ponding will occur at this interface depends on many factors including the difference between the relative permeability of the layers and the supply rate of water to the interface. One factor that can prevent ponding at the interface is the presence of a surficial layer with a lower hydraulic conductivity than the soil mixture. In the case of the BTI this layer is likely poorly defined and heterogeneous.

As in the case of the PCIB, the initial conditions of the simulations were specified using the initial moisture content option. The surface volumetric moisture content was estimated at 0.20 and the moisture content at 15 ft was saturated (0.43). Figure 102 shows the measured and average ponded depths and the intake volume for the three

simulations (isothermal conditions (20°C) and low and high temperatures). The calculated intake volumes are reasonable considering the observed total ponded depth and the time of ponding.

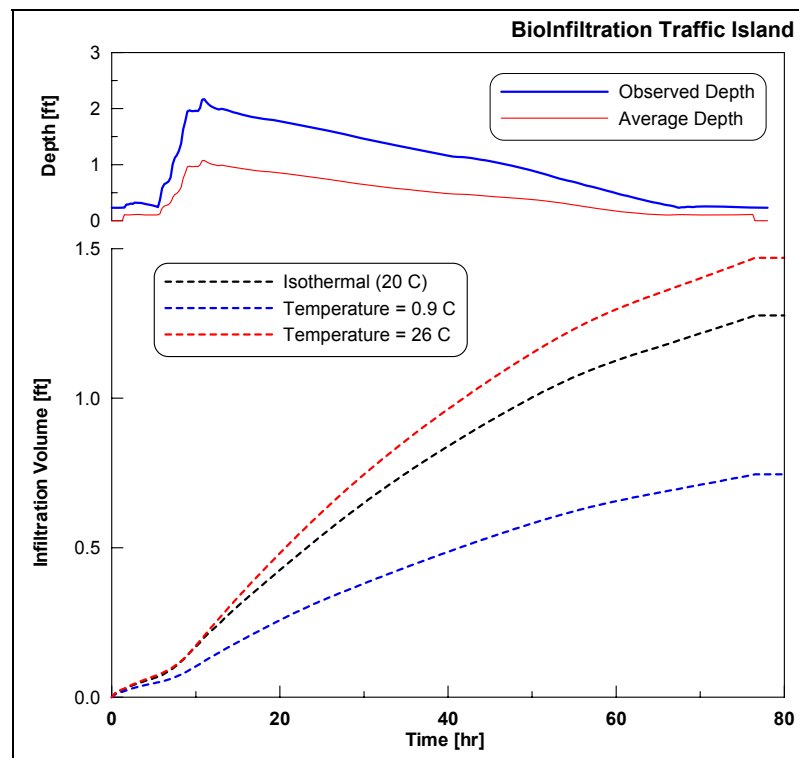


Figure 102. Bed depth and resulting soil profile intake curves for three VS2D simulations at the BTI.

Observation points which corresponded to the depths of the subsurface moisture meters at the BMP (2, 4, 8 ft) were added to the model. As discussed in Section 1.3.2, the moisture meters were difficult to calibrate. Therefore, the moisture meter data was used as an indication of the timing of the moisture front. Their response for the September 18th, 2003 storm was scaled to match the minimum and maximum of the model observation points. Also only the first 100 hours of observed moisture meter data are shown because there was additional rainfall after this time. The average ponded depth, observation point

output, and scaled observed moisture meter data are summarized in Figure 103. This storm occurred prior to the measurement of temperature at the BMP and, therefore, there is no observation of the temperature of the ponded water. However, storms at this time of year are close to 20°C at the BTI.

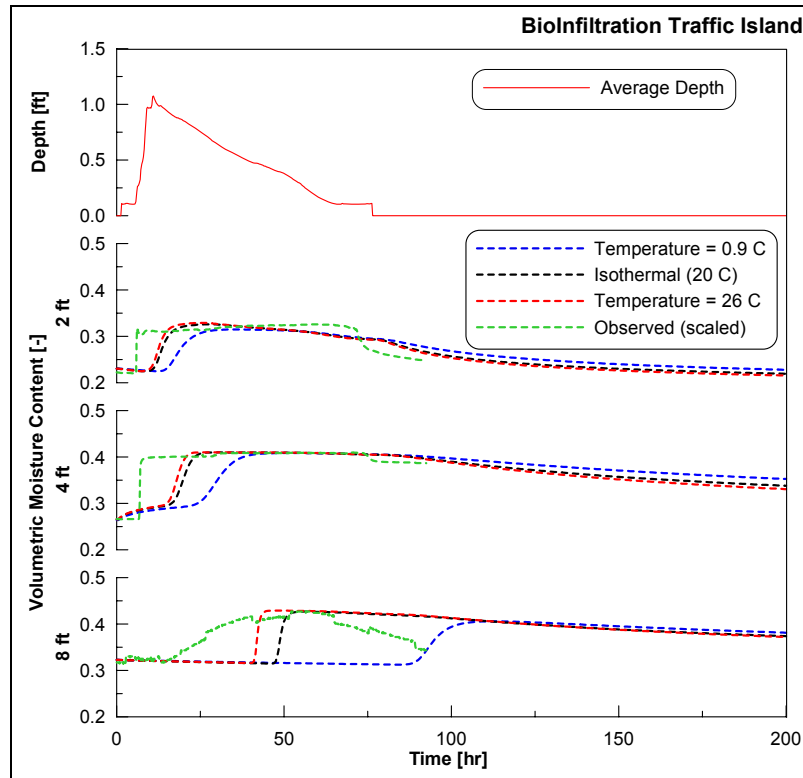


Figure 103. Total head condition (average bed depth) and resulting volumetric moisture content output for three depths in soil profile at the BTI.

The lower conductivity surficial layer prevents the composite soil mixture below from becoming fully saturated, even at the original soil interface as implied by the absence of ponded water at this location. The observation point at a depth of 2 feet only reaches 80% saturation. With the input parameters shown in Table 16, ponding does not occur at the interface with the original soil. Volumetric moisture content at that location

approaches, but does not become, saturated. The condition of no ponding at the soil interface was one of the measures used to determine the model parameters in Table 16. The total profile intake volume (1.3 ft for the isothermal run) was also used to judge the adequacy of the conceptual model. While these two measures were met, the timing of the moisture front according to the moisture meters was not well described by the model. The model predicts that the moisture front is moving much slower than the moisture meter data would imply. This discrepancy may be a result of preferential flow paths created as a result of the moisture meter installation process, or a result of the moisture meter calibration/operation. Another limitation is that it is a one-dimensional simulation and the subsurface flow process beneath the BTI becomes less and less adaptable to a one-dimensional system as the depth increases. Groundwater flow has more of an opportunity to diverge and flow laterally at increased depths.

4.4 Conclusion

In summary, VS2D has proven to be a useful tool in understanding and confirming the variably saturated flow processes that occur within the BMPs. While this modeling effort has been conceptual in nature, it has provided insight into the flow dynamics beneath the BMPs. The modeling has shown how a limiting layer can create unsaturated conditions beneath the BMPs, which compares favorably to site observations. It has also explained the absence of a perched water table at the interface between the higher permeability sand/soil mixture and the original soil of the BTI. Both models used observed depth data as input boundary conditions for the soil surface. The resulting simulations provided reasonable estimates for total soil profile intake and subsurface moisture distributions.

The results showed the substantial influence of temperature over a typical range of temperatures experienced at the BMPs.

Chapter 5. Summary and Conclusions

This research has demonstrated that properly sited and constructed infiltration BMPs can provide a long-term, long-lasting solution for the control of excess stormwater runoff volumes. Many practicing engineers in the field of stormwater management are under the assumption that infiltration features have a limited and short lifespan. This uncertainty has led to apprehension in the implementation of infiltration BMPs. This work has shown that the sustained performance of infiltration BMPs can be achieved when the design properly addresses the mechanisms and physical processes that are critical to the longevity of an infiltrating feature. Furthermore, this work has identified the magnitude and source of seasonal variations in infiltration BMP performance, which has many implications on the design, operation, and performance assessment of infiltration BMPs. In addition, this research has also examined preconstruction infiltration testing techniques and demonstrated the importance of relating these techniques to physical properties of the soil that are relevant to the design and as-built performance of infiltration BMPs.

A sustainable approach to water resource management is an increasingly important concern. Maintaining the natural hydrologic cycle is an essential part of a sustainable approach to water resource management. The conversion of forested or otherwise undisturbed land for residential and commercial uses entails the construction of impervious surfaces and the compaction of otherwise pervious areas. These impervious surfaces and newly compacted soils generate far more surface runoff than they did prior to development. The local hydrologic cycle of the site shows a significant shift with

increased surface runoff which is balanced by consequent decreases in evapotranspiration and infiltration. Past stormwater management practices have only focused on controlling the peak flow rate of the runoff generated from the developed areas. This type of methodology does not address the hydrologic modifications caused by the land development process. Unlike the hydrologic modifications it fails to address, a peak flow-based system does not function in a cumulative fashion at a watershed scale. A more sustainable and appropriate approach is to directly address the increase in the volume of runoff created by the land development process. The most commonly used technique to manage this increased volume is through engineered infiltration practices. The engineered infiltration of stormwater runoff is not a particularly new application. However, due to continued flooding and flood-related damages and the continued degradation of aquatic habitat and water resource supplies under traditional management techniques, infiltration BMPs have garnered new interest. Stormwater regulations have changed to reflect a new focus on volume control measures; specifically infiltration BMPs.

This research has provided answers to many questions related to infiltration BMP design, performance, implementation, and assessment. The primary instrument for this investigation is the analysis of continuous monitoring data from three infiltration BMPs. The construction of these three BMPs was strictly overseen and precautions were taken to avoid any unnecessary compaction of the soil beneath the BMPs.

The analysis of more than nine combined years of hydrologic monitoring data at the three infiltration BMPs has indicated that both the PCIB and the BTI are not experiencing a systematic decrease in performance. This implies that typical clogging processes related to ponded infiltration and incoming water quality are sufficiently small or adequately counteracted by processes that tend to maintain or increase the hydraulic properties of soil. This emphasizes the importance of proper design, siting, pretreatment, construction, and maintenance.

For the PCIB this continued performance can be largely attributed to the extremely low loading ratio of the BMP in addition to the characteristically low suspended solids concentration of incoming runoff. In contrast, the BTI has a moderate loading ratio and solids concentrations typical of moderately used street and parking areas. However, like the PCIB, this BMP has also exhibited a sustaining (although seasonal) level of performance. This sustained performance can be attributed to the heavily vegetated surface storage bed. The BMP has developed a protective, self-renewing, organic layer which promotes vegetation and root growth and is highly susceptible to disruptive forces of surface desiccation and freeze-thaw processes. Additionally, two rip-rap swales have provided some level of suspended solids pretreatment.

The IT is the only BMP to have demonstrated a systematic decrease in performance. This BMP was intentionally designed with an unrealistically high loading ratio which is more than 25 times the recommended ratio (PADEP 2006). Therefore, from a solids loading perspective the three year old BMP may have up to 80 years of equivalent

operation. The decrease in infiltration at the site is largely due to the high suspended solids concentrations from the heavily trafficked parking deck and the lack of pretreatment at the BMP. Furthermore, the BMP has a relatively deep storage bed. This type of deep and frequent ponding has the ability to compact depositional seals which are expected to develop in such applications. The compaction of this layer causes a further decrease in the infiltration capacity of the BMP.

Although the BMP has been in operation for six years, the longest data record analyzed in this study (>4 years) was that of the BTI. This data span is the longest of its kind; nevertheless it is too short to represent a lifecycle analysis of the BMP. A better measure of the longevity will come over a larger period of record (10-50 years). Therefore, while this represents a “long-term” study, it does not represent a lifespan analysis. However, the span of data analyzed here is longer than many of those that have reported high failure rates among similar infiltration BMPs (Lindsey, Roberts et al. 1992; Schueler 1994). Considering the increasing focus and widespread implementation of infiltration BMPs, this type of examination is essential to understanding the longevity and potential lifespan of infiltration BMPs.

All three of the infiltration BMPs exhibited a strong seasonal change in performance. The seasonal changes are roughly two-fold with the highest rates in late summer and the lowest observed in late winter. The seasonal changes are significant and result in event ponding times which vary over the course of a year between 50 to 80 hours and 80 to 120 hours on average for the PCIB and the BTI, respectively. The observed seasonal changes

in performance are similar to those expected based on the temperature dependency of the viscosity of water. This strong seasonal variation has implications for the design of infiltration BMPs and major implications for the performance assessment of infiltration BMPs.

A particle-size analysis was conducted and the soils at all three BMPs were classified according to the USDA soil classification triangle. These classifications are a valuable measure of the soil texture and allow for a direct comparison among different soils. However, they do not provide adequate estimates for the soils' hydraulic conductivity that can be used in the design and sizing of the BMP.

Various infiltration tests were performed at the three infiltration BMPs. These tests included flexible wall hydraulic conductivity tests on an undisturbed soil core, simple "percolation" tests, variations of the Maryland test well method, and constant head single-ring infiltrometer tests. The results of these tests varied widely among the methods. However, the flexible wall hydraulic conductivity method provided an acceptable estimate of the as-built performance. Additionally, the constant head single-ring infiltrometer tests were adaptable to an axisymmetric variably saturated groundwater model. Calibration of the model resulted in reasonable estimates for the soils' hydraulic conductivity. The other test methods were not appropriate for design or sizing of infiltration BMPs.

In-situ infiltration testing was performed within the BTI. Two permanently installed single-ring infiltrometers were established at the BMP. The 12 inch rings were run with a constant head method using a custom-built Mariotte reservoir. The results from the two rings provided an indication of the potential variability to be expected within an open surface vegetated infiltration BMP. Axisymmetric variably saturated groundwater modeling with heat transport was used to translate the experimental intake curves into estimates of hydraulic conductivity. The tests did not provide a good estimate of the as-built performance of the BMP. It is not known whether this discrepancy is simply a result of spatial variability within the BMP, or potential differences in air entrapment between the infiltration tests and the areal flooding during a storm event. The temperature of the soil and ponded water was monitored during all of the in-situ infiltration tests. As expected, the estimates of hydraulic conductivity found when temperature was considered differed significantly from those with no temperature consideration, highlighting the importance of temperature measurements.

Representative profiles of the PCIB and the BTI were simulated using VS2D. This modeling provided a conceptual description of the subsurface flow processes at the BMPs. The simulation explained how a surface limiting layer can create unsaturated conditions beneath an infiltration BMP. In the case of the BTI, the model demonstrated how a limiting surface layer can prevent the formation of a perched water table at the original soil and composite soil mixture interface. The one-dimensional profile simulations for both sites used an observed stage hydrograph from the data record along with the corresponding moisture meter data. Low and high temperature scenarios were

simulated to determine the influence of temperature on both the surface intake rate and the subsurface moisture profile. The effect of the temperature variation on the surface intake rate was shown to be similar to that observed in the data record for both BMPs. The temperature variation also had a significant influence on the subsurface moisture distribution within the profile.

In conclusion, stormwater infiltration BMPs are a practical and efficient method to control the increased volume of stormwater runoff from developed areas. Volume control techniques such as infiltration BMPs are an essential part of a sustainable approach to water resources management. The hydrologic benefits of an infiltration approach to stormwater management far exceed those provided by a peak flow rate method. However, the long-term benefits of such an approach can only be realized when the long-term performance of the individual infiltration BMPs can be demonstrated.

This analysis has shown that the long-term performance of infiltration BMPs is highly dependent on the specific design parameters of the BMP. Proper design and construction techniques that consider the physical processes responsible for the evolution and continued operation of an infiltrating soil surface will establish a reputation for long-lasting infiltration BMPs.

This study has also demonstrated the magnitude and source of seasonal variations in the performance of infiltration BMPs. This work has shown that these seasonal variations are significant and justify consideration during the design stage, in a multi-season

modeling effort, and especially during any type of monitoring or performance assessment.

Finally, this work has connected preconstruction infiltration tests with the as-built BMP performance they are intended to predict. Furthermore, the results of this work have been used to provide specific recommendations regarding these infiltration tests.

Chapter 6. Design Recommendations for Infiltration BMPs

The three infiltration BMPs examined in this study cover a wide range of the commonly implemented techniques for stormwater infiltration. One of the main objectives of this work is to provide information that can be applied to improve the design, implementation, and performance assessment of infiltration BMPs outside the scope of this study. An important conclusion of this study is that infiltration BMPs can be designed and constructed in such a way that their continued performance can be expected. Both the PCIB and BTI show no evidence of a systematic degradation in performance. Another important, although already to some extent established, conclusion is that an infiltration BMP can be poorly designed such that its sustained performance is not guaranteed. This conclusion is based on the drastic and systematic decrease in performance found at the IT.

One characteristic that all three of the BMPs have in common is that the construction process was strictly overseen, planned, and staged such that the infiltrating surface was not compacted due to equipment traffic and did not experience large sediment loads due to unstabilized areas during construction. Had these precautions not been taken, it would have been unlikely that any of the BMPs would have met their original design goals. The significance of proper construction techniques, while not the focus of this study, cannot be overstated.

The purpose of this chapter is to use the results and conclusions to develop specific recommendations relevant to the design, implementation and assessment of infiltration

BMPs. These recommendations include those related to investigative infiltration testing techniques, general infiltration BMP design, and the performance assessment of infiltration BMPs.

6.1 Infiltration Testing

1. *Infiltration tests used to guide the design of an infiltration BMP should be conducted with the primary objective of determining the soil's hydraulic conductivity.*

The physical property that primarily dictates the performance of any infiltration BMP is the hydraulic conductivity. The specific infiltration test conditions should be considered when translating the test results into estimates of hydraulic conductivity. This is especially true for the test geometry (e.g. ring size, depth driven, depth of ponded head, and other factors), as these parameters will have a large influence on the estimate. Tests which do not explicitly determine the hydraulic conductivity may be useful for a general comparison of other similarly tested soils, but they should not be used in the design process of an infiltration BMP. The single ring infiltrometer test was adapted to a variably saturated groundwater model to provide estimates for hydraulic conductivity based on the observed intake curve of the constant head test. This testing method does not require the use of any sophisticated equipment. Testing apparatus for this methodology is readily available or can be easily constructed from commonly used materials. A constant head single ring infiltrometer is not the only infiltration test that is adaptable to a groundwater model. However, it is one of the simplest methods to simulate due to its simple axisymmetric geometry and constant head boundary condition. Creating and running a variably saturated simulation of the

test is not as straightforward as the test itself. However, the majority of the modeling is involved with the initial setup and creation of the model (simulation domain, computational grid, and boundary conditions). Therefore, if the tests are performed in a consistent fashion the same model can be used for each test by simply changing the soil properties and temperatures.

2. *Infiltration tests should always be conducted on in-situ or otherwise undisturbed soil samples.*

This approach preserves the natural soil structure which is the primary factor influencing the hydraulic conductivity. It is the author's opinion that the infiltration tests should resemble the conditions expected during actual BMP operation. Larger sample sizes and numbers of observations improve the estimate.

3. *The temperature of the supply water should be measured and an attempt should be made to keep the temperature stable during the course of the test.*

This can be accomplished by shading the test location and/or supply water reservoir. Hydraulic conductivity is not solely a property of the soil; instead, it depends on both the porous media and the permeating fluid. This makes the outcome of any infiltration test dependent on the temperature of the supply water. If the simulation does not account for energy transport, precautions should at least be taken to ensure that the temperature of the supply water is similar to the seasonal ground temperature or ambient air temperature at the test location. The relationships developed by model simulations would relate the potential experimental steady intake rate to an isothermal

and homogeneous estimate for hydraulic conductivity. This hydraulic conductivity can then be corrected or adjusted to a reference temperature (20°C) based on the following viscosity relationship.

$$K_{20} = K_T \times \left(\frac{\mu_T}{\mu_{20}} \right) \quad (6.1)$$

Where: K_T = hydraulic conductivity at measured temperature [LT⁻¹]
 K_{20} = hydraulic conductivity at 20°C [LT⁻¹]
 μ_T = viscosity of water at the measured temperature [ML⁻¹T⁻¹]
 μ_{20} = viscosity of water at 20°C [ML⁻¹T⁻¹]

4. *In addition to the infiltration test and consequent modeling, the soil type should be determined through particle-size analysis.*

Particle-size analysis facilitates basic comparisons of soil texture, however they do not provide estimates for hydraulic conductivity that can be used in the design of infiltration BMPs. This analysis is also necessary to use estimates for unsaturated soil hydraulic parameters from existing databases. The experimental determination of these parameters (van Genuchten parameters, for example) is generally out of the scope of typical applications; additionally, sensitivity analyses have shown that they have little influence on both the infiltration test and BMP operation compared with the saturated hydraulic conductivity.

6.2 BMP Design

Due to the precautions taken during the construction process, it can be surmised that the rapid decrease in performance observed at the IT is a result of inadequate design

characteristics of the BMP and not related to the construction process. Conversely, the continued performance of the PCIB and the BTI is attributed to both the sound construction techniques and sound design considerations implemented at both these infiltration BMPs. The longevity of any infiltration BMP, regardless of design, cannot be guaranteed if proper considerations are not taken during the construction process.

1. *The design of an infiltration BMP should attempt to minimize the suspended solids loading potential of the BMP.*

The solids loading of an infiltration BMP is a combination of the land use and sediment-related characteristics of the contributing area, the level of pretreatment, and the areal loading ratio of the BMP. Therefore, the minimization of the solids loading can be accomplished by a combination of these factors. The exceedingly high loading ratio of the IT combined with the lack of pretreatment and the deep ponded depths make it likely that the IT would experience a systematic decrease in performance.

2. *Runoff from surfaces with characteristically low suspended solids concentrations should be prioritized for infiltration.*

These areas include rooftops or other impervious surfaces which are not exposed to frequent automobile traffic or that otherwise do not contain potential sediment sources. It is difficult to establish a precise loading ratio that should be followed in the design of infiltration BMPs; however as a rule of thumb, a 5:1 (DCIA:BMP) ratio is adequate with the total drainage area to BMP ratio close to 10:1. The BTI has

operated with both these ratios doubled with moderately used parking and driving areas and has not shown signs of degradation. This is due to the dense vegetation and the protective surficial soil layer with high organic matter content it has created and also due to the pretreatment provided by two rip-rap swales.

3. *From a longevity standpoint, the open vegetated storage bed has many advantages over an underground storage bed.*

The root activity of the vegetation creates macropores that may account for a large portion of infiltration under ponded conditions. The vegetation also helps create and maintain a protective soil layer with high organic matter content. A hardwood mulch layer applied after construction provides immediate protection and also encourages plant growth. In addition to root activity, the soil layer created by the mulch and vegetation is also susceptible to hydraulically beneficial impacts of surface desiccation and freeze-thaw processes. From a practical standpoint, the open bed approach is also easier to maintain if there is a sediment loading problem. Open bed infiltration features can also be designed and planted in a manner that can provide an aesthetic amenity to a site. However, there are instances where infiltration is desired or required but an open storage bed approach may not be feasible. This occurs when the area for the BMP is needed for other purposes (parking for example). All of the hydraulically beneficial processes that are present in an open storage bed are not achievable in an underground application. Additionally, the maintenance of the soil surface in an underground bed is cost prohibitive. Therefore, vegetated open bed applications should be preferred over underground beds, where they are feasible. If

an underground bed is required, extra precautions should be taken to minimize the solids loading of the BMP. The DCIA:BMP ratio should not be kept to a minimum and drainage areas with characteristically high solids concentrations should be avoided. Additionally, the runoff should have some level of pretreatment prior to entering the underground bed. Designs which exceed these guidelines will be at a considerably increased risk of failure.

4. *The design should minimize the maximum ponded depth within the infiltration BMP.*

Excessive ponded depths create an increase in the effective stress across limiting surficial layers which are expected to develop. This increase in effective stress will further compact these layers and thereby further reduce their hydraulic conductivity. The design depth is typically governed by a combination of the expected recession rate and the maximum allowable drawdown time. Shallow depths and shorter ponding times will further help to maintain a soil surface conducive to infiltration by allowing the soil surface to completely dry (desiccate) between storm events.

5. *Infiltration BMPs should be implemented in the most distributed fashion that is feasible at a site.*

This technique will support and facilitate many of the previous recommendations. This approach will minimize the loading ratio of the BMPs and also tend to create more, smaller BMPs. These smaller BMPs are easier to excavate (construct) without compacting the soil surface with unnecessary equipment traffic because, like the BTI, they can be constructed from the perimeter of the basin. Another advantage that was

not specifically a focus of this study is that a more distributed approach will minimize the potential for excessive groundwater mounding beneath the BMPs and any adverse impacts to adjacent structures the mounding might create.

6. *Proper design and simulation of infiltration BMPs should consider the roughly two-fold variation that can be expected due to temperature-induced viscosity effects.*

Neglecting to consider these temperature effects may result in a misrepresentation of event and annual BMP capture efficiencies. Storage volumes should be sized such that the infiltration BMPs will still meet their intended capture efficiencies during periods of slower infiltration. Additionally, continuous simulation of infiltration practices (over the course of various seasons) should not be based on a static representation of the infiltration process at the BMP.

In summary, infiltration BMPs must be designed and built with proper consideration given to the physical processes that will dictate their long-term performance. While there is still a need for more quantitative information regarding the relative influence of these processes, they should be considered and proactive measures should be taken to maximize their net positive impact.

6.3 Infiltration BMP Assessment

The seasonal variation of infiltration BMPs highlights the importance of long-term continuous monitoring and has many implications on the design, operation and especially the assessment of stormwater infiltration BMPs. The temperature dependency and

seasonal variation of infiltration BMPs has clear geographic and climactic implications. Therefore, infiltration BMPs should be viewed in the context of their climate and individual/local temperature regimes.

1. *BMP assessment based on one or only a few ponded infiltration observations may greatly misrepresent the BMP performance, and may give false impressions of changes in performance.*

For example, if the recession time of a ponding event in early fall is measured, and another event the following spring, the results would tend to indicate that the performance of the BMP is significantly decreasing over time. Conversely, an infiltration BMP that may actually be undergoing a systematic decrease in performance could appear to be maintaining or even improving in performance depending on when the BMP is visited.

2. *Temperature measurements should be an integral part of any monitoring effort at an infiltration BMP.*

Qualitative surveys which include details of the draw-down or recession rate should also report temperature. One method of BMP assessment that is becoming a commonly used technique is a controlled flooding event where the BMP is intentionally flooded with an artificial storm (by use of a fire hydrant or other water source). This type of test is conducted with the intention of experimentally determining the BMP drawdown time or recession rate. The measurements resulting from this type of test should be expected to be highly dependent on the temperature of

the supply water, which could potentially vary drastically from the temperature of typical incoming stormwater runoff.

3. *The seasonal variation of infiltration BMPs should be considered in the development of regulations limiting the total drawdown time of infiltration BMPs.*

Many current regulations have specific drawdown time requirements for infiltration BMPs. Often the maximum allowable drawdown time is 72 hours. This 72 hour time limit is a good design goal but it should not be used as a strict failure criteria. The drawdown time of a given infiltration BMP should be expected to vary by a factor of two over the course of the year with the longest times in late winter and the fastest in late summer. One of the main intentions of the drawdown time requirement is to prevent the BMP from providing breeding habitat for mosquitoes. Therefore, extended ponding times (greater than 72 hours) during the colder months when mosquitoes cannot reproduce may be acceptable, while during warm months when mosquitoes are active they may not.

Chapter 7. Future Work

The results and conclusions of this study have raised many other questions regarding stormwater infiltration practices. The purpose of this chapter is to highlight some of these topics and provide suggestions for further work.

1. *Continue or revisit hydrologic monitoring and assessment of infiltration BMPs.*

One of the main objectives of this work was to determine the long-term performance of infiltration BMPs. The longest continuous data record used in the analysis was over four years for the BTI. The continuation of the hydrologic monitoring effort at this site is extremely important. The current and ongoing dataset represents the longest continuous dataset for an infiltration BMP. The data examined as part of this study indicate that the BMP is not experiencing a decrease in performance. However, the ultimate confirmation of the longevity of such BMPs should come from the analysis of a much longer time period (10 - 50 years). Therefore, it is imperative that this monitoring effort continue in order to further establish the potential lifespan of such BMPs. Hydrologic monitoring of the PCIB has currently been discontinued. The conclusion of this work is that the PCIB is also not experiencing a systematic decrease. It is important that monitoring of this BMP continue in the future to further substantiate the conclusions on the longevity of this BMP. This is important because this BMP uses an underground storage bed and therefore does not benefit from the same physical processes that help maintain the infiltration performance of the BTI. Instead, this site relies on its well-designed loading ratio and low suspended solids character of the incoming runoff. Hydrologic monitoring of this BMP should be

revisited in the future to determine if the BMP is able to maintain its current level of performance. Unlike the other two BMPs, the analysis of the potential lifespan of the IT is much more definitive. The BMP displayed a drastic change in performance over the three-year monitoring period. Continued monitoring at this BMP will help confirm if the degradation observed at the BMP has ceased or if it will continue at a much slower rate than was initially observed.

2. *Investigate the role of spatial heterogeneity and macropore flow in stormwater infiltration BMPs.*

Heterogeneity and macropore flow were not directly investigated in the study. Little research has been done to quantify the role of macropores in stormwater infiltration BMPs. The spatial heterogeneity of soil properties relevant to infiltration was not thoroughly examined here. Distributed, nondestructive, bulk density estimates could be used to gauge the extent of heterogeneity. Additionally, the role of air entrapment under ponded infiltration conditions is a topic that may have significant influence on the infiltration process and yet has not been thoroughly examined.

3. *Additional investigation of the temperature dependency of stormwater infiltration BMPs.*

With regard to the seasonality and temperature dependency of the infiltration process, this study used single point measurements for temperature. Future work in this area should include multiple measurement points and temperature profiles with depth. This may explain some of the variability observed in this work.

4. *Further investigation of the role of vegetation and organic matter in stormwater infiltration BMPs.*

The role of vegetation and organic matter content in infiltration BMPs are important topics that were not rigorously studied here. Side by side, vegetated, non vegetated studies in addition to laboratory tests could help determine the precise physical processes that are relevant to continued BMP performance. This may include the natural maintenance of soil structure and evapotranspiration.

5. *Further analysis of the subsurface flow at infiltration BMPs.*

The subsurface flow processes at the BMPs could be further examined with the use of variably saturated three-dimensional groundwater models. Furthermore, nearby monitoring well data could be examined in conjunction with groundwater models to determine the BMPs' influence on the surrounding groundwater table. With regard to the subsurface flow characteristics at the BTI, the shallow observation well within the storage basin should be reexamined. This well was initially monitored for ponded water for about one year; since no ponded water was observed, this monitoring effort was discontinued. Currently, the overflow depth of the BMP is higher than the well cap due to the installation of a new, higher overflow weir. Therefore, the well should be cut above ground and lengthened such that the well cap is above the overflow elevation. The well should be monitored for ponded water to determine whether or not a transient perched water table exists at the interface between the original soil and the composite soil mixture.

6. *Role of ponded depth in deep infiltration BMPs.*

Finally, the groundwater modeling conducted at the IT has shown that the sides and the bottom of the BMP have degraded at a different rate. The modeling has shown that the bottom of the BMP is providing little to no infiltration. The majority of the continued infiltration is occurring through the near vertical sidewalls of the BMP. A tradeoff exists between the compacting effect of large ponded depths and the increased surface area provided by larger depths, especially when the sidewalls of the BMP constitute a large proportion of the total infiltrating soil surface area. This research has not investigated this tradeoff.

In conclusion, future research should be conducted to explain the factors that influence the entire infiltration process (not just late-time, post-ponding) related to stormwater BMPs. The goal of this future research should be to explain the processes that dictate inter-event, seasonal and long-term variations in performance. Long-term continuous studies similar to this work are an essential tool in the effort to enhance the current understanding of stormwater infiltration BMPs. The sustained performance of an infiltration BMP can only be guaranteed through a sound understanding of the processes that dictate their performance.

List of References

- American Sigma. (2004). *Sigma 950 Flowmeter Instrument Manual*, Loveland, CO.
- American Society of Civil Engineers (ASCE) and United Nations Educational, Scientific and Cultural Organization (UNESCO). (1998). *Sustainability Criteria for Water Resource Systems*, ASCE, Reston, VA.
- Asare, S. N., R. P. Rudra, et al. (1999). "Effect of Freeze-Thaw Cycle on the Parameters of the Green and Ampt Infiltration Equation." *Journal of Agricultural Engineering Research* **73**(3): 265-274.
- Assouline, S. (2004). "Rainfall-Induced Soil Surface Sealing: A Critical Review of Observations, Conceptual Models, and Solutions." *Vadose Zone* **3**: 570-591.
- ASTM (2000). *Standard Test Method for Measurement of Hydraulic Conductivity of Saturated Porous Materials Using a Flexible Wall Permeameter*. Conshohocken, PA, American Society for Testing and Materials.
- Barzegar, A. R., A. Yousefi, et al. (2002). "The Effect of Addition of Different Amounts and Types of Organic Materials on Soil Physical Properties and Yield of Wheat." *Plant and Soil* **247**: 295-301.
- Batroney, T. (2008). *Implications of the First Flush Phenomenon on Infiltration BMP Design*. Civil and Environmental Engineering. Villanova, PA, Villanova University. **Master of Science in Water Resources and Environmental Engineering**.
- Behnke, J. (1969). "Clogging in Surface Spreading Operations for Artificial Ground-Water Recharge." *Water Resources Research* **5**(4): 870-876.
- Benson, C. H., A. Sawangsuriya, et al. (2007). "Postconstruction Changes in the Hydraulic Properties of Water Balance Cover Soils." *Journal of Geotechnical and Geoenvironmental Engineering* **133**(4): 349-359.
- Berend, J. E. (1967). "An Analytical Approach to the Clogging Effect of Suspended Matter." *Bulletin of the International Association of Hydrology* **12**(2): 42-55.
- Bouwer, H. (1978). *Groundwater Hydrology*. New York, NY, McGraw-Hill Book Company.
- Bouwer, H. (1988). *Systems for Artificial Recharge of Ground Water*. International Symposium on Artificial Recharge of Ground Water, Anaheim, CA, ASCE.
- Bouwer, H. (1989). "Effect of Water Depth in Ground Water Recharge Basins on Infiltration." *Journal of Irrigation and Drainage Engineering* **115**(4): 556-567.

Bouwer, H. (1990). Effect of Water Depth and Groundwater Table on Infiltration from Recharge Basins. Irrigation Drainage Proceedings 1990 National Conference.

Carter, M. R. (2002). "Soil Quality for Sustainable Land Management: Organic Matter and Aggregation Interactions that Maintain Soil Functions." Agronomy Journal **95**: 38-47.

Cheviron, B., R. Guerin, et al. (2005). "Determining Long-Term Effective Groundwater Recharge by Analyzing Vertical Soil Temperature Profiles at Meteorological Stations." Water Resources Research **41**(W09501): 1-6.

Constantz, J. and F. Murphy (1991). "Temperature Dependence of Poned Infiltration under Isothermal Conditions." Journal of Hydrology **122**(1): 119.

Constantz, J., C. L. Thomas, et al. (1994). "Influence of Diurnal-Variations In Stream Temperature on Streamflow Loss and Groundwater Recharge." Water Resources Research **30**(12): 3253-3264.

Constantz, J., S. W. Tyler, et al. (2003). "Temperature-Profile Methods for Estimating Percolation Rates in Arid Environments." Vadose Zone **2**: 12-24.

Das, B. M. (1998). Principles of Geotechnical Engineering. Boston, MA, PWS Publishing.

Douglas, J. T., A. J. Koppi, et al. (1992). "Alteration of the Structural Attributes of a Compact Clay Loam Soil by Growth of a Perennial Grass Crop." Plant and Soil **139**: 195-202.

Dowman, C. E., T. P. A. Ferre, et al. (2003). "Quantifying Ephemeral Streambed Infiltration from Downhole Temperature Measurements Collected Before and After Streamflow." Vadose Zone **2**: 595-601.

Duley, F. L. and C. E. Domingo (1943). "Effect of Water Temperature on Rate of Infiltration." Proceedings of the Soil Science Society of America **8**: 129-131.

Emerson, C. H. (2003). Evaluation of the Additive Effects of Stormwater Detention Basins at the Watershed Scale. School of Environmental Engineering Science and Policy (SESEP). Philadelphia, PA, Drexel University. **Master of Science in Environmental Engineering**.

Emerson, C. H., C. Welty, et al. (2005). "Watershed-Scale Evaluation of a System of Storm Water Detention Basins." Journal of Hydrologic Engineering **10**(3): 237-242.

Ermilio, J. (2005). Characterization Study of a BioInfiltration Stormwater BMP. Civil and Environmental Engineering. Villanova, PA, Villanova University. **Master of Science in Water Resources and Environmental Engineering**.

- Fetter, C. W. (1994). Applied Hydrogeology. Upper Saddle River, NJ, Prentice Hall.
- Fox, D. M., Y. L. Bissonnais, et al. (1998). "The Effect of Ponding Depth on Infiltration in a Crusted Surface Depression." Catena **32**: 87-100.
- Freeze, R. A. and J. A. Cherry (1979). Groundwater. Englewood Cliffs, NJ, Prentice Hall.
- Fuentes, J. P., M. Flury, et al. (2004). "Hydraulic Properties in a Silt Loam Soil under Natural Prairie, Conventional Till, and No-Till." Soil Science Society of America Journal **68**: 1679-1688.
- Galli, J. (1993). Analysis of Urban BMP Performance and Longevity in Prince George's County, Maryland. M. W. C. o. Governments: 202.
- Genuchten, M. T. v. (1980). "A Closed-form Equation for Predicting the Hydraulic Conductivity of Unsaturated Soils." Soil Science Society of America Journal **44**: 892-898.
- Gibbs, J. P. (1993). "Importance of Small Wetlands for the Persistence of Local Populations of Wetland-Associated Animals." Wetlands **13**(1): 25-31.
- Gribb, M. M., R. Kodesova, et al. (2004). "Comparison of Soil Hydraulic Property Measurement Methods." Journal of Geotechnical and Geoenvironmental Engineering **130**(10): 1084-1095.
- Healy, R. W. (1990). Simulation of solute transport in variably saturated porous media with supplemental information on modifications to the U.S. Geological Survey's Computer Program VS2D. U. S. G. Survey. **Water-Resources Investigations Report 90-4025**: 125.
- Healy, R. W. and A. D. Ronan (1996). Documentation of computer program VS2DH for simulation of energy transport in variably saturated porous media--modification of the U.S. Geological Survey's computer program VS2DT. U. S. G. Survey. **Water-Resources Investigations Report 96-4230**: 36.
- Heasom, W., R. G. Traver, et al. (2006). "Hydrologic Modeling of a Bioinfiltration Best Management Practice." Journal of the American Water Resources Association **42**(5): 1329-1347.
- Hilding, K. (1996). "Longevity of Infiltration Basins Assessed in Puget Sound." Watershed Protection Techniques **1**(3): 124-125.
- Hillel, D. (1998). Environmental Soil Physics. San Diego, CA, Academic Press.

Hopmans, J. W. and J. H. Dane (1985). "Effect of Temperature-Dependent Hydraulic Properties on Soil Water Movement." Soil Science Society of America Journal **49**: 51-58.

Hopmans, J. W. and J. H. Dane (1986). "Temperature Dependence of Soil Hydraulic Properties." Soil Science Society of America Journal **50**(1): 4-9.

Hornberger, G. M., J. P. Raffensperger, et al. (1998). Elements of Physical Hydrology. Baltimore, MD, The John Hopkins University Press.

Houston, S. L., P. D. Duryea, et al. (1999). "Infiltration Considerations for Ground-Water Recharge with Waste Effluent." Journal of Irrigation and Drainage Engineering **125**(5): 264-272.

Hunt, W. F., A. R. Jarrett, et al. (2006). "Evaluating Bioretention Hydrology and Nutrient Removal at Three Field Sites in North Carolina." Journal of Irrigation and Drainage Engineering **132**(6): 1-9.

Issacs-Ricketts, K. (2008). A Soil Profile Characterization of a BioInfiltration BMP. Civil and Environmental Engineering. Villanova, PA, Villanova University. **Master of Science in Water Resources and Environmental Engineering**.

Jaynes, D. B. (1990). "Temperature Variation Effect on Field-Measured Infiltration." Soil Science Society of America Journal **54**(2): 305.

Jury, W. A. and R. Horton (2004). Soil Physics. Hoboken, NJ, John Wiley & Sons, Inc.

Kwiatkowski, M. (2004). A Water Quality Study of a Porous Concrete Infiltration Best Management Practice. Civil and Environmental Engineering. Villanova, PA, Villanova University. **Master of Science in Water Resources and Environmental Engineering**.

Kwiatkowski, M., A. L. Welker, et al. (2007). "Evaluation of an Infiltration Best Management Practice Utilizing Pervious Concrete." Journal of the American Water Resources Association **43**(5): 1208-1222.

Lado, M., A. Paz, et al. (2004). "Organic Matter and Aggregate Size Interactions in Infiltration, Seal Formation, and Soil Loss." Soil Science Society of America Journal **68**: 935-942.

Lado, M., A. Paz, et al. (2005). "Effects of Effluent Irrigation on Seal Formation, Infiltration, and Soil Loss during Rainfall." Soil Science Society of America Journal **69**: 1432-1439.

Lappala, E. G. and R. W. Healy (1987). Documentation of computer program VS2D to solve the equations of fluid flow in variably saturated porous media. U. S. G. Survey. **Water-Resources Investigations Report 83-4099**: 184.

Lentz, R. D. and D. L. Bjorneberg (1999). Influence of Irrigation Water Properties on Furrow Infiltration: Temperature Effects. 10th International Soil Conservation Organization Meeting, Purdue University.

Lin, C., D. Greenwald, et al. (2003). "Temperature Dependence of Infiltration Rate during Large Scale Water Recharge into Soils." Soil Science Society of America Journal(67): 487-493.

Lindsey, G., L. Roberts, et al. (1992). "Inspection and Maintenance of Infiltration Facilities." Journal of Soil and Water Conservation 47(6): 481-486.

Livingston, E. H. (2000). Lessons Learned About Successfully Using Infiltration Practices, Chicago, IL.

Lozada, D. S. d., P. Vandevivere, et al. (1994). "Decrease of the Hydraulic Conductivity of Sand Columns by *Methanosarcina Barkeri*." World Journal of Microbiology & Biotechnology 10: 325-333.

Maryland Dept. of the Environment (MDE). (2000). *Maryland Stormwater Design Manual*, Water Management Administration, Baltimore, MD.

McCuen, R. H. (1979). "Downstream Effects of Stormwater Management Basins." ASCE Journal of the Hydraulics Division 105(11): 1343-1356.

Neurath, S. K., A. M. Sadeghi, et al. (2005). "Spatial Variability in the Upper Soil Layer of a No-Till Field using a Small-Scale Dye Experiment." Soil Science 170(11): 881-891.

New Jersey Dept. of Environmental Protection (NJDEP). (2004). *Stormwater Best Management Practices Manual*, Division of Watershed Management, Trenton, NJ.

New Jersey Pinelands Commission. (2005). *Mullica River Watershed Stormwater Basin Assessment Project*, New Lisbon, NJ.

Pennsylvania Dept. of Environmental Protection (PADEP). (2006). *Pennsylvania Stormwater Best Management Practices Manual*, Bureau of Watershed Management, Harrisburg, PA.

Paul, M. J. and J. Meyer (2001). "Streams in the Urban Landscape." Annual Review Ecological Systems 32: 333-365.

Penman, H. L. (1948). Natural Evaporation from Open Water, Bare Soil, and Grass. Proc. R. Soc. London, London.

Princeton Hydro, LLC. (2005). *Subsurface Investigation of Recharge Basins*, Voorhees, NJ.

Prokop, M. (2003). Determining the Effectiveness of the Villanova BioInfiltration Traffic Island in Infiltrating Annual Runoff. Civil and Environmental Engineering. Villanova, PA, Villanova University. **Master of Science in Water Resources and Environmental Engineering.**

Reddi, L. N., X. Ming, et al. (2000). "Permeability Reduction of Soil Filters due to Physical Clogging." Journal of Geotechnical and Geoenvironmental Engineering **126**(3): 236-246.

Rodgers, M., J. Mulqueen, et al. (2004). "Surface Clogging in an Intermittent Stratified Sand Filter." Soil Science Society of America Journal **68**(6): 1827-1832.

Ronan, A. D., D. E. Prudic, et al. (1998). "Field Study and Simulation of Diurnal Temperature Effects on Infiltration and Variably Saturated Flow Beneath an Ephemeral Stream." Water Resources Research **34**(9): 2137-2153.

Rowe, R. K., M. D. Armstrong, et al. (2000). "Particle Size and Clogging of Granular Media Permeated with Leachate." Journal of Geotechnical and Geoenvironmental Engineering **126**(9): 775-786.

Schueler, T. (1994). "Failure Rates of Infiltration Trenches/Basins Assesses in Suburban Maryland." Watershed Protection Techniques **1**(1): 15-16.

Simmons, D. and R. Reynolds (1982). "Effects of Urbanization on Baseflow of Selected South Shore Streams, Long Island, NY." Water Resources Bulletin **18**(5): 797-805.

Simunek, J., M. T. v. Genuchten, et al. (2005). The HYDRUS-1D Software Package for Simulating the One-Dimensional Movement of Water, Heat, and Multiple Solutes in a Variably-Saturated Media, Dept. of Environmental Sciences, University of California Riverside.

Siriwardene, N. R., A. Deletic, et al. (2007). "Clogging of Stormwater Gravel Infiltration Systems and Filters: Insights from a Laboratory Study." Water Research **41**: 1433-1440.

Steffy, L. Y. and S. S. Kilham (2006). "Effects of Urbanization and Land Use on Fish Communities in Valley Creek Watershed, Chester County, Pennsylvania." Urban Ecosystems **9**(2): 119-133.

Traver, R. G. and R. A. Chadderton (1992). Accumulation Effects of Stormwater Management Detention Basins. Hydraulic Engineering: Saving a Threatened Resource - In Search of Solutions, Baltimore, MD, ASCE.

Wu, L., L. Pan, et al. (1997). "Numerical Evaluation of Ring-Infiltrimeters Under Various Soil Conditions." Soil Science **162**(11): 771-777.

Wuest, S. B. (2005). "Bias in Poned Infiltration Estimates Due to Sample Volume and Shape." Vadose Zone Journal **4**: 1183-1190.

Yaacob, O. and G. J. Blair (1981). "Effect of Legume Cropping and Organic Matter Accumulation on the Infiltration Rate and Structural Stability of a Granite Soil under a Simulated Tropical Environment." Plant and Soil **60**: 11-20.

Youngs, E. G. (1987). "Estimating Hydraulic Conductivity Values from Ring Infiltrometer Measurements." Journal of Soil Science **38**: 623-632.

Appendix A. SlopeFinder Program

The purpose of SlopeFinder is to scan through the continuous data record and identify and calculate any recession limb slopes found in the data record. Other features were subsequently added to provide more insight and understanding of the data. Another objective of the SlopeFinder program was to provide a simple method for program control and to supply output data in a convenient form that can be easily examined and further processed.

SlopeFinder is able to read a continuous data series including the following fields; date/time, depth, temperature, and rainfall. To run the program the following input fields are required; upper limit, lower limit, time interval, minimum recession time, and the row number of the final data point in the data record to be analyzed. The input upper limit represents the upper limit where the desired slope calculation can start and the lower limit is the depth where the slope calculation will end. The time interval is simply the interval of the input data, 15 minutes for example. A simplified flow chart that describes the concept and program design of SlopeFinder is presented in Figure 104. The actual Visual Basic code for SlopeFinder is provided at the end of Appendix A.

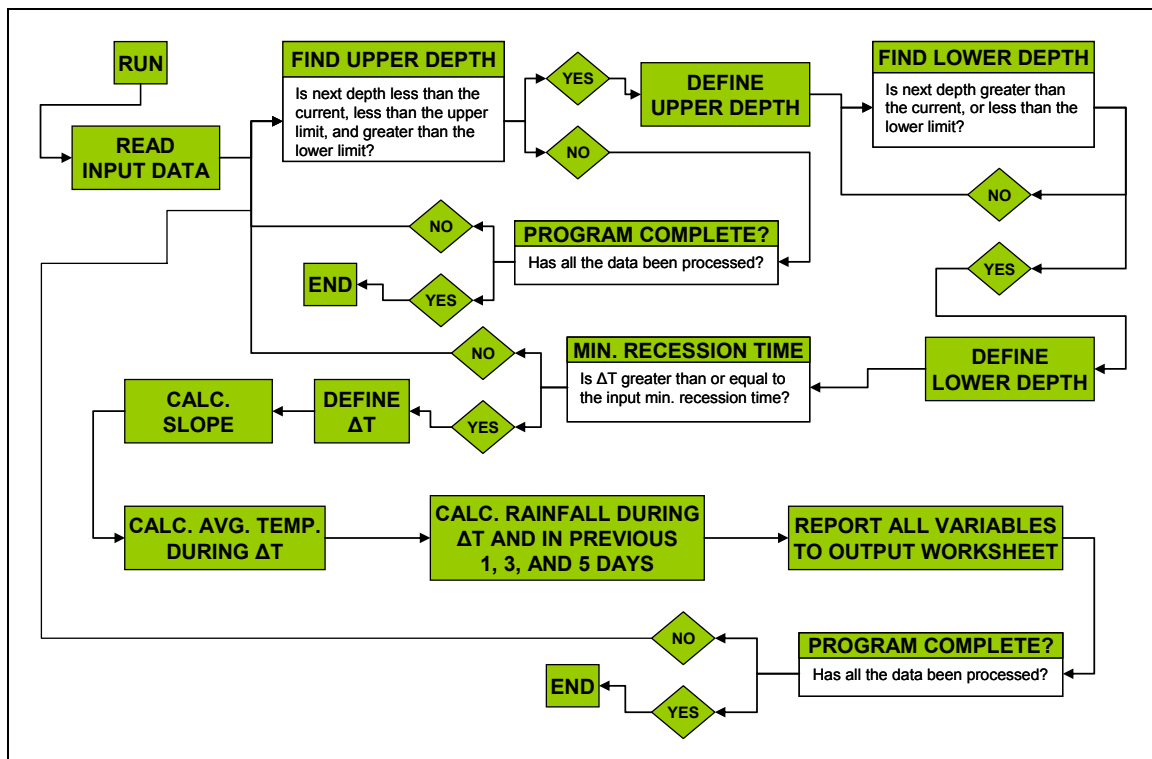


Figure 104. Conceptual program flow chart for SlopeFinder.

It should be noted that SlopeFinder will calculate any slope that occurs within the input depth range, not just those that pass through the entire range.

With SlopeFinder the user can input the desired range of depth where a slope calculation is required along with the other required program control data and the program will scan through the data and report the following information: date and time of the upper depth, upper depth found, date and time of lower depth, lower depth found, duration time of recession (min), calculated slope (in/hr), average temperature during recession, 1,3, and 5-day rainfall, the amount of rainfall that occurred during the slope calculation, and finally the total number of slopes calculated. An example output is shown in Table 17.

Table 17. Example output from SlopeFinder program.

| Upper Limit Date | Upper Depth (ft) | Lower Limit Date | Lower Depth (ft) | Time (min) | Slope (in/hr) | Avg. Temp. (C) | 1-Day Rain (in) | 3-Day Rain (in) | 5-Day Rain (in) | Rain During (in) |
|---------------------|------------------|---------------------|------------------|------------|---------------|----------------|-----------------|-----------------|-----------------|------------------|
| 1/14/2005 12:15 | 1.32 | 1/14/2005 16:15 | 1.20 | 240 | 0.35 | 7.1 | 1.68 | 2.05 | 2.05 | 0 |
| 4/3/2005 6:45 | 1.39 | 4/3/2005 10:30 | 1.21 | 225 | 0.58 | 9.2 | 2.91 | 3.75 | 3.75 | 0.01 |
| 10/9/2005 1:30 | 1.39 | 10/9/2005 4:15 | 1.20 | 165 | 0.79 | 20.4 | 4.52 | 5.48 | 5.48 | 0.02 |
| 12/16/2005 12:15 | 1.40 | 12/16/2005 17:00 | 1.21 | 285 | 0.48 | 4.2 | 1.99 | 1.99 | 2.12 | 0 |

The output table shown here was generated from the 2005 data from the PCIB with an upper limit of 1.4 ft and a lower limit of 1.2 ft. A minimum recession time of 90 min was input. It can be seen that the recession durations for this depth range in this data set are well above the minimum recession time. The first slope shown is not calculated over the full input depth range because it peaks at only 1.32 ft which is less than the input of 1.4 ft. The other three slopes that SlopeFinder identified all started at approximately 1.39 ft, shown to 2 decimal places. Therefore all the slopes in Table 17, with the exception of the first identified slope, represent “full range” slopes, or those that began prior to the upper limit depth and continued past the lower limit depth. For this analysis only these full range slopes are used. This is an effort to help eliminate slope measurements that may be significantly impacted by continued or prolonged inflow.

As previously mentioned, one of the required program control variables is the minimum recession time. This value is input in unit of minutes and it instructs SlopeFinder to report only those recession slopes which occur over a time span equal to or greater than its value. The purpose of this input is to avoid calculating and reporting miscellaneous, short-duration slopes that are not representative of the infiltration process. These small slopes can be caused by noise in the data. The utility of this variable depends on the nature of the data to be analyzed. The variable is more useful for data that is more unstable and noisy. However, attention should always be given to the value of this input variable. The depth range, defined by the upper and lower limit, divided by the minimum recession time, yields a value for slope [L/T]. If the data contains legitimate recession slopes in excess of this value they will not be reported. Therefore, the user should be

aware of the magnitude of the steepest slopes in the data set to ensure that these are not intentionally excluded by the program.

Each data set is processed with the SlopeFinder program for each incremental depth. For example, since the PCIB has seven incremental slopes and two data sets (one year duration each), it requires a total of 14 SlopeFinder runs. Then the results are sorted and slopes which are not full range measurements are deleted. All the other slopes are checked to ensure that they adequately represent the infiltration process. Slopes that may be affected directly by freezing conditions or those that are suspected to be influenced by inflow from snow and ice melt are also deleted.

SlopeFinder Visual Basic Code:

```

Sub SlopeFinder()
'activate the first worksheet
Sheets("DATA").Select
'read the number of rows to evaluate to
totalcells = Cells(1, 1).Value
'read the overflow depth, the depth under
'which we are interested in calculating the slope of the receding limb of
overflowdepth = Cells(2, 1).Value
'read the depth below which we are no longer interested in
lolim = Cells(3, 1).Value
'read the time interval of the data
timeint = Cells(4, 1).Value
'read the minimum recession time desired
mintime = Cells(5, 1).Value
'read the minimum no rain time
'norntime = Cells(6, 1).Value

'initialize all the array variables there will be one of each for every peak
Dim uplim(10000)
Dim hidte(10000)
Dim locutoff(10000)
Dim lodte(10000)
Dim timediff(10000)
Dim inperhr(10000)
Dim avgtemp(10000)
Dim onedayprecip(10000)
Dim threedayprecip(10000)
Dim fivedayprecip(10000)
Dim duringprecip(10000)
Dim slopefunc(10000)

'input data starts at row number 9
w = 9
'start the (z) count of the array variables at 1

```

z = 1

Do

For i = w To totalcells

If Cells(i + 1, 5) < Cells(i, 5) And Cells(i, 5) < overflowdepth And Cells(i, 5) >

lolim Then

'if the next depth is less than the current, and less than the overflow depth

'and greater than the lower depth threshold (to avoid looking at very small events)

'define the depth (row 5) and time (row 1) of the peak as the cell that satisfied the statement

uplim(z) = Cells(i, 5)

hidte(z) = Cells(i, 1)

Exit For

End If

Next i

'now that the peak i cell has been found, the next for loop starts with x equal to that i and follows the receding limb down to either the beginning of another peak or the lower limit

'as defined above

For x = i To totalcells

If Cells(x + 1, 5) <= lolim Or Cells(x + 1, 5) > Cells(x, 5) Then

'define the depth and time of the end of the receding limb, note that locutoff will often be

'equal to the lolim, but not always

locutoff(z) = Cells(x, 5)

lodte(z) = Cells(x, 1)

Exit For

End If

Next x

'only assign the following three variables if locutoff is assigned (ie a receding limb is found)

'and the receding limb is sufficiently long according to the input mintime

If locutoff(z) > 0 And (x - i) * timeint >= mintime Then

'calculate the time between the peak and the locutoff (min)

timediff(z) = (x - i) * timeint

'calculate the downward rate of change of the depth (in/hr)

inperhr(z) = ((uplim(z) - locutoff(z)) * 12) / (timediff(z) / 60)

'calculate the average temperature during the receding limb

avgtemp(z) = Application.Average(Range(Cells(i, 6), Cells(x, 6)))

'calculate the slope of the recession limb with the excel "slope" function

slopefunc(z) = -12 * Application.Slope(Range(Cells(i, 5), Cells(x, 5)), Range(Cells(i, 2), Cells(x, 2)))

```

'calculate the cumulative 1,3,5-day precipitation, the if statement is used to prevent an
error
'if the receding limb is within 1,3,5 days of the beginning of the data
If i - ((1 * 24 * 60) / (timeint)) >= 9 Then
onedayprecip(z) = Application.Sum(Range(Cells(i - ((1 * 24 * 60) / (timeint)), 3), Cells(i,
3)))
Else: onedayprecip(z) = Application.Sum(Range(Cells(9, 3), Cells(i, 3)))
End If
If i - ((3 * 24 * 60) / (timeint)) >= 9 Then
threedayprecip(z) = Application.Sum(Range(Cells(i - ((3 * 24 * 60) / (timeint)), 3),
Cells(i, 3)))
Else: threedayprecip(z) = Application.Sum(Range(Cells(9, 3), Cells(i, 3)))
End If
If i - ((5 * 24 * 60) / (timeint)) >= 9 Then
fivedayprecip(z) = Application.Sum(Range(Cells(i - ((5 * 24 * 60) / (timeint)), 3),
Cells(i, 3)))
Else: fivedayprecip(z) = Application.Sum(Range(Cells(9, 3), Cells(i, 3)))
End If
'calculate the precip occuring during the receding limb (except for the last cell) (these
should be small
'otherwise the depth would rise and stop the calculation.
duringprecip(z) = Application.Sum(Range(Cells((x - 1), 3), Cells(i, 3)))

'report results in second workseet
Worksheets("RESULTS").Cells(z + 1, 1).Value = hidte(z)
Worksheets("RESULTS").Cells(z + 1, 2).Value = uplim(z)
Worksheets("RESULTS").Cells(z + 1, 3).Value = lodte(z)
Worksheets("RESULTS").Cells(z + 1, 4).Value = locutoff(z)
Worksheets("RESULTS").Cells(z + 1, 5).Value = timediff(z)
Worksheets("RESULTS").Cells(z + 1, 6).Value = inperhr(z)
Worksheets("RESULTS").Cells(z + 1, 7).Value = avgtemp(z)
Worksheets("RESULTS").Cells(z + 1, 16).Value = slopefunc(z)
Worksheets("RESULTS").Cells(z + 1, 8).Value = onedayprecip(z)
Worksheets("RESULTS").Cells(z + 1, 9).Value = threedayprecip(z)
Worksheets("RESULTS").Cells(z + 1, 10).Value = fivedayprecip(z)
Worksheets("RESULTS").Cells(z + 1, 11).Value = duringprecip(z)
Worksheets("RESULTS").Cells(8, 13).Value = z
'the else statement ensures that the results will be reportrd one row after another even if
'a z has to be skipped bc of the min time constraint on the limb.
Else: z = z - 1
End If

w = x + 1
z = z + 1

Sheets("DATA").Select

```

Loop Until w >= totalcells

'go to the results sheet after execution
Sheets("RESULTS").Select

End Sub

Appendix B. Time Interval Conversion Program: Visual Basic Code

```
Sub Tldata()
```

```
total = Cells(2, 6).Value
```

```
i = 6
```

```
' 5 minute data
```

```
'For x = 6 To total
```

```
' counter variable starting at row 6
```

```
'rn = Application.Sum(Range(Cells(x, 3), Cells(x + 4, 3)))
```

```
' rn variable for rain is sum of cells x,3 to x+4
```

```
'Cells(i, 10).Value = rn
```

```
'put data from above in cells i,10
```

```
'weir = Application.Average(Range(Cells(x, 4), Cells(x + 4, 4)))
```

```
'Cells(i, 11).Value = weir
```

```
'well = Application.Average(Range(Cells(x, 5), Cells(x + 4, 5)))
```

```
'Cells(i, 12).Value = well
```

```
'x = x + 4
```

```
'i = i + 1
```

```
'Next x
```

```
'run through loop until x=total
```

```
' 10 minute data
```

```
i = 6
```

```
For j = 6 To total
```

```
rain = Application.Sum(Range(Cells(j, 2), Cells(j + 1, 2)))
```

```
Cells(i, 9).Value = rain
```

```
level = Application.Average(Range(Cells(j, 3), Cells(j + 1, 3)))
```

```
Cells(i, 10).Value = level
```

```
'well = Application.Average(Range(Cells(j, 5), Cells(j + 1, 5)))
```

```
'Cells(i, 12).Value = well
```

```
j = j + 1
```

```
i = i + 1
```

```
Next j
```

```
' 15 minute data
```

```
i = 6
```

```
For k = 6 To total
```

```
rain = Application.Sum(Range(Cells(k, 2), Cells(k + 2, 2)))
```

```
Cells(i, 15).Value = rain
```

```
level = Application.Average(Range(Cells(k, 3), Cells(k + 2, 3)))
```

```
Cells(i, 16).Value = level
```

```
'well = Application.Average(Range(Cells(k, 5), Cells(k + 2, 5)))  
'Cells(i, 18).Value = well
```

```
k = k + 2
```

```
i = i + 1
```

```
Next k
```

```
End Sub
```

Appendix C. Monte Carlo Green and Ampt Sensitivity Analysis

The infiltration of water into an initially unsaturated soil profile is a complex process. Therefore many simplified semi-empirical models have been created to approximate the infiltration process. One of the most widely used methods is the one-dimensional Green and Ampt infiltration model. The Green and Ampt method makes many simplifying assumptions of the infiltration process. The first major assumption is that the wetting front is infinitely sharp, with the moisture content of the soil going from a dry state to a wetted state instantaneously as the depth of the wetting front passes. The Green and Ampt model simply requires input of the difference between the two volumetric moisture contents (wet and dry), often referred to as the volumetric moisture deficit ($\Delta\theta$). The other major assumptions of the model are that the wetting front maintains a constant soil moisture potential (suction) and the wetted region or “transmission zone” is homogeneous with a constant hydraulic conductivity. This is an idealized representation of the infiltration process. However it often provides a satisfactory approximation of the infiltration process with only limited input data requirements and a relatively simple implementation. For these reasons the Green and Ampt model is one of the most widely used infiltration models.

The Green and Ampt model provides an efficient way to estimate the accuracy of the hydraulic conductivity estimates used in this analysis for the PCIB and the BioInfiltration Traffic Island. Therefore the Green and Ampt method was run over the same depth range from which the hydraulic conductivity estimate was taken. For the PCIB this range is 0.8 to 0.6 ft and for the BioInfiltration Traffic Island the range is 1.4 to 0.4 ft. Since the storage bed geometry of the BioInfiltration Traffic Island is known, this depth range (as measured by the level detector) can instead be represented by the average ponded depth in the basin which is 0.74 to 0.24 ft over the same range.

The Green and Ampt method requires the following input data: hydraulic conductivity of the transmission zone, soil moisture potential (suction) at the wetting front, and the initial moisture deficit. In addition to these commonly used inputs, this approximation also requires the initial depth of the wetting front. This is required because the simulation is occurring after the onset of surface infiltration, usually hours after. All of these input parameters are highly simplified and largely hypothetical quantities, the magnitude of which is unknown. However, realistic bounds can be placed on the magnitude of these input parameters with some level of confidence. Therefore the Green and Ampt model can be used with a Monte Carlo-like approach to determine how realistic parameter bounds will influence the model.

A Visual Basic macro was programmed in the Microsoft Excel environment with the purpose of comparing the calculated recession rate (slope) of the ponded water surface over time (from a hypothetical Green and Ampt model) to the hydraulic conductivity used within the Green and Ampt model. A randomly selected value within the input parameter range was chosen for each input parameter. Then the set of inputs are used with the Green and Ampt model to calculate a recession curve from the upper depth of interest to the lower depth of interest (as previously mentioned for each BMP). After this

calculation was completed the slope of the hypothetical recession limb is calculated and can be easily compared to the randomly selected (within some input range) value for hydraulic conductivity. The macro allows this process to be automated and run with a user selected number of iterations. A scatter plot is then created from the recession rates and randomly selected hydraulic conductivities. If this plot were a perfect 1:1 line, this would imply perfect agreement between the two variables. Based on the Green and Ampt formulation it is clear that the recession rate will always be larger than the hydraulic conductivity, based on the relative contribution of other factors including the depth of ponded water and soil moisture potential gradient over the distance of the wetting front depth.

Table 18 summarizes the input parameter ranges and depth ranges for both BMPs. The table also displays the results of the sensitivity analysis with the ratio of the hydraulic conductivity and the recession rate between the input depth ranges, expressed as the average percentage of the recession rate that the hydraulic conductivity is equal to. This percentage simply represents the best fit slope of the scatter plot of recession rate vs. hydraulic conductivity, as shown in Figure 105 for the BioInfiltration Traffic Island. Both simulations were run with 1,000 iterations for each BMP. A screenshot of the spreadsheet used to implement the macro is provided in Figure 106 and the Visual Basic code for the macro are provided at the end of this section.

Table 18. Summary of the Monte Carlo Green and Ampt sensitivity analysis.

| | Input Parameter Ranges | | | | | | | | | | % of Rec. Rate [%] |
|----------------------------------|------------------------|------------------|--------------------|------|------------------------|-----|--------------------|------|-----------------------|---|--------------------|
| | Upper Depth [ft] | Lower Depth [ft] | Hyd. Cond. [in/hr] | | Wet. Frt. Suction [ft] | | Moist. Deficit [-] | | Int. Front Depth [ft] | | |
| Pervious Conc. Inf. Basin | 0.8 | 0.6 | 0.025 | 0.25 | 0.1 | 0.5 | 0.35 | 0.45 | 2 | 4 | 75 |
| BioInf. Traff. Island | 0.73 | 0.24 | 0.01 | 1.0 | 0.1 | 0.5 | 0.35 | 0.45 | 2 | 4 | 81 |

As expected both analyses indicate that over the indicated depth ranges, the recession rate will tend to be an over prediction of the hydraulic conductivity according to the Green and Ampt infiltration model. Due to the idealized nature of the Green and Ampt model and the uncertainty related to the largely theoretical input parameters of the model, these estimates of hydraulic conductivity from the recession rate analysis were not adjusted based on the results of this sensitivity analysis.

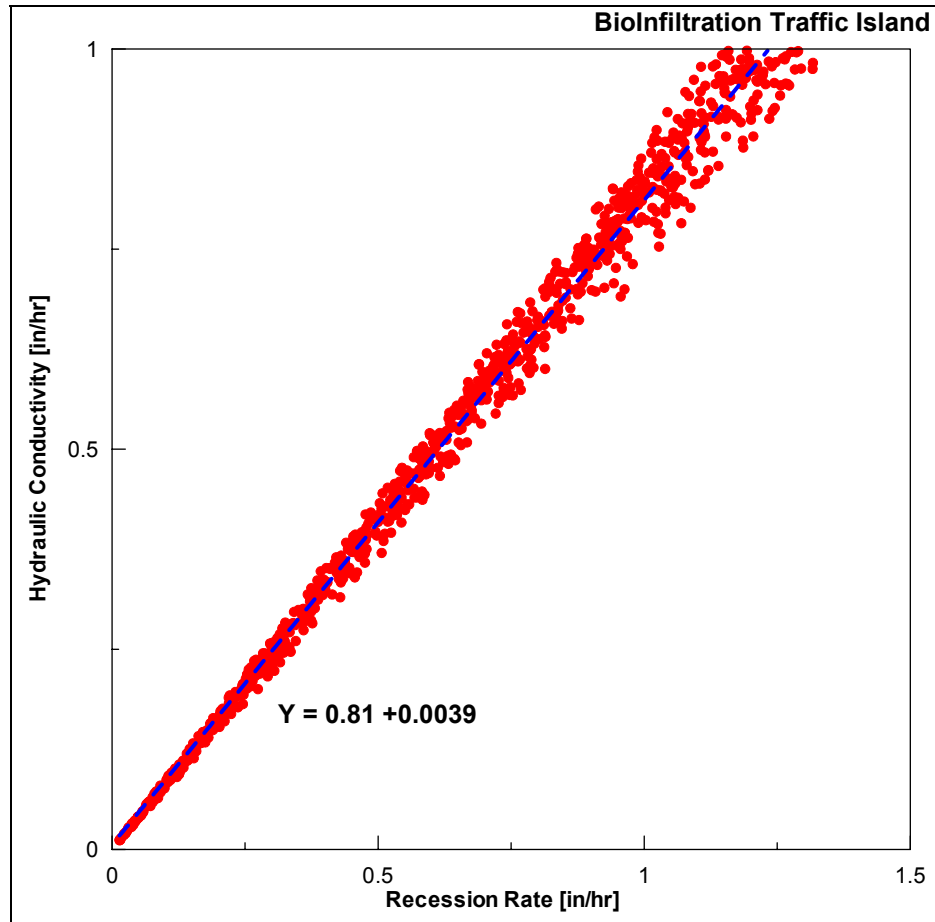


Figure 105. Recession rate vs. hydraulic conductivity for Green and Ampt sensitivity analysis for the BioInfiltration Traffic Island.

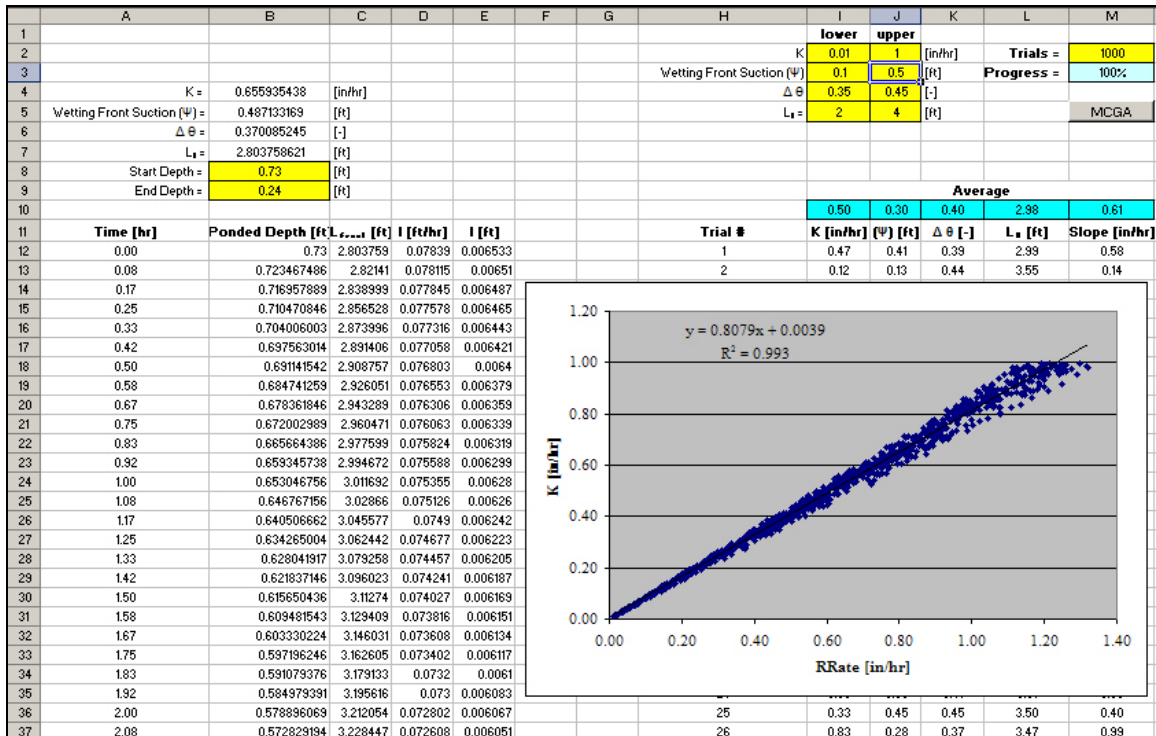


Figure 106. Screenshot of the spreadsheet used to implement the Monte Carlo Green and Ampt sensitivity analysis, results for the BioInfiltration Traffic Island shown.

Visual Basic code for the Monte Carlo Green and Ampt sensitivity analysis macro:

Sub MCGA()

```
'clear previous run results
Range("H12:M65536").ClearContents
```

```
trials = Cells(2, 13).Value
StartDepth = Cells(8, 2).Value
EndDepth = Cells(9, 2).Value
K_low = Cells(2, 9).Value
K_high = Cells(2, 10).Value
Psi_low = Cells(3, 9).Value
Psi_high = Cells(3, 10).Value
DelTheta_low = Cells(4, 9).Value
DelTheta_high = Cells(4, 10).Value
L_low = Cells(5, 9).Value
L_high = Cells(5, 10).Value
```

```
Dim K(1000000)
Dim Psi(1000000)
Dim DelTheta(1000000)
```

```

Dim L(1000000)
Dim RRate(1000000)
Dim RTime(1000000)
Dim LowDepth(1000000)

n = 1

Do

For n = 1 To trials
  'Choose random K's within set range
  K(n) = ((K_high - K_low + 0) * Rnd + K_low)
  Psi(n) = ((Psi_high - Psi_low + 0) * Rnd + Psi_low)
  DelTheta(n) = ((DelTheta_high - DelTheta_low + 0) * Rnd + DelTheta_low)
  L(n) = ((L_high - L_low + 0) * Rnd + L_low)

  'Write them to the output table
  Cells(11 + n, 8).Value = n
  Cells(11 + n, 9).Value = K(n)
  Cells(11 + n, 10).Value = Psi(n)
  Cells(11 + n, 11).Value = DelTheta(n)
  Cells(11 + n, 12).Value = L(n)

  'Plug these values into the GA model
  Cells(4, 2).Value = K(n)
  Cells(5, 2).Value = Psi(n)
  Cells(6, 2).Value = DelTheta(n)
  Cells(7, 2).Value = L(n)

  'GA model should automatically update
  'calculate average slope between start depth (TI=0.73 ft, PC=0.8 ft) and end depth
  (TI=0.24 ft, PC=0.6 ft)

  'find the time when the depth is calculated to past the end depth
  m = 1

  Do
    If Cells(11 + m, 2) <= EndDepth Then
      RTime(n) = Cells(11 + m, 1).Value
      LowDepth(n) = Cells(11 + m, 2).Value
      m = 10001
    Else
      m = m + 1
    End If

  Loop While m <= 10000

```

```
RRate(n) = ((StartDepth - LowDepth(n)) * 12) / RTime(n)  
Cells(11 + n, 13) = RRate(n)
```

```
'Progress meter  
Cells(3, 13).Value = n / trials
```

```
Next n
```

```
Loop While n <= trials
```

```
End Sub
```

Appendix D. Method to Correct for Oscillations in Level Data from the BTI

The ultrasonic transducer measures the time required to reflect sound waves off the water surface and converts it into an equivalent depth. Since the speed of sound in air is a function of temperature the transducer is stated to be equipped with a temperature correction feature. However, in order for the transducer to have an accurate estimate of air temperature it must be properly shielded from the sun (American Sigma 2004). The transducer head is black and has not been fully shielded from the sun during the data record. Therefore the failure of the transducer to properly correct for ambient air temperature was determined to likely be the cause of the oscillation. This is further confirmed with Figure 107 which shows a week of depth data from the ultrasonic transducer and the corresponding temperature data which is recorded by a completely independent datalogger. This data is from the first week of August 2005 when there was no rainfall and a dry storage bed. As is evident from the plot, the oscillation of the ultrasonic transducer appears to be highly correlated with the measured temperature.

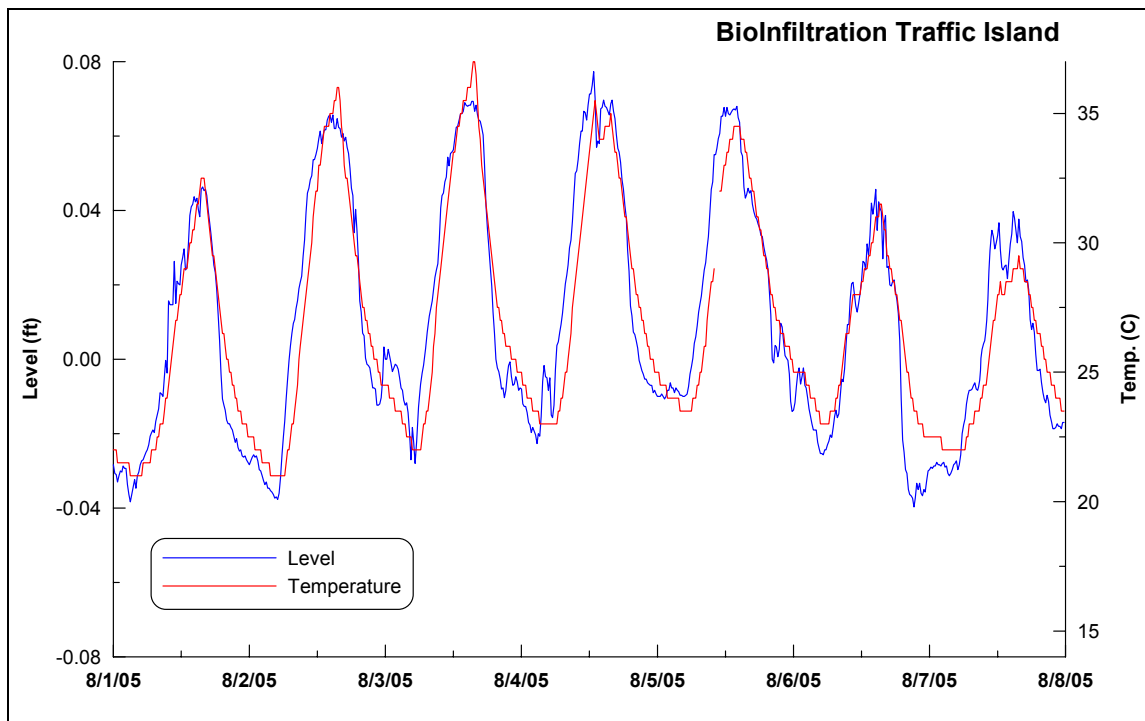


Figure 107. Ultrasonic transducer oscillations and temperature at the BioInfiltration Traffic Island.

Since the on-site temperature measurement does not span the entire span of the depth record and its location is submerged when the storage basin has water in it, there is no on-site measurement of ambient air temperature. Therefore it is not possible derive a function based on temperature measurements that explains the oscillation and could be

used to correct the level record. Instead the oscillation would have to be considered and the slope measurement method modified to avoid its impact.

Figure 108 shows the transducer oscillation and a calculated three-hour slope of the oscillation. It can be seen that the slope of the oscillation exceeds 0.2 in/hr on both the up and down slope for the period examined here. A slope of 0.2 in/hr is well in the range of the water surface recession slopes observed at the BioInfiltration Traffic Island.

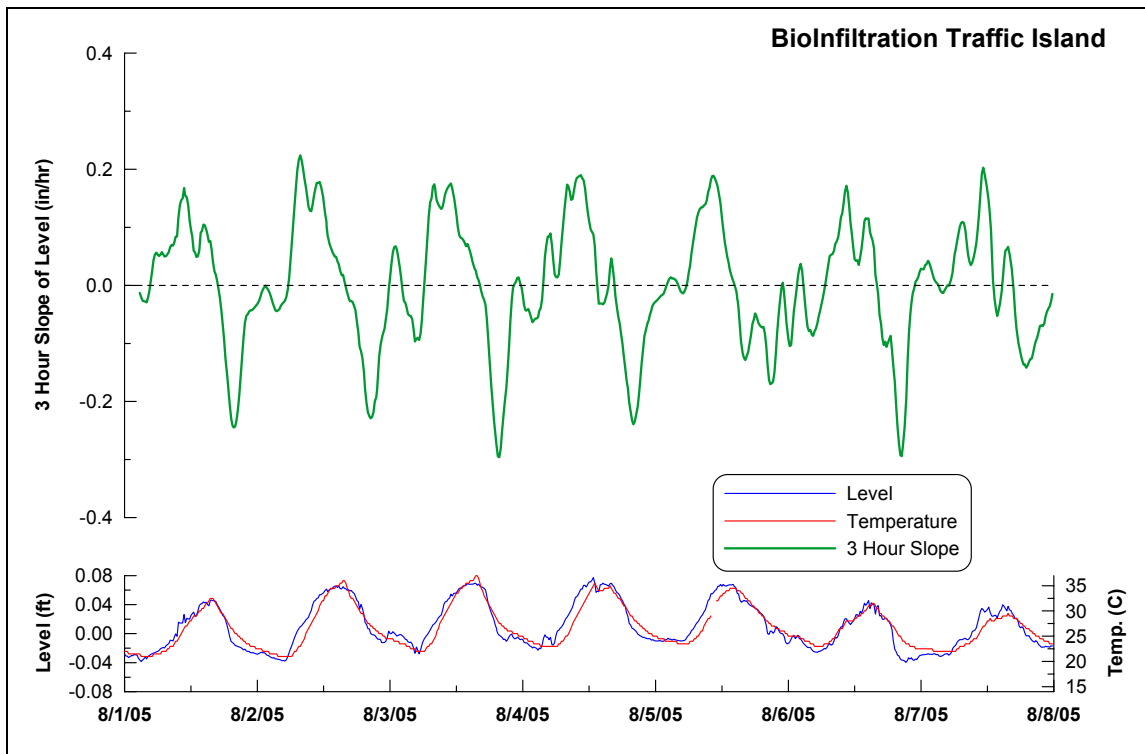


Figure 108. Running calculation of a three-hour slope of the ultrasonic transducer oscillation.

When this oscillation is combined with the actual water level recession it yields recession limbs that are not perfectly linear. Additionally if the rising slope of the oscillation (late morning) occurs during a recession and its slope is greater than the actual water surface recession, the depth record will indicate a brief increase during those time steps. This increase will cause the SlopeFinder program to end a slope calculation at the depth corresponding to the increase, and begin another calculation once the sum of the natural recession slope and the oscillation are again negative. This results in there being multiple (usually two) slopes calculated for a single storm event. These multiple slopes often differ by more than 0.02 in/hr. An example of this problem is shown in Figure 109.

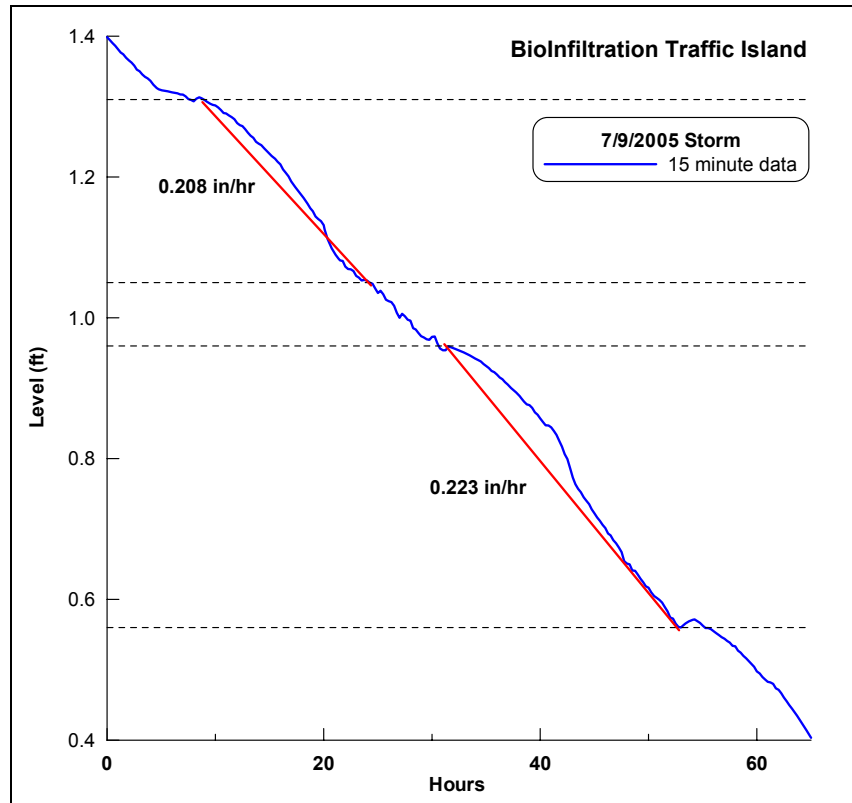


Figure 109. Recession limb (from 1.4 to 0.4 ft) for the July 9th 2005 storm, showing two calculated slopes as found with the SlopeFinder program.

The two slopes labeled on the plot are those calculated by SlopeFinder. It should be noted that a best fit (linear regression) line from 1.4 to 0.4 ft for this storm results in a slope of 0.188 in/hr. This best fit slope is likely the most accurate estimate of the true recession rate of the water surface.

In order to prevent SlopeFinder from calculating multiple slopes for a single recession limb, the data was resampled to a longer time interval. A time interval of two hours was found to be adequate. The data was transformed using a modification to the original time interval conversion program which can be found in Appendix B. Figure 110 shows the results of the time interval conversion for the same storm event.

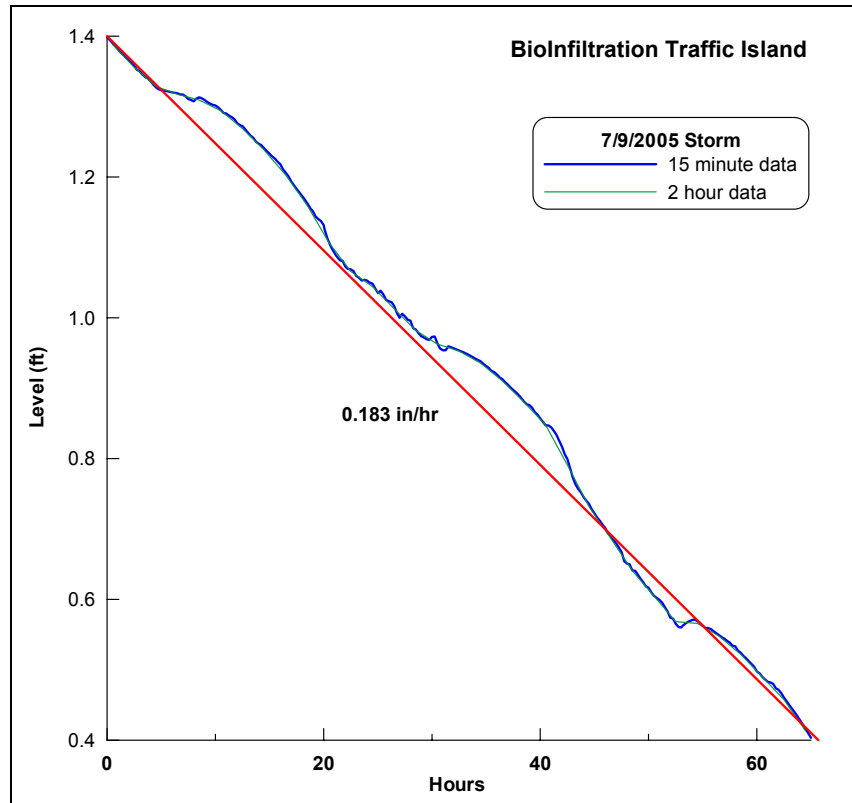


Figure 110. Recession limb for July 9th 2005 storm showing both 15-minute and two-hour data.

The two-hour time conversion was enough to smooth out the brief periods of positive slope that are evident in the recession limbs of the 15-minute data. Therefore when the SlopeFinder program is run it will not break the recession limb into multiple slopes. Figure 110 shows the slope found by the program for this storm event. A slope of 0.183 in/hr was found between the depths of 1.4 and 0.4 ft. The linear regression for this same set of data yields a slope of 0.188 in/hr. In an effort to further avoid potential influences of the instrument oscillations the SlopeFinder program was modified to calculate the slope both by the original method as described in Section 2.2.1, and by use of the Excel “Slope” function which provides a slope of a linear regression line through the input data points. The range of data used as input to the “Slope” function is the same range of data used in the original slope calculation in the program. This process was run for the entire dataset.

Since the characteristic recession limb of the BioInfiltration Traffic Island is much more linear than the other two infiltration BMPs, it was only necessary to use a single depth range for slope calculations. A range of 1.4 to 0.4 ft was chosen because it was well below the overflow level of 1.49 ft and it was long enough to obtain a representative slope calculation. A minimum recession time of 24 hours was input, this time limit over the input depth range would result in a slope of 0.5 in/hr which exceeds the slopes that can be found in the dataset for the BioInfiltration Traffic Island. First, only full range

slopes were examined; these are storm events that filled the basin past the upper limit of 1.4 ft and infiltrated down below the lower limit of 0.4 ft without any secondary peaks in between. Additionally if there was more than 0.02 in of rainfall recorded during the period of slope calculation the data point was not used in the analysis. Within the four-year dataset there were a total of 31 recession limbs that met these requirements. Both the original two-point method for slope calculation and the linear regression slope method produce similar results from the two-hour data. The average difference between the two methods is only 0.002 in/hr with the two point method producing a higher slope on average. Figure 111 compares the results from both methods of slope measurement.

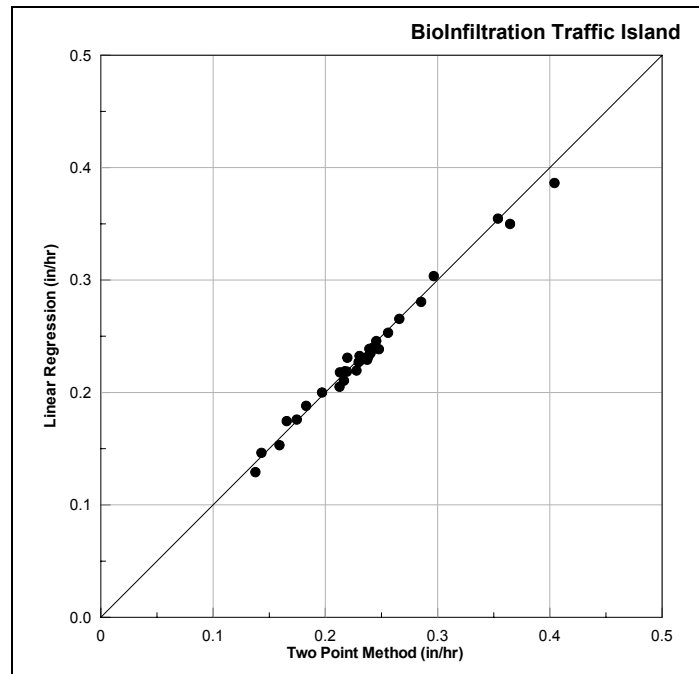


Figure 111. Comparison of original two-point method and linear regression method for the BioInfiltration Traffic Island.

Appendix E. Infiltration Trench Model (McKsat)

The modeling process for a given storm is described as follows. First, the observed recession limb of interest is input into the worksheet. The worksheet automatically creates an observed infiltration hydrograph and an observed rating curve (infiltration vs. depth) based on the known geometry. These plots are created by interpolating storage and consequent change in storage based on the observed recession limb depth record. The initial range for the hydraulic conductivities is generally set at 0 to 2 in/hr for *both* the conductivities. The reason the same range is used for both is to ensure that the model is not initially biased by assuming one value is greater than the other. The program is then run with one thousand iterations. After the run is completed both ranges are narrowed down to plus and minus ten percent of the optimal hydraulic conductivities found from the first run of one thousand iterations. With the narrower range the program is run again with five thousand iterations. The resulting hydraulic conductivities found after five thousand iterations are typically the same (to two significant figures) or very close to those found with only one thousand iterations. This indicates that the model is narrowing down on the optimal set of parameters. It was decided that five thousand iterations of this method was an adequate number because only two significant figures are being carried from the analysis. If either value is close to the minimum or maximum value input for the range the program is run again with an adjusted range. A program flow chart is provided in Figure 112, and a worksheet screenshot and program code are also provided below.

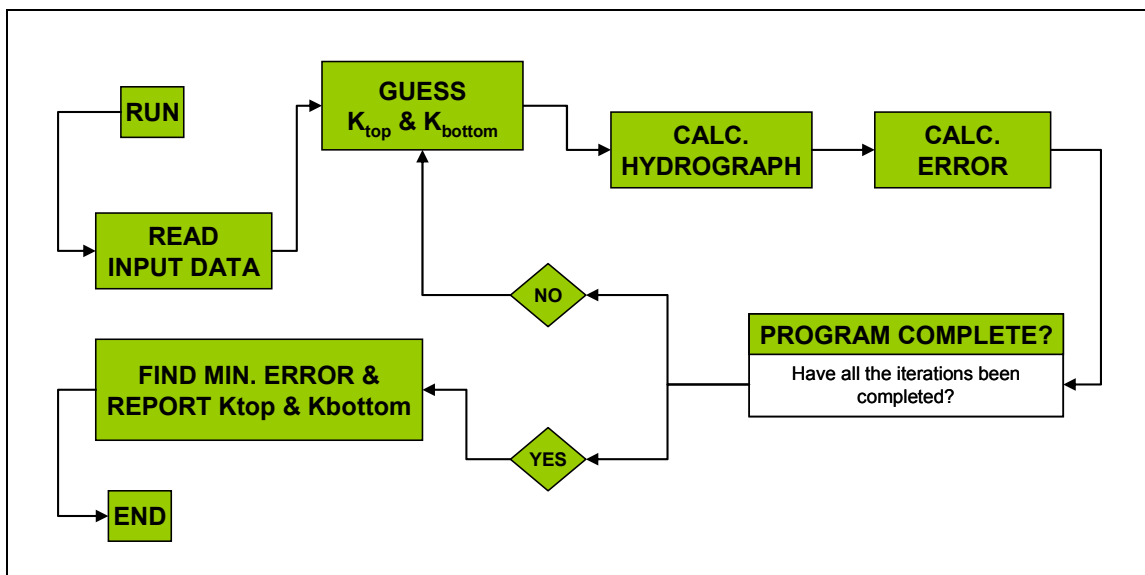


Figure 112. Program flow chart for the McKsat model of the IT.

McKsat Visual Basic Code:

```
Sub MCKsat()
```

```
'clear previous run results
Range("S11:V65536").clearcontents
```

```
trials = Cells(3, 16).Value
Kbottom_low = Cells(3, 13).Value
Kbottom_high = Cells(3, 14).Value
Ksides_low = Cells(4, 13).Value
Ksides_high = Cells(4, 14).Value
```

```
Dim Kbottom(1000000)
Dim Ksides(1000000)
Dim SSErr(1000000)
```

```
'start the (n) count of the guesses at 1
n = 1
```

```
Do
```

```
For n = 1 To trials
```

```
    'Choose random K's within set range
```

```
    Kbottom(n) = ((Kbottom_high - Kbottom_low + 0) * Rnd + Kbottom_low)
```

```
    Ksides(n) = ((Ksides_high - Ksides_low + 0) * Rnd + Ksides_low)
```

```
    'Plug these K's into the model
```

```
    Cells(1, 7).Value = Kbottom(n)
```

```
    Cells(3, 7).Value = Ksides(n)
```

```
    'Assign the SSErr associated with the chosen K's
```

```
    SSErr(n) = Cells(6, 11).Value
```

```
    'Report trial number, K's and SSErrs
```

```
    Cells(n + 10, 19).Value = n
```

```
    Cells(n + 10, 20).Value = Kbottom(n)
```

```
    Cells(n + 10, 21).Value = Ksides(n)
```

```
    Cells(n + 10, 22).Value = SSErr(n)
```

```
    'Progress meter
```

```
    Cells(4, 16).Value = n
```

```
Next n
```

```
'Next find the lowest SSErr and report the associated K's
```

```
Loop While n <= trials
```

```
Do
```

```
For n = 1 To trials
```

```
    If SSErr(n) = Cells(6, 16).Value Then
```

```
        Cells(7, 16).Value = Cells(n + 10, 20).Value
```

```
        Cells(8, 16).Value = Cells(n + 10, 21).Value
```

```
        Cells(9, 16).Value = n
```

```
    Else  
    End If  
Next n  
Loop While n <= trials  
  
End Sub
```

Appendix F. Green and Ampt Model for Infiltration BMPs

Soil testing and site investigation give estimates of soil properties related to the infiltration process. The behavior of an infiltration BMP is then dictated by these soil properties. One way of using these properties to simulate or predict the performance of an infiltration BMP is apply the Green and Ampt model for ponded infiltration. This appendix describes the original Green and Ampt infiltration model and how it can be modified and applied to stormwater infiltration BMPs. The Visual Basic code and the spreadsheet example can be used to model any existing or proposed infiltration BMP. The only part of the code that would require modifications is the overflow calculation which is based here on the 90° V-notch weir.

The Green and Ampt model is a one dimension, physically-based model of the infiltration process. The approach is to assume a slug or piston-like infiltration process with a sharp wetting front. The Green and Ampt model has the following important assumptions. First it assumes that the wetting front is infinitely sharp. That is that the moisture content of the soil goes from a dry state to a wetted state instantaneously as the depth of the wetting front passes. The dry condition moisture content need not be equal to the residual moisture content (θ_r). Additionally the wet condition moisture content does not need to equal the saturated moisture content (θ_s). The Green and Ampt model simply uses the difference between these two volumetric moisture contents, this is often referred to as the volumetric moisture deficit ($\Delta\theta$). The other major assumptions of the model are that the wetting front maintains a constant soil moisture potential (suction) and the wetted region or “transmission zone” is homogeneous with a constant hydraulic conductivity. The following figure shows approximately three weeks of rainfall, depth and two foot depth moisture meter readings for July of 2004. The plots illustrate the concept of this volumetric moisture deficit and show that it is indeed a good approximation of the infiltration process at the BioInfiltration traffic Island.

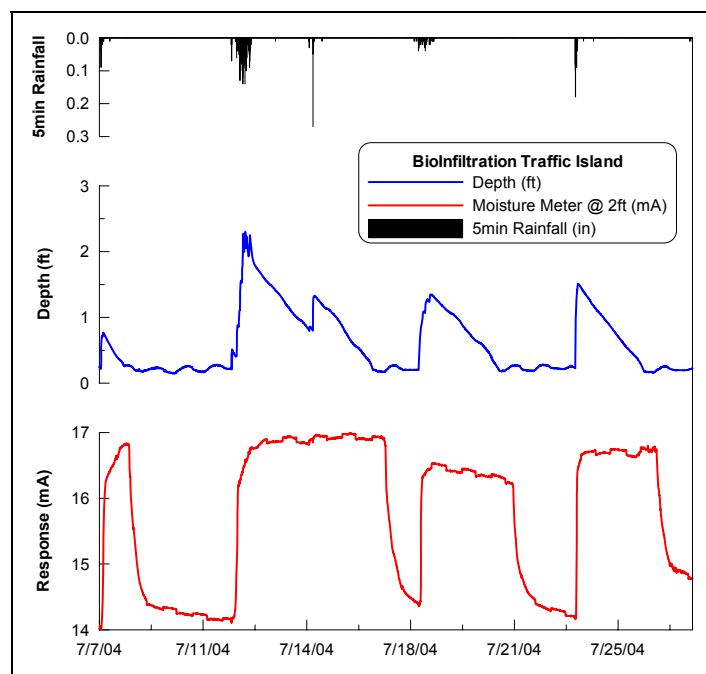


Figure 113. BioInfiltration Traffic Island readings for depth, rainfall and two foot depth moisture meter, July 2004.

Background and Purpose

The original impetus for the model was to use a Green and Ampt procedure to simulate the BioInfiltration Traffic Island. There is an existing, calibrated, hydrologic model of the BMP's drainage area which has been run for numerous years of measured rainfall data collected at the site. This model uses the kinematic wave method to route runoff from both the impervious and pervious areas within the drainage area. It also happens to use the Green and Ampt methodology to calculate losses on the pervious areas. It should be noted that the model does not account for any losses over the impervious area. This is not a bad assumption but may tend to slightly over predict the runoff from impervious area because pavement will likely have some abstractions although they are usually too small to be accurately measured (Heasom, Traver et al. 2006). Using the measured rainfall at the site the model can be used to create a time series record of inflow. The program was written to perform the Green and Ampt procedure on this variable inflow data (time series) and give time series output for the infiltration, storage, and depth in the BMP. The output depth time series could then be compared to the ultrasonic depth measurements recorded at the BMP.

Storage Basin Geometry

Originally the program was written to refer to tables of pertinent geometric data for the BMP. This table format data relates the BMP's depth to its volume, wetted area, and

average depth of infiltration. Where the average depth of infiltration [ft] is computed as follows.

$$\bar{d}_{\text{infiltration}} = \frac{V_{\text{pond}}}{A_{\text{wetted}}}$$

Where: V_{pond} = volume of storage within open pond of BMP at a given depth [ft³]
 A_{wetted} = wetted area of the BMP at a given depth [ft²]

It should also be noted that the volume of pond storage in the BMP does not include storage that occurs in the weir inlet box and connecting pipe. The storage volume described below includes this additional amount of storage. The wetted area is approximated as the plan view area encompassed by the water surface at a given depth. This data was created by and based on a survey of the BioInfiltration Traffic Island done in 2001 by Bill Heasom. A graphical representation of these four variables is provided in the following figure.

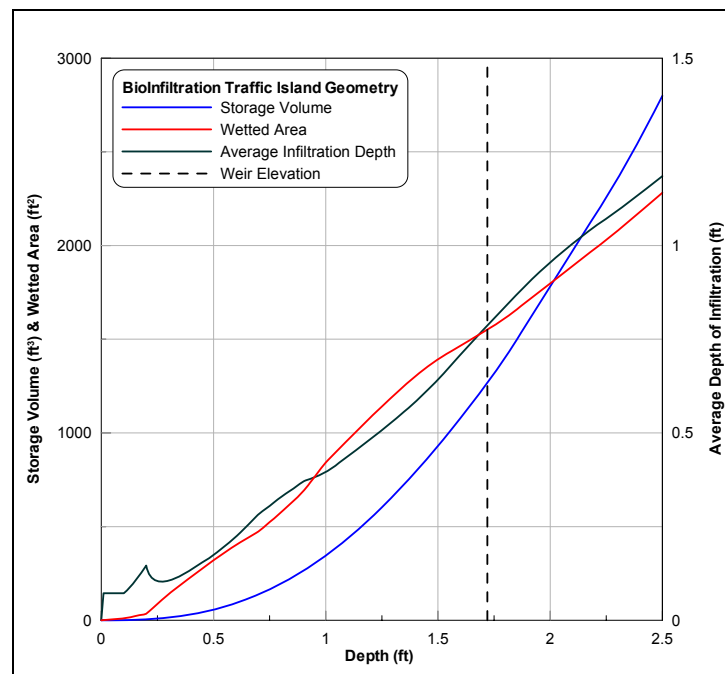


Figure 114. Bioinfiltration Traffic Island storage basin geometry.

Based on the BMP topography the average infiltration depth is not a monotonically increasing function of depth. This is due to a relatively small sump at the bottom of the BMP followed by a larger, flatter area. This complicates the program by requiring that the code always use storage as the independent look up variable because for a given storage there is only one average infiltration depth. If average infiltration depth were

used there would be instances where the incorrect storage and or wetted area were returned due to the multi-valued nature of the average infiltration depth function. This problem was avoided by always using storage as the independent lookup variable.

The need to use an average infiltration depth arises because when the basin is in a ponded condition, the ponded depth above the soil surface varies from 0 ft along the edges to a maximum of the current actual depth at the low point of the bowl. Since the Green and Ampt model considers only one dimension, it is necessary to use an average representative depth over the current wetted area when calculating the rate of surface infiltration. Other more important dimensional problems arise as well. Each time the current step's infiltration volume is calculated it is divided by the wetted area and volumetric soil moisture deficit to determine the new depth of the wetting front. However since the infiltrating area is not constant over a storm, the model can not properly (dimensionally) account for the downward progress of wetting front. At early times when the basin is filling the infiltrating area is small and the wetting front is predicted to move faster than it would on average over a larger wetted area. However as the basin continues filling there are dry upper areas experiencing ponding for the first time. At this point the depth of the wetting front is artificially large and the model would tend to under-predict the basin-wide rate of infiltration. In an effort to better account for early infiltration an attempt was made to use a constant infiltrating area equal to the average wetted area between an empty and completely full (onset of weir flow) depth (0 – 1.72 ft). For the BioInfiltration Traffic Island this results in an area of approximately 710 ft². Even after this modification the model still could not account for the amount of early infiltration that the observed data was exhibiting.

Finally this leads to the most significant shortcoming of this approach to the Green and Ampt model of the BioInfiltration Traffic Island. While the table geometric data of the storage basin topography is based on an extremely precise and detailed survey it does not adequately provide estimates of the wetted area over the time-course of a storm event. This is due to the hysteretic and largely unknown relationship between the depth and the infiltrating area. At the onset of precipitation and consequent inflow the runoff enters the storage basin from three locations; not including the precipitation that falls directly in the bowl. These locations include two unlined riprap swales at the eastern side of the BMP and the 12 in pipe carrying runoff from the storm drain and diversion weir inlet. The pipe from the weir inlet basically flows directly into the low point of the basin. However the two rip-rap swales are located at the opposite end of the basin. Therefore this runoff must first flow through these unlined swales and over the large unchanneled upper section of the basin. Undoubtedly there is a large amount of infiltration that occurs before any of this runoff reaches the low point where it can begin to be accounted for in the ponded depth measurements. The model on the other hand essentially assumes that all of the runoff is entering the basin at the low point where it would be immediately accounted for by the storage basin depth. The infiltration process as modeled by the Green and Ampt method is characterized by high rates of infiltration at early times for a dry soil condition, with the rate asymptotically decreasing and approaching the hydraulic conductivity. This will tend to magnify the inaccuracies mentioned above that exist

especially at early times during a storm event. Therefore at early times it is not possible to reliably predict what the actual wetted area and consequent infiltration may be.

In summary, the variability and unknown nature of the wetted area combined with the previously mentioned dimensional conflicts makes an accurate Green and Ampt simulation of the BioInfiltration Traffic Island unfeasible. Due to these shortcomings the Green and Ampt model with the tabled geometric data underestimates early infiltration but tracks the observed depth fairly well at later times during the storm.

Simulation and Results

The following figure shows the observed data and predicted data for a storm event that took place on August 27th 2005 at the BioInfiltration Traffic Island. This storm event was chosen first because it occurred during the warmest part of the year and after a long period (~10 days) without precipitation and therefore would tend to have the driest initial soil conditions making it ideal for the Green and Ampt method. This storm was also chosen because it did not produce any weir flow (overflow). The Green and Ampt parameters used for the simulation are also shown in the figure.

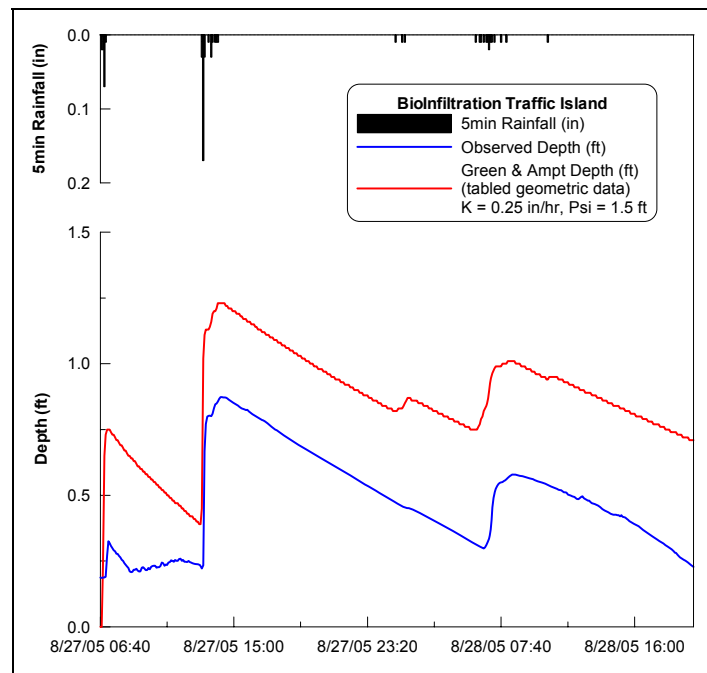


Figure 115. Observed and simulated depth using Green and Ampt model with tabled geometric data.

Figure 115 shows that the model under predicts early infiltration and this extra volume is carried throughout the entire storm event.

At later times when the storage basin is relatively full and the incoming runoff does not need to travel over large areas of dry soil, the model will better represent the infiltration process. Additionally, during the recession period when there is no more inflow, the depth and wetted area relationship is relevant. Figure 116 illustrates how the model can be used to simulate just the recession limb of the storm.

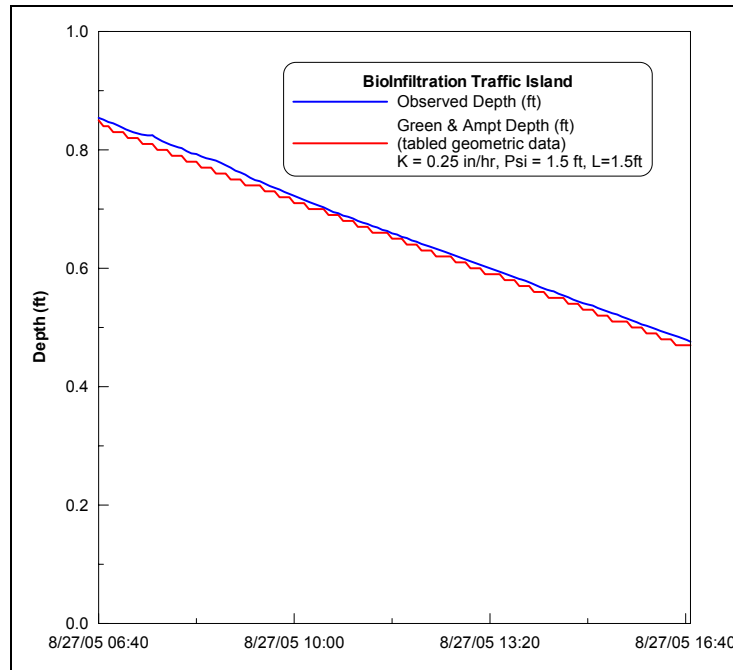


Figure 116. Green and Ampt model used to simulate recession limb of BioInfiltration Traffic Island for same storm mentioned previously.

The figure shows that the model can accurately predict the recession limb. This is accomplished with what appear to be very reasonable infiltration parameters, with a hydraulic conductivity of 0.25 in/hr. Input hydraulic conductivity is referenced at 20°C and temperature is a model input therefore the program automatically adjusts the input hydraulic conductivity to the input temperature. This type of simulation does not include the early infiltration process, which is complicated by the aforementioned factors. In order to simulate the just the recession limb, the initial ponded depth must be set to the observed value at the onset of the recession limb. It is also necessary to input an estimated depth of the wetting front at that time.

In order to properly use the Green and Ampt model with accurate estimates of wetted area and without violating its one-dimensional assumptions it is necessary to assume that the infiltration BMP has a truly flat bottom and that the inflow is evenly distributed over the flat bottom. It should be noted that the BioInfiltration Traffic Island has a relatively flat bottom with a rise of 1.72 ft over the approximate 45 ft between the lowest point and the farthest point along the wetted perimeter at the onset of weir flow. As previously

described, problems arise even with this relatively small slope when the ponded depth in the basin, and to a lesser extent storage, is used to determine the how well the model is predicting observed data.

Generally it is a common and recommended design practice to construct infiltration basins with a flat bottom (MDE 2000; NJDEP 2004; PADEP 2006). This flat bottom geometry will minimize the time of ponding and help prevent nuisance ponding in low points that could potentially provide habitat for breeding mosquitoes. A flat bottom provides a means of helping ensure that all areas of the infiltration basin experience equal hydraulic loading. Therefore the Green and Ampt program was simplified to be based on this flat-bottom design approach where the wetted area is only a function of the bottom dimensions and does not vary with depth. This also assumes that there is no infiltration from the sides, an assumption that improves with increased bottom area and decreased total depth. Both of these conditions are recommended for maintaining the infiltration capacity of an infiltration BMP. With these geometric assumptions the storage within the basin is simply the current depth multiplied by the bottom area.

The best approximation of the BioInfiltration Traffic Island using a flat bottom geometry is one where the storage at the onset of weir flow is equal between both the actual geometry and the flat bottom geometry. For this condition a wetted area of approximately 737 ft² is required. For the previously presented storm the flat bottom Green and Ampt model was run and compared to observed data. This comparison is somewhat trivial due to the significant differences in basin geometry. It is shown here however for the purpose of illustrating the similarities between the recession limbs even with the differing geometries.

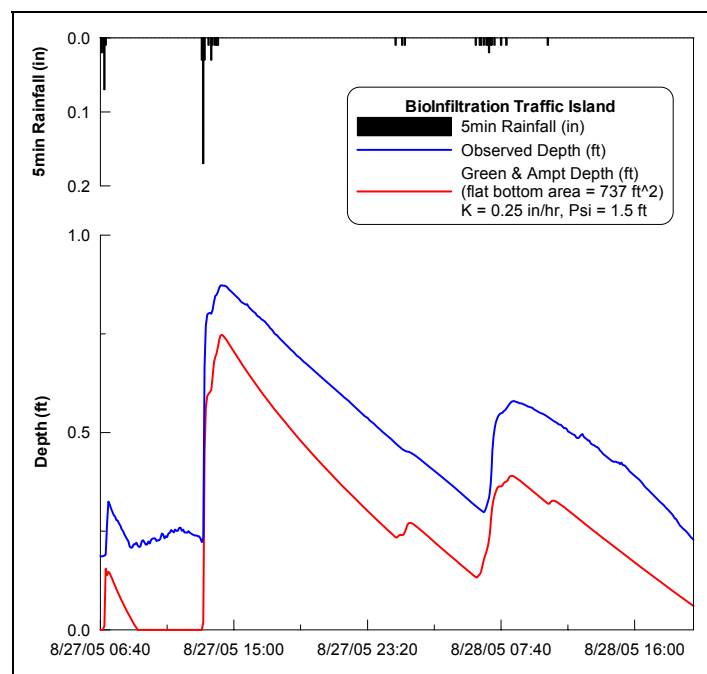


Figure 117. Green and Ampt model with flat bottom approximation of BioInfiltration Traffic Island.

Modification for Continuous Simulation

As previously mentioned one of the main assumptions of the Green and Ampt model is that the moisture moves downward in a piston-like manner. Therefore the hydraulic gradient between the soil surface and the wetting front can only decrease over time. This makes continuous simulation impossible. The Green and Ampt method does not provide any information on the redistribution or recovery of soil moisture within the transmission zone. As previously described, the infiltration process, including redistribution, is described by a nonlinear form of Darcy's equation for unsaturated flow (commonly referred to as the Richards equation), where the soil moisture potential and hydraulic conductivity are nonlinear functions of the moisture content. The assumptions of the Green and Ampt method vastly simplify this equation but provide no direct means for soil moisture recovery. Therefore to enable continuous simulation a hypothetical and empirical method of simulating soil moisture recovery is proposed.

The Green and Ampt program used here does not calculate infiltration unless there is a depth of ponded water above the soil surface. Consequently progress of the wetting front ceases when the ponded depth reaches 0 ft. The final depth of the wetting front represents a volume of water stored within the soil. There are two major processes that will theoretically remove water from this storage. First there is the continued downward movement of gravity and potentially soil suction driven forces that will contribute recharge to the groundwater table beneath the BMP. Secondly there is the upward movement of water caused by direct soil surface evaporation and root uptake with

consequent transpiration. For the purpose of simplification we can assume that both the upward and downward forces can be represented by in a linear fashion and summed to represent the net removal of soil moisture within the wetting front. This linear removal rate [in/day], or soil moisture recovery rate (SMRR) can then be used to decrease the volume of water stored in the soil. Consequently the volume of soil water can then be expressed as a decreasing depth of the wetting front. As the depth of the wetting front is theoretically decreased the infiltration capacity as calculated by the Green and Ampt method will increase. Therefore, providing there is no additional inflow, the soil surface will eventually reach a fully dry state with a maximum infiltration capacity. If additional inflow occurs before the soil reaches a fully dry state the Green and Ampt calculation will proceed as usual with the initial wetting front depth being a function of the previously calculated depth of wetting front, the calculated antecedent time without ponding, and the input soil moisture recovery rate. Clearly there are many problems and shortcomings associated with this highly simplified approach. The method ignores any physical process governing the subsurface drainage processes and also does not incorporate climatic and other conditions that will have influence on the upward movement of water in the soil profile. The equations used to for the entire Green and Ampt program are explained in following section and the visual basic code for the entire Green and Ampt model is supplied at the end of this appendix.

Clearly this is a highly simplified and idealized representation of extremely complex processes. However the method does provide a somewhat physically-based conservation of mass modification to the Green and Ampt approach to enable soil moisture recovery. This simplified method provides a basic structure for further improvements and modifications to create a better continuous simulation model. The following figure shows observed data and modeled data for the months of July and August 2005. The observed depths are included however it should be noted that the assumed flat geometry is different than the actual BMP. The geometry used in this model simulation is a flat bottom area equal to 737 ft² which results in a storage at the onset of weir flow equal to that of the BioInfiltration Traffic Island.

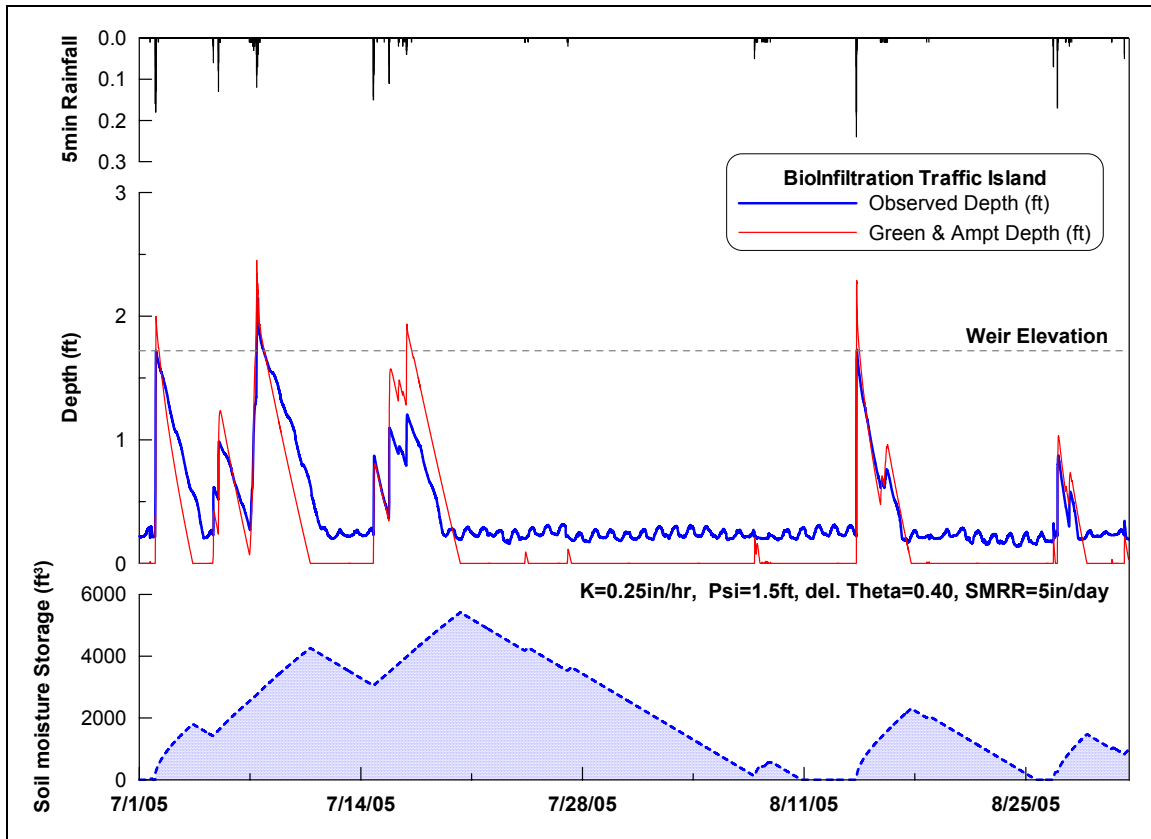


Figure 118. Observed data and Green and Ampt continuous simulation data for July and August 2005.

Figure 118 shows that the continuous simulation model is able to empirically simulate soil moisture recovery. The figure shows a storm event that occurred on August 14th 2005. By this time the model had predicted a full recovery of the soil moisture; back to a fully dry condition. The storm began with a relatively intense period of rainfall with 0.97 in of rainfall in a 45 min period. More rainfall occurred approximately 36 hours later while there was still a ponded depth in the basin. The total precipitation for the event was 1.31 in. The rainfall-runoff model for the BMP's drainage area predicted that the rainfall would result in a total of approximately 3,200 ft³ of inflow to the BMP. The observed data indicates that the initial rainfall filled the storage in the BMP right up to the weir elevation. Since the installation of a pressure transducer in the weir inlet it has been observed that there are periods where weir flow occurs before the BMP depth measurement would predict it. This is due to a difference in water surface elevations between the pond and the inlet/weir box that occurs when there are times of intense rainfall and consequent inflow. While the observed level data indicates there was some trivial amount of weir flow, it likely underestimates the true water surface elevation in the weir box and therefore may be underestimating weir flow. The Green and Ampt model with a flat bottom geometry predicted approximately 880 ft³ of overflow. Therefore the total predicted infiltration for the storm event was approximately 2,300 ft³. This infiltration volume can be seen graphically in Figure 118 with the soil moisture storage reaching the 2,300 ft³ on August 18th at 9:10 which corresponds with the completion of

ponded infiltration. From that time on the soil moisture storage is decreased by a constant rate as indicated by the soil moisture recovery rate of 5 in/day. Therefore the BMP would regain its full infiltration capacity in approximately 7.5 days. As previously mentioned the observed depth data is somewhat irrelevant due to the geometric differences between the modeled flat bottom geometry and the actual surveyed geometry of the BioInfiltration Traffic Island. However, when compared over the two-month period, the two depth records are somewhat similar and provide comparable estimates for event specific ponded duration.

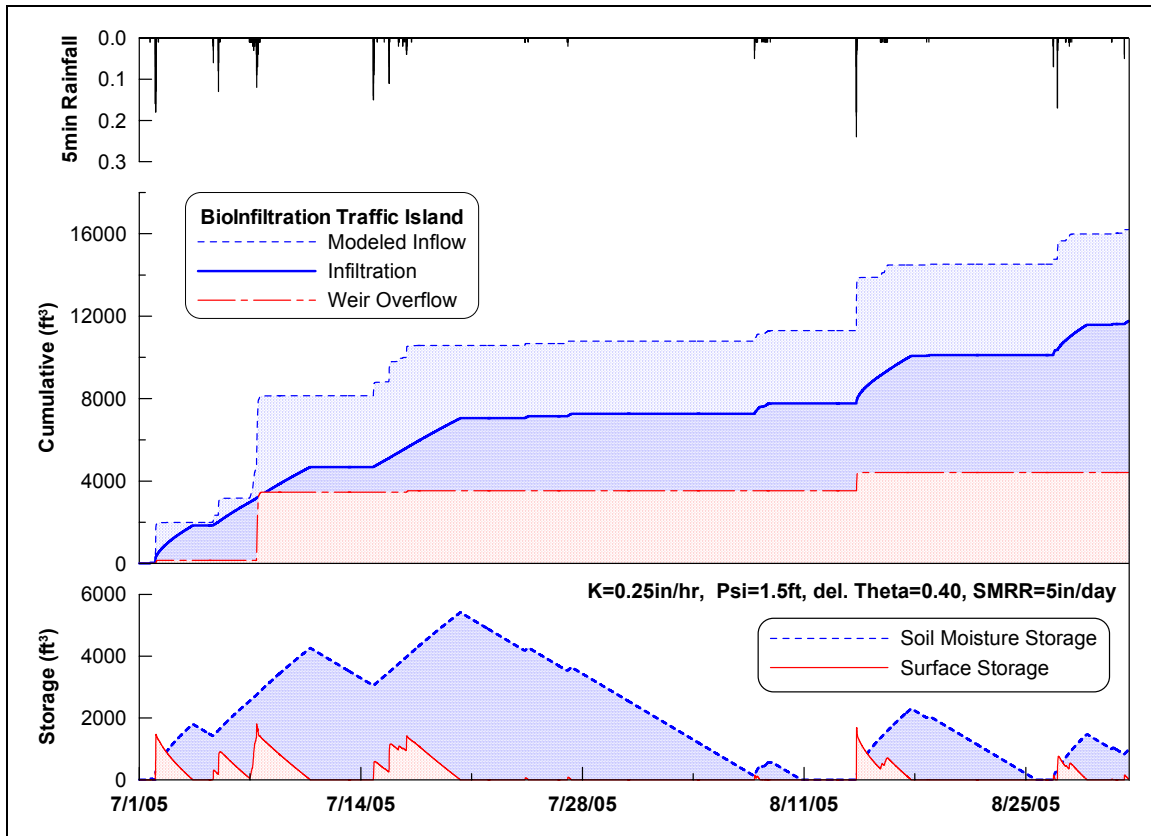


Figure 119. Cumulative plot for two month simulation period.

Figure 119 shows the same model results in a mass balance fashion with running summations for total inflow (from the HEC-HMS model), total infiltration, and total weir overflow. For the two-month period simulated here the BMP is predicted to receive a total of 16,000 ft³ of inflow as a result of the 7.78 in of precipitation. The flat-bottom geometry Green and Ampt model predicts that 12,000 ft³ of this inflow will be infiltrated and the remaining 4,000 ft³ flowing over the weir as overflow.

Governing Equations and Program Format

Before the iterative calculations can begin the input data must be processed. First the input hydraulic conductivity is adjusted for temperature based on a ratio of the viscosity of water at the reference temperature of 20°C and the input temperature (Constantz and Murphy 1991).

$$K_T = K_{20} \times \left(\frac{\mu_{20}}{\mu_T} \right)$$

Where: K_T = hydraulic conductivity at input temperature [in/hr]
 K_{20} = hydraulic conductivity at 20 degrees C [in/hr]
 μ_T = viscosity of water at the input temperature [Ns/m²]

The following empirical formula is used to describe the dependency of the viscosity of water with temperature (Ronan, Prudic et al. 1998).

$$\mu(T) = 0.00002414 \times 10^{[247.8/(T+133.16)]}$$

Where: T = input temperature [°C]

Other input data that requires some processing includes calculating the area based on the input bottom width and length and converting the soil moisture recovery rate from in/day to ft/min. After the variables have all been initialized for the first time step, the following series of iterative equations solves the Green and Ampt infiltration model for ponded infiltration. First the elapsed time is updated.

$$t_j = t_{j-1} + \Delta t$$

Where: Δt = input time step [min]

Secondly the depth of the wetting front is calculated based on the previous step's wetting front depth and infiltration volume. In the following equation $\Delta\theta$ represents the change in volumetric water content expected as the soil goes from dry conditions to wet.

Theoretically it cannot exceed the soil's porosity.

$$L_j = L_{j-1} + \frac{(I_{j-1} / A)}{\Delta\theta}$$

Where: L = depth of wetting front [ft]
 I = infiltration volume [ft³]
 A = infiltrating area [ft²]
 $\Delta\theta$ = change in volumetric moisture content expected as soil is wetted [-]

If there is no ponding and a positive value (non-zero) for soil moisture recovery rate has been entered, the program decreases L with the following equation. It also keeps a running track of the amount of dry time since the last time of ponding.

$$L_j = L_{j-1} - \frac{(SMRR \times \Delta t)}{\Delta \theta}$$

Where: $SMRR$ = user specified volumetric abstraction [in/day]

Finally, before the current one-dimensional infiltration flux can be calculated the depth of ponded head is updated. Each volumetric term is divided by the infiltrating area and by the porosity of the storage basin. For open storage beds the porosity would be input as 1. For a stone storage bed with 40% void space this parameter would be entered as 0.4.

$$h_j = h_{j-1} + \frac{Inflow_{j-1}}{A \times n_{storage}} - \frac{I_{j-1}}{A \times n_{storage}} - \frac{Outflow_{j-1}}{A \times n_{storage}}$$

Where: h = depth of ponded head [ft]
 $Inflow$ = inflow read from input time series [ft³]
 $n_{storage}$ = porosity of storage basin [-]
 $Outflow$ = the calculated outflow [ft³]

Once the necessary inputs have all been determined the Green and Ampt equation is computed as follows, with the hydraulic conductivity units being converted from in/hr to ft/min.

$$i_j = \left(K_r \times \frac{1}{12} \times \frac{1}{60} \right) \times \frac{h_j + \psi + L_j}{L_j}$$

Where: ψ = soil moisture potential (suction) entered as a positive value [ft]
 i = incremental step infiltration rate [ft/min]

The Green and Ampt infiltration flux is then converted to an incremental volume by multiplying by the time step and infiltrating area.

$$I_j = i_j \times \Delta t \times A$$

The code keeps track of the storage within the BMP by multiplying the current depth by the infiltrating area and accounting for storage basing porosity.

$$S_j = h_j \times A \times n_{storage}$$

Where: S = storage in BMP [ft³]

The code uses the equation for flow over a 90 degree v-notch weir with a weir coefficient of 2.47 (US customary units). The flow rate [cfs] is calculated as an incremental volume by multiply by the input time step and converting seconds to min.

$$Outflow_j = 2.47 \times (h_j - h_{overflow})^{\frac{5}{2}} \times \Delta t \times 60$$

The program uses an ‘If’ statement to ensure that the calculated depth remains positive. This is accomplished simply by checking that the previous step’s infiltration volume is not greater than the volume of water that is available for infiltration. When the program calculates an otherwise negative value for depth, it sets the depth to zero. It also sets the previous step’s infiltration volume equal to the previous storage volume. This condition is generally relevant at two specific times in a given storm. First when the storm begins the early inflow volumes are often small. Additionally at early time when the depth of the wetting front is still small (shallow) the soil has its highest potential infiltration flux. Therefore, generally the soil is able to infiltrate the entire step’s incremental inflow volume. In other words, the actual infiltration flux is equal to the inflow rate until the inflow rate exceeds the potential infiltration flux and ponding occurs. The second time a negative depth could be calculated is at the time corresponding to the end of ponding. For both of these cases another ‘If’ statement is used that sets the incremental infiltration volume equal to only the volume of water that was available for infiltration. A spreadsheet screenshot and the visual basic code for the Green and Ampt program area included below.

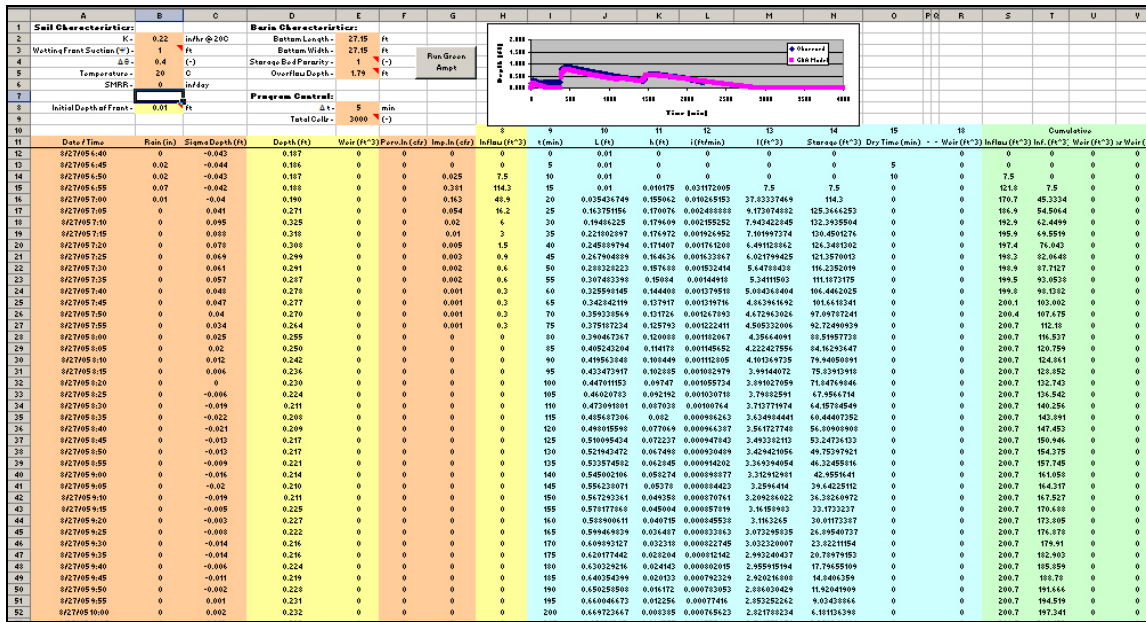


Figure 120. Screenshot of spreadsheet used to implement Green and Ampt infiltration BMP model.

Visual Basic code for Green and Ampt infiltration BMP model with flat bottom geometry:

Sub GreenAmptFlat1ET1()

```

*****
**
'housekeeping

'activate the first worksheet
Sheets("GA").Select
'clear old results
Range("I12:R65536").ClearContents

*****
**

'read user set program control data

'read the k of the transmission zone, in/hr at 20 deg C
K20C = Cells(2, 2).Value
'read the suction at the wetting front
frontsuction = Cells(3, 2)
'read the change in moisture content expected as the front progresses
deltheta = Cells(4, 2).Value
'read the initial depth of wetting front
    
```

```

initialLfront = Cells(8, 2).Value
'read the storage porosity
storpor = Cells(4, 5).Value
'read the time step
delttime = Cells(8, 5).Value
'read the number of rows to evaluate to
totalcells = Cells(9, 5).Value
'read the overflow depth
overflowdepth = Cells(5, 5).Value
'read the bottom length
bottomlength = Cells(2, 5).Value
'read the bottom width
bottomwidth = Cells(3, 5).Value
'calculate bottom area
area = bottomlength * bottomwidth
'read the temperature, deg C
temperature = Cells(5, 2).Value
'read in the "ET" rate and convert to ft/min
ETinday = Cells(6, 2)
ET = ETinday * (1 / (12 * 24 * 60))

*****
**
'convert input K20 to k at given temperature
'calc viscosity at given temperature
viscosityattemperature = 0.00002414 * 10 ^ (247.8 / (temperature + 133.16))
viscosityat20C = 0.00002414 * 10 ^ (247.8 / (20 + 133.16))
K = K20C * (viscosityat20C / viscosityattemperature)

*****
**
'initialize the variables

'input data starts at row number 12
w = 12

'set initial time
Cells(w, 9) = 0

'input initial depth of front
Cells(w, 10) = initialLfront

'initialize the depth column, by default it starts empty, unless there is inflow on the first
step
'Cells(w, 11) = Application.Max(0, (Cells(w, 8) / (area * storpor)))
Cells(w, 11) = 0

```

'initialize the infiltration rate

Cells(w, 12) = 0

'initialize the inf vol (cf)

Cells(w, 13) = 0

'initialize the storage

'Cells(w, 14) = Cells(w, 11) * (area * storpor)

Cells(w, 14) = 0

'initialize the weir outflow

Cells(w, 18) = 0

'initialize the dry time counter

ADT = 0

**

'begin the iterative calculations

Do

w = w + 1

'calc the step time

Cells(w, 9) = Cells(w - 1, 9) + deltime

'calc the depth, if the step's depth is negative ($I > h$), there is no ponding for this
'step. therefore the step's depth should be 0.

If Cells(w - 1, 11) - (Cells(w - 1, 13) / (area * storpor)) + (Cells(w - 1, 8) / (area *
storpor)) - (Cells(w - 1, 18) / (area * storpor)) <= 0 Then

Cells(w, 11) = 0

Else

'otherwise, the depth is: previous depth - previous inf depth + next inflow depth -
previous weir outflow depth

Cells(w, 11) = Cells(w - 1, 11) - (Cells(w - 1, 13) / (area * storpor)) + (Cells(w - 1, 8) /
(area * storpor)) - (Cells(w - 1, 18) / (area * storpor))

End If

'calc the new depth of front (previous depth + ((InfVol/Area)/deltheta)

'if there is no ponding decrease L based on the ET and ADT (dry time)

If Cells(w, 11) = 0 Then

ADT = ADT + deltime

```

Cells(w, 10) = Application.Max(Cells(w - 1, 10) - ((deltime * ET) / deltheta),
initialLfront)
Else
Cells(w, 10) = Cells(w - 1, 10) + ((Cells(w - 1, 13) / area) / deltheta)
ADT = 0
End If

Cells(w, 15) = ADT

'calc i only if there is ponding (no ponding, no infiltration/recovery)
If Cells(w, 11) > 0 Then
Cells(w, 12) = (K / (12 * 60)) * (((Cells(w, 11) + frontsuction) + Cells(w, 10)) / Cells(w,
10))
Else
Cells(w, 12) = 0
End If

'calc infiltration volume, if the step's (i * deltime * area) is greater than the step's depth *
area (no more ponding) then,
'the step's infiltration volume is simply the depth times the area. Otherwise simply
calculate it.
If (Cells(w, 12) * deltime) / storpor >= Cells(w, 11) Then
Cells(w, 13) = Cells(w, 11) * area * storpor
Else
Cells(w, 13) = (Cells(w, 12) * deltime) * area
End If

'calc weir flow 90degree v-notch cd=2.47 (must also convert cfs to cf)
Cells(w, 18) = (Application.Max(Cells(w, 11), overflowdepth) - overflowdepth) ^ (5 / 2)
* 2.47 * deltime * 60

'calc the storage
Cells(w, 14) = Cells(w, 11) * area * storpor

Loop Until w >= totalcells

End Sub

```